


UNIVERSITY OF BIRMINGHAM

# Influence of periodontal pathogens on induction of epithelial-mesenchymal transition (EMT) in oral keratinocytes

By

Satvir Singh Shoker

A thesis submitted to the University of Birmingham for the degree of

DOCTOR OF PHILOSOPHY

School of Dentistry

College of Medical and Dental Sciences

University of Birmingham

December 2021

UNIVERSITY OF
BIRMINGHAM

## University of Birmingham Research Archive

### e-theses repository

This unpublished thesis/dissertation is copyright of the author and/or third parties. The intellectual property rights of the author or third parties in respect of this work are as defined by The Copyright Designs and Patents Act 1988 or as modified by any successor legislation.

Any use made of information contained in this thesis/dissertation must be in accordance with that legislation and must be properly acknowledged. Further distribution or reproduction in any format is prohibited without the permission of the copyright holder.

## ABSTRACT

Epithelial-mesenchymal transition (EMT) is a process where epithelial cells gain migratory and invasive properties and is associated with dissolution of epithelial integrity. Inflammatory mediators released as a host response to periodontal pathogens are known to induce EMT. This project investigated the ability of these periodontal pathogens to induce EMT *in vitro* and to identify whether the natural EMT-inhibitor curcumin could interfere with this process. A 2D-oral epithelium model using H400 oral keratinocytes was exposed to *Escherichia coli* lipopolysaccharide (LPS) (positive control) and heat-killed (HK) or oxygen-killed (OK) periodontal pathogens *Porphyromonas gingivalis*, *Fusobacterium nucleatum* and *Treponema denticola* for 8-days. EMT-related changes were assessed by quantitative real time-polymerase chain reaction (qRT-PCR), enzyme linked immunosorbent assay (ELISA), immunofluorescence, Ibidi culture-insert (2-well) wound healing assay and trans-epithelial electrical resistance (TEER). Scanning electron microscopic analysis showed that heat-killing resulted in loss of *T. denticola* morphology but was maintained after oxygen-killing. Further analysis by mass spectrometry-based proteomics of *T. denticola* isolated membrane, revealed that heat-killing was more detrimental to *T. denticola* proteins than oxygen-killing. Stimulation of oral keratinocytes by *E. coli* LPS and all HK and OK pathogens for 8-days, increased secretion of pro-inflammatory cytokines interleukin (IL)-1β, IL-8 and transforming growth factor-β1 (TGF-β1) and gene expression of EMT-related transcription factors snail-1, snail-2 and twist-1, resulting in down-regulated expression of epithelial markers, E-cadherin, desmoplakin-1 and cytokeratin 5. Concomitantly, expression of mesenchymal markers, N-cadherin, vimentin and matrix metalloproteinase-9 (MMP-9), were up-regulated. Molecular changes were associated with compromised epithelial barrier integrity and increased cell

migration. Simultaneous treatment with 5μM curcumin suppressed gene expression of OK pathogen induced pro-inflammatory cytokines and snail-1. In addition, curcumin inhibited OK pathogen induced down-regulation of epithelial markers and inhibited up-regulated expression of mesenchymal markers. Curcumin inhibited OK *P. gingivalis* and *T. denticola* induced cell migration. These data indicated that naturally derived EMT-inhibitors, such as curcumin, may inhibit periodontal pathogen induced EMT, therefore maintaining the epithelial barrier and potentially preventing the progression of periodontitis.

## ACKNOWLEDGEMENTS

Firstly, I would like to thank my supervisors Professor Michael Milward, Professor Gabriel Landini, Dr Richard Shelton and Professor Paul Cooper for their continuous support and guidance over the past 4 years. Their constant encouragement to do better and constructive criticism during my PhD have helped me become a more competent researcher and I could not have asked for a better supervisory team.

I would also like to thank all the technicians at the school of dentistry who have been extremely helpful providing me with training and offering advice during my PhD. I would especially like to thank Gay Smith, Helen Wright, Jiangou Liu, Michelle Holder and Khawla Doudin. I would also like to thank Dr Sarah Kuehne and Dr Melissa Grant for their help throughout my PhD.

I am also grateful for the support provided by my supervisors at GSK, Dr Martin Ling and Dr Jonathan Pratten. Thank you for always making me feel welcome at GSK visits and offering guidance during my PhD.

A massive thank you also goes to my friends and colleagues at the school of dentistry past and present. The constant support, insightful conversations and of course laughs have made this journey much more enjoyable and I am extremely grateful for you all.

Most of all I would like to thank my wonderful family who have sacrificed so much for me to achieve my goals. The endless support and motivation you have all provided me throughout my PhD have made this journey achievable.

## TABLE OF CONTENTS

**1. INTRODUCTION ..... 1**

1.1 General introduction ..... 2

1.2 Epithelium ..... 3

1.2.1 Gingival epithelium ..... 6

1.2.2 Gingival connective tissue ..... 7

1.2.3 Gingival inflammation ..... 8

1.3 Epithelial-mesenchymal transition ..... 9

1.3.1 Overview of EMT ..... 9

1.3.2 Molecular events in EMT ..... 10

1.3.2.1 Loss of epithelial cell-cell contacts ..... 10

1.3.2.2 Cytoskeletal changes and acquisition of migratory properties ..... 14

1.3.2.3 ECM changes ..... 15

1.3.3 Biomarkers of EMT ..... 18

1.3.4 Types of EMT ..... 20

1.3.4.1 Type 1 EMT ..... 20

1.3.4.2 Type 2 EMT ..... 21

1.3.4.3 Type 3 EMT ..... 22

1.3.5 EMT-inducing pro-inflammatory cytokines in periodontitis ..... 23

1.3.5.1 IL-1β ..... 23

1.3.5.2 IL-8 ..... 24

1.3.5.3 TGF-β1 ..... 25

1.4 Periodontitis ..... 26

1.4.1 Systemic disease association ..... 27

1.4.2 Risk factors for periodontitis ..... 30

1.4.3 *In vitro* models of periodontitis ..... 32

1.5 Oral microbiome ..... 33

1.5.1 Oral bacteria and inflammation ..... 38

1.5.2 Bacteria and EMT ..... 39

1.6 Bacterial inactivation for use in epithelial stimulation ..... 41

1.7 EMT inhibitors ..... 42
1.7.1 Curcumin ..... 46
1.7.1.1 Anti-inflammatory properties ..... 47
1.7.1.2 Clinical studies ..... 48
1.7.1.3 Curcumin as an EMT inhibitor ..... 49

1.8 Aims and objectives ..... 51

**2. MATERIALS AND METHODS ..... 53**

2.1 Bacterial cultivation ..... 54
2.1.1 New oral spirochete (mNOS) medium ..... 54
2.1.1.1 Volatile fatty acid (VFA) mix ..... 55
2.1.1.2 Thiamine pyrophosphate–volatile fatty acid (TPP-VFA) ..... 55

2.2 Determining bacterial concentration ..... 57

2.3 Bacterial preparation ..... 58
2.3.1 Heat-killing ..... 58
2.3.2 Oxygen-killing ..... 58

2.4 Characterisation of periodontal pathogens ..... 59
2.4.1 Gram staining ..... 59
2.4.2 Bacteria identification by polymerase chain reaction (PCR) ..... 59
2.4.2.1 Visualisation of PCR product by gel electrophoresis ..... 61

2.5 Scanning electron microscopy (SEM) sample preparation ..... 61
2.5.1 Artificial saliva ..... 62

2.6 Cell Culture ..... 63
2.6.1 Culture of H400 cells ..... 63
2.6.2 Sub-culturing ..... 64
2.6.3 Cryopreservation ..... 64

2.7 Cell counts and viability ..... 65
2.7.1 Manual cell counting and viability assay using haemocytometer ..... 65
2.7.2 Automated cell counting and viability assay using Tecan Spark® ..... 66

2.8 Exposure of oral keratinocytes to oral pathogens ..... 66

2.9 Enzyme-linked Immunosorbent Assay (ELISA) ..... 67

2.9.1 IL-1β and IL-8 ELISA protocol ..... 67
2.9.2 TGF-β1 ELISA protocol ..... 68

2.10 Polymerase chain reaction assay ..... 71
2.10.1 H400 cell culture preparation for qRT-PCR ..... 71
2.10.2 Cell lysis ..... 71
2.10.3 RNA extraction ..... 72
2.10.4 RNA quantification ..... 73
2.10.5 cDNA conversion ..... 73
2.10.6 Determining primer efficiency: ..... 74
2.10.7 Identification of a suitable housekeeping gene ..... 77
2.10.8 Gene expression analysis of target genes ..... 77

2.11 Cell migration assays ..... 81
2.11.1 Mitomycin C preparation and determining optimum mitomycin C concentration ..... 81
2.11.2 Scratch wound assay ..... 82
2.11.3 Cell migration assay using culture-inserts ..... 82

2.12 Trans-epithelial electrical resistance ..... 85
2.12.1 TEER protocol ..... 85

2.13 Immunofluorescence ..... 88
2.13.1 Positive and negative controls ..... 88
2.13.2 Staining procedure ..... 89
2.13.3 Determining localisation of snail-1 ..... 90

2.14 Curcumin addition to inhibit bacterial-induced EMT ..... 93
2.14.1 Curcumin preparation and optimisation ..... 93

2.14.1.1 Curcumin dissolved in DMSO with PBS ..... 93
2.14.1.2 Curcumin dissolved in NaOH with PBS ..... 94

2.15 Analysis of curcumin EMT inhibition ..... 96

2.16 Mass spectrometry of live, heat and oxygen-killed *Treponema denticola* ..... 96
2.16.1 Isolation of outer membrane ..... 97
2.16.2 Bicinchoninic acid (BCA) assay ..... 97
2.16.3 Filter-aided sample preparation (FASP) digestion ..... 98
2.16.4 Fluorometric peptide assay ..... 99
2.16.5 TMT™ labelling protocol ..... 100
2.16.6 Desalting with Sep-pak filter ..... 101
2.16.7 Liquid chromatography tandem mass spectrometry (LC-MS/MS) ..... 102

2.17 Statistical analysis ..... 102

**3. PERIODONTAL PATHOGEN CHARACTERISATION AND 2D ORAL EPITHELIAL MODEL DEVELOPMENT FOR EPITHELIAL-MESENCHYMAL TRANSITION ANALYSIS ..... 103**

3.1 Introduction ..... 104

3.2 Periodontal pathogen characterisation ..... 107
3.2.1 Identification by culture ..... 107
3.2.1.1 Analysis of bacterial cultures ..... 107
3.2.2 Characterisation by Gram stain ..... 109
3.2.2.1 Analysis of Gram stains ..... 109
3.2.3 Characterisation by PCR ..... 111
3.2.3.1 Analysis of PCR results ..... 111

3.3 Periodontal pathogen growth curves ..... 113
3.3.1 Analysis of growth curves ..... 113

3.4 Oxygen-killing of periodontal pathogens ..... 116
3.4.1 Analysis of periodontal pathogen killing by exposure to oxygen ..... 116

3.5 Effects of heat and oxygen-killing on pathogen morphology by Gram stain ..... 120
3.5.1 Analysis of Gram stain images after heat and oxygen-killing ..... 120

3.6 Effects of heat and oxygen-killing on pathogen morphology by scanning electron microscopy ..... 124
3.6.1 Analysis of scanning electron microscope images after heat and oxygen-killing of pathogens ..... 124

3.7 Manual (haemocytometer) vs Automatic (Tecan Spark) cell counts/viability ..... 128
3.7.1 Analysis of manual and automatic counting on cell counts/viability ..... 128

3.8 Development of a 2D oral epithelial model for EMT analysis ..... 130
3.8.1 Optimising cell seeding density with percentage cell confluency ..... 130
3.8.1.1 Effects of increasing cell density on cell confluency ..... 131
3.8.2 Cell growth models ..... 133
3.8.2.1 Effects of alterations to cell culture media on cell growth and viability ..... 133
3.8.3 Using hypoxic conditions for H400 growth ..... 140
3.8.3.1 Effects of hypoxia on cell growth and viability ..... 140

3.9 Discussion ..... 142
3.9.1 Characterisation of periodontal pathogens by culture, Gram stain and PCR ..... 142
3.9.2 Pathogen growth curves ..... 143
3.9.3 Oxygen killing of bacterial pathogens ..... 144
3.9.4 Effects of heat and oxygen-killing on bacterial morphology ..... 146
3.9.5 Manual vs automatic cell counting ..... 148
3.9.6 Percentage cell confluency in different cell models ..... 149
3.9.7 Normoxia vs Hypoxia ..... 150

**4. EPITHELIAL-MESENCHYMAL TRANSITION INDUCTION OF H400 ORAL EPITHELIAL CELLS BY HEAT AND OXYGEN-KILLED PERIODONTAL PATHOGENS ..... 152**

4.1 Introduction ..... 153

4.2 Effect of heat-killed and oxygen-killed periodontal pathogens on epithelial cell growth and viability ..... 155
4.2.1 Analysis of heat-killed and oxygen-killed periodontal pathogens on epithelial cell growth and viability ..... 155

4.3 Real-time PCR analysis of EMT related markers after heat and oxygen killed pathogen challenge ..... 161
4.3.1 Gene expression of epithelial markers in oral keratinocytes ..... 161
4.3.1.1 Effects of pathogen exposure on epithelial marker gene expression ..... 161
4.3.2 Gene expression of mesenchymal markers in oral keratinocytes ..... 166
4.3.2.1 Effects of pathogen exposure on mesenchymal marker gene expression ..... 166
4.3.3 Gene expression of EMT-related transcription factors in oral keratinocytes ..... 170
4.3.3.1 Effects of pathogen exposure on EMT-related transcription factor gene expression ..... 170
4.3.4 Gene expression of EMT-inducing pro-inflammatory cytokines in oral keratinocytes ..... 174
4.3.4.1 Effects of pathogen exposure on EMT- inducing pro-inflammatory cytokine gene expression ..... 174

..... 178

4.4 Pro-inflammatory cytokine expression by Enzyme-linked immunosorbent assay ..... 179
4.4.1 Analysis of IL-1β secretion ..... 179
4.4.2 Analysis of IL-8 secretion ..... 183
4.4.3 Analysis of TGF-β1 secretion ..... 186

4.5 Immunofluorescence for E-cadherin, Vimentin and Snail-1 proteins in oral keratinocytes after stimulation with heat and oxygen-killed pathogens ..... 189
4.5.1 Effects of heat and oxygen-killed pathogens on E-cadherin, Vimentin and Snail-1 protein expression in oral keratinocytes ..... 189
4.5.1.1 Localisation of Snail-1 in oral keratinocytes after oxygen-killed *T. denticola* exposure ..... 193

4.6 Cell migration of oral keratinocytes after exposure to heat and oxygen-killed periodontal pathogens ..... 195
4.6.1 Optimising mitomycin C concentration for inhibition of proliferation ..... 195
4.6.1.1 Effects of increasing mitomycin C concentration on epithelial cell viability ..... 195
4.6.2 Cell migration of oral keratinocytes after heat-killed *P. gingivalis* and *F. nucleatum* exposure using scratch wound assay ..... 198
4.6.2.1 Analysis of oral keratinocyte wound gap closure after heat-killed pathogen exposure ..... 198
4.6.3 Cell migration of oral keratinocytes after heat and oxygen-killed pathogen exposure using Ibidi 2-well culture insert method ..... 200
4.6.3.1 Analysis of oral keratinocyte wound gap closure after heat-killed and oxygen-killed pathogen exposure ..... 200

4.7 Trans-epithelial electrical resistance of oral keratinocyte monolayers after heat and oxygen-killed pathogen exposure ..... 206
4.7.1 Effects of pathogen exposure on trans-epithelial electrical resistance in oral keratinocyte monolayers ..... 206

4.8 Discussion ..... 210
4.8.1 Effect of heat and oxygen-killed pathogens on epithelial cell growth and viability ..... 210
4.8.2 Heat and oxygen-killed periodontal pathogens compromise epithelial integrity ..... 211
4.8.3 Heat and oxygen-killed periodontal pathogens promote mesenchymal phenotype ..... 214
4.8.4 Heat or oxygen-killed pathogens can activate EMT related transcription factors ..... 216
4.8.5 Oxygen-killed pathogens promote greater expression of EMT-related pro-inflammatory cytokines ..... 219
4.8.6 Heat and oxygen-killed periodontal pathogens promote oral keratinocyte cell migration ..... 223

**5. INHIBITION OF PATHOGEN-INDUCED EPITHELIAL-MESENCHYMAL TRANSITION IN ORAL KERATINOCYTES ..... 226**

5.1 Introduction ..... 227

5.2 Curcumin solubilised in DMSO for oral keratinocyte exposure ..... 229

5.2.1 Effects of DMSO and curcumin concentrations on cell growth and viability .....229

5.3 Curcumin solubilised in NaOH for oral keratinocyte exposure .....232
5.3.1 Effects of NaOH concentrations on oral keratinocyte cell viability .....232

5.4 Optimising curcumin concentration for use on oral keratinocytes .....234
5.4.1 Effects of increasing curcumin concentrations on H400 cell growth and viability ...234

5.5 Curcumin and oxygen-killed *T. denticola* exposure of oral keratinocytes .....238
5.5.1 Effects of curcumin on oxygen-killed *T. denticola* induced oral keratinocyte cell growth and viability .....238

5.6 Oxygen-killed pathogen induced cell migration of oral keratinocytes and curcumin .....240
5.6.1 Analysis of curcumin on oxygen-killed pathogen induced oral keratinocyte wound gap closure .....240

5.7 EMT-related gene expression changes in oral keratinocytes stimulated with oxygen-killed pathogens and curcumin .....248
5.7.1 Gene expression of epithelial markers .....248
5.7.1.1 Effects of curcumin on oxygen-killed pathogen induced epithelial-related gene expression changes .....248
5.7.2 Gene expression of mesenchymal markers .....251
5.7.2.1 Effects of curcumin on oxygen-killed pathogen induced mesenchymal-related gene expression .....251
5.7.3 Gene expression of EMT-related transcription factors .....254
5.7.3.1 Effects of curcumin on oxygen-killed pathogen induced expression of EMT-related transcription factors .....254
5.7.4 Gene expression of EMT-inducing pro-inflammatory cytokines .....257
5.7.4.1 Effects of curcumin on oxygen-killed pathogen induced EMT-related pro-inflammatory cytokine gene expression .....257

5.8 Trans-epithelial electrical resistance of oral keratinocyte monolayers exposed to oxygen-killed *T. denticola* and *E. coli* LPS with curcumin .....261
5.8.1 Analysis of curcumin on trans-epithelial electrical resistance in oxygen-killed *T. denticola* and *E. coli* LPS exposed monolayers .....261

5.9 Discussion....263
5.9.1 Curcumin inhibits oxygen-killed *T. denticola* induced oral keratinocyte growth ....263
5.9.2 Curcumin inhibits oxygen-killed *P. gingivalis* and *T. denticola* induced oral keratinocyte cell migration ....264
5.9.3 Curcumin inhibits oxygen-killed pathogen induced epithelial marker repression ....265
5.9.4 Curcumin potentially inhibits oxygen-killed pathogen-induced mesenchymal gene expression ....266
5.9.5 Curcumin selectively inhibits oxygen-killed pathogen induced gene expression of EMT-related transcription factors....267
5.9.6 Curcumin selectively inhibits oxygen-killed pathogen induced gene expression of EMT promoting pro-inflammatory cytokines....269

**6. MASS SPECTROMETRY ANALYSIS OF LIVE, HEAT AND OXYGEN-KILLED *T. DENTICOLA* PROTEINS ....272**

6.1 Introduction ....273

6.2 Isolated *T. denticola* outer membrane proteins ....274
6.2.1 Analysis of *T. denticola* outer membrane proteins ....274

6.3 Analysis of *T. denticola* proteins....280
6.3.1 Live vs heat-killed *T. denticola* protein analysis ....280
6.3.2 Live vs oxygen-killed *T. denticola* protein analysis ....287

6.4 Discussion....291
6.4.1 Proteins involved in *T. denticola* structure ....292
6.4.2 Proteins involved in heat shock response ....293
6.4.3 Proteins potentially involved in oxidative stress response ....295
6.4.4 Proteins potentially involved in EMT responses ....295

**7. CONCLUSIONS AND FUTURE WORK....297**

7.1 Main conclusions....298

7.2 Limitations and future work ....301

7.3 Concluding remarks.....303

**8. REFERENCES .....305**

**9. APPENDICES.....353**

9.1 List of proteins and abundances of isolated live, heat and oxygen-killed *T. denticola* outer membrane proteins .....354

9.2 Conference abstracts.....369

## LIST OF FIGURES

### Chapter 1

**Figure 1.1:** Diagram of keratinised epithelial cells and cell junctions. .....5
**Figure 1.2**: Diagram of an epithelial cell undergoing epithelial-mesenchymal transition. .....13
**Figure 1.3**: Illustration of a fibroblastic cell within the ECM. .....17
**Figure 1.4**: Oral bacteria of subgingival plaque clustered into Socransky complexes. .....37

### Chapter 2

**Figure 2.1**: Inoculation of *Treponema denticola*. .....56
**Figure 2.2**: Overview of sandwich ELISA protocol .....70
**Figure 2.3**: qPCR amplification curves for housekeeping gene GAPDH .....76
**Figure 2.4**: Melting curve of GAPDH .....76
**Figure 2.5**: Cell culture images for cell migration analysis using ImageJ .....84
**Figure 2.6**: Diagram of how TEER was measured using the EVOM2™ epithelial voltohmmeter and STX2 electrodes. .....87
**Figure 2.7**: Overview of direct and indirect immunofluorescence staining .....92

### Chapter 3

**Figure 3.1**: Photographs of *P. gingivalis*, *F. nucleatum* and *T. denticola* cultures .....108
**Figure 3.2**: Gram stain images of *P. gingivalis*, *F. nucleatum* and *T. denticola* .....110
**Figure 3.3**: PCR amplification of species-specific genomic sequences in *P. gingivalis*, *F. nucleatum* and *T. denticola*. .....112
**Figure 3.4**: Optical density readings for *P. gingivalis*, *F. nucleatum* and *T. denticola* .....114
**Figure 3.5**: Optical density readings plotted against CFU/ml for *P. gingivalis*, *F. nucleatum* and *T. denticola* .....115
**Figure 3.6**: Atmospheric oxygen exposure of *P. gingivalis* for 72 hours .....117
**Figure 3.7**: Atmospheric oxygen exposure of *F. nucleatum* for 72 hours. .....118
**Figure 3.8**: Atmospheric oxygen exposure of *T. denticola* for 72 hours. .....119
**Figure 3.9**: Gram stain images of live, heat and oxygen-killed *P. gingivalis* .....121

**Figure 3.10**: Gram stain images of live, heat and oxygen-killed *F. nucleatum*.....122
**Figure 3.11**: Gram stain images of live, heat and oxygen-killed *T. denticola*.....123
**Figure 3.12**: SEM images captured of live, heat and oxygen-killed *P. gingivalis*. .....125
**Figure 3.13**: SEM images captured of live, heat and oxygen-killed *F. nucleatum*. .....126
**Figure 3.14**: SEM images captured of live, heat and oxygen-killed *T. denticola* .....127
**Figure 3.15**: Comparison of the manual (haemocytometer) and automated (Tecan Spark®) methods for cell counting .....129
**Figure 3.16**: Well images showing cell confluence and % confluency values obtained using the Tecan Spark® multiplate reader. .....132
**Figure 3.17**: Growth curve and % cell viability of H400 cells over a 10-day period cultured in 2ml DMEM media supplemented with 10% FBS with media change every 2 days.....136
**Figure 3.18**: Growth curve and % cell viability of H400 cells over 8 days cultured in 2ml DMEM media supplemented with 10% FBS with no media change but addition of 1ml media every 2 days .....137
**Figure 3.19**: Growth curve and % cell viability of H400 cells over 8 days cultured in 5ml DMEM media supplemented with 10% FBS with no media change .....138
**Figure 3.20**: Light microscope images of H400 cells seeded at 10,000 cells in 5ml supplemented media with no media change .....139
**Figure 3.21**: Cell number and % cell viability of H400 cells grown in normoxic and hypoxic conditions over 8 days .....141
**Figure 3.22**: Light microscope images of H400 cells after 8-days growth in normoxia and hypoxia .....142

**Chapter 4**

**Figure 4.1**: Cell growth over 8-days challenge with heat or oxygen-killed *P. gingivalis*. ....158
**Figure 4.2**: Cell growth over 8-days challenge with heat or oxygen-killed *F. nucleatum* ....159
**Figure 4.3**: Cell growth over 8-days challenge with heat or oxygen-killed *T. denticola* .....160
**Figure 4.4**: Epithelial marker gene expression after heat-killed pathogen exposure.....164
**Figure 4.5**: Epithelial marker gene expression after oxygen-killed pathogen exposure.....165
**Figure 4.6**: Mesenchymal marker gene expression after heat-killed pathogen exposure.....168
**Figure 4.7**: Mesenchymal marker gene expression after oxygen-killed pathogen exposure.169
**Figure 4.8**: Transcription factor gene expression after heat-killed pathogen exposure.....172

**Figure 4.9**: Transcription factor gene expression after oxygen-killed pathogen exposure....173
**Figure 4.10**: Cytokine gene expression after heat-killed pathogen exposure.....176
**Figure 4.11**: Cytokine gene expression after oxygen-killed pathogen exposure.....177
**Figure 4.12**: IL-1β ELISA analysis after heat and oxygen-killed pathogen stimulation.....182
**Figure 4.13**: IL-8 ELISA analysis after heat and oxygen-killed pathogen stimulation.....185
**Figure 4.14**: TGF-β1 ELISA analysis after heat and oxygen-killed pathogen stimulation...188
**Figure 4.15**: IF for E-cadherin, Vimentin and Snail-1 after exposure to heat and oxygen killed pathogens .....192
**Figure 4.16**: DAPI, snail-1 and UBF-1 IF staining of H400 cells.....194
**Figure 4.17**: Determining optimum mitomycin C (MMC) concentration.....197
**Figure 4.18**: Cell migration over 24 hours of cultures after 8 days stimulation with heat-killed *P. gingivalis* and *F. nucleatum* .....199
**Figure 4.19**: H400 cell migration of cells stimulated with heat/oxygen-killed pathogens.....202
**Figure 4.20**: H400 cell migration of cells stimulated with heat/oxygen-killed *P. gingivalis* 203
**Figure 4.21**: H400 cell migration of cells stimulated with heat/oxygen-killed *F. nucleatum* .....204
**Figure 4.22**: H400 cell migration of cells stimulated with heat/oxygen-killed *T. denticola* .205
**Figure 4.23**: TEER readings of oral keratinocyte monolayers across 8-days with different initial cell seeding densities without or with changing media every 2 days. .....208
**Figure 4.24**: TEER readings after heat/oxygen-killed pathogen exposure.....209

**Chapter 5**

**Figure 5.1**: Effect of DMSO only (vehicle control) and increasing concentrations of curcumin dissolved in DMSO on H400 cell growth and % cell viability .....231
**Figure 5.2**: % cell viability of day-8 H400 cultures exposed to increasing concentrations of NaOH determined by Alamar blue assay. .....233
**Figure 5.3**: Effect of NaOH only (vehicle control) and increasing concentrations of curcumin dissolved in NaOH on H400 cell growth and % cell viability .....236
**Figure 5.4**: % cell viability of day-8 H400 cultures exposed to increasing concentrations of curcumin dissolved in NaOH determined by Alamar blue assay. .....237
**Figure 5.5**: Cell growth of oral keratinocytes incubated with oxygen-killed *T. denticola* and curcumin from day 4-8. .....239

**Figure 5.6**: H400 cell migration after oxygen-killed *P. gingivalis* and curcumin exposure..243
**Figure 5.7**: H400 cell migration after oxygen-killed *F. nucleatum* and curcumin exposure.245
**Figure 5.8**: H400 cell migration after oxygen-killed *T. denticola* and curcumin exposure...247
**Figure 5.9**: Epithelial marker gene expression with curcumin .....250
**Figure 5.10**: Mesenchymal marker gene expression with curcumin .....253
**Figure 5.11**: EMT-related transcription factor gene expression with curcumin.....256
**Figure 5.12**: Cytokine gene expression with curcumin .....259
**Figure 5.13**: TEER readings after oxygen-killed *T. denticola* and curcumin exposure .....262

**Chapter 6**

**Figure 6.1**: STRING visualization of identified *T. denticola* proteins. .....279
**Figure 6.2**: LC-MS/MS analysis of live vs heat-killed *T. denticola* proteins.....282
**Figure 6.3**: STRING visualization of lower abundance *T. denticola* proteins affected by heat-killing.....284
**Figure 6.4**: STRING visualization of higher abundance *T. denticola* proteins affected by heat-killing.....286
**Figure 6.5**: LC-MS/MS analysis of live vs oxygen-killed *T. denticola* proteins.....288
**Figure 6.6**: STRING visualization of higher abundance *T. denticola* proteins affected by oxygen-killing.....290

## LIST OF TABLES

### Chapter 1

**Table 1.1**: Molecular markers differentially expressed during EMT. .....19
**Table 1.2:** A summary of naturally derived compounds that inhibit EMT. .....44
**Table 1.3**: Synthesised compounds that can inhibit EMT .....45
**Table 1.4**: An overview of curcumins EMT inhibitory effects in different diseases.....50

### Chapter 2

**Table 2.1**: Primers and PCR conditions used to identify bacteria .....60
**Table 2.2**: List of reagents and volumes used in each well for qRT-PCR of target genes. .....77
**Table 2.3**: PCR conditions used at each stage to perform qRT-PCR for target genes. .....78
**Table 2.4**: Human genes and primer sequences used to perform qRT-PCR .....79
**Table 2.5**: Fluorochrome-conjugated antibodies provided in the R&D human EMT 3-colour immunocytochemistry kit used to stain for EMT markers E-cadherin, snail and vimentin. ....88
**Table 2.6**: Volumes of BSA and PBS needed to prepare standards for BCA assay.....98
**Table 2.7**: Volumes of diluent and digest assay standard needed to prepare peptide digest assay standards .....100
**Table 2.8**: TMTsixplex™ mass tagging reagents (labels) used to label live, heat-killed and oxygen-killed *T. denticola* proteins .....101

### Chapter 3

**Table 3.1**: Absorbance readings of *T. denticola* after exposure to atmospheric oxygen. .....120

### Chapter 4

**Table 4.1**: Summary of gene expression ratios of EMT related markers after exposure to heat and oxygen-killed pathogens .....178

### Chapter 5

**Table 5.1**: Summary of gene expression ratios of EMT related markers after oxygen-killed pathogen exposure with and without curcumin. .....260

## Chapter 6

**Table 6.1**: GO term analysis of *T. denticola* genes showing cellular component .....276
**Table 6.2**: GO term analysis of *T. denticola* genes showing biological processes.....276
**Table 6.3**: GO term analysis of *T. denticola* genes showing molecular function. .....277
**Table 6.4**: *T. denticola* genes involved in molecular pathways.....278
**Table 6.5**: Proteins decreased after heat-killing of *T. denticola* .....283
**Table 6.6**: Proteins increased after heat-killing of *T. denticola*.....285
**Table 6.7**: Proteins increased after oxygen-killing of *T. denticola*.....289

## Appendices

**Table 9.1**: Abundances of isolated *T. denticola* outer membrane proteins (live, heat and oxygen-killed) after performing quantitative mass spectrometry-based analysis using tandem mass tags (TMT™).....354

## LIST OF EQUATIONS

**Equation 2.1**: Equation used to calculate % cell viability after Alamar Blue staining .....95

# LIST OF ABBREVIATIONS

| | |
|---|---|
| ACN | Acetonitrile |
| AD | Alzheimer’s disease |
| Akt | Protein kinase B |
| ANOVA | Analysis of variance |
| ATCC | American type culture collection |
| BM | Basement membrane |
| BCA | Bicinchoninic acid protein assay |
| BSA | Bovine serum albumin |
| CagA | Cytotoxin-associated gene A |
| cDNA | Complimentary deoxyribonucleic acid |
| CFU | Colony forming unit |
| CLR | C-type lectin receptors |
| CVD | Cardiovascular disease |
| DMEM | Dulbecco’s modified Eagle’s medium |
| DMSO | Dimethyl sulfoxide |
| DNA | Deoxyribonucleic acid |
| Dnase I | Deoxyribonuclease I |
| *E . coli* | *Escherichia coli* |
| ECM | Extracellular matrix |
| eDNA | Extracellular deoxyribonucleic acid |
| EDTA | Ethylenediaminetetraacetic acid |
| EGF | Epidermal growth factor |

| | |
|---|---|
| ELISA | Enzyme-linked immunosorbent assay |
| EMT | Epithelial-mesenchymal transition |
| EndMT | Endothelial-mesenchymal transition |
| EPS | Extracellular polymeric substances |
| FBS | Foetal bovine serum |
| FITC | Fluorescein isothiocyanate |
| *F. nucleatum* | *Fusobacterium nucleatum* |
| FSP-1 | Fibroblast specific protein-1 |
| GAPDH | Glyceraldehyde-3-phosphate dehydrogenase |
| gDNA | Genomic deoxyribonucleic acid |
| HMDS | Hexamethyldisilazane |
| HGF | Human growth factor |
| HK | Heat-killed |
| IAA | Indole-3-acetic acid |
| IF | Immunofluorescence |
| IL | Interleukins |
| IκB-kinase | Inhibitor of NF-κB kinase |
| LC-MS/MS | Liquid chromatography tandem mass spectrometry |
| LEF-1 | Lymphoid enhancer-binding factor-1 |
| LOS | Lipooligosaccharide |
| LPS | Lipopolysaccharide |
| MAPK | Mitogen-associated protein kinase |
| MET | Mesenchymal-epithelial transition |

| | |
|---|---|
| MMC | Mitomycin C |
| MMP | Matrix metalloproteinases |
| mNOS | New oral spirochete medium |
| mTOR | Mammalian target of rapamycin |
| MUPP1 | Multi-PDZ domain protein 1 |
| NF-κB | Nuclear factor kappa-light-chain-enhancer of activated B cells |
| NLRs | Nucleotide-binding oligomerization domain-like receptors |
| OD | Optical density |
| OK | Oxygen-killed |
| OSCC | Oral squamous cell carcinoma |
| *P. aeruginosa* | *Pseudomonas aeruginosa* |
| PAMPs | Pathogen-associated molecular patterns |
| PAR | Partitioning defective protein |
| PBS | Phosphate buffered saline |
| PCR | Polymerase chain reaction |
| PDGF | Platelet-derived growth factor |
| *P. gingivalis* | *Porphyromonas gingivalis* |
| PI3K | Phosphatidylinositol 3-kinase protein kinase B (Akt) |
| PRRs | Pattern-recognition receptors |
| qRT-PCR | Quantitative real time polymerase chain reaction |
| RLRs | Retinoid acid-inducible gene I-like receptors |
| RNA | Ribonucleic acid |
| RTK | Receptor tyrosine kinase |

| | |
|---|---|
| sCD40L | Soluble cluster of differentiation 40 ligand |
| SEM | Scanning electron microscope |
| STAT3 | Signal transducer and activator of transcription 3 |
| sVCAM-1 | Soluble vascular cell adhesion molecule-1 |
| TCEP | Tris (2-carboxyethyly) phosphine |
| *T. denticola* | *Treponema denticola* |
| TEAB | Triethylammonium bicarbonate |
| TEER | Transepithelial electrical resistance |
| TFA | Trifluoroacetic acid |
| TGF-β | Transforming growth factor-β |
| TLRs | Toll-like receptors |
| TMT™ | Tandem mass tags |
| TNF-α | Tumour necrosis factor-α |
| TPP-VFA | Thiamine pyrophosphate–volatile fatty acid |
| TSB | Trypticase soy broth |
| UA | Urea |
| VFA | Volatile fatty acid |
| WHO | World health organisation |
| WIF-1 | Wnt inhibitory factor-1 (WIF-1) |
| ZEB | Zinc-finger E-box-binding |
| ZO | Zonula occludens |
| α-SMA | α-smooth muscle actin |

# 1. Introduction

## 1.1 General introduction

The research field of epithelial-mesenchymal transition (EMT) has grown considerably over the last 20 years with more than half of all articles being published in the past 5 years (Yang et al., 2020). EMT is a cellular process by which epithelial cells lose some epithelial features and present some mesenchymal-like characteristics, which lead to functional changes (Chen et al., 2017c). EMT has been implicated in a wide array of physiological (section 1.3.4.1) and pathological conditions (section 1.3.1) and it is driven by several distinct molecular processes orchestrated by a conserved set of inducing signals, transcriptional regulators and downstream effectors. EMT is typically categorised into three subtypes, types 1, 2 and 3, according to the functional and physiological outcomes and the context of tissue involved (Kalluri and Weinberg, 2009).

Periodontitis is a severe form of periodontal disease that is characterised by gingival tissue loss, deterioration of periodontal ligament and alveolar bone loss in susceptible patients and if not appropriately managed can ultimately result in tooth loss. It is the result of a persistent non-resolving and excessive immunoinflammatory response to pathogenic bacteria that have accumulated on the tooth and in the subgingival crevice (Preshaw, 2015). Predominance of Gram-negative anaerobic bacteria, such as *Porphyromonas gingivalis* and *Fusobacterium nucleatum* which are commonly detected in sub-gingival pockets (Baelum and López, 2013) can trigger host responses leading to the release of pro-inflammatory cytokines, some of which have been linked with inducing EMT (Abdulkareem et al., 2017). The resulting EMT response could compromise epithelial barrier integrity possibly facilitating the initiation and propagation of periodontitis. The role of other key periodontal pathogens (*Treponema denticola*) to induce EMT and potentially predispose a patient to periodontitis is yet to be

elucidated. In addition, naturally occurring EMT inhibitors such as curcumin and its potential in inhibiting pathogen induced EMT for the management of periodontitis remains to be understood.

### 1.2 Epithelium

Epithelium forms a major component of the human body and has a primary function in providing a physical barrier protecting the host against physical, chemical and biological environmental challenges. In addition, it plays vital roles in secretion, absorption and transportation of macromolecules to allow for efficient functioning of tissue (Biga et al., 2020). Furthermore, epithelium exposure to bacterial stimulus can elicit pro-inflammatory responses including recruitment of cytokines that are also implicated in inducing EMT (Kinane et al., 2008). The epithelium is composed of tightly packed continuous epithelial cells, either in monolayer or forming stratification. Epithelial cells are derived from three major embryonic layers including the ectoderm, endoderm and mesoderm, with the epithelia lining parts of the oral cavity developing from the ectoderm (Koller and Sapra, 2021). Epithelial cells are linked intercellularly by cell junctions and integrity of these junctions maintains the epithelial barrier. These cell junctions include tight, gap and adherens junctions and desmosomes (Figure 1.1), which allow varying levels of interaction between cells (Biga et al., 2020). Epithelial cells at the interface with the surrounding connective tissue attach to the basement membrane (BM) through interactions between laminin and integrin receptors (Belkin and Stepp, 2000).

Epithelium can be composed of different cell morphologies and varying number of layers allowing for classification of the tissue depending on these two characteristics. The epithelial

cell shapes include squamous, cuboidal and columnar. A single cell layer is known as a simple epithelium whereas organisation into multiple layers is known as stratified epithelium with pseudostratified epithelium being composed of a single layer of irregular shaped cells (Biga et al., 2020), giving the appearance of multiple layers while all reaching the BM. In addition, epithelial cells have apical-basal polarity due to the composition of different phospholipids and protein complexes (Wu and Mlodzik, 2009). Apical-basal polarity is regulated by three main polarity complexes, the partitioning defective protein (PAR) complex, Crumbs and Scribble complexes and loss of epithelial cell polarity is implicated in initial stages of EMT (Jung et al., 2019).

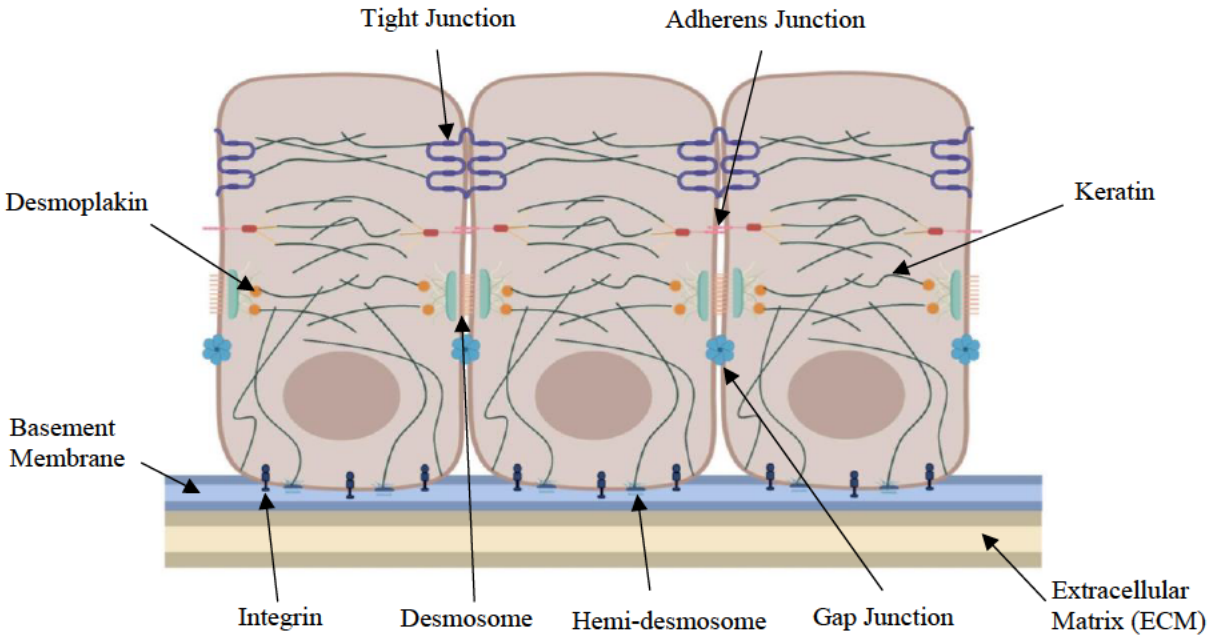



**Figure 1.1:** Diagram of keratinised epithelial cells connected by junctions including: tight junctions, adherens junctions, desmosomes and gap junctions. Desmoplakin link desmosomes to keratin and epithelial cells are connected to basement membrane via integrins and hemi-desmosomes (created with Biorender.com).

### 1.2.1 Gingival epithelium

The gingival epithelium is subdivided into three sections including: oral/outer epithelium, sulcular epithelium and junctional epithelium which are composed of stratified and squamous tissue (Tribble and Lamont, 2010). The oral/outer epithelium covers the external surface of the gingiva whilst the sulcular epithelium is located on the gingival sulcus and extends from the coronal limit of the junctional epithelium to the crest of the gingival margin (Carranza et al., 2006). The junctional epithelium maintains a direct attachment to the tooth and is located at the junction of periodontal hard and soft tissue (Jiang et al., 2014). The oral epithelium is composed of stratified squamous epithelium and is keratinised to varying levels in different regions of the oral cavity (Presland and Dale, 2000). The sulcular and junctional epithelium are non-keratinized whereas the oral/outer epithelium is keratinized (Berkovitz, Holland and Moxham, 2009). Keratins provide a scaffold in epithelial cells protecting against mechanical stress and maintain structural integrity which is an important requirement of the gingival epithelium (Schroeder and Listgarten, 1997).

Epithelial cells from this anatomical region share common characteristics with epithelium at other body sites, including protecting the underlying tissues from bacterial invasion. It was previously understood that epithelium only acted as an inert barrier, but research now indicates that it can respond to bacterial challenge by initiating an inflammatory response and release defence related molecules (Milward et al., 2007). The crevicular epithelium is closely associated with the plaque biofilm that develops on the root surface. The nature of the interaction between the plaque biofilm and crevicular epithelium can lead to an excessive inflammatory response and periodontitis in susceptible individuals (Tribble and Lamont, 2010).

### 1.2.2 Gingival connective tissue

Underlying the gingival epithelium is gingival connective tissue and collectively is known as gingiva (Cho et al., 2021). Gingival connective tissue is commonly referred as the lamina propria and is subdivided into two layers, papillary and reticular layer (Dawson et al., 2013). The papillary layer which is immediately beneath the epithelium is formed by irregular oriented thin collagen fibres that connect with the epithelium through undulating papillae ridges (Chen et al., 2015). The deeper reticular layer is formed by thicker collagen fibres and is located between the papillary layer and the underlying submucosa or periosteum (Brizuela and Winters, 2022). These thicker fibres which are perpendicularly connected to the periosteum are called mucoperiosteum and they can resist compression and shear to the oral mucosa via strong connections to the bone (Fleisch and Austin, 1978). Collagen and elastin are the two main fibres found in the connective tissue with type I and III collagen being the predominant ones (Tayebi and Moharamzadeh, 2018).

The gingival connective tissue is composed of cells including fibroblasts, mast cells, immune cells (macrophages, neutrophils and lymphocytes) and extracellular matrix (ECM) components consisting of collagen fibres, vessels and nerves (Gehrig, Shin and Willmann, 2020). In contrast to the gingival epithelium which has an abundance of cells and sparse extracellular matrix (ECM), the gingival connective has an abundance of ECM and few cells (compromising about 5% of the gingival connective tissue) (Gehrig, Shin and Willmann, 2020). The gingival connective tissue primarily functions to provide solidity to the gingiva through a dense network of collagen fibres which secure and hold the connective tissues together (Bartold, 1991).

### 1.2.3 Gingival inflammation

The well-known four stages of periodontal disease first explained by Page and Schroeder (1976) include the initial, early, established and advanced lesion with the advanced lesion indicating periodontitis (Page and Schroeder, 1976). The accumulation of bacteria at the dento-gingival margin leads to a host response where an inflammatory cell infiltrate is produced in the tissue (Page and Schroeder, 1976). Host responses to bacterial biofilm trigger epithelium cells to produce cytokines and chemokines resulting in neutrophil migration to the site of inflammation, followed by clearance of cellular debris by monocytes and macrophages and this is known as the initial lesion (Cekici, Kantarci, Hasturk and Van Dyke, 2013). The early lesion is where clinical signs of gingivitis are noticed such as redness and bleeding from the gingiva. It is defined by an increased number of neutrophils and leukocytes in addition to loss of collagen which can reach up to 70% in the affected area (Schroeder, Münzel-Pedrazzoli and Page, 1973). Proteolytic enzymes released by neutrophils can disrupt the epithelial barrier leading to deeper penetration by pathogens into the lamina propria resulting in further inflammation (Bosshardt and Lang, 2005). The following stage is the established lesion where the innate immune response transitions to the adaptive response and macrophages, plasma cells and T and B lymphocytes dominate. Collagenolytic activity is also increased and a gingival pocket develops (Cekici, Kantarci, Hasturk and Van Dyke, 2013). Degradation of connective tissue ECM occurs through activation of MMPs, release of reactive oxygen species and phagocytosis (Bartold and Narayanan, 2006). The advanced lesion is the transition to periodontitis where plasma cells continue to predominate and irreversible attachment loss and bone loss are observed (Page and Schroeder, 1976), with the inflammatory lesion extending deeper and affecting the alveolar bone (Carranza et al., 2006).

## 1.3 Epithelial-mesenchymal transition

### 1.3.1 Overview of EMT

EMT is the process by which epithelial cells obtain mesenchymal-like characteristics through the loss of cell polarity, cell-cell adhesion and gain migratory and invasive properties (Chen et al., 2017c). EMT has been implicated in several disease processes including fibrosis in the liver (Zeisberg et al., 2007b), lung (Kim et al., 2006), heart (Zeisberg et al., 2007a) and kidney (Fragiadaki and Mason, 2011), tumour metastasis (Davis et al., 2014) and Crohn's disease (Jiang, Shen and Ran, 2017). The concept of epithelial cells acquiring some mesenchymal characteristics whilst simultaneously losing some epithelial characteristics was first observed by Elizabeth Hay in the late 1960s' (Hay, 1968). Hays' study involved the chick primitive streak, a first sign of gastrulation and structure formed early in avian, reptile and mammalian development. It was proposed that epithelial cells can undergo phenotypic changes that are characteristic of mesenchymal cells and considered degradation of the BM, during mesoderm formation in the chick embryo, as one of the key features of EMT. After this initial observation, others investigated this further using 3D collagen gel models, where it was shown the ability of epithelial cells to lose polarity and gain more mesenchymal-like characteristics (Greenburg, 1982). In the intervening years there have been many studies proposing EMT in the pathogenesis of several processes including cancer progression (Wei et al., 2015), inflammation (Correa-Costa et al., 2014) and embryogenesis (Yoshino et al., 2014). It is now understood that a plethora of molecular processes are involved in EMT including activation of transcription factors, regulation of cell surface and extracellular proteins, cytoskeletal reorganisation and up-regulation of extracellular matrix (ECM) - degrading enzymes (Kalluri and Weinberg, 2009).

### 1.3.2 Molecular events in EMT

Although the exact molecular events occurring during EMT are dependent on tissue type and the physiological context, there are similarities which include initial changes associated with disassembly of epithelial cell-cell contacts, loss of apical-basal polarity, suppression of epithelial genes and activation of mesenchymal genes. As EMT progresses, cells lose apical-basal polarity and reorganise the cytoskeleton resulting in changes from a cuboidal epithelial structure into an elongated mesenchymal shape (Nelson et al., 2008) (Figure 1.2). However, it should be noted that Nelson et al. (2008) study was on mammary epithelial cells and that not all epithelial cells are cuboidal. Furthermore, these EMT-associated changes include formation of lamellipodia, filopodia and invadopodia which enable cells to migrate and invade (explained further in section 1.3.2.2). This is accompanied with increased expression of MMPs which degrade ECM proteins and facilitate cell migration and invasiveness. Transcription factors such as snail-1, snail-2, twist, lymphoid enhancer-binding factor-1 (LEF-1), zinc-finger E-box-binding (ZEB)-1 and ZEB-2 (see Table 1.1) can induce these changes through activation or suppression of downstream target genes. These transcription factors are ultimately regulated by pathways involved in EMT such as TGF-β (Xu, Lamouille and Derynck, 2009), Wnt/β-catenin (Mylavarapu et al., 2019) receptor tyrosine kinase (RTK) (Shetty et al., 2020) and notch signalling (Wang et al., 2010).

#### 1.3.2.1 Loss of epithelial cell-cell contacts

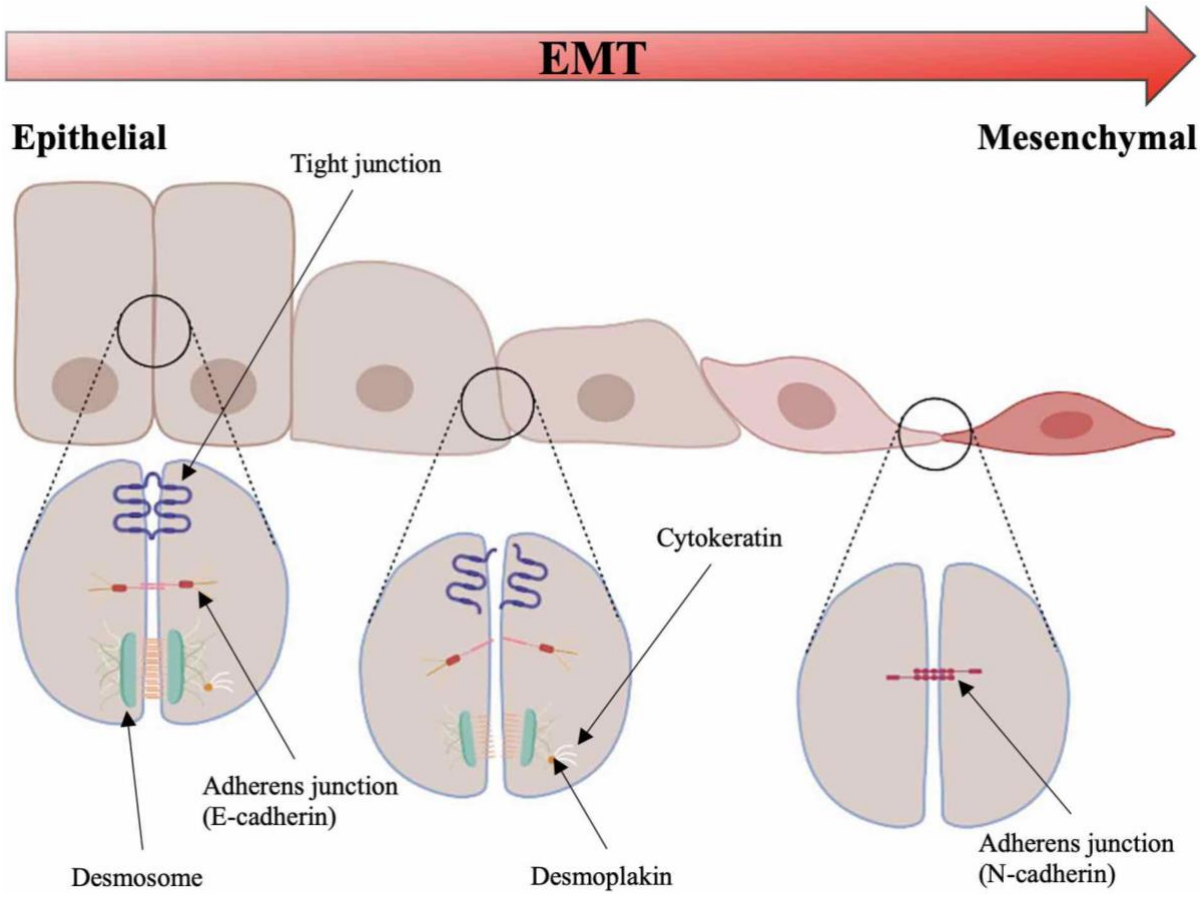
Epithelial cells are linked by cell junctions including tight junctions, gap junctions, adherens junctions, gap junctions and desmosomes. In adherens junctions, epithelial cadherin (E-cadherin), is a protein that facilitates adhesion between epithelial cells. It is often cited that loss of this key epithelial cell marker is suggestive of EMT induction (Hay, 1995) and can

lead to increased cell migration and invasion as seen in EMT (Vleminckx et al., 1991). The replacement of E-cadherin by N-cadherin, which is commonly referred to as the 'hallmark' of EMT, causes modification of the adherens junction and is known as the 'cadherin switch' (Prieto-García et al., 2017; Cavallaro, Schaffhauser and Christofori, 2002) (Figure 1.2). The suppression of E-cadherin is the result of activated EMT-related transcription factors including snail-1, snail-2 (slug) (Cano et al., 2000), ZEB-1, ZEB-2 (Peinado, Olmeda and Cano, 2007) and Twist (Lo et al., 2007) with snail being the most recognised suppressor of E-cadherin expression (Zeisberg and Neilson, 2009). The cytoplasmic domains of E-cadherin bind tightly to β-catenin which is a cytoplasmic protein that interacts with α-catenin. The actin cytoskeleton binds to α-catenin and this interaction enhances adhesion between cells through greater stability of the adhesion complexes (Xu, Lamouille and Derynck, 2009). During EMT, E-cadherin is degraded and disassembled leading to weakened cell-cell adhesion (Lamouille, Xu and Derynck, 2014). In addition, disassembled E-cadherin means that β-catenin can no longer interact with E-cadherin, therefore further weakening cell-cell adhesion. The loss of E-cadherin initiates a sequence of signalling events and major cytoskeletal reorganisation associated with EMT (Xu, Lamouille and Derynck, 2009).

Desmosomes are intercellular junctions that join adjacent epithelial cells and provide strong adhesion between cells due to intracellular binding to the cytoskeletal intermediate filament, keratin (Garrod and Chidgey, 2008). Desmosomes are composed of five main proteins including desmoglein, desmocollin, plakoglobin, plakophilin and desmoplakin (McHarg et al., 2014). Desmosomes are connected to keratin, through desmoplakin and cells that have undergone EMT experience a loss of desmosomal proteins such as desmoplakin (Serrano-

Gomez, Maziveyi and Alahari, 2016) (Figure 1.2). This results in breakdown of epithelial cell-cell adhesion and integrity of the epithelial barrier (Lamouille, Xu and Derynck, 2014).

Tight junctions are the most apical of the cell junctions and form the closest cell-cell interactions (Samiei et al., 2019). These junctions are composed of integral and peripheral membrane proteins and some of these integral proteins include claudins, occludin, tricellulin, marvelD3 and junctional adhesion molecules. Some of the peripheral membrane proteins include the multi-PDZ domain protein 1 (MUPP1) and zonula occludens (ZO)-1, ZO-2 and ZO-3 (Kyuno et al., 2014). Peripheral proteins can attach to actin filaments, thus contributing to the strength and integrity of tight junctions (Samiei et al., 2019). During the early stages of EMT, tight junctions are disassembled resulting in the redistribution of ZO proteins, claudins and occludin (Xu, Lamouille and Derynck, 2009). Claudins are major components of tight junctions and form an integral part of the epithelial barrier and transportation system (Markov, Aschenbach and Amasheh, 2015). Disassembly of tight junctional proteins leads to weakening of the epithelial barrier and loss of cell adhesion leading to increased migratory ability (Kyuno et al., 2014). An example of an epithelial cell undergoing EMT and the effects on cell junctions are shown in Figure 1.2.




**Epithelial**

- Cell junctions such as tight junctions, adherens junction (E-cadherin) and desmosomes
- Apical-basal polarity
- Limited migration potential

**Mesenchymal**

- Tight junctions and desmosome disassociation
- Replacement of E-cadherin with N-cadherin
- Front-back polarity
- Migratory potential
- Spindle-like shape

**Figure 1.2**: Diagram of an epithelial cell undergoing epithelial-mesenchymal transition and the effects on cell junctions including the 'cadherin switch', where the adherens junction E-cadherin is replaced with N-cadherin which is known as the hallmark of EMT (created with Biorender.com).

### 1.3.2.2 Cytoskeletal changes and acquisition of migratory properties

The cytoskeletal intermediate filaments in epithelial cells are composed of cytokeratins and the replacement of these filaments with vimentin (Figure 1.3) is associated with EMT (Liu et al., 2015). Keratin has also been shown to direct E-cadherin to the membrane whilst vimentin does not and thus promotes lack of cell-cell adhesion and cell motility (Toivola et al., 2005). The transcription factor snail-1 has been implicated in down-regulating cytokeratin expression (Guaita et al., 2002) and up-regulating vimentin expression (Cano et al., 2000) and this results in reorganisation of the cortical actin cytoskeleton. This is associated with formation of actin-rich membrane protrusions such as lamellipodia, filopodia, blebs and invadopodia (Ridley, 2011). These protrusions are formed at the leading edge of the cell and are uniquely responsible for cell movement. Lamellipodia form thin sheet like protrusions which can extend relatively long distances through the ECM *in vivo* allowing cells to pull through the tissue (Friedl and Gilmour, 2009). Whereas filopodia are distinguished by thin finger-like protrusions that extend from the leading edge of the cell and play key role in exploring the cells surroundings (Gupton and Gertler, 2007). Invadopodia are long and slender structures that have the capacity to degrade ECM components through secretion of proteases such as MMPs. This facilitates cell invasion into tissue, particularly when cells cross the BM (Buccione, Caldieri and Ayala, 2009).

Another characteristic change during EMT is the formation of actin stress fibres (Figure 1.3) which increases cell contractility and facilitates movement (Yeung and Yang, 2016). This formation is mediated by proteins such as moesin (Haynes et al., 2011) and the small guanosine triphosphatase (GTPase), RhoA (Girouard et al., 2016). The induction of EMT by TGF-β requires the activation of RhoA to form actin stress fibres and RhoA can also interrupt

localisation of E-cadherin ultimately attenuating cell adhesion (Bhowmick et al., 2001). Rho GTPases are also involved in lamellipodia and filopodia formation. The Rho GTPases ras-related C3 botulinum toxin substrate 1 (RAC1) is involved in lamellipodia formation (Wu et al., 2009), whilst cell division cycle 42 (CDC42) induces filopodia formation through reassembly of its targets which contributes to filopodium initiation and extension (Ahmed, Goh and Bu, 2010).

#### 1.3.2.3 ECM changes

ECM provides structural support and information to epithelial cells within tissues and integrins are responsible for linking the ECM to the cytoskeleton of cells and communicating biochemical information (Cichon and Radisky, 2014). During EMT, the ECM is remodelled and this requires changes in the composition of integrins. One of the epithelial integrins that is down-regulated during EMT is α6β4 which is phosphorylated and released from hemi-desmosomes (Rabinovitz, Toker and Mercurio, 1999). α6β4 is required for the formation of hemi-desmosomes which link cytokeratin to the BM and are essential for maintaining integrity of the epithelial monolayer (Borradori and Sonnenberg, 1999). A specific group of integrins including α5β1, αvβ5 and αvβ6 have been associated with migration and proliferation (Sheppard, 1996). In addition, these integrins have also been shown to be up-regulated in keratinocytes during wound healing (Zambruno et al., 1995). Fibronectin is another ECM protein that is also over-expressed in cells during EMT (Lee et al., 2006) and which facilitates cell migration (Park and Schwarzbauer, 2013). It has been observed that over-expression of integrin α5β1 increases adhesion to fibronectin, therefore assisting cell motility (Maschler et al., 2005; Mise et al., 2012).

The change in integrin expression during EMT is accompanied by the increased expression of MMPs (Figure 1.3) which aids protein degradation and remodelling of the ECM to assist cell migration and invasion (Nistico, Bissell and Radisky, 2012; Scheau et al., 2019). MMPs are proteolytic enzymes consisting of 23 human family members (Nagase, Visse and Murphy, 2006) that degrade ECM components (Makela et al., 1994). Of these 23, MMP-2 and MMP-9 contain specialized, fibronectin-like gelatin binding domains which can bind and degrade type IV collagen (Gilles et al., 2000). Type IV collagen is the main collagen component of the BM and breakdown of this by increased MMP-9 production facilitates the migration and invasion of cells as is seen in EMT. In addition, some MMPs such as MMP-3 (Lochter et al., 1997) and MMP-7 (Lynch et al., 2010) can also cleave and breakdown E-cadherin resulting in loss of cell adhesion thus promoting cell migration.

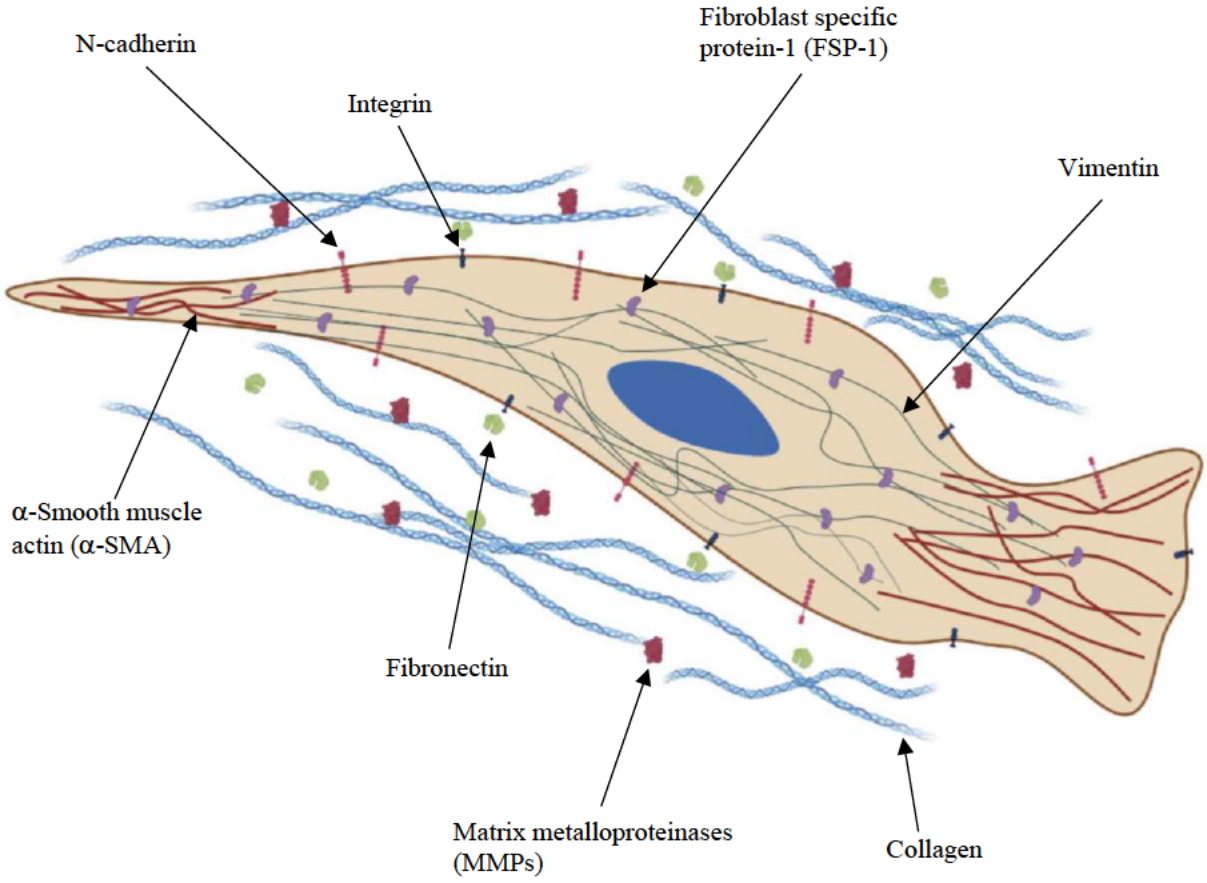



**Figure 1.3**: Illustration of a fibroblastic cell within the ECM expressing markers associated with a mesenchymal phenotype such as N-cadherin, vimentin, α-smooth muscle actin (α-SMA) and fibroblast specific protein-1 (FSP-1). ECM degrading proteolytic enzymes, matrix metalloproteinases (MMPs), which are secreted from the cell can facilitate cell migration and invasion into the basement membrane (created with Biorender.com).

### 1.3.3 Biomarkers of EMT

The induction of EMT involves an array of processes which leads to changes in expression of transcription factors, cell-cell adhesion, cell-BM and cytoskeletal molecules. These changes are associated with several markers and the induction of EMT is defined by the up or down-regulation of these biomarkers (Table 1.1) (Zeisberg and Neilson, 2009).

**Table 1.1**: Molecular markers differentially expressed during the EMT process highlighting the plethora of cell surface, cytoskeletal and ECM changes along with increased activity of transcriptional factors and proteolytic enzymes.

| Type of marker | Biomarker | EMT related change | Reference |
|---|---|---|---|
| **Cell surface** | E-cadherin | Downregulated | (Huber, Kraut and Beug, 2005) |
| | Claudins/Occludins | Downregulated | (Ikenouchi et al., 2003) |
| | Desmoplakin | Downregulated | (Serrano-Gomez, Maziveyi and Alahari, 2016) |
| | ZO-1 | Downregulated | (Huang, Guilford and Thiery, 2012) |
| | N-cadherin | Upregulated | (Zhang et al., 2013) |
| **Cytoskeletal** | β-catenin | Downregulated | (Tian et al., 2011) |
| | Cytokeratin | Downregulated | (Savagner, 2010) |
| | Fibroblast-specific protein 1 (FSP-1) | Upregulated | (Osterreicher et al., 2010) |
| | Vimentin | Upregulated | (Liu et al., 2015) |
| | α-Smooth Muscle actin (α-SMA) | Upregulated | (Ohbayashi et al., 2014) |
| **Extracellular proteins** | Fibronectin | Upregulated | (Li et al., 2017a) |
| | Laminin | Downregulated | (Scanlon et al., 2012) |
| | α1 collagen | Upregulated | (Medici and Nawshad, 2010) |
| | α3 collagen | Upregulated | (Zeisberg and Neilson, 2009) |
| **Cell-basement membrane attachment proteins** | α6β4 | Downregulated | (Rabinovitz, Toker and Mercurio, 1999) |
| | αVβ3 | Upregulated | (Shah, Fong and Kakar, 2011) |
| | αVβ5 | Upregulated | (Ricono et al., 2009) |
| | αVβ6 | Upregulated | (Lamouille et al., 2014) |
| | α5β1 | Upregulated | (Renner et al., 2016) |
| **Transcriptional factors** | Snail1 | Upregulated | (Kaufhold and Bonavida, 2014) |
| | Snail2 (Slug) | Upregulated | (Mathsyaraja and Ostrowski, 2012) |
| | Twist | Upregulated | (Wang et al., 2016) |
| | LEF-1 | Upregulated | (Sun et al., 2017) |
| | ZEB1 | Upregulated | (Zhang, Sun and Ma, 2015) |
| | ZEB2 | Upregulated | (DaSilva-Arnold et al., 2018) |
| | NF-κB | Upregulated | (Julien et al., 2007) |
| **Proteolytic enzymes** | MMP-2 | Upregulated | (Li and Luo, 2019) |
| | MMP-3 | Upregulated | (Si-Tayeb et al., 2006) |
| | MMP-7 | Upregulated | (Lin et al., 2017) |
| | MMP-9 | Upregulated | (Bai et al., 2017) |

### 1.3.4 Types of EMT

The process by which epithelial cells transition to mesenchymal cells follows a conserved programme and shares common characteristics. However, dependent on cell type, signals that activate EMT and tissue context, EMT mechanisms can vary ultimately resulting in different functional and physiological outcomes. EMT is classified into three different subtypes (types 1, 2 and 3) and these are detailed below (Kalluri and Weinberg, 2009).

#### 1.3.4.1 Type 1 EMT

Type 1 EMT occurs in implantation, embryogenesis and organ development. Mesenchymal cells generated via type 1 EMT have the capacity to undergo mesenchymal-epithelial transition (MET) generating secondary epithelia, which can then again undergo EMT (Kalluri and Weinberg, 2009). This type of EMT is associated with embryo implantation and early stages of placenta formation. More specifically the trophectoderm layer of the incoming embryo undergoes changes via EMT to produce invasive trophoblastic cells prior to coming into contact and adhering with maternal luminal epithelial cells of the endometrium. These cells lose polarity (Aplin and Ruane, 2017) and experience down-regulation of E-cadherin and increased motility and protrusive ability (Owusu-Akyaw et al., 2018). These initial events facilitate invasion and eventual formation of the placenta. In addition, the maternal endometrial epithelium also undergoes EMT which aids embryo implantation. MicroRNAs (miRNAs), which regulate post-transcriptional gene expression through RNA silencing are implicated in promoting EMT in endometrium epithelium during the receptive stage (Owusu-Akyaw et al., 2018). The miR-429 has displayed down-regulated expression which led to an increase in mesenchymal markers, whilst enhanced expression of miR-429 resulted in decreased migratory and invasive properties (Li et al., 2015). Gastrulation during

embryogenesis is the process by which three germ layers are produced via initial formation of the primitive streak. The primitive streak then forms the mesendoderm which eventually separates to give rise to the mesoderm and endoderm via EMT (Hay, 1995). In addition, EMT also occurs in neuroectodermal cells to form migratory neural crest cells during embryogenesis (Duband and Thiery, 1982). These cells gain migratory properties allowing movement to different parts of the embryo and have been shown to express genes such as snail (Sauka-Spengler and Bronner-Fraser, 2008) and slug (Knecht and Bronner-Fraser, 2002), which are key EMT-related transcription factors. Canonical Wnt signalling is fundamental in controlling EMT associated with gastrulation during embryogenesis (Skromne and Stern, 2001).

#### 1.3.4.2 Type 2 EMT

The second type of EMT is related with tissue regeneration and organ fibrosis. Fibrosis is an exaggerated wound healing process resulting in excessive overgrowth and/or scarring of tissue which affects normal functioning of organs (Wynn, 2008). The deposition of ECM components such as collagen contributes to this overgrowth. Chronic inflammatory responses provoked by repeated injury, autoimmune reactions and persistent infection can lead to the induction of fibrosis (Wynn and Ramalingam, 2012). ECM-producing myofibroblasts are a common feature of fibrosis and are implicated in all types of fibrotic diseases. These cells are generated from mesenchymal cells or epithelial and endothelial cells via an epithelial/endothelial-mesenchymal transition (EMT/EndMT). It has been shown that EMT induction by macrophage-derived TGF-β1 can promote differentiation of epithelial cells into myofibroblasts (Wynn, 2008). In addition, pro-inflammatory cytokines such as IL-1β can induce EMT leading to activation of myofibroblasts through a TGF-β1-mediated mechanism

(Fan et al., 2001). Reliable markers for differentiating between mesenchymal cells and epithelial cells generated after EMT during fibrosis include fibroblast-specific protein 1 (FSP-1) (Strutz et al., 1995), α-Smooth muscle actin (α-SMA) (Hinz, 2021) and collagen I (Duffield, 2014). In addition, markers such as vimentin, desmin and discoidin domain receptor (DDR2) have proved invaluable in detecting EMT prior to fibrotic events (Kalluri and Weinberg, 2009).

#### 1.3.4.3 Type 3 EMT

Type 3 EMT is associated with cancer progression and metastasis. Epithelial tumour cells gain migratory and invasive properties via EMT and eventually leave a primary tumour nodule via blood circulation to form secondary tumours at distant sites. Interestingly, newly formed secondary tumours exhibit epithelial properties resulting in these cells undergoing MET as observed in type 1 EMT during embryogenesis (see section 1.3.4.1) (Kalluri, 2009). As with type 2 EMT, FSP-1 is also used as a marker for type 3 EMT (Xue et al., 2003). Other specific markers such as β6 integrin have been used and detected at relatively high levels in colon cancer cells that have undergone type 3 EMT, whereas epithelial cells that have not undergone type 3 EMT expressed low levels of this integrin (Bates et al., 2005). Vimentin is also a regularly used marker to distinguish epithelial cells that are undergoing type 3 in cancers (Boyer et al., 1989 and Yang et al., 2004). Also, EMT transcription factor twist-1 was implicated in developing metastatic cancer cells via type 3 EMT and twist-1 can in turn up-regulate expression of mesenchymal markers N-cadherin and fibronectin (Yang et al., 2004). This type of EMT is induced by signals originating from the tumour including human growth factor (HGF) (Smith and Bhowmick, 2016), epidermal growth factor (EGF) (Kim et al., 2016), platelet-derived growth factor (PDGF) (Wu et al., 2013) and TGF-β (Hao, Baker and

ten Dijke, 2019). Overall, the primary roles of type 3 EMT are to prepare epithelial tumour cells for migration, invasion and metastasis, whilst type 2 EMT focusses on generating myofibroblasts for tissue repair (Xue et al., 2003).

### 1.3.5 EMT-inducing pro-inflammatory cytokines in periodontitis

Periodontal pathogens can initiate host pro-inflammatory cytokine release leading to migration of leucocytes such as neutrophils and macrophages. Activated leucocytes can initiate further production of pro-inflammatory cytokines resulting in a chronic cycle of migration and persistent inflammatory response as is observed in patients with periodontitis (Garlet, 2010). The pro-inflammatory cytokines IL-1β (Aleksandrowicz et al., 2021), IL-8 (Lagdive et al., 2013) and TGF-β1 (Gürkan et al., 2006) have been commonly detected as being upregulated in patients with periodontitis. In addition, IL-1β (Li et al., 2020), IL-8 (Zhao et al., 2017) and TGF-β1 (Kasai et al., 2005) have been associated with inducing EMT in previous investigations.

#### 1.3.5.1 IL-1β

The IL-1 family of cytokines consists of 11 members which are linked with damaging inflammation more so than other cytokine families. Of these, IL-1α and IL-1β can bind to the IL-1R1 receptor. This leads to structural changes to IL-1R1 allowing the co-receptor IL-1R3 to bind forming a trimeric complex, which results in a cascade of kinases being produced that can induce pro-inflammatory signals (Dinarello, 2017). The potent pro-inflammatory cytokine, IL-1β, is the most well characterised and studied cytokine of the IL-1 family (Lopez-Castejon and Brough, 2011). It has been implicated in inducing EMT in several studies. One study has shown IL-1β to down-regulate expression of several epithelial markers

including E-cadherin, gamma-catenin and cytokeratin 18. In addition, mesenchymal markers such as vimentin, N-cadherin, smooth muscle actin (SMA) and fibronectin were simultaneously up-regulated in lung cancer cells after IL-1β exposure. Furthermore, key EMT transcription factors, snail-2 and ZEB-1 were both up-regulated after IL-1β exposure (Li et al., 2020). In addition, IL-1β can induce α-SMA expression and fibronectin production in human proximal tubule cells (Vesey et al., 2002). Also, IL-1β has been shown to increase invasiveness of oral squamous cell carcinoma (OSCC) cells through downregulation of E-cadherin, upregulation of snail-1, snail-2, vimentin and cause alterations in morphology associated with the mesenchymal phenotype (Lee et al., 2014).

#### 1.3.5.2 IL-8

IL-8 is a pro-inflammatory cytokine that belongs to the CXC chemokine family. It is a relatively small protein that can act as a chemoattractant for neutrophils, basophils and T cells (Jiang et al., 2011). IL-8 binds to IL-8 receptors which consists of two heterotrimeric G protein-coupled receptors, CXCR1 and CXCR2 (Long et al., 2015). Once bound, IL-8 can induce angiogenesis (Végran et al., 2011) and promote progression of cancers including ovarian cancer (Shahzad et al., 2018), prostate cancer (Araki et al., 2007), melanoma (Rofstad and Halsør, 2000), non-small cell lung carcinoma (Millar et al., 2008) and has been shown to induce EMT in several studies. In one of these studies IL-8 induced invasion, increased expression of fibronectin and down-regulated expression of E-cadherin in human carcinoma cells (Fernando et al., 2011). In addition, IL-8 could also promote human ovarian cancer cell migration possibly enhancing ovarian cancer cell metastasis (Yin et al., 2014). It was also observed in this study that expression of E-cadherin was decreased whilst β-catenin was increased. IL-8 could also up-regulate the activity of MMP-2 in human melanoma cells

enhancing invasion of host stroma by tumour cell and facilitating metastasis (Luca et al., 1997). In another study, IL-8 has been shown to regulate migration/invasion of oral cancer cell lines and promote EMT by down-regulating E-cadherin and up-regulating vimentin via signal transducer and activator of transcription 3 (STAT3) signalling pathway (Hsu et al., 2021).

#### 1.3.5.3 TGF-β1

TGF-β1 binds to TGF-β type I and type II receptors which in turn initiates the TGF-β signalling pathway (Hao, Baker and ten Dijke, 2019), which is the most common pathway through which EMT is induced (Avila-Carrasco et al., 2019). This leads to activation of targets genes including the snail, ZEB and basic helix-loop-helix (bHLH) family of transcription factors which are responsible for regulating EMT related genes such as snail-1, snail-2 and twist-1 (Xu, Lamouille and Derynck, 2009). A previous study has shown that TGF-β1 treatment of cholangiocarcinoma cell lines could activate cell migration, invasion and induce fibroblastic morphological changes. Exposed cells also demonstrated a switch in cadherin expression where E-cadherin was down-regulated and N-cadherin was up-regulated (Araki et al., 2011). TGF-β1 has also been associated with inducing expression of the EMT transcription factor, snail-1 in epithelial cell lines (Peinado, Quintanilla and Cano, 2003) and twist-1 in prostate cancer cells (Cho et al., 2013). In another study, TGF-β1 induced EMT in alveolar epithelial cells in a time and concentration dependent manner. EMT changes were identified by morphological alterations consistent with a fibroblastic phenotype and up-regulated expression of vimentin accompanied with E-cadherin down-regulation (Kasai et al., 2005). Furthermore, TGF-β1 treatment of OSCC cells could also increase expression of twist-

1 and N-cadherin, whilst simultaneously down-regulating E-cadherin expression (Quan et al., 2013).

### 1.4 Periodontitis

Periodontal diseases are commonly occurring destructive inflammatory diseases affecting between 20% to 50% of the global population (Albandar and Rams, 2002). The World Health Organisation (WHO) states that almost 10% of the global population has severe periodontal disease which may result in tooth loss (World Health Organization, 2021). Periodontal diseases are subdivided into gingivitis and periodontitis. Gingivitis presents as inflammation of the periodontal tissues as a response to plaque that has been allowed to accumulate on the surface of the tooth. It is a reversible non-destructive periodontal disease as there is no loss of soft or hard tissue and it can be treated by removal of the plaque biofilm. However, if left untreated, gingivitis may progress to periodontitis in susceptible patients. Within the UK, periodontitis imposes a considerable financial healthcare burden on the NHS costing almost £19 billion if 90% of all diagnosed were managed correctly (Economist Intelligence Unit, 2021).

Periodontitis is characterised by a non-resolving chronic inflammatory condition as a result of an aberrant host response that leads to loss of connective tissue, deterioration of periodontal ligament and alveolar bone (Carranza et al., 2006). If not diagnosed early and left untreated periodontitis can ultimately result in multiple tooth loss which can affect an individual's nutrition, quality of life and self-esteem (Chapple et al., 2015). Generally, periodontitis destruction of the periodontal tissues occurs slowly and it can occur at any age but is most prevalent in adults. Patients diagnosed with Grade C disease with none of the characteristic

risk factors and in younger patients can show a more rapid profile of disease progression (formally termed aggressive periodontitis) (Caton et al., 2018). As gingivitis progresses to periodontitis there is a shift in the microbial community from Gram positive to Gram negative and aerobic to anaerobic, with periodontitis patients having a microbial flora that is predominantly Gram-negative and anaerobic (Baelum and López, 2013). The disease is initiated by an aberrant or excessive host response to these pathogenic bacteria that are present in the plaque biofilm. However, the increasingly accepted 'keystone species' concept suggests that low abundance species can have a major influence on the microbial community, which can ultimately promote disease progression (Ebenman and Jonsson, 2005; Power et al., 1996). A previous study has noted that the key periodontal pathogen, *P. gingivalis*, at low colonization levels is required for maintaining high numbers of oral bacteria which are linked with enhanced inflammatory bone loss and that identifying and targeting these keystone pathogens may help prevent inflammatory diseases of polymicrobial etiology (Hajishengallis et al., 2011).

In recent years the importance of periodontitis has been raised by a number of associations with systemic diseases.

### 1.4.1 Systemic disease association

The relationship between periodontitis and systemic disease is commonly described as being 'two-way' or 'bi-directional', however the directionality is hard to determine within many of these observational epidemiological studies due to limitations in study design (Winning and Linden, 2017). Although periodontitis has been linked to several systemic diseases including cardiovascular disease (Humphrey et al., 2008), respiratory disease (Zeng et al., 2012),

diabetes (Borgnakke et al., 2013), cancer (Fitzpatrick and Katz, 2010) and Alzheimer's (Cerajewska, Davies and West, 2016) and adverse pregnancy outcomes (Ide and Papapanou, 2013), it is difficult to establish whether these associations play a part in causation (Winning and Linden, 2017). Reported positive associations between periodontitis and a systemic condition show that a certain cohort of people with periodontitis have a higher chance of suffering from a certain systemic condition. Whereas causation would suggest that development of periodontitis caused the onset and progression of a systemic condition and these causations are very rarely reported in the literature (Leite, Peres and Nascimento, 2019).

It should also be noted that observational studies may be influenced by common confounding factors that are difficult to measure such as socioeconomic status, postnatal environment (Zhou, Dong, Zha and Liao, 2021) and behavioural factors (Christakis and Fowler, 2007). These confounding factors may bias reported associations found between periodontal disease and systemic diseases. Confounding remains a challenging issue in the interpretations of the associations found between periodontitis and systemic disease (Winning and Linden, 2017) and appropriate methods such as Mendelian randomisation (MR) may be used to identify confounding and should be considered in study design (Shungin et al., 2015).

Cardiovascular diseases (CVD) are very common, accounting for 29% of deaths worldwide (Amar and Han, 2003). A study involving 108 subjects had shown that 91% of patients with CVD had moderate to severe periodontitis and a statistically significant correlation between coronary artery disease and periodontitis was also observed (Geerts et al., 2004). In addition, a meta-analysis involving 86,092 patients showed that individuals with periodontal disease had 1.14 times greater risk of developing coronary heart disease in comparison with controls

(Bahekar et al., 2007). This association between periodontitis and cardiovascular diseases may be due to increased presence of periodontal pathogens such as *Tannerella forsythia*, *P. gingivalis* and *Aggregatibacter actinomycetemcomitans* in serum or atheromatous plaques (Haraszthy et al., 2000). These pathogens can induce atherogenesis by direct invasion of the arterial wall (Haraszthy et al., 2000) or stimulating the release of inflammatory mediators that can promote atherogenesis (Loos et al., 2000). One of these mediators, serum C-reactive protein (CRP) (Amar et al., 2003), has been shown to play a role in endothelial dysfunction and increased levels of CRP may promote CVD (Joshipura et al., 2004). Furthermore, an extensive review of observational studies supported positive associations between periodontal disease and CVD independent of known confounders, however it did not support a causative relationship (Lockhart et al., 2012). It was also determined from Lockhart et al. (2012) review that periodontal interventions did not confirm prevention of or modify the clinical course of heart disease. In addition, another review suggested that it was too early to mark periodontal disease as a causal factor of CVD and interventional studies could not examine the effect of periodontal therapy on prevention of CVD (Zardawi et al., 2021). Further *in vivo*, *in vitro* and long-term interventional studies are therefore needed to determine the cause-effect relationship between periodontal disease and CVD and whether periodontal treatment can translate into reduction of CVD occurrence (Zardawi et al., 2021).

Alzheimer's disease (AD) is one of the leading causes of dementia and it is becoming common in the aging population (Gaur and Agnihotri, 2014). A study which investigated the relationship between chronic periodontitis and cognitive impairment by using tooth loss as a measure for periodontitis, noticed a significant relationship between cognitive impairment and tooth loss (Grabe et al., 2009). However, it should be noted from Grabe et al.'s (2009) study

that tooth loss was used as a surrogate measure and was not a direct measure of periodontitis. The association between chronic periodontitis and AD could be due to periodontopathogens, including *P. gingivalis, T. forsythia, and T. denticola*, which have been shown to spread to the brain from closely related anatomical pathways. Inadequate neutralisation of these pathogens can lead to the accumulation of inflammatory molecules ,which can alter cyto-architectural integrity and cause loss of vital neurons resulting in memory loss (Singhrao et al., 2014).

### 1.4.2 Risk factors for periodontitis

The risk factors for periodontitis are generally divided in to two, modifiable and non-modifiable. Modifiable risk factors are usually environmental or behavioural such as smoking, diabetes mellitus and psychological stress. Factors such as age, excessive inflammatory immune host response and genetic factors are currently non-modifiable.

Smoking is one of the main risk factors for periodontitis and elevates the risk of disease by 5 to 20-fold in comparison to a non-smoker (Bergström, 2004). Smokers display increased susceptibility, greater severity and faster progression of periodontitis with more loss of teeth in comparison with non-smokers (Nociti, Casati and Duartes, 2014). The greater progression of periodontal tissue breakdown in smokers maybe related to microbiological differences between smokers and non-smokers. It was observed that disease associated pathogens, *A. actinomycetemcomitans, P. gingivalis* and *T. forsythia* were detected at higher levels in smokers in comparison with non-smokers (Winkelhoff et al., 2001). In another study, the prevalence of disease associated pathogens such as *Campylobacter*, *Fusobacterium*, *Bacteroides* and *Treponema* were significantly more abundant in smokers when compared with non-smokers (Shchipkova, Nagaraja and Kumar, 2010). Furthermore, smoking can also

alter the immunoinflammatory systems in periodontal tissue and may explain the differences in disease severity between smokers and non-smokers. For example, increased levels of pro-inflammatory cytokines tumour necrosis factor-alpha (TNF-α) (Boström, Linder and Bergström, 1999), IL-4, IL-6 and IL-8 (Giannopoulou, Kamma and Mombelli, 2003) were detected in gingival crevicular fluid (GCF) of smokers in comparison with non-smokers.

Other well-established risk factors for periodontitis include types 1 and 2 diabetes (predominantly type 2) and a review of the literature by Kinane and Chestnutt, (1997) found significant evidence to suggest a direct relationship between diabetes and periodontitis (Kinane and Chestnutt, 1997). The risk of periodontitis is increased threefold in individuals with diabetes compared with non-diabetic individuals (Mealey and Ocampo, 2007). A study in the United States revealed that adults with diabetes (HbA1C levels of > 9%) had a significantly higher prevalence of severe periodontitis compared with non-diabetic individuals (Tsai, Hayes and Taylor, 2002). A cross-sectional study involving 10,000 individuals from 2009 to 2012 in the USA revealed that adults with diabetes suffered from more moderate or severe periodontitis compared with those with normal glucose levels. Also, prevalence of moderate/severe periodontitis was greater in those with poorly controlled diabetes compared to participants without diabetes in both sexes (Borgnakke, Genco, Eke and Taylor, 2018). Furthermore, a meta-analysis involving 53 studies between 1948 to 2018 showed that type 2 diabetes mellitus patients had a significantly worse periodontal status than those without diabetes and that type 2 diabetes could elevate the risk of developing periodontitis by 34% (Wu et al., 2020). Many other studies have also observed a direct relationship between poor glycaemic control and parameters of periodontal disease (Cutler et al., 1999; Guzman et al., 2003; Tervonen et al., 1994). It has been observed that the subgingival microbiota of diabetic

and non-diabetic patients has relatively few differences (Sastrowijoto et al., 1989). This suggests that the immunoinflammatory response may be altered in diabetic individuals leading to impaired neutrophil adherence, phagocytosis and chemotaxis and increased pro-inflammatory cytokine production (Manouchehr-Pour et al., 1981; Salvi et al., 1997). A previous study has shown that diabetic individuals (HbA1C levels of > 8%) had twice the levels of IL-1β in GCF in comparison with subjects whose HbA1C levels were < 8% (Engebretson et al., 2004). This impairment in immunoinflammatory responses within diabetic individuals may facilitate the persistence of bacteria and inflammation resulting in increased periodontal destruction.

However, the most important risk factor for periodontitis is the accumulation of a dysbiotic plaque biofilm which is responsible for the persistent and destructive host inflammatory immune response in susceptible patients (Chapple et al., 2015).

### 1.4.3 *In vitro* models of periodontitis

Simple *in vitro* cell culture models of periodontitis typically apply bacteria to a monolayer of confluent eukaryotic cells and these basic models can be used to determine cellular responses to bacteria and any specific interactions which may occur (Pan et al., 2009; Stathopoulou, Benakanakere, Galicia and Kinane, 2010; Saito, Inagaki and Ishihara, 2009). *In vitro* 2D models have been widely used to mimic periodontitis and some of these have utilised the OSCC H400 cell line (Abdulkareem et al., 2017; Bugueno et al., 2018; Grant et al., 2010). In addition, primary gingival epithelial cells (Yilmaz, Young, Lamont and Kenny, 2003), human gingival fibroblasts (Dabija-Wolter et al., 2022), oral carcinoma cell lines (Mintz and Fives-Taylor, 1994) and models utilising multiple eukaryotic cells have been used for 2D models of

periodontitis (Bodet, Chandad and Grenier, 2006). However, the periodontium is 3D in structure, therefore 2D cell culture models do not fully represent the *in vivo* tissue architecture and any cell interactions/signals that occur.

Many 3D models have been developed to mimic the oral mucosa with some of these models utilising fibroblast-containing collagen gel with oral keratinocytes cultured on the surface at the air-liquid interface (Dongari-Bagtzoglou and Kashleva, 2006; Schaller et al., 2006). In addition, decellularized matrix used as a scaffold for human keratinocytes and fibroblasts have been utilised and show more similar immunohistological and proliferation characteristics to normal mucosa when compared with a 2D oral cell line (Yadev, Murdoch, Saville and Thornhill, 2011). Furthermore, a 3D co-culture model using collagen-fibroblast gel with surface epithelial cells cultured at the air-liquid interface and exposed to *P. gingivalis* showed significant differences when compared with monolayer cultures of epithelial cells (Pinnock et al., 2014). It was determined from Pinnock et al. (2014) study that 3D co-culture systems were important in understanding interactions between cell types after pathogen exposure. 3D oral mucosa models are more representative of the oral cavity and can be used to model periodontitis, however there is no current universal system available and significant optimisation may be required if deciding to use a 3D model (Duval et al., 2017).

### 1.5 Oral microbiome

One of the most heavily colonised parts of the human body is the oral cavity, harbouring approximately 700 types of bacterial species that colonize hard and soft tissues, including the teeth and the oral mucosa (Kilian et al., 2016). The sites within the oral cavity all have unique bacterial profiles because of differences in the local niches that will favour specific bacterial

growth (Aas et al., 2005). In healthy individuals these bacteria live with their host rarely causing health-related issues. The host-microbe interactions which involves the immune system is key to maintaining homeostasis and to avoid unwanted activation of the immune response (Devine, Marsh and Meade, 2015). Oral commensal bacteria can maintain homeostasis and prevent disease progression by occupying the niche preferred by disease-associated pathogens and by hindering the ability to multiply (Socransky and Haffajee, 1992). Changes to the oral symbiotic microbiome can be instigated by poor oral hygiene, genetics and a compromised immune system (Zarco, Vess and Ginsburg, 2011). This shift in the well-balanced oral microbiome from commensal bacteria to an increased presence of disease-causing pathogens is known as dysbiosis (Kilian et al., 2016). Dysbiotic microbial communities can disrupt normal functioning of the host immune system predisposing to development of periodontitis (Darveau, 2010).

Biofilms are complex structures of microorganisms that colonise surfaces within the oral cavity, with dental plaque being one of the commonly known multispecies biofilms that forms as layers on tooth surfaces (Flemmig and Beikler, 2010). The dental plaque biofilm also consists of a matrix containing extracellular polymeric substances (EPS), which is composed of carbohydrates (glucans and fructans), proteins, extracellular deoxyribonucleic acid (eDNA), peptidoglycans and lipids (Jakubovics et al., 2021). In periodontitis, dental plaque consists of supragingival dense filament-containing plaque and subgingival plaque consisting mostly of flagellated bacteria, spirochetes and small Gram-negative bacteria (Listgarten and Hellden, 1978). Some of these pathogens that are found in subgingival plaque include *A. actinomycetemcomitans, P. gingivalis, Prevotella intermedia, F. nucleatum, T. forsythia,* and *Eikenella corrodens* and *T. denticola* (Zarco, Vess and Ginsburg, 2011).

Current clinical treatment methods for periodontitis are focused on restoring homeostasis between the host and its microbial community by controlling the subgingival dysbiotic dental biofilm (Lasserre, Brecx and Toma, 2018).

*Streptococci* species, such as *S. gordonii, S. oralis, S. mitis* and *S. sanguinis* and the *Actinomyces* species have long been known to be early colonizers of dental plaque and are involved in initiating biofilm formation (Ximénez-Fyvie, Haffajee and Socransky, 2000). Once colonized by binding to the salivary pellicle on the surface of the tooth, late colonisers that are generally Gram-negative bacteria start to aggregate and plaque development occurs (Lee and Davey, 2017). These late colonisers attach to early colonisers through adhesions and tend to bind to other metabolically compatible species (Kuboniwa and Lamont, 2010). Late colonisers, such as *P. gingivalis* (Yao et al., 1996) and *F. nucleatum* (Kolenbrander et al., 2002) can bind to early colonisers and form a connection or 'bridge' for other later colonisers. *P. gingivalis* and *F. nucleatum* have also been shown to co-aggregate with each other through carbohydrate-protein specific binding (Kolenbrander and Andersen, 1989). In addition, *T. denticola* can also aggregate with *F. nucleatum* through galactose containing receptors present in the outer sheath membrane of *T. denticola* (Rosen, Genzler and Sela, 2008). Furthermore, *T. denticola* and *P. gingivalis* also form dual-species biofilms possibly through activities of *T. denticola* dentilisin (Cogoni et al., 2012) and *P. gingivalis* gingipains (Ito et al., 2010).
The subgingival biofilm consists of many bacterial species which can be divided into 5 complexes that consist of: red, orange, green, yellow and purple, having first been described by Socransky and his colleagues in 1998 (Socransky et al., 1998) (see Figure 1.4). The red complex pathogens are the most important in adult forms of periodontal disease and they appear later in biofilm development (Holt and Ebersole, 2005). Both, red and orange complex

bacteria have strong associations with clinical parameters of periodontitis in comparison with the other complexes (Socransky et al., 1998).

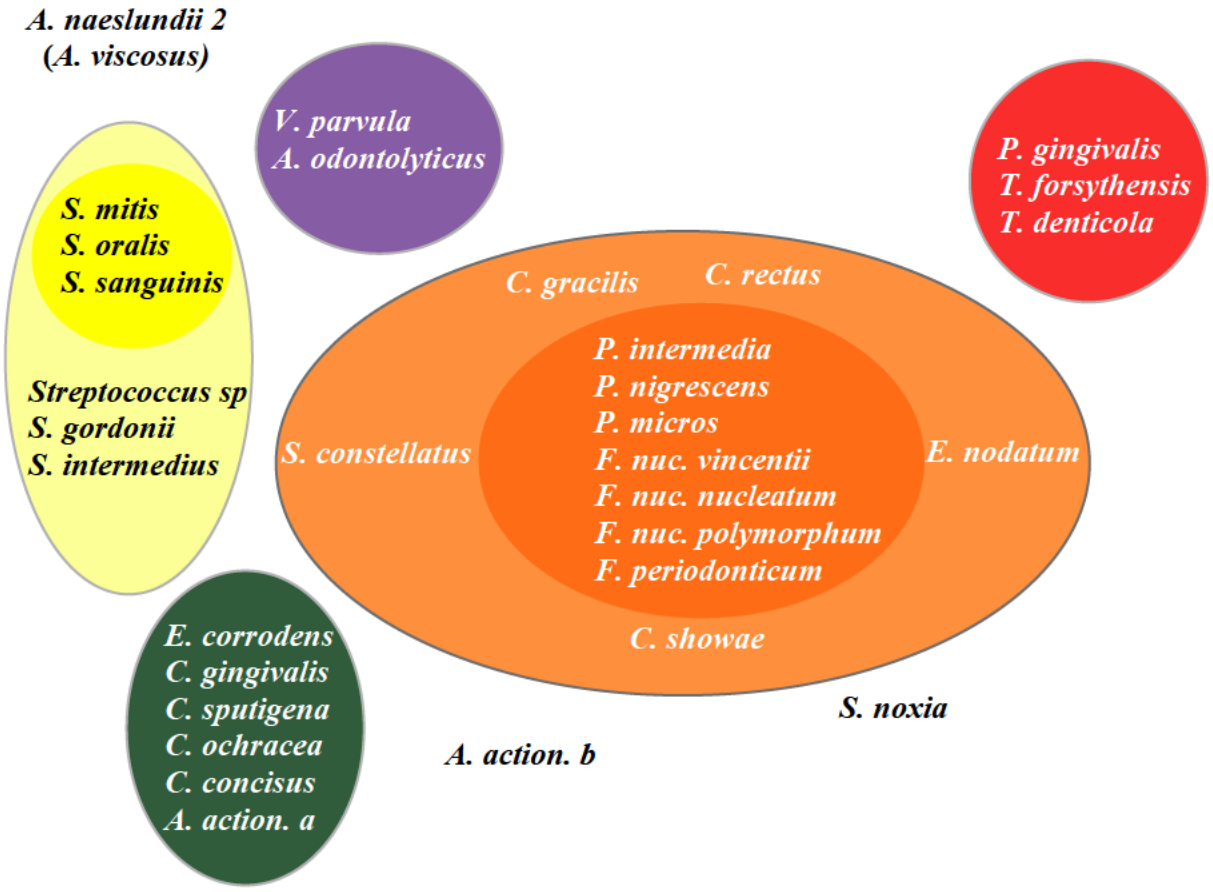



**Figure 1.4**: Oral bacteria of subgingival plaque clustered into different coloured complexes (red, orange, green, yellow and purple) that are grouped based on virulence and are also known as Socransky complexes. The pathogens compromising the yellow, purple and green complexes are early colonisers with purple complex pathogens having low to moderate pathogenicity. Whilst green complex pathogens are facultative anaerobes that have moderate pathogenicity. Orange complex pathogens can co-aggregate with red complex pathogens facilitating the formation of multispecies biofilms. Species within the red and orange complexes are generally associated with periodontitis (adapted from (Socransky et al., 1998)).

### 1.5.1 Oral bacteria and inflammation

It has been shown that some oral commensal bacteria are able to supress pro-inflammatory cytokine secretion in epithelial cells. *Streptococcus salivarius* K12 inhibited activation of NF-κB resulting in down-regulated IL-8 secretion in oral keratinocytes (Cosseau *et al.*, 2008). However, dysbiotic plaque biofilms concomitant with periodontitis contain pathogenic bacterial communities that can initiate an immunological response within the host causing the release of pro-inflammatory mediators. Continuous immunoinflammatory responses leads to destruction of the host tissue which eventually manifests in the symptoms associated with periodontitis (Singh et al., 2011).

Oral bacteria initiate the innate immune response through activation of receptors known as pattern-recognition receptors (PRRs), which are located on antigen presenting cells, immune and tissular structural cells (Medzhitov and Janeway, 2000). Different types of PRR's include Toll-like receptors (TLRs), retinoid acid-inducible gene I-like receptors (RLRs), nucleotide-binding oligomerization domain-like receptors (NLRs) and C-type lectin receptors (CLR) (Creagh and O'Neill, 2006; Hoving, Wilson and Brown, 2014). These receptors recognise pathogen associated molecular patterns (PAMPs) which are highly conserved molecular patterns or structures which provide exogenous signals to the immune system (Tang et al., 2012).

*P. gingivalis* (Ding et al., 2020a) and *T. denticola* (Miyamoto, Ishihara and Okuda, 2006) have previously been shown to induce secretion of the pro-inflammatory cytokine, IL-1β. Previous findings have also revealed that virulence factors present in these pathogens can stimulate production of cytokines. For example, the *P. gingivalis* surface virulence factor,

fimbriae, has been shown to induce IL-1β secretion (Amano et al., 2004). In addition, *F. nucleatum*, which is also associated with periodontitis can promote the secretion of IL-1β in epithelial cells (Bui et al., 2016). Another pro-inflammatory cytokine, IL-8 has been shown to be up-regulated after *P. gingivalis* (Milward et al., 2007) and *F. nucleatum* (Koike et al., 2020) exposure in epithelial cells. These processes may be connected with another *P. gingivalis* virulence factor, arg-gingipain (Oido-Mori et al., 2001), or *F. nucleatum* virulence factor FadA (Rubinstein et al., 2013), which have both been shown to induce IL-8 secretion. TGF-β1 secretion can also be stimulated by periodontal pathogens including *P. gingivalis, F. nucleatum* (Abdulkareem et al., 2017) and *T. denticola* (Bakthavatchalu et al., 2010). Lipopolysaccharide (LPS) is the dominant glycolipid that forms a central component of the outer membrane in Gram-negative bacteria and plays a key role in pathogenesis (Maldonado, Sá-Correia and Valvano, 2016). The LPS associated with *F. nucleatum* has previously been demonstrated to induce secretion of pro-inflammatory cytokines such as IL-6, IL-1β and TNF-α (Karpiński, 2019).

### 1.5.2 Bacteria and EMT

The role of bacteria in inducing EMT has been investigated in many different studies under various conditions. One of these studies examining the effects of flagellin on TLR5 stimulation in pulmonary fibrosis, identified induction of EMT (Kondo et al., 2012). Bacterial species in the subgingival plaque commonly include flagellated bacteria (Germano et al., 2013) such as *T. denticola* (Ng et al., 2019) and *Campylobacter rectus* (Ihara et al., 2003). Flagellin is a structural component of the flagella that enables cell motility and is mostly associated with Gram-negative bacteria (Hajam et al., 2017). The adenocarcinomic human alveolar basal epithelial cell line, A549, treated with flagellin exhibited activation of the

nuclear factor kappa-light-chain-enhancer of activated B cells (NF-κB) pathway and treatment with TGF-β1 which is a key factor in EMT induction caused similar up-regulation of genes compared with flagellin exposure. Also, flagellin increased the amount of fibronectin protein and decreased levels of E-cadherin thus demonstrating its involvement in EMT and possible role in pulmonary fibrosis (Kondo et al., 2012).

Furthermore, the oncoprotein cytotoxin-associated gene A (CagA) found in the Gram-negative bacterium *Helicobacter pylori* has been shown to trigger cancer stem cell-like properties through EMT in gastric epithelial cells (Bessède et al., 2013). It was observed in this study that mesenchymal markers snail-1, vimentin and ZEB-1 were up-regulated whilst epithelial markers cytokeratin 7 and osteopontin were down-regulated. LPS from Gram-negative bacteria has also been shown to induce EMT in previous studies using oral epithelial cells (Jing et al., 2012; Ding et al., 2020b). An additional study which investigated the effects of LPS to induce EMT in human intrahepatic biliary epithelial cells (HIBEpiCs), reported an increased expression of mesenchymal markers, S100A and α-SMA through a TGF-β mediated pathway (Zhao et al., 2011).

In a study investigating the link between the presence of *F. nucleatum* in 280 colorectal cancer stage III/IV patients, data showed that the level of *F. nucleatum* in the tumours was correlated with several markers associated with EMT, including E-cadherin, sox-2, oct-4, N-cadherin and nanog. *F. nucleatum* levels were negatively correlated with E-cadherin expression and positively correlated with expression of N-cadherin, highlighting *F. nucleatums'* potential contribution to EMT-cancer stem cell cross talk in colorectal cancer (Xuebing et al., 2017). Furthermore, previous work from our group has demonstrated EMT

induction of OSCC cells after stimulation with the periodontal pathogens *P. gingivalis* and *F. nucleatum* (Abdulkareem et al., 2017). A significant release of EMT-inducing pro-inflammatory cytokines TGF-β1, TNF-α, and EGF was observed. In addition, expression of E-cadherin, cytokeratin 14, and β-Catenin were down-regulated, whilst N-cadherin, vimentin, snail, MMP-2 and MMP-9 were simultaneously up-regulated (Abdulkareem et al., 2017).

### 1.6 Bacterial inactivation for use in epithelial stimulation

Long-term cell culture models of periodontitis (>3 days) have historically and most commonly utilised heat-killed bacterial pathogens as opposed to live bacteria (Abdulkareem et al., 2017; Bugueno et al., 2018; Grant et al., 2010). This approach has been used because of issues with contamination of the cultures and bacterial overgrowth in long-term models using live bacteria (Cross et al., 2004; Kim et al., 2015). It has been proposed that heat-killed pathogens can elicit similar responses in oral epithelial cells as viable bacteria, therefore heat-killed pathogens have frequently been used as a suitable alternative to avoid the common problems associated with using live bacteria (Laheij et al., 2013). In contrast, it has been noted that heat-killing of bacteria can damage the outer membrane (Katsui et al., 1982), inner membrane (Russell and Harries, 1967) and deoxyribonucleic acid (DNA) (Woodcock and Grigg, 1972). In addition, this killing approach causes ribosomal degradation (Tomlins and Ordal, 1971) and protein denaturation (Rosenberg et al., 1971) in bacteria. Therefore, the use of heat-killed bacteria could result in unrealistic bacterial-epithelial cell interactions which would be unrepresentative of the subgingival bacterial – host interaction. In addition, in the gingival crevice there are more likely to be obligate anaerobic bacteria killed by oxygen and not by heat. The bacterial species intended for use in this study, *P. gingivalis* and *T. denticola*, are obligate anaerobes whilst *F. nucleatum* is a facultative anaerobe. It is known that

anaerobes do not possess the defences needed to survive in oxygen long-term which ultimately results in their death (Baron and Hentges, 1996). Exposing anaerobes to oxygen as a means of bacterial killing may be less disruptive to bacteria architecture and protein expression when compared with heat-killing and would better represent viable bacteria.

### 1.7 EMT inhibitors

EMT is implicated in diseases such as cancer and fibrosis and involves numerous pathways and mediators (see 1.3.2 and 1.3.3). The treatment of cancer is facing serious challenges related to drug resistance and EMT has been recently implicated for its role in cancer drug resistance (Du and Shim, 2016). Therefore, drugs that target EMT mediators or pathways may provide potential therapies for fibrosis and cancer treatment. Naturally derived inhibitors such as curcumin (see 1.7.1.3) and synthetic compounds such as Sepantronium bromide, have been widely reported to inhibit EMT by targeting different mediators (Feng et al., 2019).

One of these natural compounds, resveratrol, which is commonly found in grapes, berries and peanuts (Pirola and Fröjdö, 2008) has been shown to inhibit EMT in pancreatic cancer cells (Li et al., 2013). It was observed that EMT was inhibited via suppression of the PI3K/Akt/NF-κB pathway leading to up-regulation of E-cadherin and down-regulation of N-cadherin and vimentin. In addition, migratory and invasive abilities were also inhibited with resveratrol exposure (Li et al., 2013). Another natural compound, Ergone, which is found in a medicinal mushroom (*Polyporus umbellatus*) (Lee, Park and Ahn, 2007) was shown to inhibit EMT in renal fibrosis via the Wnt/β-catenin pathway, resulting in snail-1, twist, MMP-7, fibronectin, α-SMA and vimentin down-regulation, whilst E-cadherin expression was restored

(Chen et al., 2017a). A summary of natural EMT-inhibitors and the pathways affected are shown in Table 1.2.

Synthetic compounds have also been reported to inhibit EMT in numerous studies. Notably, one of these synthesised compounds, Sepantronium bromide (YM155), has been shown to inhibit EMT in glioblastoma cells via STAT3 signalling leading to increased E-cadherin expression whilst N-cadherin, β-catenin, slug and ZEB-1 expression were decreased (Zhang et al., 2018). Another synthetic compound, Trichostatin A, has also been demonstrated to repress EMT by increasing expression of E-cadherin and decreasing expression of α-SMA in experimental lung fibrosis (Li et al., 2017b). An overview of synthetic compounds known to inhibit EMT and the pathways involved are shown in Table 1.3.

**Table 1.2:** A summary of naturally derived compounds that inhibit EMT in various conditions and the signalling pathways involved.

| **Compound** | **Species** | **Disease** | **Signalling pathway** | **References** |
|---|---|---|---|---|
| Curcumin | *Curcuma longa* | Breast cancer cells, Pancreatic cancer cells, intestinal fibrosis, bladder cancer | Wnt/β-catenin, c-MET/PI3K/Akt/mTOR, PPARγ, NF-κB-Snail, miR-34a | (Gallardo, Ponce-Cusi and Calaf, 2017; Li et al., 2018; Xu et al., 2017b and Deng et al., 2016) |
| Resveratrol | *Vitis vinifera, Vaccinium macrocarpon, Morus alba, Pistacia vera* and *Arachis hypogaea* | Lung and renal fibrosis, gastric cancer, HCT-116 colorectal cancer cells | PTEN/Akt, miR200c, TGF-β, p38-mitogen-associated protein kinase (MAPK), TGF-β | (Zhang et al., 2015a; Choi et al., 2016; Dermani et al., 2016 and Xu et al., 2017a) |
| Hispolon | *Phellinus linteus* | Human epithelial cancer cells | TGF-β-Snail/Twist | (Hong et al., 2017) |
| Ergone | *Polyporus umbellatus* | Renal fibrosis | Wnt/β-catenin | (Chen et al., 2017a) |
| Arctigenin | *Arctium lappa* and *Saussurea heteromalla* | Human lung cancer cells | TGF-β, ERK and β-catenin | (Xu, Lou and Lee, 2017) |
| Carnosol | *Rosmarinus officinalis* | Human glioblastomas | TNF-α/TGF-β | (Giacomelli et al., 2017) |
| Codonolactone | *Atractylodes* | Breast cancer | TGF-β | (Fu et al., 2015) |
| Jatrophone | *Jatropha isabelli* and *Jatropha gossypiifolia* | Breast cancer | Wnt/β-catenin | (Fatima et al., 2017) |
| Epicatechin-3-gallate | *Camellia sinensis* | Human Lung cancer cells | TGF-β | (Huang et al., 2016) |
| Oxymatrine | *Sophora flavescens* | Liver, pulmonary, myocardial and skin scar tissue fibrosis | TGF-β1/Smad | (Shi and Li, 2005; Chen et al., 2008; Shen et al., 2011 and Fan et al., 2012) |

**Table 1.3**: Synthesised compounds that can inhibit EMT in different conditions via their effects on various signalling pathways.

| **Compound** | **Disease** | **Signalling pathway** | **References** |
|---|---|---|---|
| Decitabine | Non-small-cell lung cancer PC9 cells | MiR-200/ZEB | (Zhang et al., 2017) |
| Sepantronium bromide | Glioblastoma | STAT3 | (Zhang et al., 2018) |
| Ubenimex | Renal cell carcinoma | Akt | (Liu et al., 2016b) |
| GW788388 | Renal fibrosis | TGFβRI | (Petersen et al., 2008) |
| FH355 | Radioresistant oesophageal cancer cell line | Wnt/β-catenin | (Su et al., 2015a) |
| RO4929097 | Cervical cancer cells | Notch | (LoConte et al., 2014) |
| Trichostatin A | Lung fibrosis | Akt | (Li et al., 2017b) |
| Galunisertib | Human hepatocellular carcinoma cell lines | TGFβRI | (Lahn et al., 2015) |
| Oxymatrine | Kidney NRK-52E cells | TGF-β1/Smad | (Liu et al., 2016a) |
| Losartan | Hyperglycemia | RAS | (Yao et al., 2018) |

### 1.7.1 Curcumin

Turmeric is a rhizomatous herbaceous perennial plant (*Curcuma longa*) that is derived from the ginger family (Priyadarsini, 2014) and it is normally cultivated in tropical and subtropical regions (Aggarwal, Deb and Prasad, 2014). The health benefits of turmeric have been known for almost 4000 years with its first being used as an antiseptic and antibacterial agent for cuts and burns in many south Asian countries (Prasad and Aggarwal, 2011). In addition, it has been traditionally used as a treatment for coughs, colds, sore throats and in a paste form for viral diseases including measles, chicken pox and smallpox thus demonstrating its pleiotropic effects (Krishnaswamy, 2020). However, the mechanisms and bioactive components responsible for these health benefits have only been discovered in the past 60 years (Gupta, Patchva and Aggarwal, 2013).

Turmeric contains curcuminoids which are natural phenols responsible for the yellow colour of turmeric and consist of compounds such as curcumin, demethoxycurcumin and bis-demethoxycurcumin (Priyadarsini, 2014). These all share the same structure with two benzenemethoxy rings joined by a seven-carbon unsaturated chain (Amalraj et al., 2017). Curcumin (1, 7-bis(4-hydroxy-3-methoxyphenyl) often referred as diferuloylmethane is the most active and widely reported curcuminoid (Stohs et al., 2020). Curcumin has been shown to possess anti-inflammatory properties (Fadus et al., 2017) and has been utilised in several clinical studies (Gupta, Patchva and Aggarwal, 2013). In addition, its EMT inhibitory effects are well reported (Bahrami, Majeed and Sahebkar, 2019).

#### 1.7.1.1 Anti-inflammatory properties

Curcumin's anti-inflammatory properties are well reported and it has been shown to inhibit secretion and expression of cytokines implicated in pro-inflammatory disease. In one study that modelled chronic inflammation in metabolic diseases, pre-treatment of intestinal epithelial cells and macrophages with curcumin was able to inhibit LPS-induced secretion of IL-1β (Wang, Ghosh and Ghosh, 2017a). In addition, curcumin has been demonstrated to attenuate gene expression of IL-1β in immortalised human keratinocytes (Cho, Lee and Kim, 2007). Furthermore, curcumin could down-regulate IL-8 gene expression in a study modelling oesophageal inflammation using human oesophageal epithelial cells in response to acidic pH during gastroesophageal reflux disease (Rafiee et al., 2009). Activation of NF-κβ can suppress apoptosis and induce cell proliferation, invasion, metastasis and inflammation (Nakanishi and Toi, 2005). Curcumin treatment has also been shown to down-regulate secretion and gene expression of IL-8 in OSCC cells via the NF-κB pathway through increased activity of the inhibitor of NF-κB kinase (IκB-kinase) (Cohen et al., 2009). It has been demonstrated that curcumin can also inhibit TGF-β1 secretion in breast epithelial cells via the NF-κB pathway (Mohankumar et al., 2015). The pro-inflammatory cytokine, TNF-α is a key mediator in inducing inflammation in many diseases and it can elicit its effects through activation of the transcription factor NF-κB. Curcumin has also shown to down-regulate expression of TNF-α and decrease NF-κB activity in ankle joints of patients with rheumatoid arthritis (Aggarwal, Gupta and Sung, 2013) and in experimentally induced arthritis in rats (Cai et al., 2015). In addition, curcumin can ameliorate ulcerative colitis symptoms by suppressing expression of TNF-α (Camacho-Barquero et al., 2007). Curcumin can target a wide range of inflammatory mediators as reviewed by Aggarwal, Gupta and Sung, (2013).

#### 1.7.1.2 Clinical studies

Many clinical trials have been performed to evaluate curcumins health benefits. One of these, a short-term double-blind cross over study, investigated the potential of curcumin to alleviate symptoms in rheumatoid arthritis. A daily dose of curcumin (1200mg) for 2 weeks was able to improve morning stiffness, walking time and joint swelling (Deodhar, Sethi and Srimar, 2013). In addition, an interventional unblinded clinical trial in osteoarthritis patients demonstrated significant reductions in inflammatory markers (including IL-1β, IL-6, soluble cluster of differentiation 40 ligand (sCD40L) and soluble vascular cell adhesion molecule-1 (sVCAM-1)) after a daily dose of curcumin (200mg) for 8 months (Belcaro et al., 2010). Furthermore, in an unblinded clinical trial, curcumin applied in ointment form has shown to provide symptomatic relief including reduction of itching, dry lesions and lesion size and pain in patients with malignant skin lesions (Kuttan, Sudheeran and Josph, 1987). Additionally, a phase II unblinded clinical trial (pilot study) involving patients with peptic ulcers showed ulcer resolution and a decrease in abdominal pain and discomfort after treatment with curcumin (3000mg/day) for 12 weeks (Prucksunand et al., 2001). A randomised, controlled clinical trial has also indicated that curcumin can reduce body fat, reduce BMI, increase waistline reduction and reduce hip circumference in 44 obese subjects after 30 days treatment, however the strength of this study is limited as it is not double-blinded (Di Pierro et al., 2015).

#### 1.7.1.3 Curcumin as an EMT inhibitor

Curcumin has shown to inhibit EMT in multiple studies investigating different conditions. One of these studies showed curcumin to reduce expression of proteolytic enzymes, including MMP-2 and MMP-9, leading to reduced invasiveness of OSCC cells (Lee et al., 2015). It was also observed that expression of snail and twist were both down-regulated with curcumin treatment. In another study using DU145 prostate cancer cells, curcumin down-regulated expression of snail and vimentin via inhibition of c-Met expression (Hu et al., 2015). Furthermore, curcumin has been shown to prevent EMT in a rat model of intestinal fibrosis via repression of the TGF-β1/Smad pathway, resulting in up-regulation of E-cadherin and down-regulation of α-SMA and fibronectin (Xu et al., 2017b). An overview of curcumin and its EMT inhibitory effects in different disease conditions is shown in Table 1.4.

**Table 1.4**: An overview of curcumins EMT inhibitory effects in different diseases.

| Disease condition | EMT inhibitory effects by curcumin | Model used | Reference |
|---|---|---|---|
| **Cancer** | | | |
| Oral | • Induction of p53 gene repressed EMT<br>• Down-regulation of snail, twist, MMP-2 and MMP-9 | *In vitro* (OSCC cell line, SCC25) | (Lee et al., 2015) |
| Pancreatic | • Reduction of mesenchymal markers vimentin and α-SMA in cancer associated fibroblasts<br>• Up-regulation of E-cadherin<br>• Curcumin inhibited metastasis *in vivo* | *In vitro* (cancer associated fibroblasts) and *in vivo* (mice) | (Wang et al., 2017b) |
| | • Blocked the phosphatidylinositol 3-kinase (PI3K)/protein kinase B (Akt)/NF-κB signalling pathway | *In vitro* (human pancreatic cancer cell lines – BxPC-3 and Panc-1) | (Li et al., 2018) |
| Lung | • Up-regulation of Wnt inhibitory factor-1 (WIF-1) protein expression inhibited Wnt signalling pathway in metastatic lung cancer cells | *In vitro* (invasive lung cancer cell lines – 95C and 95D) | (Xu et al., 2015) |
| | • Blocked phosphorylation of the receptor tyrosine kinase c-Met and PI3K/Akt/mammalian target of rapamycin (mTOR) pathways | *In vitro* (human lung cancer cell line, A549) | (Jiao et al., 2016) |
| Thyroid | • Down-regulated Smad2 and Smad3 signalling pathways<br>• Increased expression of E-cadherin and repressed expression of vimentin, MMP-2 and MMP-9 | *In vitro* (human papillary thyroid carcinoma BCPAP cells) | (Zhang et al., 2016) |
| Prostate | • Down-regulated snail and vimentin expression through inhibition of phosphorylated c-Met | *In vitro* (human prostate cancer cell line, DU-145) | (Hu et al., 2015) |
| Breast | • Inhibited β-catenin nuclear translocation resulting in inhibited slug trans-activation leading to up-regulated E-cadherin gene expression | *In vitro* (human breast cancer stem cell line, MCF-7) | (Mukherjee et al., 2014) |
| **Fibrosis** | | | |
| Intestinal | • Supressed TGF-β1 induced Smad pathway leading to decreased gene expression of α-SMA and fibronectin<br>• Increased expression of E-cadherin<br>• Reduced TGF-β1 and increased E-cadherin staining *in vivo* | *In vitro* (rat small intestinal epithelial cell line, IEC-6) and *in vivo* (rats) | (Xu et al., 2017b) |

| | | | |
|---|---|---|---|
| Renal | • Inhibited of Akt/mTOR pathway<br>• Increased expression of E-cadherin and cytokeratin<br>• Decreased expression of vimentin, α-SMA and FSP-1 | *In vitro* (human renal proximal tubular cell line, HKC) | (Zhu et al., 2017) |

### 1.8 Aims and objectives

Whilst it is known that periodontitis is the result of a persistent non-resolving immunoinflammatory response to pathogenic bacteria, some aspects which underpin the breakdown of gingival tissue are still unclear. EMT which is implicated in many diseases, is a process where epithelial cells gain migratory and invasive properties resulting in a breakdown of epithelial integrity (Chen et al., 2017c). It has been shown to be induced by bacteria (see section 1.5.2) and inflammatory mediators (see section 1.3.5) that are implicated in periodontitis. EMT may therefore be a driver of periodontitis leading to associated changes and may be a process to potentially target for the treatment of periodontitis. This thesis therefore aims to use a suitable 2D epithelium model of periodontitis that simulates the *in vivo* situation and to provide evidence of EMT induction by periodontal pathogens. This project will also determine if natural EMT inhibitors could be used to down regulate or block EMT induction as a potential therapeutic strategy in the management of periodontitis. The objectives which underpin these aims are described below:

**Objective 1:** To develop a suitable 2D-oral epithelium model which replicates the chronic persistent inflammatory response observed in patients with periodontitis using an immortalized cell line (H400) for the induction of EMT. To explore the use of oxygen-killing of anaerobic periodontal pathogens as an alternative to heat-killing for use in the model.

**Objective 2:** To investigate the potential of heat-killed (HK) and oxygen-killed (OK) *P. gingivalis*, *F. nucleatum* and *T. denticola* to induce EMT-related changes *in vitro*.

**Objective 3:** To evaluate whether curcumin can inhibit periodontal pathogen induced EMT *in vitro*.

**Objective 4:** To further elucidate the effects of heat and oxygen-killing on *T. denticola* and to understand the different EMT responses observed after HK and OK *T. denticola* exposure.

# 2. Materials and methods

All materials used were acquired from Sigma, UK unless otherwise stated.

### 2.1 Bacterial cultivation

Stocks of *P. gingivalis* (ATCC 33277) and *F. nucleatum (polymorphum)* (ATCC 10953) were originally purchased from American Type Culture Collection (ATCC, Rockville, MD) and *T. denticola* (ATCC 35405) was kindly gifted from the laboratory of Dr. Angela Nobbs at the University of Bristol. UK. *P. gingivalis* and *F. nucleatum* were cultured for 7 and 3 days respectively on horse blood agar (Oxoid, UK) in an anaerobic chamber (Don Whitley, UK) with 80% nitrogen, 10% carbon dioxide and 10% hydrogen at 37ºC. Broth cultures were prepared by inoculating 20ml of sterile Trypticase soy broth (TSB) with 3-4 representative colonies of *P. gingivalis* or *F. nucleatum* in anaerobic conditions. *T. denticola* was cultured in new oral spirochete (mNOS) semi-solid agar by inserting a sterile loop containing bacteria directly through the centre of the media (Figure 2.1) and broth cultures were prepared in 20ml mNOS medium in anaerobic conditions. Growth of all three bacteria were indicated by visible turbidity in suspension. The components of mNOS are detailed below:

#### 2.1.1 New oral spirochete (mNOS) medium

mNOS medium consisted of 1.25g brain heart infusion broth (Oxoid, UK), 1.00g trypticase peptone (Becton, Dickinson and company, UK), 0.25g yeast extract, 0.05g sodium thioglycolate, 0.1g L-cysteine (Acros organics, USA), 0.025g L-asparagine, 0.2g glucose (BDH laboratory supplies, UK) and 0.1ml filter sterilized 0.1% w/v resazurin in 94ml distilled water ($dH_2O$) and then autoclaved. Semi-solid agar was produced by adding 0.5% Schaedler anaerobe agar and 0.5% gelatin (Merck, UK) prior to autoclaving. After autoclaving 2.67ml filter sterilized 7.5% w/v $NaHCO_3$, 2ml heat-inactivated rabbit serum (Cellect, Israel) and 2ml filter sterilized thiamine pyrophosphate–volatile fatty acid (TPP-VFA) mix were added.

#### 2.1.1.1 Volatile fatty acid (VFA) mix

The VFA component of the TPP-VFA consisted of 0.5ml isobutyric acid (Alfa-Aesar, USA), 0.5ml 2-methylbutyric acid (Alfa-Aesar, USA), 0.5ml isovaleric acid, 0.5ml valeric acid and 98ml 0.1M NaOH which was then filter sterilized using a 0.22µm pore size MF-Millipore™ membrane filter (Merck Millipore, Ireland) and needleless syringe (Terumo® corporation, Philippines) and stored at 4$^{o}$C until required.

#### 2.1.1.2 Thiamine pyrophosphate–volatile fatty acid (TPP-VFA)

TPP-VFA mix consisted of 8.5ml $dH_2O$, 1.5ml 0.2% thiamine pyrophosphate and 1ml VFA mix which was filter sterilized and stored at 4$^{o}$C.

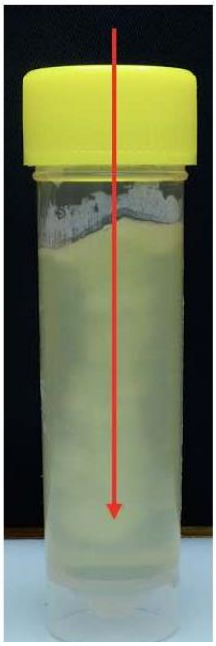


**Figure 2.1**: A sterile universal tube containing 20ml of semi-solid mNOS agar was inoculated by inserting a sterile loop containing *T. denticola* directly through the centre of the media (indicated by the red arrow).

## 2.2 Determining bacterial concentration

To determine bacterial concentration in suspension a standard curve was produced (optical density vs. bacterial count) by measuring the suspension optical density (OD) at a wavelength of 600nm ($OD_{600nm}$) with a spectrophotometer (Jenway, Dunmow, UK) using 1ml semi-micro cuvettes (Sarstedt, UK). OD readings were obtained every hour from 1-8 hours and then finally at 24 and 48 hours. Simultaneously blood agar plates and mNOS were inoculated using the Miles and Misra (Miles, Misra and Irwin, 1938) method. The spectrophotometer was first blanked with TSB or mNOS broth only before every reading was taken. Absorbance readings and colony forming units (CFU) were plotted in a scatter graph using Excel software (Microsoft, US) and the linear regression equation produced was used to determine the number of viable bacteria in the suspension. This could also be used to determine how many CFU were present in new bacterial suspensions by reading the OD and using the straight-line equation.

After determining the number of bacteria per ml, bacterial suspensions were centrifuged (MSE Harrier, UK) at 3000rpm for 10 mins to produce a bacterial pellet. Supernatants were removed aseptically and pellet containing bacteria was re-suspended in 10ml phosphate-buffered saline (PBS). PBS was prepared by dissolving 8g sodium chloride (NaCl), 1g sodium phosphate dibasic ($Na_2HPO_4$), 0.2g potassium chloride (KCl) and 0.2g of potassium phosphate monobasic ($KH_2PO_4$) in 1L $dH_2O$ and then sterilised by autoclaving before use. Suspensions were centrifuged again and re-suspended in PBS before being either heat or oxygen-killed following the protocol described in section 2.3. A final suspension of $4x10^8$ bacteria/ml was produced by diluting the suspension appropriately with sterile PBS and then stored at -20°C. Prior to heat or oxygen-killing, aliquots of live cultures stored at -20°C were spared for SEM analysis.

## 2.3 Bacterial preparation

### 2.3.1 Heat-killing

Bacteria were first grown in respective agars and overnight cultures were prepared as described in section 2.1. After 48-72 hrs growth, bacterial cultures were washed twice in PBS before being heat-killed at 80$^{o}$C for 1 hour in a N-Biotek NB-205 shaking incubator (N-Biotek, UK). To determine successful heat-killing, 50µl of bacterial suspension was re-plated into respective media and incubated anaerobically for 7 and 3 days for *P. gingivalis* and *F. nucleatum* and 4 – 6 days for *T. denticola*. Visible absence of growth indicated successful heat killing of bacteria. Heat-killed bacterial suspensions were then stored at $4x10^{8}$ in 1ml aliquots at -20$^{o}$C.

### 2.3.2 Oxygen-killing

Bacteria were grown in respective media and overnight cultures were prepared as described in section 2.1. Bacteria were washed twice in PBS and then exposed to atmospheric oxygen for up to 48 hrs and plated onto respective agar plates every 2 hrs up to 8 hrs then at 24 and 48 hours. A 5µl volume disposable inoculating loop (Thermo Fisher Scientific, UK) was used to streak bacterial cultures on respective agars at the time points indicated. For *T. denticola,* mNOS medium was used to inoculate *T. denticola* at each time point to determine optimum time needed to oxygen-kill, as growth of *T. denticola* was more easily detected in mNOS medium than mNOS agar. The time required for each bacterium to be oxygen-killed was indicated by the absence of growth in the respective media following incubation. This timeframe was subsequently used for the oxygen killing of bacteria. Oxygen-killed bacterial suspensions were then diluted with PBS to produce a solution containing $4x10^{8}$ bacteria/ml, which was distributed into 1ml aliquots and stored at -20$^{o}$C prior to use.

## 2.4 Characterisation of periodontal pathogens

### 2.4.1 Gram staining

A single colony of bacteria was harvested from their respective agar plates and emulsified into a single drop of PBS (0.5ml) on a clear glass microscope slide (Fisherbrand, UK). After air-drying it was heat-fixed on a hot plate (Corning PC-420D, USA) at 100ºC for 1 minute and allowed to cool before being flooded with 0.3% crystal violet (Prolab, diagnostics, UK) for 1 minute. This was rinsed with $dH_2O$ and then flooded with iodine solution (Prolab, diagnostics, UK) for 1 minute and then rinsed with $dH_2O$ again. The slide was then treated with decolourizer (Prolab, diagnostics, UK) for 5 seconds and rinsed with $dH_2O$. This was followed by counter-staining with 0.25% safranin (Prolab, diagnostics, UK) for 30 seconds and rinsed with $dH_2O$. Following staining the slide was dried using absorbent tissue paper and viewed using oil-immersion microscopy at 100x objective magnification and images were captured under the Olympus® BX50 microscope (Olympus, UK) using the QImaging camera (Teledyne Imaging, USA). Pink staining indicated Gram-negative bacteria whereas purple staining would indicate Gram-positive bacteria and possible contamination by another species.

### 2.4.2 Bacteria identification by polymerase chain reaction (PCR)

To further characterise bacteria, PCR was utilised to amplify specific genes for each bacterial species. The primer sequences used in this study were obtained from existing literature (see Table 2.1). $1x10^6$ bacteria was suspended in 1µl molecular biology grade water (Corning, USA) with 12.5µl REDTaq ReadyMix PCR reaction mix, 10.5µl molecular biology grade water and 0.5µl each of the forward and reverse primer (25µM). The amplification was performed in GeneAMP® PCR system 2700 (Applied Biosystems, USA) and initial denaturation was undertaken at 94ºC for 5 mins which also served to lyse bacteria. A

specified number of cycles including a denaturing step at 94$^{o}$C for 20 secs followed by a primer annealing step (specific temperature provided in Table 2.1) and an extension step at 72$^{o}$C for 20 secs, were performed. Finally, an extension step at 72$^{o}$C for 10 mins was undertaken.

**Table 2.1**: Primers and PCR conditions used to identify bacteria

| **Bacterial species (*gene*)** | **Primer sequence (5' → 3')** | **Number of cycles** | **Annealing conditions** | **Source** |
|---|---|---|---|---|
| *Porphyromonas gingivalis (16s rRNA)* | F - AGGCAGCTTGCCATACTGC<br>R - ACTGTTAGCAACTACCGATGT | 40 | 55$^{o}$C for 30 secs | (Mahendra et al., 2013) |
| *Fusobacterium nucleatum 10953 (16s rRNA)* | F - CTAAATACGTGCCAGCAGCC<br>R - CGACCCCCAACACCTAGTAA | 33 | 55$^{o}$C for 20 secs | (Külekçi et al., 2001) |
| *Treponema denticola* 35405 (16s rRNA) | F-TAGTCATGCGAATAAGCCCC<br>R-TTGCTACGCTGCCATATCTC | 40 | 60$^{o}$C for 1 min | (Külekçi et al., 2001) |

#### 2.4.2.1 Visualisation of PCR product by gel electrophoresis

During PCR product synthesis a 1.5% agarose gel was prepared by dissolving 0.9g molecular grade agarose (Bioline, UK) in 60ml tris-acetate ethylenediamine tetraacetic acid (EDTA) electrophoresis buffer (TAE; Thermo Fisher Scientific, UK) and heated for 2 minutes in a Sharp Easy Chef II microwave (Sharp, Japan) at 850W until completely dissolved. After heating, the mixture was immediately cooled by gently swirling under cold tap water until safe to handle without heat-resistant gloves. Five µl of highly sensitive Invitrogen™ SYBR™ safe DNA gel stain, which is a safer alternative to ethidium bromide for DNA visualization, was added to the solution before being poured into a gel tray with a comb to generate 4mm wide loading wells. Once the gel had set at room temperature, 5µl of PCR products were loaded into wells and 5µl of Quick-Load® 100 bp DNA ladder (New England BioLabs®, UK) was also loaded to determine product bp length. Gels were then electrophoresed using a VWR® 300V gel electrophoresis power supply (Avantor, USA) set at 120V for 30 mins in a VWR® electrophoresis tank (Avantor, USA) filled with 1x TAE. Products were then visualised under transillumination (EtBr/UV filter) using a Syngene G:BOX HR (SynGene, UK) gel doc system and images were captured using the GeneSnap software (SynGene, UK).

### 2.5 Scanning electron microscopy (SEM) sample preparation

SEM was performed on live, heat and oxygen-killed bacteria to further analyse the effects of both types of preparation on bacterial morphology. Nunc™ Thermanox® coverslips (Thermo Fisher Scientific, UK) were placed in 24 well plates (Thermo Fisher Scientific, UK) and artificial saliva was added into each well prior to adding bacterial cultures. Artificial saliva was used to mimic the dental pellicle (composed mainly of salivary proteins), which is essential for oral biofilm formation and bacterial adhesion (Darrene and Cecile, 2016).

Bacterial cultures were then grown on artificial saliva coated coverslips and some cultures were heat or oxygen-killed prior to being fixed and processed for SEM analysis.

### 2.5.1 Artificial saliva

0.35g sodium chloride, 0.2g potassium chloride, 0.2g calcium chloride ($CaCl_2$), 2g yeast extract, 1g Oxoid™ lab lemco powder (Thermo Fisher Scientific, UK), 2.5g hog gastric mucin (Type III, partially purified) and 5g Bacto™ Proteose peptone (Thermo Fisher Scientific, UK) was added sequentially to 1L $dH_2O$ whilst being mixed with a magnetic stirrer. This was mixed for 1hr and then autoclaved. After autoclaving, 1.25ml of 40% sterile filtered urea was then added and prepared media was wrapped in foil and stored at 4$^oC$ to exclude light and prevent protein degradation.

Artificial saliva (200µl) was added into each well for 20 minutes and then removed and 1ml of overnight cultures were added to each well. Single species biofilms were grown for 3 days and samples were then prepared for SEM.

- Culture medium was removed carefully, and biofilms were rinsed in 3x PBS to ensure culture medium was completely removed.
- Samples were then fixed in 2.5% EM grade glutaraldehyde in 0.1M sodium cacodylate buffer, pH 7.3 for 10 minutes. 10ml of fixative was prepared using 4ml $dH_2O$, 5ml of 0.2M sodium cacodylate buffer pH 7.3 (Agar Scientific, UK) and 1ml of 25% EM grade glutaraldehyde (Agar Scientific, UK).
- After fixation, samples were dehydrated using increasing concentrations of ethanol at 20, 30, 40, 50, 60, 70, 90, 95 twice and 100% twice for 10 mins each time.
- Alcohol was then removed by using a VWR® plastic transfer pipette and hexamethyldisilazane (HMDS) was added to samples in a fume cupboard due to

toxicity. Samples were completely covered with HMDS and its addition was undertaken relatively quickly to ensure samples did not become desiccated. HMDS was allowed to evaporate overnight in a fume cupboard.

Once the samples were dry, coverslips were removed from wells and placed on carbon tabs stuck to aluminium stubs which were connected with copper tape and placed in a Quorum Emitech K550X automatic sputter coater (Quorum Technologies Ltd, UK) and gold coated twice. An Edwards RV3 vacuum pump (Edwards, UK) was connected to the sputter coater to create a vacuum in the sputter coaters gas chamber.

Gold coated samples were then placed in the Zeiss Evo MA10 (Zeiss, Germany) scanning electron microscope and SEM images were captured at 15kV accelerating voltage using second electron imaging.

### 2.6 Cell Culture

#### 2.6.1 Culture of H400 cells

H400 cells (ECACC 06092006) were from a human oral squamous cell carcinoma (OSCC) first isolated from a 55 year old female patient's squamous cell carcinoma of the alveolar process. H400 cells with passages between 23 and 26 were removed from liquid nitrogen storage and rapidly thawed in a pre-warmed water bath at 37$^{o}$C for 30-60 secs. After rapid thawing, cells were transferred to a Falcon tube containing 1ml of growth media under aseptic conditions inside a class II tissue culture cabinet (Monmouth Scientific, UK). Growth medium consisted of Dulbecco's modified Eagle's medium (DMEM) with 2.5mM L-Glutamine supplemented with 25µl 10mg/ml hydrocortisone, 10ml penicillin/streptomycin (0.0365% final concentration) and 10% foetal bovine serum (FBS) (Biosera, UK). Cells were then centrifuged (Jouan, UK) at 1000rpm for 5 mins until a pellet was formed and supernatant was

removed. The resulting cell pellet was re-suspended in 1ml of growth medium and transferred into a T75 Nunc™ EasYFlask (Thermo Fisher Scientific, UK) flask containing 15ml of growth medium and placed in a humidified Heracell™ 150i $CO_2$ incubator (Thermo Fisher Scientific, UK) at 37ºC with 5% $CO_2$. Cells were checked daily using an inverted Zeiss Primovert microscope (Zeiss, Germany) to assess culture health and monitor degree of confluency. Growth media was replaced every 2 days and cells were sub-cultured (passaged) once cultures had reached 80% confluence.

### 2.6.2 Sub-culturing

Growth media was first removed from cell cultures and cells washed twice with 5ml pre-warmed sterile PBS to remove DMEM and FBS as this may inhibit the action of trypsin. PBS was then removed and 5ml pre-warmed 0.25% trypsin-EDTA was applied to cells and placed in the incubator at 37ºC for 10 mins, or gently agitated periodically until cells were completely detached from the surface of the flask and this was observed through microscopic examination. Enzymatic activity of trypsin was stopped by adding equal amounts of medium supplemented with 10% FBS to cell suspension. Cell suspension was then centrifuged at 1000rpm for 5 min to form a pellet. The supernatant was then removed and the pellet re-suspended in 10ml of pre-warmed growth media and desired number of cells transferred to a T75 Flask with 15ml growth medium and incubated at 37ºC with 5% $CO_2$.

### 2.6.3 Cryopreservation

H400 cells were cryopreserved to maintain a low passage number to enable use in future studies. Following trypsinisation, $1x10^6$ cells were suspended in 1ml of cryomedia which consisted of 700µl DMEM, 200µl FBS and 100µl dimethyl sulfoxide (DMSO). Vials were labelled appropriately and stored at -80ºC overnight before being transferred to long term storage in the vapour phase of liquid nitrogen.

## 2.7 Cell counts and viability

### 2.7.1 Manual cell counting and viability assay using haemocytometer

Manual cell counts were performed using a haemocytometer (Improved Neubauer, Hawksley, UK). For H400 cells grown in hypoxic condition, cells were incubated in a New Brunswick Galaxy 48R (Eppendorf, Germany) hypoxia chamber at 37$^{o}$C with 1.8% oxygen and 5% $CO_2$, prior to measuring cell counts and viability from day 4-8. H400 cell cultures were trypsinised using 0.25% trypsin-EDTA until cells were completely detached as determined by microscopic examination and the reaction deactivated by addition of equal volumes of DMEM supplemented with 10% FBS. The mixture was centrifuged at 1000rpm for 5 mins and the supernatant was removed. The remaining cell pellet was re-suspended in fresh growth media. A volume of 100µl of suspended cells were pipetted into an Eppendorf containing an equal volume of Trypan blue (0.4%) and vortex mixed (Starlab, UK) to ensure uptake of dye into cells. A cover slip moistened with exhaled air was applied on top of the haemocytometer and confirmation of visible Newton's diffraction rings was ensured to confirm correct application. After, 10µl of thoroughly mixed trypan blue cell suspension was pipetted beneath the edge of the cover slip and the counting chamber filled through capillary action. The haemocytometer was examined using a phase contrast microscope (Primovert, Zeiss, Germany) at 10x magnification and cells in the primary square were counted with the middle line of the three lines being the boundary. Cells touching right and lower lines were not counted whereas cells touching top and left lines were to ensure consistency throughout the counts. Viable cells do not stain blue whereas non-viable cells stain blue because of a damaged cell membrane (Tran et al., 2011). Viable and non-viable cells were counted to determine the percentage of viable cells from 3 wells with 6 counts from each well resulting

in a total of 18 readings. Subsequently, mean cell counts and percentage cell viability was calculated.

### 2.7.2 Automated cell counting and viability assay using Tecan Spark®

The Tecan Spark® multimode microplate reader uses Cell chips™ to perform high throughput label free automated cell counts and determination of cell viability. A bright-field cell imaging module present in the Spark® detects cells through differences in absorption fields of cells compared with its surroundings. The use of Cell chips™ was explored to count cells more rapidly when compared with manual cell counting.

H400 cells were trypsinised and re-suspended in Trypan blue as explained in section 2.7.1. A volume of 10µl of cell suspension was pipetted into both loading chambers of the Cell chip™ adapter. A total of 4 Cell chips™ could be placed in the Cell chip™ adapter resulting in a maximum of 8 counts per run. The adapter was placed in the microplate holder of the Tecan Spark® and cell counting protocol was selected with the correct cell size of 13µm entered to ensure only cells were counted. Cell chips™ values for cell counts and % cell viability were highly variable as indicated in section 3.7.1. Therefore, the haemocytometer counting method was used for all future experiments.

## 2.8 Exposure of oral keratinocytes to oral pathogens

Oral H400 keratinocytes were seeded at $1x10^4$ cell seeding density in 6-well plates and stimulated by the three periodontal pathogens *P. gingivalis*, *F. nucleatum* and *T. denticola*. Bacteria were either heat or oxygen-killed and applied to cell monolayers at a ratio of 100 bacteria per oral epithelial cell to mimic the ratio identified in the periodontal pocket (Dierickx et al., 2002). The bacteria to epithelial cell ratio was maintained by addition of bacteria every 2 days to compensate for increased H400 cell number. The number of bacteria

needed to be added at each time point was determined from a previously generated growth curve that determined cell number at each time point over an 8-day period. LPS from Gram negative bacteria has been shown to induce EMT in previous studies using oral epithelial cells, therefore LPS was used as a positive control in this study (Jing et al., 2012 and Ding et al., 2020b). A ready-made solution of 1mg/ml *E. coli* LPS serotype O26:B6 was applied to cells at a final of concentration of 20µg/ml.

### 2.9 Enzyme-linked Immunosorbent Assay (ELISA)

This study investigated release of cytokines IL-1β (Li et al., 2012), IL-8 (Wen et al., 2019) and TGF-β1 (Chen et al., 2017b) which have been shown to promote EMT in previous studies. All ELISA kits (R&D systems, UK) contained the streptavidin conjugated to horseradish-peroxidase (Streptavidin-HRP), recombinant standards and capture and detection antibodies. The DuoSet ELISA ancillary reagent kit 2 (R&D systems, UK) contained the reagents and consumables required to perform ELISA for IL-1β and IL-8 whilst the DuoSet ancillary reagent kit 1 (R&D systems, UK) and sample activation kit 1 (R&D systems, UK) was needed to perform ELISA for TGF-β1. Recombinant standards, capture and detection antibodies were all prepared according to manufacturer's instructions and stored at -20$^{o}$C until needed. Pro-inflammatory cytokine levels were measured in supernatants collected at days 1, 5 and 8 from H400 cells challenged with heat or oxygen-killed bacteria and performed in clear high-binding, flat-bottom polystyrene 96-well microplates provided in the ancillary reagent kits.

#### 2.9.1 IL-1β and IL-8 ELISA protocol

The capture antibody was diluted to its working concentration with the supplied PBS and 100µl was added per well and left overnight at room temperature. Wash buffer was also prepared by adding 24ml of 25x wash buffer to 576ml of deionised water. Wells were then

washed three times using the Biotek ELx50 automatic plate washer (Biotek, USA) and then blocked by adding 300µl of 1x reagent diluent 2 (1% BSA in PBS, pH 7.2-7.4) per well and incubated for 1 hour at room temperature. After 1 hour, wells were washed 3 times using the plate washer followed by adding 200µl of standards at working concentration to wells A1-3 and 100µl of 1x reagent diluent 2 to wells B1-H1, B2-H2 and C3-H3. Standards were then serially diluted by transferring 100µl into each well and mixing by pipetting up and down and this was done up to wells G1-3 and H1-3 which were left as blanks. 100µl of supernatants were then added to wells and left for 2 hours at room temperature until being washed again 3 times using the automatic plate washer. After washing, 100µl of detection antibody at working concentration was added per well and left for 2 hours until being washed 3 times. 100µl Streptavidin HRP at working concentration was then added per well and left for 25 mins at room temperature and then washed 3 times. After this, 100µl of an equal ratio of substrate solution A and substrate solution B was added to each well and left for 25 mins in the dark at room temperature. This was followed by a final step of adding 50µl of stop solution per well. Absorbance values were determined using a Biotek ELx800 microplate reader (Biotek, USA) at wavelengths 450nm and 570nm. The absorbance values obtained at the 570nm wavelength were background readings and were subtracted from the 450nm values to obtain true absorbance readings.

### 2.9.2 TGF-β1 ELISA protocol

Capture antibody was diluted to its working concentration and 100µl was added to each well and left to incubate overnight at room temperature. Wells were then washed three times and blocked using 300µl of 1x reagent diluent 3 (25% Tween 20 solution in PBS) for 1 hour at room temperature. Wells were then washed three times and 200µl of standards at working

concentration and 100µl of 1x reagent diluent 1 were added to wells and serially diluted as previously described in the IL-1β and IL-8 protocol. Samples were first activated before addition to wells by adding 20µl of 1N HCL to 100µl of supernatants and then mixing well before being incubated for 10 mins at room temperature. After, acidified samples were neutralised by adding 20µl of 1.2N NaOH/0.5M HEPES and checking the pH was between 7.2-7.6 before adding to wells for 2 hours at room temperature. The assay was then completed as described in the IL-1β and IL-8 protocol in section 2.9.1. As the samples were diluted the final concentration of TGF-β1 was multiplied by 1.4 to determine the actual cytokine concentration present in the cell supernatants.

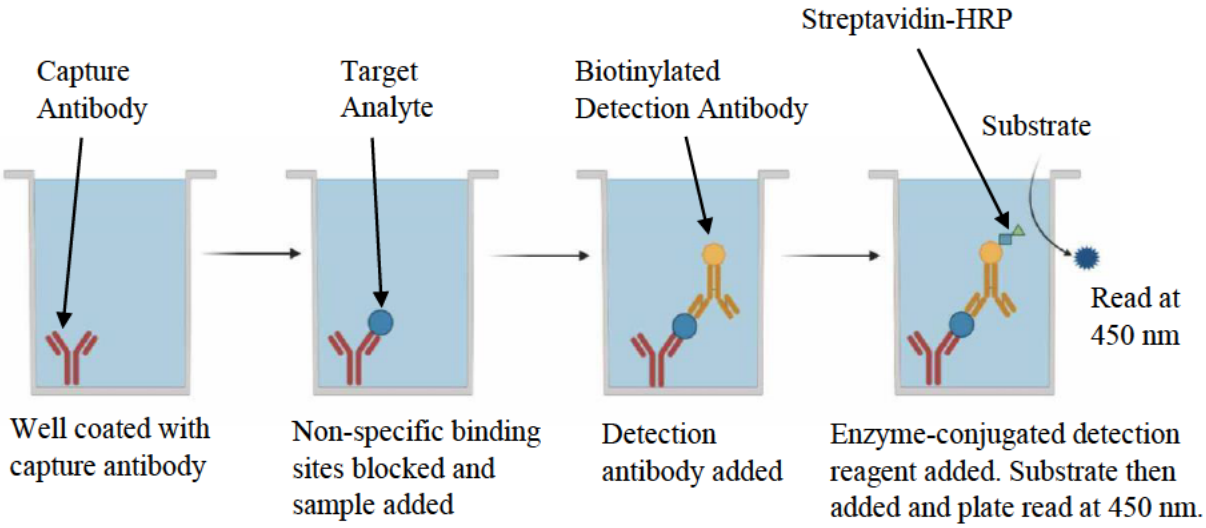



**Figure 2.2**: Overview of sandwich ELISA protocol used in this study to detect presence of secreted EMT-inducing pro-inflammatory cytokines (created with Biorender.com).

## 2.10 Polymerase chain reaction assay

This study utilised quantitative real time polymerase chain reaction (qRT-PCR) to assess for any key EMT related gene expression changes in day 8 H400 cultures challenged with heat and oxygen-killed bacteria and the methods are detailed below. Gene expression analysis was performed using LightCycler® 480 SYBR green I master fluorescent dye (Roche, UK) and Roche LightCycler® 480 system (Roche, UK). White LightCycler® 480 96 well plates (Roche, UK) tailor made for the LightCycler® 480 instrument were used to perform qRT-PCR.

### 2.10.1 H400 cell culture preparation for qRT-PCR

Firstly, oral keratinocytes were seeded in T75 flasks at $5x10^4$ cells in 20ml DMEM media supplemented with 10% FBS. Cultures were challenged after 24 hrs post-seeding with 20μg/ml *E. coli* LPS, heat or oxygen-killed bacteria for 8 days. Media was not changed during the 8-day challenge period to allow for build-up of inflammatory markers that aims to mimic the chronic inflammatory nature of periodontitis.

### 2.10.2 Cell lysis

After the 8-day incubation period cell lysates were obtained for ribonucleic acid (RNA) extraction. Firstly, media was removed and cultures washed 3x with PBS and then trypsinised until all cells had detached. Once detached trypsin was deactivated with equal amounts of pre-warmed DMEM media supplemented with 10% FBS and then centrifuged at 1000rpm for 5 mins. The supernatant was removed and cells subsequently washed 3x with 10ml PBS before cells were lysed with 350μl buffer RLT which is provided in the RNeasy mini kit (Qiagen, UK). The RNA was extracted immediately or stored at -80$^o$C for future RNA extraction.

### 2.10.3 RNA extraction

RNA extraction was performed using the buffers and consumables provided in the RNeasy minikit (Qiagen, UK).

- Firstly, cell lysates were transferred to mini spin columns and an equal volume of 70% ethanol was added and centrifuged at 10000rpm for 30 seconds in an Eppendorf® 5415D digital centrifuge (Eppendorf, Germany). The resulting flow-through was discarded.
- 350μl of RW1 buffer was then added into each sample and spun at 10000rpm for 30 seconds and flow-through discarded.
- The next step involved DNase digestion which was performed to eliminate genomic DNA (gDNA) from total RNA preparations as trace amounts of DNA can lead to false positive detection of complimentary DNA (cDNA)-derived amplicons during sensitive amplifications such as RT-PCR. 10ul of deoxyribonuclease I (DNase I) was added to 70μl of DNase digest buffer provided in the On-Column DNase I digestion set (Sigma-Aldrich, UK). This was mixed well by gently inverting the tube (not vortexing as this leads to physical denaturation and decreased enzyme activity). The resulting mixture was then added to each sample and incubated at room temperature for 15 minutes.
- 350μl of RW1 buffer was then added to each tube and centrifuged as previously described and flow-through discarded.
- Next, 500μl of RPE buffer was added to each sample and centrifuged as before and flow-through discarded.
- 500μl of RPE buffer was then added to spin columns and centrifuged at 10000rpm for 2 mins and subsequent flow-through discarded.

- Samples were then centrifuged at 13100rpm for 1 min to remove remaining alcohol and the spin columns were transferred to new collection tubes.
- 30µl of RNA free water was added to the columns and centrifuged at 10000rpm for 1 min to elute the RNA.

### 2.10.4 RNA quantification

The RNA amount and purity were determined using the Jenway® Genovanano spectrophotometer (Cole-Parmer®, UK). Settings on the spectrophotometer were changed to output RNA concentration in µg/ml and purity values were assessed using the absorbance ratio of 260/280nm ($OD_{260/280nm}$). RNA has a purity value of 2.0 but values between 1.8-2.1 are generally accepted as pure and can be used in downstream applications. The spectrophotometer was first blanked using 2µl of RNase free water. Once blanked, upper and lower read heads were cleaned using lint free cloth before addition of RNA. 2µl of RNA sample was then pipetted on the lower read head ensuring there were no bubbles present in the sample and concentration and purity was measured. A total of 3 measurements were taken for each sample and the average used as the final RNA concentration.

### 2.10.5 cDNA conversion

Extracted RNA was then converted to cDNA using the Tetro cDNA conversion kit (Bioline, UK) and the steps followed are outlined below:

- Firstly, solutions were vortexed and briefly centrifuged before use to ensure all contents were suspended in the tube and not in the lid.
- The priming premix was then prepared on ice in an RNase-free reaction tube by adding 1µl oligo $(dT)_{18}$, 1µl 10mM dNTP mix, 4µl 5x RT buffer, 1µL ribosafe RNase inhibitor, 1µl tetro reverse transcriptase (200u/µl) which was prepared for each

sample. 8µl of mastermix was added to 1-1.5µg of RNA plus DEPC-treated water to make a total of 20µl.

- Samples were then incubated for 1 hour at 45ºC annealing temperature in an GeneAMP® PCR system 2700 (Applied Biosystems, USA).
- The enzymatic reaction was then terminated by incubating at 85ºC for 5 minutes followed by incubation at 4ºC to allow for short term storage to maintain product integrity.
- Then 50µl RNase free water was added to produce a total of 70µl cDNA.
- Samples were either stored at -20ºC for long term storage or qRT-PCR was performed immediately.

### 2.10.6 Determining primer efficiency:

Before performing real-time PCR, the amplification efficiency of each primer was calculated which is an important consideration for relative quantitation as calculations with incorrect efficiency values leads to inappropriate correction factors resulting in over or underestimated starting concentrations (Liu and Saint, 2002). An optimum primer efficiency is considered as 2.0 which assumes that PCR product concentration doubles with every cycle during the exponential phase of the reaction (Gibson, Heid and Williams, 1996). However, primer efficiency values ranging between 1.8 and 2.2 (equivalent to 90% to 110%) are considered acceptable as stated in MIQE (Bustin et al., 2009) and manufacturer guidelines (Roche Diagnostics GmbH, 2011). To test primer efficiencies, cDNA from each sample to be tested was pooled and serial dilutions (100%, 50%, 10%, 1%, 0.1% and 0%) were prepared from this using RNase free water. A real-time assay was performed in duplicate for each dilution and primer and efficiency was calculated using the LightCycler® 480 software version 1.5 (Roche, UK). The purity of reaction products following real-time qPCR was also assessed by

melt curve genotyping analysis with multiple melt peaks indicating the presence of nonspecific DNA products or primer-dimers (Fisher et al., 2000).

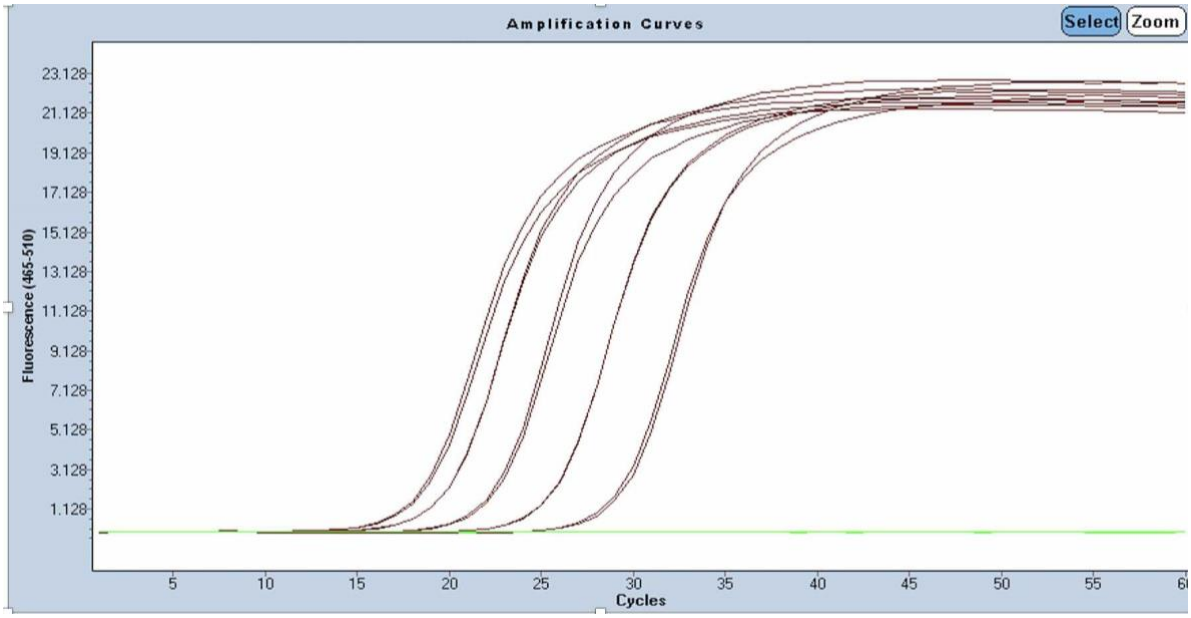



**Figure 2.3**: qRT-PCR amplification curves for housekeeping gene GAPDH for serially diluted pooled cDNA (100%, 50%, 10%, 1%, 0.1% and 0%) to determine primer efficiency.

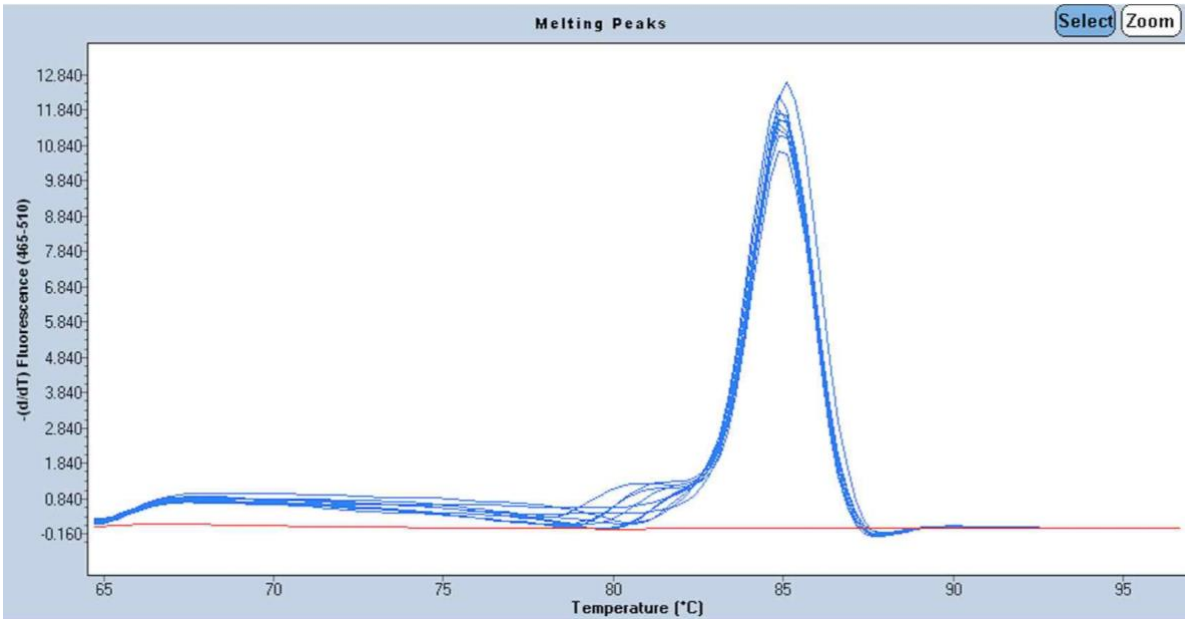



**Figure 2.4**: Melting curve of GAPDH produced using meltcurve genotyping analysis shows the presence of a single melting point suggesting that the desired target was amplified. If multiple melting points had been shown this would indicate amplification of multiple targets which implies that primers are inefficient and primers would need to be redesigned or assays optimised.

### 2.10.7 Identification of a suitable housekeeping gene

The BestKeeper (Pfaffl et al., 2004) statistical analysis tool supplied as an add-on for Excel (Microsoft, US) was used to determine the best housekeeping gene (HKG). A total of 4 HKGs: β-actin (ACTB), β2-microglobulin (B2M), tyrosine 3-monooxygenase/tryptophan 5-monooxygenase activation protein zeta (YWHAZ) and GAPDH were tested and the most stable housekeeping gene was selected as determined by a SD <1. The GAPDH housekeeping gene was selected as the most suitable gene for normalisation to ensure correct gene expression analysis of target genes.

### 2.10.8 Gene expression analysis of target genes

The target genes used and primer sequences are outlined in Table 2.4. To determine gene expression levels of target genes in samples, 96 well LightCycler® 480 microplates were prepared with a final well volume of 10µl. Each well consisted of the components outlined in Table 2.2.

**Table 2.2**: List of reagents and volumes used in each well for quantitative real-time PCR of target genes.

| **Component** | **Volume (µl)** |
|---|---|
| SYBR green I master fluorescent dye | 5 |
| Forward primer | 0.05 |
| Reverse primer | 0.05 |
| PCR grade water | 3.9 |
| cDNA | 1 |

Once samples were loaded as duplicates, plates were sealed with a plastic sealing foil and centrifuged at 3200rpm (Hettich 320R, Germany) for 2 mins to ensure all liquid remaining in the wells were captured. Plates were then loaded into the plate holder of the Lightcycler® 480

PCR machine and PCR performed using the run set-up outlined in Table 2.3. Analysis of gene expression levels were automatically performed using the second derivative maximum method available in the LightCycler® 480 version 1.5 software. The Cp values and inputted efficiency values generated previously were used to perform calculations on gene expression changes which were presented as fold changes.

**Table 2.3**: PCR conditions used at each stage to perform real time PCR for target genes.

| **Stage** | | **Temperature (°C)** | **Time (mins)** | **Number of cycles** |
|---|---|---|---|---|
| **Pre-incubation** | | 95 | 5:00 | 1 |
| **Amplification** | **Denaturation** | 95 | 0:20 | 60 |
| | **Annealing** | 60 | 0:20 | |
| | **Extension** | 72 | 0:30 | |
| **Melting curve** | | 97 | Continuous until complete | 1 |
| **Cooling** | | 40 | 0:30 | 1 |

**Table 2.4**: Human genes and primer sequences used to perform quantitative RT-PCR and accession numbers were obtained from GenBank. The efficiency values shown represent how well each primer amplifies its target each PCR cycle with 2.0 denoting 100% efficiency.

| **Gene name** | **Gene symbol** | **Accession number** | **Sequence (5'→3')** | **Product (bp)** | **Efficiency** |
|---|---|---|---|---|---|
| Glyceraldehyde-3-phosphate dehydrogenase | *GAPDH* | AJ005371 | F-TCTAGACGGCAGGTCAGGTCC<br>R-CCACCCATGGCAAATTCCATG | 1102 | 1.973 |
| E-cadherin | *CDH1* | NM_004360 | F-CAAGTGCCTGCTTTTGATGA<br>R-GCTTGAACTGCCGAAAAATC | 339 | 2.144 |
| Cytokeratin-5 | *CK5* | NM_000424.4 | F-CCAAGCCAATTGCAGAACCA<br>R-AAATTTGGGATTGGGGTGGG | 199 | 1.986 |
| Desmoplakin-1 | *DPI* | NM_001008844.3 | F-TGCCCCAAAACCAAATTAAA<br>R-AGCAACCACTCCCAACTGAC | 313 | 1.871 |
| N-cadherin | *CDH2* | NM_001792. 3 | F-GCCCGGTTTCATTTGAGGGCACA<br>R-TGACGGCCGTGGCTGTGTTT | 418 | 1.887 |
| Snail-1 | *SNAI1* | NM_005985. 3 | F-CGGACCCACACTGGCGAGAAG<br>R-CAGCTGCCCTCCCTCCACAGA | 433 | 2.132 |
| Snail-2 | *SNAI2* | NM_003068. 4 | F-CAACGCCTCCAAAAAGCCAA<br>R- GGCCAGCCCAGAAAAAGTTG | 1145 | 2.071 |
| Vimentin | *VIM* | NM_003380. 3 | F-CGGGAGAAATTGCAGGAGGA<br>R-ACGAAGGTGACGAGCCATTT | 588 | 2.076 |

| | | | | | |
|---|---|---|---|---|---|
| Twist family bHLH transcription factor 1 | *TWIST1* | NM_000474 | F-AGACCTAGATGTCATTGTTTCCAGA<br>R-CAGGCCAGTTTGATCCCAGT | 454 | 2.08 |
| Matrix metalloproteinases 9 | *MMP-9* | NM_004994. 2 | F-TTCGACGGGAAGGACGGGCT<br>R-ACCGTCGAGTCAGCTCGGGT | 470 | 1.966 |
| Transforming growth factor-β1 | *TGF-β1* | NM_014266 | F- CGCCTTAGCGCCCACTGCTCCTGT<br>R-GGGGCGGGACCTCAGCTGCAC | 533 | 1.897 |
| Interleukin-8 | *IL-8* | NM_000584. 2 | F-TAGCAAAATTGAGGCCAAGG<br>R-GGACTTGTGGATCCTGGCTA | 205 | 2.046 |
| Interleukin-1β | *IL-1β* | NM_000576. 2 | F-TCCAGGGACAGGATATGGAG<br>R-TTCTGCTTGAGAGGTGCTGA | 2250 | 1.815 |

## 2.11 Cell migration assays

This study utilised two different methods of gap generation to measure rate of oral epithelial cell migration after exposure with heat or oxygen-killed bacteria and the most suitable cell migration assay was selected based on creation of a consistent initial cell free gap area and uniformity of the wound. This allowed for more reliable comparisons between control and test wound areas ultimately improving assay reproducibility.

### 2.11.1 Mitomycin C preparation and determining optimum mitomycin C concentration

A 0.5mg/ml stock solution of mitomycin C (Roche, UK) was prepared in $dH_2O$ and filter sterilised using a 0.22µM pore size MF-Millipore™ membrane filter (Merck Millipore, Ireland) and needleless syringe (Terumo® corporation, Philippines) prior to storage in the dark at $4^oC$ until needed. Mitomycin C has been used widely in epithelial cell migration studies to inhibit proliferation; therefore, closure of the wound would be due to migration and not proliferation (Yang et al., 2011; Glenn, Messner and Meldrum, 2016). H400 cells ($1x10^4$) were seeded in 6 well plates and grown to confluence and cells were then treated with differing mitomycin C concentrations of 0, 2, 4, 6, 8 and 10µg/ml for 2 hours. The exposure period of 2 hours was selected because 5µg/ml mitomycin C exposure for 2 hours has previously shown to inhibit proliferation without affecting cell viability (Shikatani et al., 2012). Therefore, the optimum mitomycin C concentration was determined by selecting the highest concentration before a decrease in cell viability was observed which may indicate mitomycin C having a toxic effect (Kabiri et al., 2019; Varankar and Bapat, 2018). Cell viability was determined using the Trypan blue exclusion viability assay as outlined in 2.7.1.

### 2.11.2 Scratch wound assay

H400 cells were initially grown in T75 flasks, passaged and re-seeded into 6-well plates at a cell seeding density of $1x10^4$ per well with 5ml supplemented DMEM. Cells were then challenged with either heat or oxygen-killed bacteria for 8-days at an 100:1 multiplicity of infection (MOI). Cultures were then treated with 8 μg/ml mitomycin C for 2 hours to inhibit proliferation before washing three times with PBS to completely remove mitomycin C. A scratch wound was introduced through the centre of the monolayer using a sterile 10μl pipette tip and was performed in one quick and steady movement to ensure a linear and even wound gap was produced. Cultures were then washed twice with PBS to remove any cell debris caused by scratching and 2ml serum free media was added and images captured at 0, 12 and 24 hours using the 10X objective of an inverted Zeiss Primovert microscope with Axiocam ERc 5s HD camera attached (Zeiss, Germany). The correct reorientation of wound areas to be imaged were ensured by visible markings drawn on the bottom of the plate.

### 2.11.3 Cell migration assay using culture-inserts

H400 cells were seeded at $1x10^4$ cells per well in a 6-well plate and exposed to heat or oxygen-killed bacteria for 8 days at a 100:1 MOI. After the exposure period, cells were trypsinised and $7.5x10^5$ cells were reseeded into each well of two well tissue inserts (Ibidi, Germany), which were self-inserted using sterile forceps into a 6-well plate. Following attachment, cells were treated with 8μg/ml mitomycin C for 2 hours to further inhibit proliferation. After treatment, media was aspirated, and cells cultures were washed three times with PBS to ensure full removal of mitomycin C. The inserts were then carefully removed using sterile forceps making sure cell cultures were not disrupted and 2ml serum free media was added to wells and images were captured at 0, 12, 24 and 48 hours using the 4x objective of the Nikon Eclipse TE300 phase contrast microscope (Nikon, Japan). The cell free

gap was measured using the MRI wound healing tool plug-in available on the open-source image analysis software ImageJ (Schneider, Rasband and Eliceiri, 2012) as shown in Figure 2.5. Images were captured from 4 different areas for each time point and correct reorientation of wound areas was ensured by visible markings drawn on the bottom of the plate.

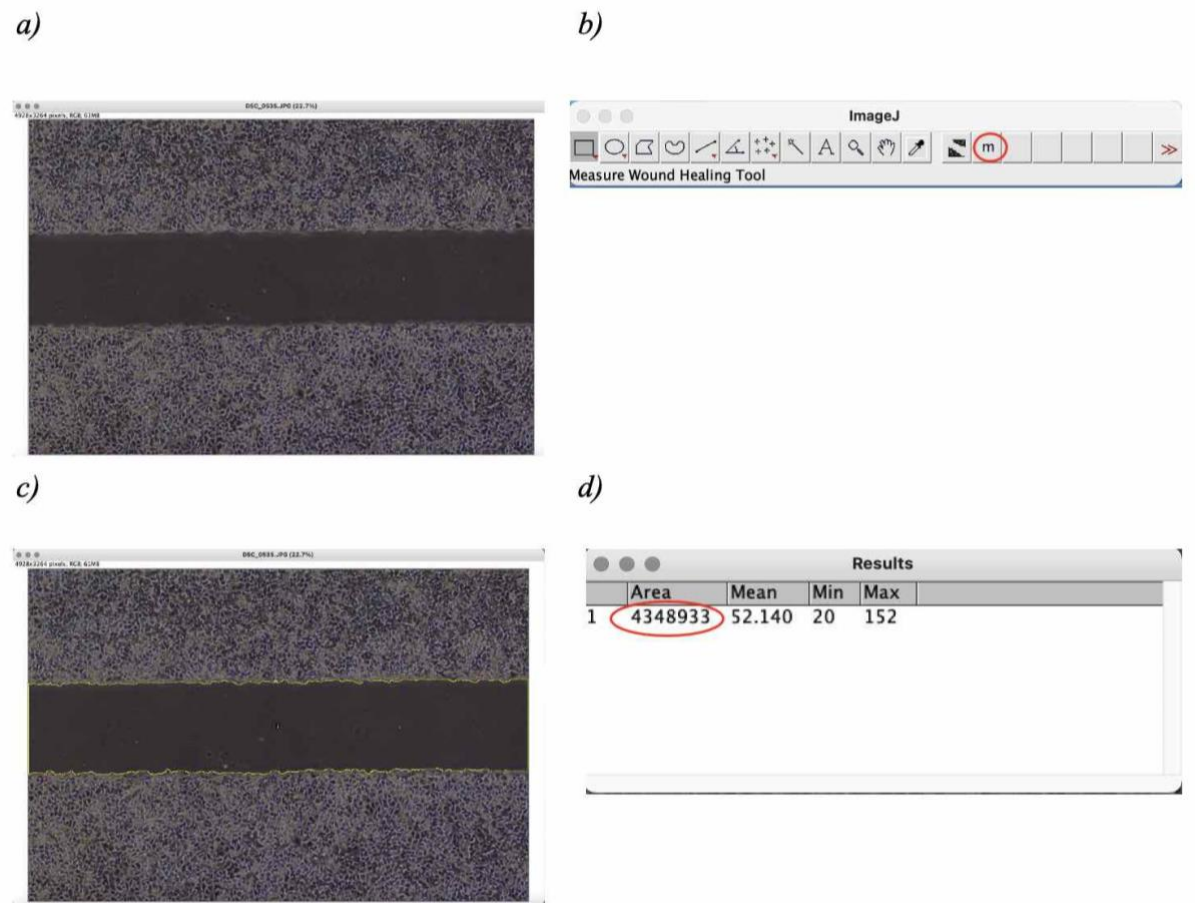



**Figure 2.5**: Cell culture images acquired for cell migration analysis using ImageJ. (a) Cell culture images were loaded into the image analysis software ImageJ, (b) the MRI wound healing tool as highlighted by the red circle was selected to measure the cell free gap area. The area measured was then shown by a yellow outline in (c). (d) displays a separate pop-up 'results' tab which includes cell free gap area shown in square pixels as highlighted by the red oval.

### 2.12 Trans-epithelial electrical resistance

Trans-epithelial electrical resistance (TEER) measurements have been widely used in the last two decades as the most efficient way to evaluate growth and epithelial cell barrier integrity in 2D epithelial cell models *in vitro* (Srinivasan et al., 2015). The EVOM2™ epithelial ohm meter and STX2 electrodes (World Precision Instruments, USA) were used to measure resistance across epithelial monolayers challenged with either HK or OK bacteria as outlined in Figure 2.6. Loss of cell-cell attachment would lead to decreased resistance readings when compared with intact monolayers (control) as current passes more easily through intercellular spaces than a confluent epithelial sheet.

#### 2.12.1 TEER protocol

H400 cells were seeded at $7x10^4$ in 0.4µm pore tissue culture inserts (Grenier, Bio-one, UK) placed in a 24 well plate. 200µl of supplemented DMEM media was added to inserts and 500µl into the wells. Inserts containing media only were used as blanks. 20µg/ml *E. coli* LPS, HK or OK bacteria at 100:1 MOI were added to cultures and TEER readings were recorded daily from day 2 to day 8. The media in the insert and wells were replaced every 2 days as it was noted in initial studies that as media is utilised by cells, electrical resistance is also reduced. TEER readings were measured using the EVOM2™ epithelial ohmmeter and STX2 electrodes. Before being used, both STX2 electrodes were disinfected by placing in 70% ethanol for 20 mins before rinsing with growth media and used for TEER readings. The outer electrode (outer pair) was carefully placed in the insert ensuring the cell monolayer was not disrupted and the inner electrode (inner pair) was placed in the well so that the electrode touched the base of the well each time to increase reproducibility of readings (see Figure 2.6). The outer electrode passes current through the cell monolayer which was detected by the inner electrode and resistance was recorded once stable values were displaying on the

EVOM2™ device. Both electrodes were held vertically and flexing or angling of the electrodes was avoided as this can affect resistance measurements. Electrodes were rinsed with growth media before taking readings from different samples to avoid contamination.

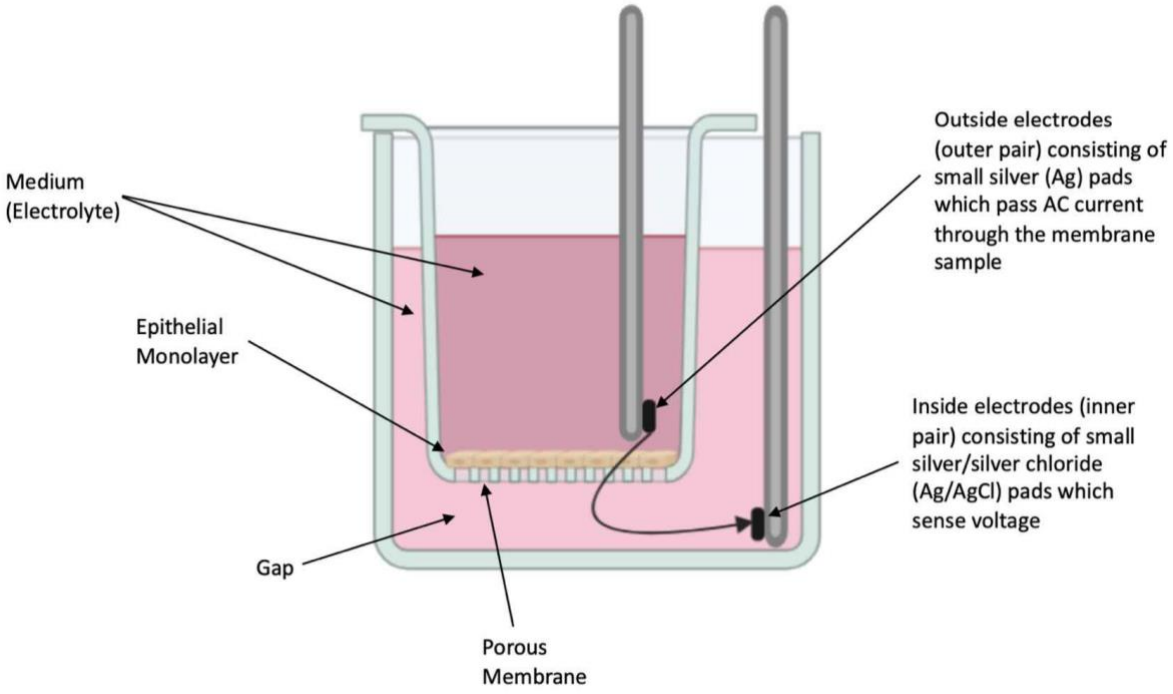



**Figure 2.6**: Diagram of how TEER was measured using the EVOM2™ epithelial voltohmmeter and STX2 electrodes. TEER was measured across an epithelial monolayer seeded within a tissue insert mounted in a 24 well plate (created with Biorender.com).

### 2.13 Immunofluorescence

Immunofluorescence (IF) staining was performed to assess changes in protein levels of key EMT markers E-cadherin, snail and vimentin after HK or OK bacterial challenge. Initially, 22mm glass coverslips (Chance Propper LTD., UK) were sterilized and placed in 6 well plates and $1x10^4$ H400 cells seeded on top for 8-day culture with HK or OK bacteria as outlined in section 2.8 or without bacteria (media only control). The human EMT 3-colour immunocytochemistry kit (R&D systems, USA) consisting of fluorochrome-conjugated antibodies outlined in Table 2.5 were used to stain samples for E-cadherin, snail and vimentin. After 8-day challenge with bacteria, cell cultures were first fixed and then stained in non-sterile conditions.

**Table 2.5**: Fluorochrome-conjugated antibodies provided in the R&D human EMT 3-colour immunocytochemistry kit used to stain for EMT markers E-cadherin, snail and vimentin.

| **Antibody** | **Fluorochrome-NorthernLights™ (NL)** | **Absorption maximum (nm)** | **Emission maximum (nm)** |
|---|---|---|---|
| Anti-human Snail NL557-Conjugated Goat IgG | NL557 | 493 | 514 |
| Anti-human E-Cadherin NL637-Conjugated Goat IgG | NL637 | 557 | 574 |
| Anti-human Vimentin NL493-Conjugated Rat IgG2A | NL493 | 637 | 658 |

#### 2.13.1 Positive and negative controls

The 3T3 fibroblast cell line is a mesenchymal cell line of murine embryonic origin (Todaro and Green, 1963) and was used as a positive control as it has been shown to express EMT markers snail (Francí et al., 2006) and vimentin (Feliksiak et al., 2020). As with the other assays, cells treated with 20µg/ml *E. coli* LPS were used as a positive control as LPS can

induce EMT in epithelial cells detected through increased vimentin and snail-1 expression whilst simultaneously decreasing E-cadherin expression (Jing et al., 2012; Abdulkareem et al., 2017).

Negative control slides were prepared by cultures in media only and weren't exposed to LPS or HK and OK bacteria. In addition, slides stained by excluding each primary antibody were utilised as negative controls. These slides would show no signal intensity when acquiring an image during confocal microscopy and was used for calibrating the microscope for future image analysis. This would also ensure that any non-specific binding and false-positive signals were excluded by the secondary antibody.

### 2.13.2 Staining procedure

In a fume hood (Premier Laboratory Systems, UK), cell culture media was removed using a VWR® plastic transfer pipette and 800µl 4% paraformaldehyde in PBS (PFA, Alfa-Aesar, USA) was added to each well for 10 mins ensuring complete coverage of the cover slips. PFA was then removed from each well using a transfer pipette and cultures were washed 3x with PBS making sure cells do not dry out as this can lead to unreliable staining intensities caused by an uneven spread of antibodies on the cell layer. To ensure staining of intracellular proteins snail and vimentin, cells were permeabilised with 0.5% Triton™ X-100 for 10 mins ensuring limited exposure as prolonged exposure of Triton™ X-100 can be toxic to cells. Cells were then washed 3x with PBS ensuring PBS was completely removed before addition of 800µl blocking solution into each well for 1 hour. Blocking solution was prepared by adding donkey serum to PBS in a 1:5 ratio. Blocking solution was then removed but samples were not washed with PBS after this step. Antibody diluent was then prepared using 20ml PBS, 0.6g BSA and 10µl Tween-20 (Thermo Fisher Scientific, UK) and all three antibodies (snail, E-cadherin and vimentin) supplied at 10x stock were diluted to working concentration

(1x) in antibody diluent. 100µl of antibodies were then added to each coverslip for 2 hours at room temperature in the dark. After 2 hours, coverslips were removed from the wells and mounted onto clear glass microscope slides (Fisherbrand, UK) using Invitrogen™ fluoromount mounting medium with DAPI (Thermo Fisher Scientific, UK). This was left to set for 1 hour or until the cover slip was fully mounted to the glass slide and stored at 4°C in the dark until needed. Images were then acquired using x63 oil immersion objective on the Zeiss LSM 710 confocal microscope (Zeiss, Germany).

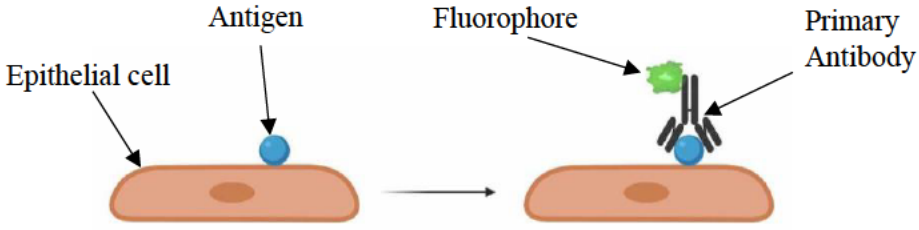
### 2.13.3 Determining localisation of snail-1

To determine the localisation of snail in the nucleus after OK *T. denticola* exposure, H400 cells were also stained with Invitrogen™ human upstream binding factor-1 (UBF-1) rabbit IgG polyclonal unconjugated antibody (Thermo Fisher Scientific, UK), which binds nucleolar organizer regions (NORs) in the nucleolus. This was applied to cells at a 1/100 dilution in antibody diluent alongside conjugated snail antibody outlined in Table 2.5. It was ensured that both primary antibodies were of different species as secondary antibodies will detect both conjugated and unconjugated primary antibodies leading to cross-reactivity. Cover slips were then washed 3x with PBS after 2 hour incubation with both conjugated and unconjugated primary antibodies. A volume of 100µl fluorescein isothiocyanate (FITC) labelled secondary goat anti-rabbit IgG antibody (Abcam, UK) was then applied to cover slips at 1/500 dilution in secondary antibody diluent which consisted of 0.05g BSA, 4.5ml PBS, and 500µl (10% of total volume) of AB plasma. Cells were stained with secondary antibody for 1 hour in the dark at room temperature and then washed 3x with PBS before being mounted onto clear glass microscope slides using Invitrogen™ fluoromount mounting medium with DAPI. Stained samples were stored at 4°C in the dark until needed and images were then acquired

using x63 oil immersion objective on the Zeiss LSM 710 confocal microscope (Zeiss, Germany).

The same staining procedure described above (see 2.13.2), using the antibodies outlined in Table 2.5, was repeated on 3T3 cells, which was used as one of the positive controls in this study.

**Direct Immunofluorescence**




**Indirect Immunofluorescence**

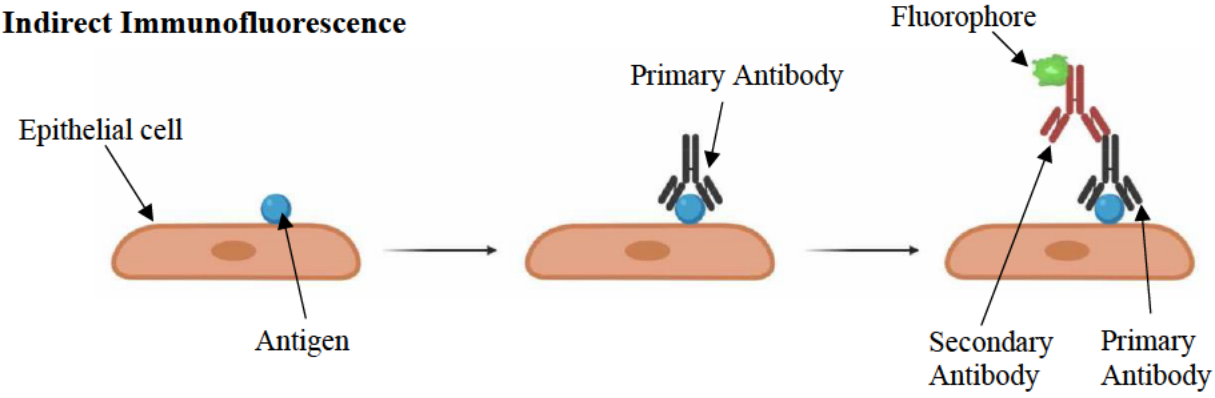



**Figure 2.7**: Overview of the methodology behind the two types of immunofluorescence techniques used to stain for EMT markers e-cadherin, snail-1 and vimentin and to determine co-localisation of snail-1 using upstream binding factor-1 (UBF-1) (created with Biorender.com).

### 2.14 Curcumin addition to inhibit bacterial-induced EMT

Curcumin is one of the main active ingredients in turmeric and it has been shown to inhibit EMT in many studies using epithelial cells (Hu et al., 2015; Lee et al., 2015; Xu et al., 2015). Curcumin was employed in this study to inhibit the migratory, gene expression and epithelial barrier changes seen after bacterial exposure. Curcumin is known to be poorly soluble in water but is soluble in organic solvents such as DMSO or bases such as sodium hydroxide (NaOH) (Farooqui and Farooqui, 2019; Kurien and Scofield, 2007). Therefore, curcumin was dissolved in two solutes DMSO with PBS and NaOH with PBS in this study. Both curcumin preparations were prepared and used in the dark due to its light sensitivity. Initially the effects of different curcumin concentration dissolved in DMSO with PBS on epithelial cell growth and viability were assessed. Data indicated that the use of DMSO with PBS resulted in cell toxicity, therefore curcumin dissolved in NaOH and PBS was used in further studies to inhibit EMT. Curcumin concentrations at 5µM (Chhunchha et al., 2011; Ferreira et al., 2015) and 10µM (Hollborn et al., 2013; Platania et al., 2018) have shown to be effective in epithelial cells without affecting cell viability, therefore these were selected along with higher and lower concentrations to determine the optimum curcumin concentration needed for use in the 8-day EMT model.

#### 2.14.1 Curcumin preparation and optimisation

##### 2.14.1.1 Curcumin dissolved in DMSO with PBS

A 10mM solution of curcumin in 90% PBS/10% DMSO was prepared and the solution was mixed by vortexing and heated at 37$^{o}$C a water bath (Gem Scientific, UK) to accelerate the solubilisation of curcumin. Curcumin was fully dissolved by indication of a dark orange solution without any precipitation. This solution was filter sterilised and distributed in 1ml aliquots and stored at -20$^{o}$C in the dark until needed. Ten(mM) curcumin and filter sterilised

DMSO was then used to prepare 500µl master stocks of 0µM, 5µM, 10µM, 15µM, 20µM and 50µM curcumin. Twenty-five(µl) of each concentration of curcumin was then added to cells creating a final DMSO concentration of 0.5%. Cell growth and viability was then measured using the method described in section 2.7.1

#### 2.14.1.2 Curcumin dissolved in NaOH with PBS

To determine the optimum concentration of NaOH with PBS for use in oral epithelial cell cultures, concentrations ranging from 0.05M to 0.5M were prepared. NaOH was dissolved in PBS by vortexing and then filter sterilised to create concentrations of 0.05M, 0.1M, 0.15M, 0.2M, 0.25M, 0.3M, 0.35M, 0.4M, 0.45M and 0.5M. A volume of 25µl of each concentration was added to cells. The Alamar Blue assay as described in section 2.14.1.2.1 was used to measure cell viability on day 8 cultures.

The optimum concentration of 0.15M NaOH with PBS for 8-day oral keratinocyte exposure was determined by the Alamar Blue assay and subsequently used to dissolve curcumin for use in further studies. A 0.5M NaOH solution was initially prepared in 200ml $dH_2O$. A 10mM solution of curcumin in 0.15M NaOH was prepared by 30% 0.5M NaOH/70% PBS and then filter sterilised and fully dissolved. From this, 500µl stock concentrations of 1µM, 2.5µM, 5µM, 10µM, 15µM, 20µM curcumin were prepared by diluting in 0.15M NaOH with PBS and 25µl was added to each well. This ensured that equal amounts of NaOH with PBS were added to each well. Cell growth and viability was then measured from day 4-8 as described in section 2.7.1 and the Alamar Blue reagent assay was used to confirm cell viability as described below.

#### 2.14.1.2.1 Measuring cell viability using Alamar Blue

Resazurin, the active ingredient in Alamar Blue, changes from blue to red when added to viable cells, this colour change is caused by the reducing environment when viable cells are present. The magnitude of this colour change can be detected by measuring absorbance at 570nm and 600nm wavelengths which measure the reduced and oxidised environment respectively. An amount of 0.015g of Invitrogen™ Resazurin (Thermo Fisher Scientific, UK) was dissolved by vortexing in 15ml PBS. This was then filter sterilised and stored at 4°C in the dark until needed. After 8 days, culture media was removed and 10% Alamar Blue in 2ml serum free media was added to each well for 4 hours and incubated in a humidified Heracell™ 150i $CO_2$ incubator (Thermo Fisher Scientific, UK) at 37°C with 5% $CO_2$. Serum free media was used as FBS has shown to interfere with the assay (Goegan, Johnson and Vincent, 1995). Absorbance was then measured at 570nm and 600nm using the Tecan Spark® and number of viable cells was calculated using Equation 2.1.

$$Percentage\ of\ viable\ cells\ relative\ to\ control = \frac{(O2\ X\ A1) - (O1\ X\ A2)}{(O2\ X\ P1) - (O1\ X\ P2)} \times 100$$

*Where:*

*O1 = molar extinction coefficient (E) of oxidized Alamar Blue at 570nm which was 80586*

*O2 = E of oxidized Alamar Blue at 600nm which was 117216*

*A1 = absorbance of test wells at 570nm*

*A2 = absorbance of test wells at 600nm*

*P1 = absorbance of positive growth control well (Alamar Blue with cells and without test agent) at 570nm*

*P2 = absorbance of positive growth control well (Alamar Blue with cells and without test agent) at 600nm*

**Equation 2.1**: Equation used to calculate % cell viability from 600nm and 570nm absorbance values attained by the Tecan Spark® after 4hrs staining with Alamar Blue.

### 2.15 Analysis of curcumin EMT inhibition

Curcumin was applied to oral epithelial cell cultures 1-day after cell seeding along with OK bacteria as outlined in section 2.8 and cell growth/viability was initially assessed using the method described in section 2.7.1. The ability of curcumin to inhibit cell migration was then evaluated using the methodology for the 2-well insert wound migration assay described in section 2.11.3 and gene expression profiling for key EMT related genes was performed using the steps outlined for qRT-PCR in section 2.10. In addition, the effect of curcumin to increase TEER readings across an epithelial monolayer after bacterial challenge was evaluated using the method explained in section 2.12.

### 2.16 Mass spectrometry of live, heat and oxygen-killed *Treponema denticola*

The effects of heat and oxygen-killing *T. denticola* were further explored by quantitative mass spectrometry-based proteomics. This was performed on live, HK and OK *T. denticola* outer membrane proteins using Thermo Scientific tandem mass tags (TMT ™) which are isobaric compounds meaning they have the same mass and structure with a different number of heavy isotopes. Each mass tag/label has a signature mass peak which can be used for sample identification and to compare the relative abundance of target proteins. The outer membrane proteins were first isolated before being denatured, reduced, alkylated and digested with trypsin. Once digested with trypsin, peptides were TMT™ labelled live, HK or OK *T. denticola* in duplicate and then combined. Labelled proteins were then desalted for removal of salts and urea to improve peptide ionization efficiency during mass spectrometry analysis. After desalting, peptide samples were speed vacuum dried and sent to University of Birmingham's advanced mass spectrometry facility for liquid chromatography tandem mass spectrometry analysis (LC-MS/MS).

### 2.16.1 Isolation of outer membrane

*T. denticola* was cultured in 70ml mNOS medium by inoculating with 3-4 representative colonies under anaerobic conditions as previously described in section 2.1. Cultures were then either heat or oxygen-killed as described in section 2.3 and treated cultures were then stored in PBS at -20ºC until needed. Prior to cell lysis, 350µl (1/200) protease inhibitor cocktail powder for use with bacterial extracts was added to cultures and mixed by inverting the tube. This was to improve the yield of intact proteins by inhibiting any unwanted enzyme activity. Protease inhibitor was initially prepared by adding 5ml DMSO and 20ml $dH_2O$ to the lyophilized powder. Cells were thoroughly re-suspended before being lysed in a Avestin EmulsiFlex-C3 high pressure homogenizer (Avestin, Inc., Canada) at 100 MPa and the sample collected on ice. This was performed three times with a further aliquot of 140µl protease inhibitor added after the first passage. Unbroken cells were then removed by centrifugation at 6000g for 15 mins at 4ºC. The supernatant was the 'cell soluble' sample whilst the pellet was the 'cell membrane'. The pellet was thoroughly re-suspended in 5ml cold PBS using a MSE Soniprep 150 ultrasonic processor (MSE, UK) connected to a 3mm tapered microtip at 21% amplitude for 2 mins. The suspension was then collected in a 15ml Falcon tube and stored at -80ºC until needed.

### 2.16.2 Bicinchoninic acid (BCA) assay

The amount of protein in each sample was quantified using a BCA assay. Firstly, standards were prepared by adding bovine serum albumin (BSA) 2mg/ml protein standard to PBS as per the volumes outlined in Table 2.6 and added in duplicates into a 96 well plate. Samples were first diluted 1:10 with $dH_2O$ as visual cloudiness indicated high amounts of protein. Ten-µl diluted samples were loaded in triplicate into wells alongside the standards. BCA reagent was then prepared by adding bicinchoninic acid solution to copper sulphate solution in the ratio

50:1. A volume of 200µl reagent was then added to standards and samples and incubated for 30 mins at 37ºC and absorbances read at 570nm wavelength in a Tecan Spark® multimode microplate spectrophotometer (Tecan Group Ltd., Switzerland). A standard line was constructed by plotting absorbance (y-axis) against the known quantity in the standards (x-axis) and the unknown sample absorbances were converted to µg of protein from the standard line.

**Table 2.6**: Volumes of BSA and PBS needed to prepare standards for BCA assay to quantify amount of protein in each sample.

| Standard (µg) | Volume of BSA (µl) | Volume of PBS (µl) |
|---|---|---|
| 10 | 5 | 5 |
| 8 | 4 | 6 |
| 6 | 3 | 7 |
| 4 | 2 | 8 |
| 2 | 1 | 9 |
| 0 | 0 | 10 |

### 2.16.3 Filter-aided sample preparation (FASP) digestion

One-ml per sample of urea (UA) was prepared by adding 8M urea in 0.1M Tris/HCl at pH 8.5. A protein extract of 100µg was mixed with 200µl UA in the micron centrifugal filter ultracel PL-30 (Merck Millipore, Ireland) and centrifuged at 14,000 x g for 15 mins in an Eppendorf® 5418 R centrifuge (Eppendorf, Germany) to unfold protein. Another 200µl UA was added to filter units and centrifuged at 14,000 x g for 15 mins and flow-through was discarded from the collection tubes. A volume of 0.1M triethylammonium bicarbonate (TEAB) was prepared by adding 1M TEAB (Thermo Fisher Scientific, UK) to 9ml of $dH_2O$ and added to each filter unit which acted as a buffer to wash out UA from the filter. Tris (2-carboxyethyly) phosphine (TCEP) at 200mM concentration was then prepared by adding 70µl

0.5M TCEP (Thermo Fisher Scientific, UK) to 70µl ultrapure water and 35µl 1M TEAB. Ten-µl of TCEP was then added to each filter and incubated at 55ºC for 1 hour. Temperatures above 60ºC were avoided as urea-based carbamylation of lysines and protein N-termini can occur. A volume of 0.1ml per 1 sample of indole-3-acetic acid (IAA) solution was then prepared by adding 0.05M iodoacetamide in UA. Then, 100µl IAA was added to each filter unit and combined at 600 rpm in an Eppendorf® 5350 thermomixer (Eppendorf, Germany) for 1 min and incubated without mixing for 20 mins in the dark. After incubation, filter units were centrifuged at 14,000 x g for 10 mins and then 100µl UA was added and centrifuged at 14,000 x g for 15 mins, the addition of UA and centrifugation was repeated twice. A volume of 100µl of TEAB was then added to filter units and centrifuged at 14,000 x g for 10 mins and this was repeated twice. Then, 40µl TEAB with trypsin was added and mixed at 600 rpm in a thermomixer for 1 min and incubated in a wet chamber at 37ºC for 18 hrs. Filter units were then transferred to new collection tubes and centrifuged at 14,000 x g for 10 mins. A volume of 40µl TEAB was then added and centrifuged at 14,000 x g for 10 mins and collected sample was made up to 100µl with TEAB in preparation for TMT labelling.

### 2.16.4 Fluorometric peptide assay

The Pierce quantitative fluorometric peptide assay kit (Thermo Fisher Scientific, UK) was used to perform the fluorometric peptide assay to quantify protein concentration present in samples. Firstly, kit components were equilibrated to room temperature before opening and loading. Peptide digest assay standards were serially diluted as per Table 2.7 so a standard curve (Fluorescence vs µg/ml) can be generated and unknown sample protein concentrations could be extrapolated. The standards were diluted using the same diluent in the sample which was TEAB in this study.

**Table 2.7**: Volumes of diluent and digest assay standard needed to prepare peptide digest assay standards for fluorometric analysis to determine sample protein concentrations.

| Centrifuge tubes | Volume of diluent (µL) | Volume of digest assay standard (µL) | Final standard concentration for peptide mixture (µg/mL) |
|---|---|---|---|
| A | 0 | 150 of stock | 1000 |
| B | 75 | 75 of A | 500 |
| C | 75 | 75 of B | 250 |
| D | 75 | 75 of C | 125 |
| E | 75 | 75 of D | 62.5 |
| F | 75 | 75 of E | 31.25 |
| G | 75 | 75 of F | 15.6 |
| H | 75 | 75 of G | 7.8 |
| Blank | 75 | 0 | 0 |

Ten-µl each standard or sample were loaded in duplicate into wells of a black, fluorescent-compatible 96-well microplate (Thermo Fisher Scientific, UK). Then, 70µl fluorometric peptide assay buffer was added to each well, followed by 20µl fluorometric peptide assay reagent then incubated at room temperature for 5 mins. Fluorescence was then measured using excitation/emission at 390nm/475nm in a Tecan Spark® spectrophotometer and peptide concentrations of each unknown sample were calculated using the standard curve.

### 2.16.5 TMT™ labelling protocol

The TMTsixplex™ contains six labels which were used to label live, HK and OK *T. denticola* in duplicate as per Table 2.8. Immediately before use the TMTsixplex™ isobaric label reagent set, 1 x 0.8mg (Thermo Fisher Scientific, UK) TMT™ label reagents were equilibrated to room temperature and 41µl anhydrous acetonitrile was added to each tube. The reagent was allowed to dissolve for 5 mins with vortexing and then briefly centrifuged to combine all the

solution. Twenty-five-µg of each reduced and alkylated protein digest was carefully added to 41µl of each TMT™ label reagent and incubated for 1 hour at room temperature. Eight-µl of 5% hydroxylamine was added to each sample and incubated for 15 mins to quench the reaction. All samples were then combined in a new microcentrifuge tube before being desalted with a Sep-pak® C18 plus light cartridge filter (Waters, UK).

**Table 2.8**: TMTsixplex™ mass tagging reagents (labels) used to label live, heat-killed and oxygen-killed *T. denticola* prior to LC-MS/MS analysis to identify and quantify target proteins.

| **Label/Mass tag** | ***T. denticola*** |
|---|---|
| $TMT^6$ – 126 (yellow vial) | Live |
| $TMT^6$ – 127 (red vial) | Live |
| $TMT^6$ – 128 (blue vial) | Heat-killed |
| $TMT^6$ – 129 (orange vial) | Heat-killed |
| $TMT^6$ – 130 (purple vial) | Oxygen-killed |
| $TMT^6$ – 131 (green vial) | Oxygen-killed |

### 2.16.6 Desalting with Sep-pak filter

After isolation of peptides, salts and buffers may still remain which can affect mass spec analysis. Desalting with Sep-pak® C18 plus light cartridge filter was utilised to capture peptides whilst salts and buffers were washed off. The Sep-pak cartridge was connected to a needleless syringe and initially washed with 4ml 100% acetonitrile (ACN). It was then conditioned with 1.5ml 50% ACN/0.5% acetic acid (HAcO) and equilibrated with 4ml 0.1% trifluoroacetic acid (TFA). The sample was then loaded and washed/desalted with 4ml 0.1% TFA. Following desalting, 1ml 0.5% HAcO was passed through to wash the sample before being eluted in 2ml 50% ACN/0.5% HAcO. Samples were transferred to Eppendorfs in 1ml aliquots and speed vacuum dried using an Eppendorf® concentrator plus speed vac (Eppendorf, Germany) until no liquid was present and then stored at -20ºC until needed.

### 2.16.7 Liquid chromatography tandem mass spectrometry (LC-MS/MS)

The TMT™ labelled sample was then processed for mass spectrometry 3 (MS3) analysis using a Thermo orbitrap eclipse mass spectrometer (Thermo Fisher Scientific, UK) equipped with a Advion TriVersa Nanomate® electrospray system (Advion Inc., USA) and Dionex™ direct nano-flow LC system (Dionex™, USA). Analysis was performed using a 1-hour LC gradient time and results were searched against the reviewed UniProt knowledgebase (UniProtKb) protein database (The UniProt Consortium) using the Proteome Discoverer™ version 2.4 software (Thermo Fisher Scientific, UK) and the Excel (Microsoft, US) file containing protein details and abundances was exported for analysis.

## 2.17 Statistical analysis

Statistical analysis for all data presented in this thesis was performed using GraphPad Prism 9 software (GraphPad, USA). Significance between two data sets obtained from the same cell culture, such as manual vs automatic cell counts/cell viability, was evaluated by paired t-test. Also paired t-test was performed to determine significant difference between live vs HK or OK *T. denticola* protein abundance. Whereas significance between two data sets from different cultures, such as cell viability on different days was evaluated by unpaired t-test. Significance between multiple groups was performed by one-way analysis of variance (ANOVA) followed by a *post-hoc* Tukey Test. Significance was considered when $P<0.05$ and was expressed as follows * = $P<0.05$, ** = $P<0.01$ and *** = $P<0.001$.

# 3. Periodontal pathogen characterisation and 2D oral epithelial model development for epithelial-mesenchymal transition analysis

## 3.1 Introduction

This chapter aimed to describe a suitable long-term 2D-oral epithelium model for the induction of EMT by periodontal pathogens using an immortalized H400 cell line. Bacteria that have been strongly associated with periodontitis were investigated. Red complex pathogens *P. gingivalis* and *T. denticola* are highly prevalent in patients with periodontitis (Scapoli et al., 2012) and *P. gingivalis* has demonstrated the potential to induce EMT along with the orange complex pathogen, *F. nucleatum* (Abdulkareem et al., 2017). *T. denticola* was selected because of strong associations with periodontitis and investigated to identify if it induced EMT in oral epithelial cells as it has been previously shown to induce IL-8 secretion (Okuda et al., 2007) and increased IL-8 expression is known to promote EMT (Zhao et al., 2017). Prior to undertaking cell-based studies, periodontal pathogens *P. gingivalis, F. nucleatum* and *T. denticola* were characterised by culture growth and colony morphology, Gram stain and PCR. This was to ensure use of non-contaminated stocks with the correct bacteria.

Long-term cell culture models of periodontitis have commonly utilised heat-killed bacterial pathogens as opposed to live bacteria, because of issues with contamination and bacterial overgrowth in long-term models using live bacteria (Cross et al., 2004 and Kim et al., 2015). However, heat killing is damaging to bacteria (see section 1.6) meaning bacteria-epithelial cell interactions would be unrepresentative of the subgingival bacterial – host interaction. There is more likely to be strict anaerobic bacteria killed by oxygen rather than heat in the gingival crevice and oxygen-killing should theoretically be less disruptive to bacteria than heat-killing. Therefore, oxygen-killing of anaerobic pathogens as a potential alternative to heat-killing was investigated.

An immortal H400 oral epithelial cell line was used as it has been used in several studies (Abdulkareem et al., 2017, Milward et al., 2007 and Grant et al., 2010) and is well characterised with similarities to gingival epithelium (Prime et al., 1990) indicating its suitability for use in this model system. An 8-day model where media was replaced every 2 days was selected based on previous experiments carried out by Abdulkareem et al. (2017) and that EMT was achieved in this time frame. However, during periodontitis there is cumulative release of cytokines in the sub-gingival pocket as a result of a persistent chronic inflammatory response (Yucel-Lindberg and Båge, 2013). This suggests a build-up of inflammatory markers and mediators in the sub-gingival region, therefore media replenishment in this cell culture model would suggest the removal of cytokines released at early stages and this would inaccurately represent the sub-gingival environment. Therefore, changes to media addition or using large volumes of media without replacing media were explored and effect on cell growth and cell viability were investigated.

The automatic cell counting method using the Tecan Spark® and Cell chips™ provides quicker results compared with the traditional method of manual cell counting using the haemocytometer. In addition, automated methods remove the issue of subjectivity that occurs with manual cell counting where variations in counts can occur between individuals. Therefore, cell number and cell viability readings were validated against the gold standard which is haemocytometer counting to determine if the automated approach could be utilised in on-going experiments.

It is known that established subgingival plaque mostly consists of anaerobic bacteria, suggesting that the periodontal pocket environment is anaerobic and previous studies have elucidated the oxygen tension ($pO_2$) within this region to be hypoxic at 1.8% oxygen

(Mettraux, Gusberti and Graf, 1983). Therefore, H400 cells cultured in 1.8% oxygen would provide similarities with the periodontal pocket environment and represent physiological conditions more closely than growing cells in atmospheric oxygen (21%). Considering this, H400 cell growth and viability were compared in cultures grown in hypoxia and normoxia to clarify whether hypoxic conditions could be used to better mimic the *in vivo* situation.

These characterisation steps to better mimic the clinical environment and the use of oxygen-killed bacteria would provide a more suitable and clinically relevant alternative to using heat-killed bacteria in inducing EMT in an 8-day 2D oral epithelial model.

## 3.2 Periodontal pathogen characterisation

### 3.2.1 Identification by culture

Periodontal pathogens *P. gingivalis*, *F. nucleatum* and *T. denticola* were grown on respective agars as outlined in section 2.1 until bacterial cultures were formed. This step would provide an initial basis for the identification of bacteria and would help confirm purity of the bacterial stock.

#### 3.2.1.1 Analysis of bacterial cultures

Figure 3.1 shows cultures of *a) P. gingivalis* ATCC 33277 and *b*) *F. nucleatum* ATCC 10953 grown on horse blood agar and *c) T. denticola* ATCC 35405 which was grown in a universal tube containing mNOS semi-solid agar. Cultures of *P. gingivalis* showed classical, black-pigmented colonies after 5-7 days growth in anaerobic conditions with β-haemolysis occurring in blood agar (zone of red cell lysis). *F. nucleatum* produced classic grey translucent colonies on horse blood agar with no signs of haemolysis (γ-haemolysis) after 2-3 days anaerobic growth. *T. denticola* produced typical white colonies in groups after 5-7 days anaerobic growth around the site of loop insertion

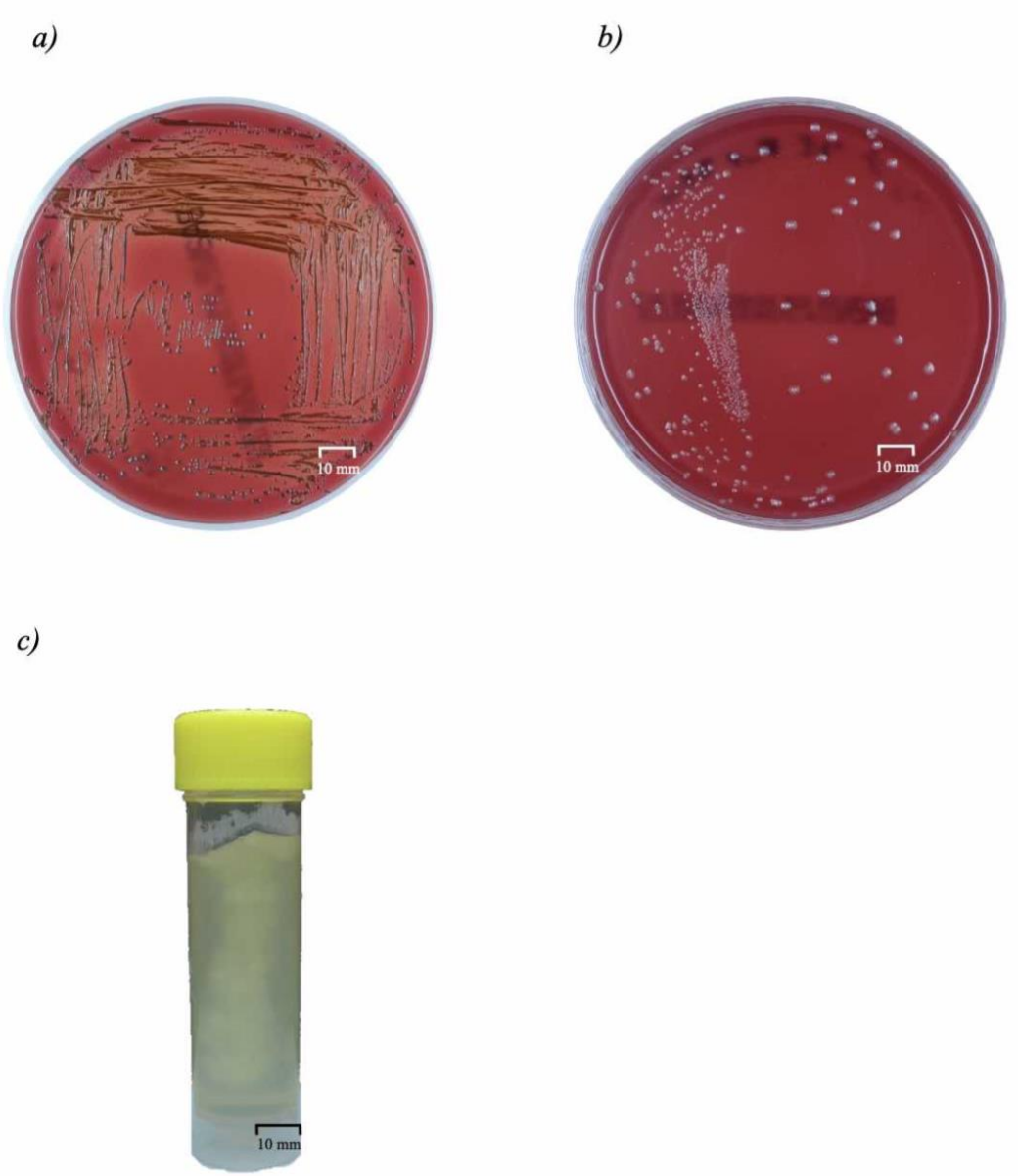



**Figure 3.1**: Photographs of periodontal pathogen cultures grown in anaerobic conditions at 37ºC. (a) *P. gingivalis* ATCC 33277 produced black-pigmented colonies with β-haemolysis and (b) *F. nucleatum* ATCC 10953 produced grey translucent colonies with no haemolysis occurring on horse blood agar. (c) *T. denticola* ATCC 35405 produced white grouped colonies in mNOS semi-solid agar. Scale bars = 10 mm.

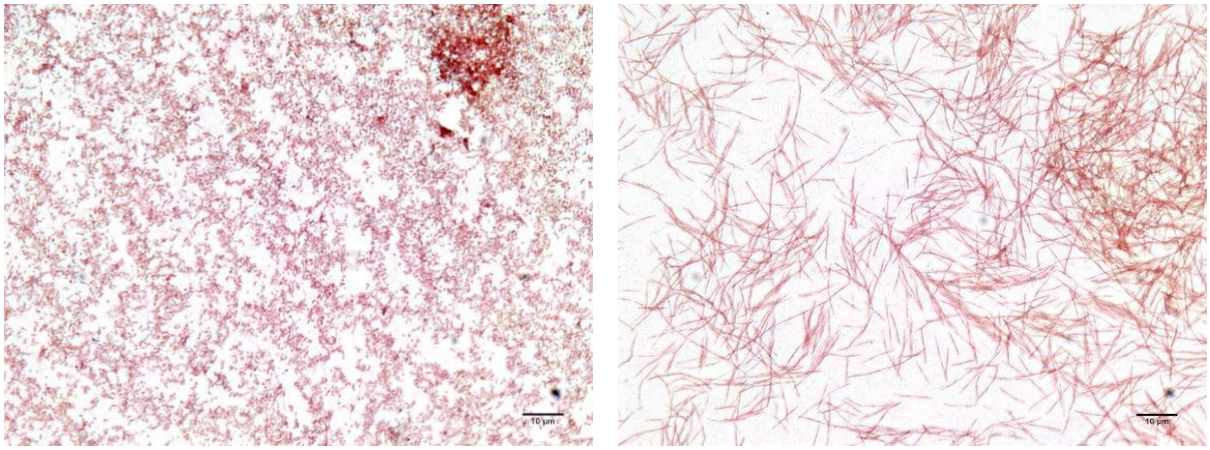
### 3.2.2 Characterisation by Gram stain

To further confirm the identity of pathogens, Gram staining was performed to determine the microscopic bacterial morphology (shape and cell wall composition). The pathogens used in this study were all Gram-negative.

#### 3.2.2.1 Analysis of Gram stains

Cultures proposed to be *P. gingivalis* stained red/pink and showed coccobacilli morphology (a shape intermediate between cocci (sphere) and bacilli (rod)) (Figure 3.2a). *F. nucleatum* also stained red/pink with long spindle-shaped rod morphology (Figure 3.2b) and *T. denticola* stained pink with long helical-shaped rod morphology (Figure 3.2c). In all the cultures examined, morphology and Gram staining supported that these were the correct bacteria and that there was no evidence of bacterial contamination.

*a)* *b)*



*c)*

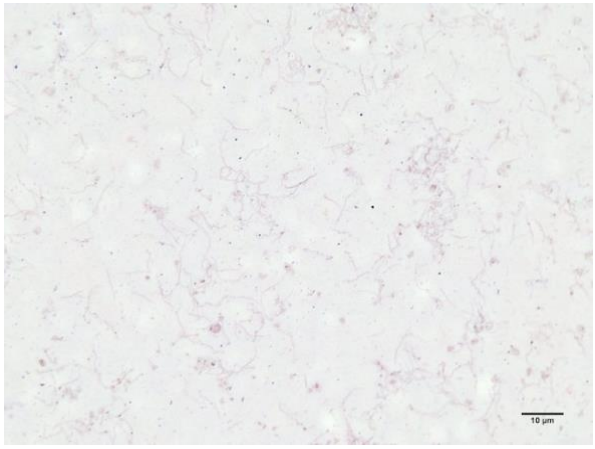


**Figure 3.2**: Representative Gram stain images of (a) *P. gingivalis* ATCC 33277, (b) *F. nucleatum* ATCC 10953 and (c) *T. denticola* ATCC 35405. A single colony of bacteria was acquired from the agar plate and emulsified in 50µl saline on glass slides. All three Gram negative bacteria stained red/pink with *P. gingivalis* having coccibacilli morphology whilst *F. nucleatum* morphology showed long, spindle shaped rods with sharp pointed ends. *T. denticola* morphology showed long helical-shaped rods. Scale bars = 10µm.

### 3.2.3 Characterisation by PCR

PCR was performed on *P. gingivalis*, *F. nucleatum* and *T. denticola* using the amplification conditions and species-specific primers outlined in section 2.4.2. This aimed to determine if the bacteria were indeed correct and to look at possible contamination with other bacterial species.

#### 3.2.3.1 Analysis of PCR results

From Figure 3.3 bands were present at 350, 300 and 550bp for *a) P. gingivalis*, *b) F. nucleatum* and *c) T. denticola* respectively, these bands were consistent with the primers specific to the individual bacterial strains, there were also no signs of additional bands which would signify contamination with other bacterial species. Results from these experiments (culture, morphology and PCR) provided confidence that the bacteria used were indeed the bacteria to be investigated and that no contamination was present. As a result, the bacteria were suitable for use in subsequent experimentation.

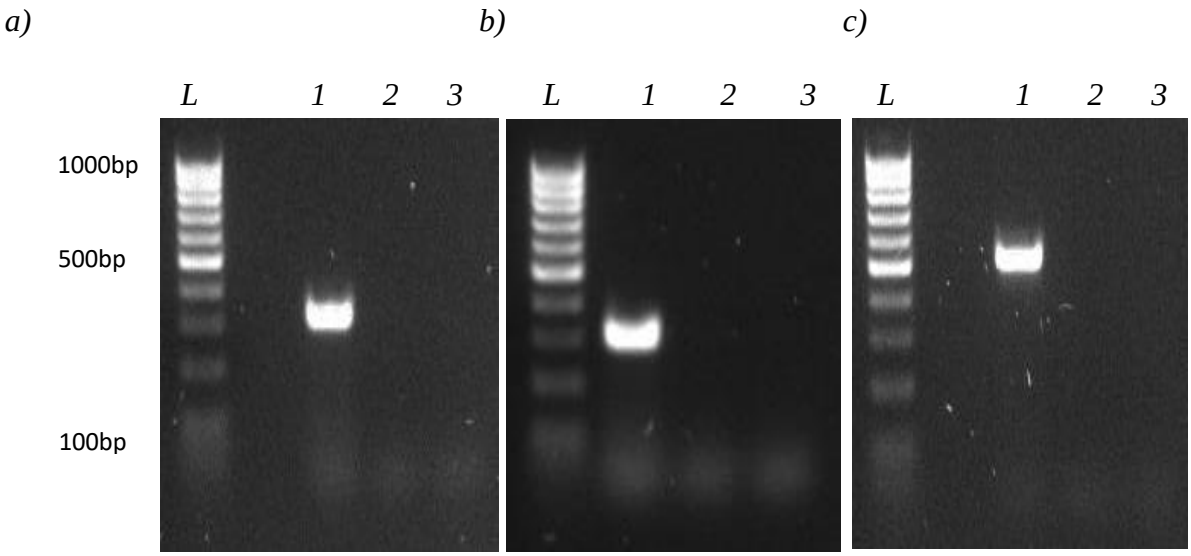



**Figure 3.3**: PCR amplification of species-specific genomic sequences in bacteria. 8µl of PCR product was electrophoresed on a 1.5% agarose gel stained with Invitrogen™ SYBR™ safe DNA gel stain. L represents the Quick-Load® DNA ladder and lane 1 contains PCR product of bacteria plus bacterial primer pairs only. Successful identification of bacteria by PCR is seen in (a) *P. gingivalis* ATCC 33277, (b) *F. nucleatum* ATCC 10953 and (c) *T. denticola* ATCC 35405 with bands present at 350, 300 and 550bp respectively. Lane 2 contains PCR product of bacterial primer pairs plus a different bacterium other than the one expected ((a) *F. nucleatum* ATCC 10953, (b) *P. gingivalis* ATCC 33277 and (c) *P. gingivalis* ATCC 33277) to test for contamination. Lane 3 contains PCR product of bacterial primer pairs plus molecular grade water which acts as a negative control.

### 3.3 Periodontal pathogen growth curves

The growth curves of bacteria were established to determine CFU/ml in bacterial stocks. The correct volume of bacteria could then be applied to epithelial cells to achieve a 100:1 bacterium to oral epithelial cell ratio. Growth curves were determined by measuring liquid culture media turbidity (OD readings) over a 72-hour growth period and using the Miles and Misra (Miles, Misra and Irwin, 1938) method to plate and enumerate bacteria at each time point.

#### 3.3.1 Analysis of growth curves

Figure 3.4 shows $OD_{600nm}$ readings over a 72-hour period for *P. gingivalis, F. nucleatum* and *T. denticola* after inoculation of respective broths with 2 – 3 representative colonies of bacteria. The spectrophotometer was initially zeroed using respective growth media before reading samples with an increase in $OD_{600nm}$ indicating increased bacterial growth. All three pathogens showed increasing OD, *i.e.,* growth over a 72-hour period with *T. denticola* showing a longer lag phase of 24 hours as compared with 8 and 4 hours for *P. gingivalis* and *F. nucleatum,* respectively. *F. nucleatum* entered the decline or 'death' phase after 24 hours growth, whereas *P. gingivalis* and *T. denticola* did not enter this phase within 72 hours. Simultaneously, the Miles and Misra method of plating bacteria was utilised at each time point to determine the CFU/ml for each pathogen. These CFU/ml values were obtained and plotted against $OD_{600nm}$ to produce a standard curve and linear regression equation for each bacterium as seen in Figure 3.5. The CFU/ml for new bacterial suspensions were subsequently calculated by reading the OD and using the equations in Figure 3.5 to solve for *'y'*.

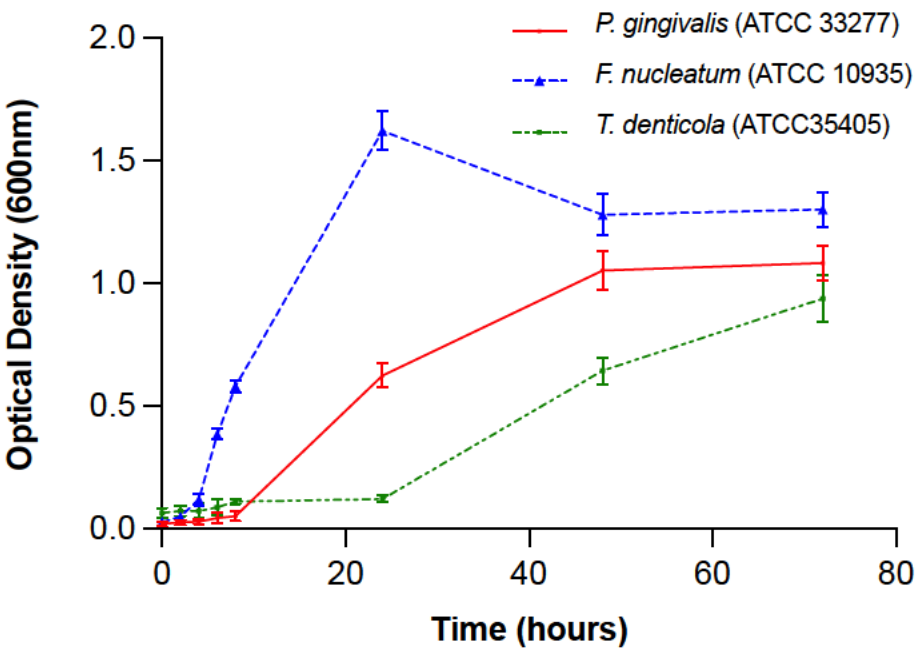



**Figure 3.4**: Optical density readings at wavelength 600nm ($OD_{(600nm)}$) at 0, 2, 4, 6, 8, 24, 48 and 72 hour periods using a Jenway® spectrophotometer for *P. gingivalis, F. nucleatum* and *T. denticola* after inoculation of respective broths with a single colony of bacteria. Increase in bacterial growth occurred across all three pathogens over the 72-hour period with *T. denticola* having a longer lag phase of 24 hours compared with 8 and 4 hours for *P. gingivalis* and *F. nucleatum* respectively. *P. gingivalis* and *T. denticola* did not enter the decline or 'death' phase within 72 hours whereas *F. nucleatum* entered this phase after 24 hours. Experiments were performed in triplicate.

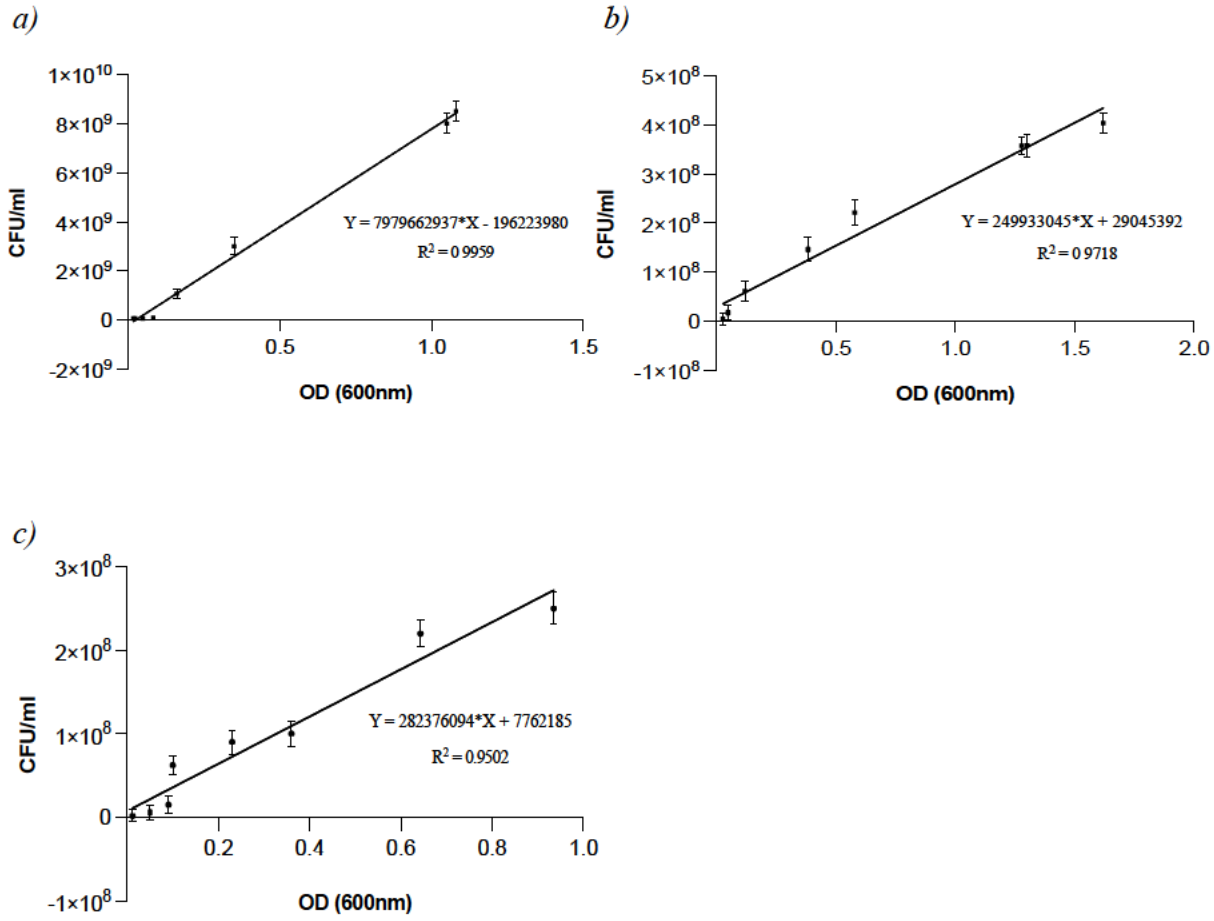



**Figure 3.5**: Optical density readings at wavelength 600nm ($OD_{600nm}$) plotted against CFU/ml for (a) *P. gingivalis*, (b) *F. nucleatum* and (c) *T. denticola* to produce a standard curve and linear regression equation which was used to determine CFU values in new bacterial suspensions. The Miles and Misra method of plating bacteria was performed concurrently alongside taking $OD_{600nm}$ readings to determine CFU/ml at each time point, therefore $OD_{600nm}$ readings were relative to CFU/ml for each pathogen. Experiments were performed in triplicate.

### 3.4 Oxygen-killing of periodontal pathogens

The detrimental effects of using heat-killing of bacteria have been previously reported (see section 1.6). An alternative method to bacterial killing for use in long term epithelial cell cultures was explored to better preserve bacteria morphology and protein integrity, with the aim of creating a model better representing the *in vivo* situation. Oxygen killing was used as it is known that anaerobic bacteria cannot survive in the presence of oxygen, therefore initial experiments investigated the optimum time taken for each pathogen to be killed in the presence of oxygen, which would ultimately be used in on-going experiments.

#### 3.4.1 Analysis of periodontal pathogen killing by exposure to oxygen

The oxygen tolerance of all pathogens was observed over a 72-hour period and experiments performed in triplicate. Results indicated that *P. gingivalis* was killed after 8-24 hours exposure (Figure 3.6) to atmospheric oxygen in a shaking incubator at 37ºC. The streaked agar plates showed no observable growth of *P. gingivalis* occurring after the 8-hour time point. Furthermore, the orange complex pathogen *F. nucleatum* was killed between 2-4 hours exposure to atmospheric oxygen which is apparent in Figure 3.7 where there was no observable growth of *F. nucleatum* on blood agar plates after the 2-hour time point. The oxygen tolerance of *T. denticola* was similar to *P. gingivalis,* where it was killed between 8-24 hours exposure to atmospheric oxygen (Figure 3.8). *T. denticola* absorbance readings were also read at each time point and the readings at 24, 48 and 72 hour time points were '0' indicating no growth of *T. denticola,* further confirming killing by atmospheric oxygen (Table 3.1).

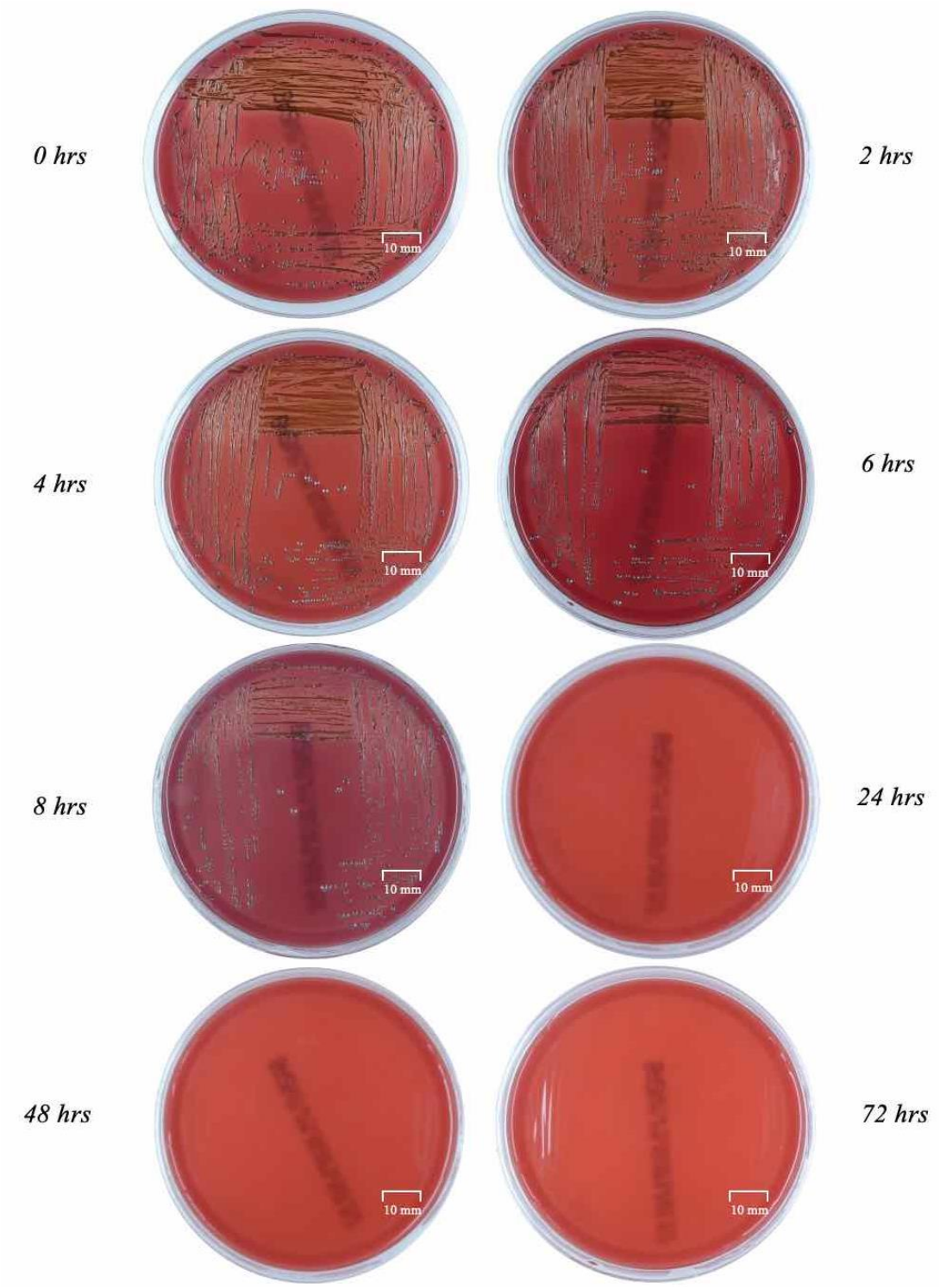



**Figure 3.6**: 1x10$^8$ *P. gingivalis* cells in 10ml TSB exposed to atmospheric oxygen in a shaking incubator (N-Biotek) at 37ºC for 72 hours. A disposable inoculating loop of 5µl volume was used to streak cultures at 0, 2, 4, 6, 8, 24, 48 and 72 hours on horse blood agar and allowed to grow in anaerobic conditions. *P. gingivalis* was killed between 8 and 24 hours exposure to atmospheric oxygen. Images were captured using a Nikon D5100 camera with 18-55 mm lens and images shown are representative of experiments performed in triplicate. Scale bars = 10 mm.

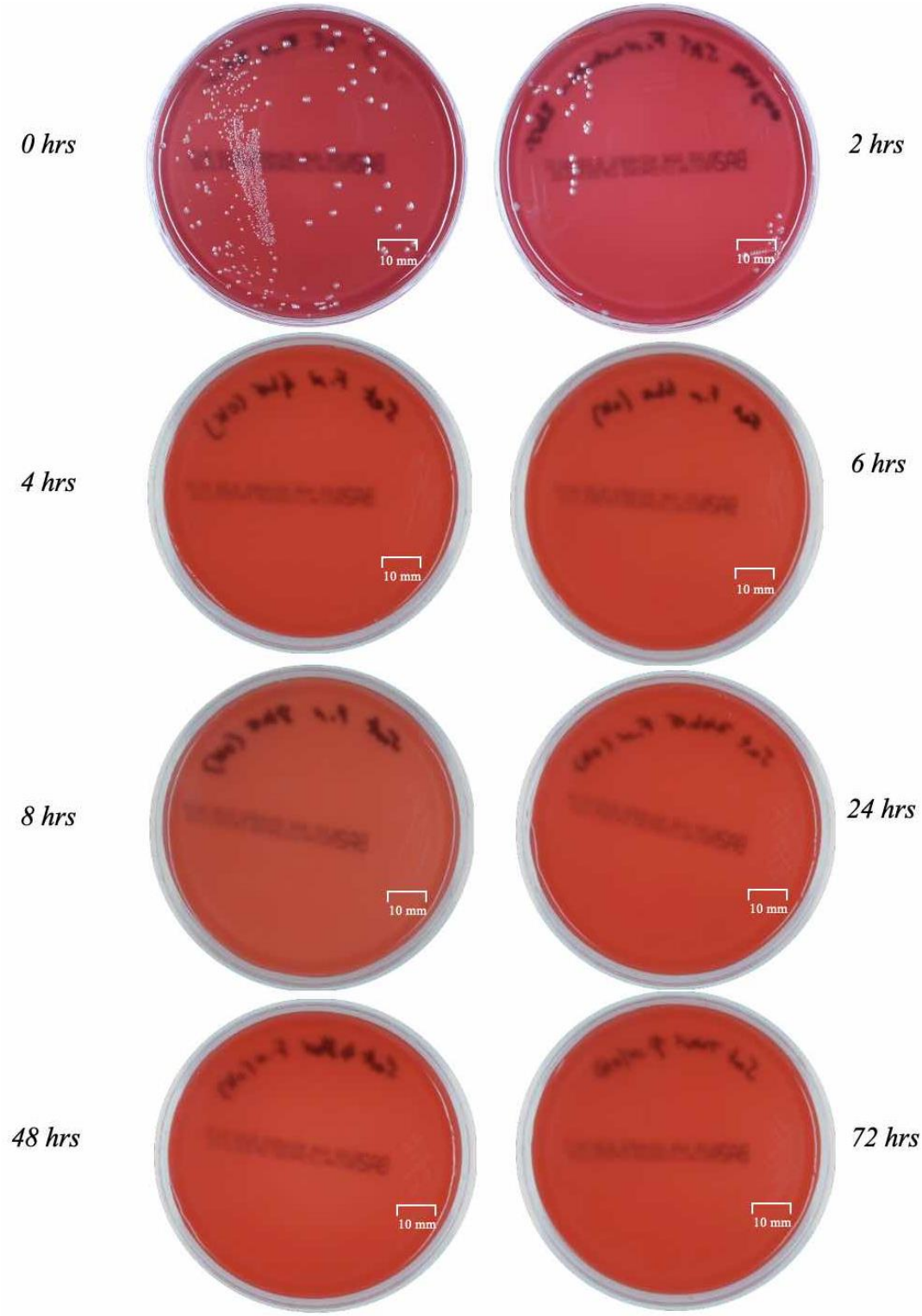



**Figure 3.7**: 1x10$^8$ *F. nucleatum* cells in 10ml TSB exposed to atmospheric oxygen in a shaking incubator (N-Biotek) at 37$^o$C for 72 hours. A disposable inoculating loop of 5µl volume was used to streak cultures at 0, 2, 4, 6, 8, 24, 48 and 72 hours on horse blood agar and allowed to grow in anaerobic conditions. *F. nucleatum* was killed between 2 and 4 hours exposure to atmospheric oxygen. Images were taken using a Nikon D5100 camera and images shown are representative of experiments performed in triplicate. Scale bars = 10 mm.

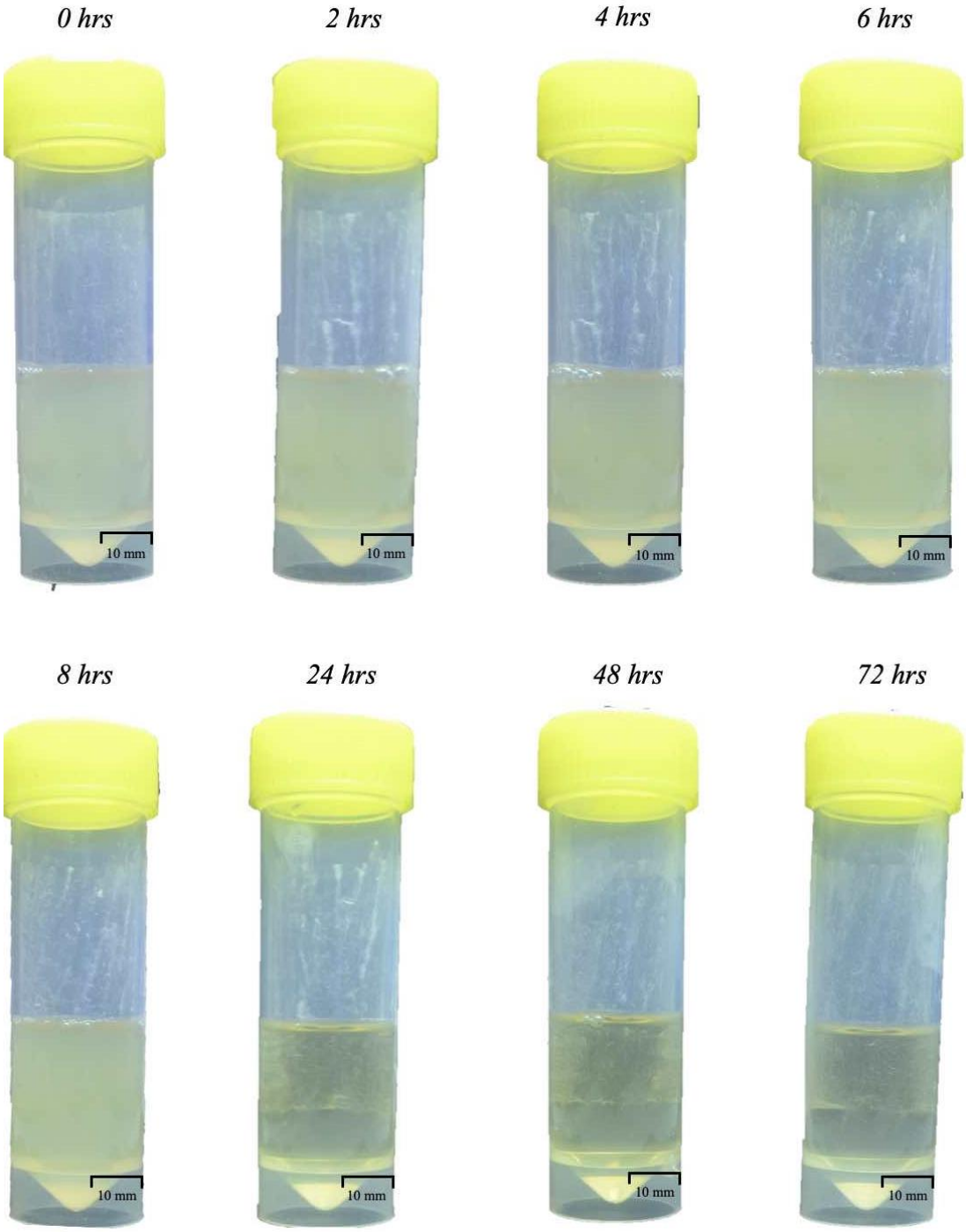



**Figure 3.8**: 1x10$^8$ *T. denticola* cells in 10ml mNOS medium exposed to atmospheric oxygen in a shaking incubator (N-Biotek) at 37$^o$C for 72 hours. A disposable inoculating loop of 5µl volume was used to inoculate 10ml pre-conditioned mNOS medium at 0, 2, 4, 6, 8, 24, 48 and 72 hours and allowed to grow overnight in anaerobic conditions. *T. denticola* was killed between 8 and 24 hours exposure to atmospheric oxygen. Images were taken using a Nikon D5100 camera and images shown are representative of experiments performed in triplicate. Scale bars = 10 mm.

**Table 3.1**: Overnight $OD_{600nm}$ absorbance readings of *T. denticola* cultures after inoculation from $1x10^8$ *T. denticola* culture in 10ml mNOS medium after 0, 2, 4, 6, 8, 24, 48 and 72 hours exposure to atmospheric oxygen in a shaking incubator (N-Biotek) at 37°C for 72 hours. No absorbance was observed after 24 hours exposure to atmospheric oxygen, n=3.

| **Hours** | **$OD_{600nm}$ Absorbance readings** |
|---|---|
| 0 | 0.462667 |
| 2 | 0.428 |
| 4 | 0.439667 |
| 6 | 0.477 |
| 8 | 0.406667 |
| 24 | 0 |
| 48 | 0 |
| 72 | 0 |

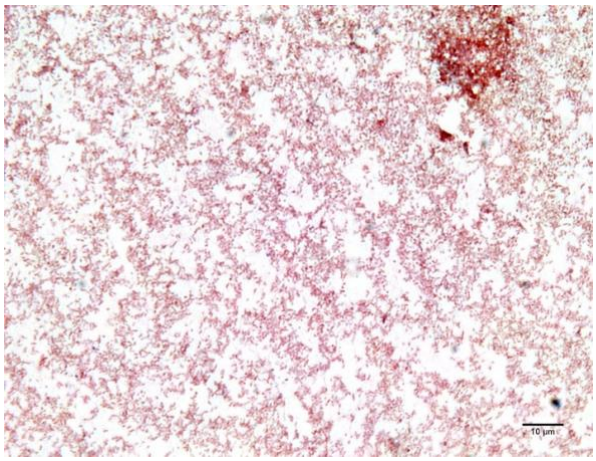
### 3.5 Effects of heat and oxygen-killing on pathogen morphology by Gram stain

With the negative effects of heat-killing on bacteria previously being reported (see section 1.6) the effects of oxygen killing on bacterial cell morphology were also explored. The morphology of *P. gingivalis*, *F. nucleatum* and *T. denticola* were assessed by Gram stain after heat and oxygen-killing and compared with live bacterial cultures.

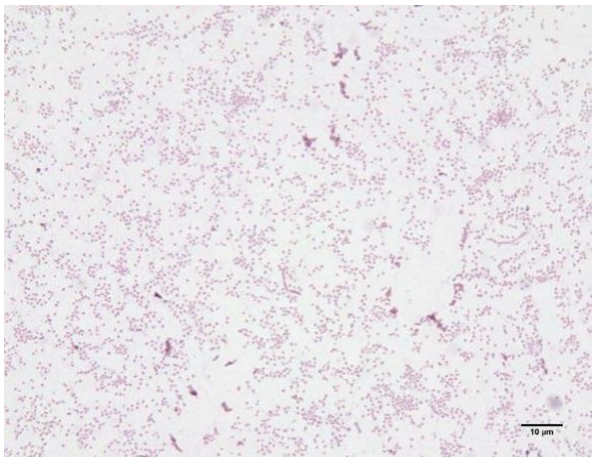
#### 3.5.1 Analysis of Gram stain images after heat and oxygen-killing

Heat or oxygen-killing of *P. gingivalis* resulted in no observable changes in morphology compared with viable control bacterial cultures, however there was a suggestion of more bacterial clumping after oxygen-killing (Figure 3.9). The straight, rigid rod structure of *F. nucleatum* cells was distorted with visible increases in curvature noticed after heat and oxygen-killing as seen in Figure 3.10. Heat-killing also resulted in loss of *T. denticola* helical shaped structure; however oxygen-killing did not cause any observable change in morphology (Figure 3.11).

*a)*



*b)*



*c)*

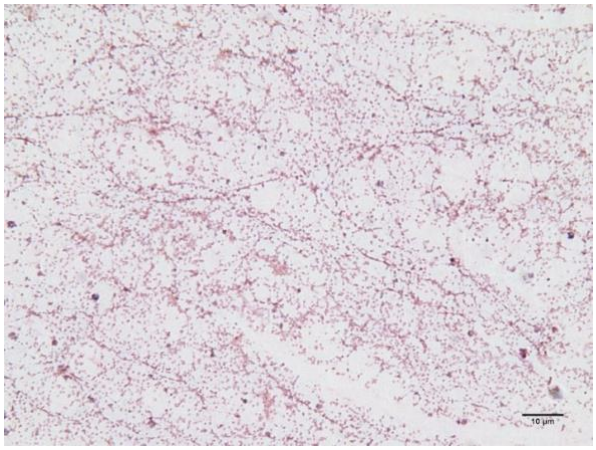


**Figure 3.9**: Representative Gram stain images of (a) live *P. gingivalis*, (b) heat-killed *P. gingivalis* and (c) oxygen-killed *P. gingivalis.* Bacterial cultures were emulsified in 50µl saline on glass slides. Effects of heat and oxygen killing on *P. gingivalis* morphology were indistinguishable through Gram staining however oxygen-killing resulted in more clumping of bacteria.

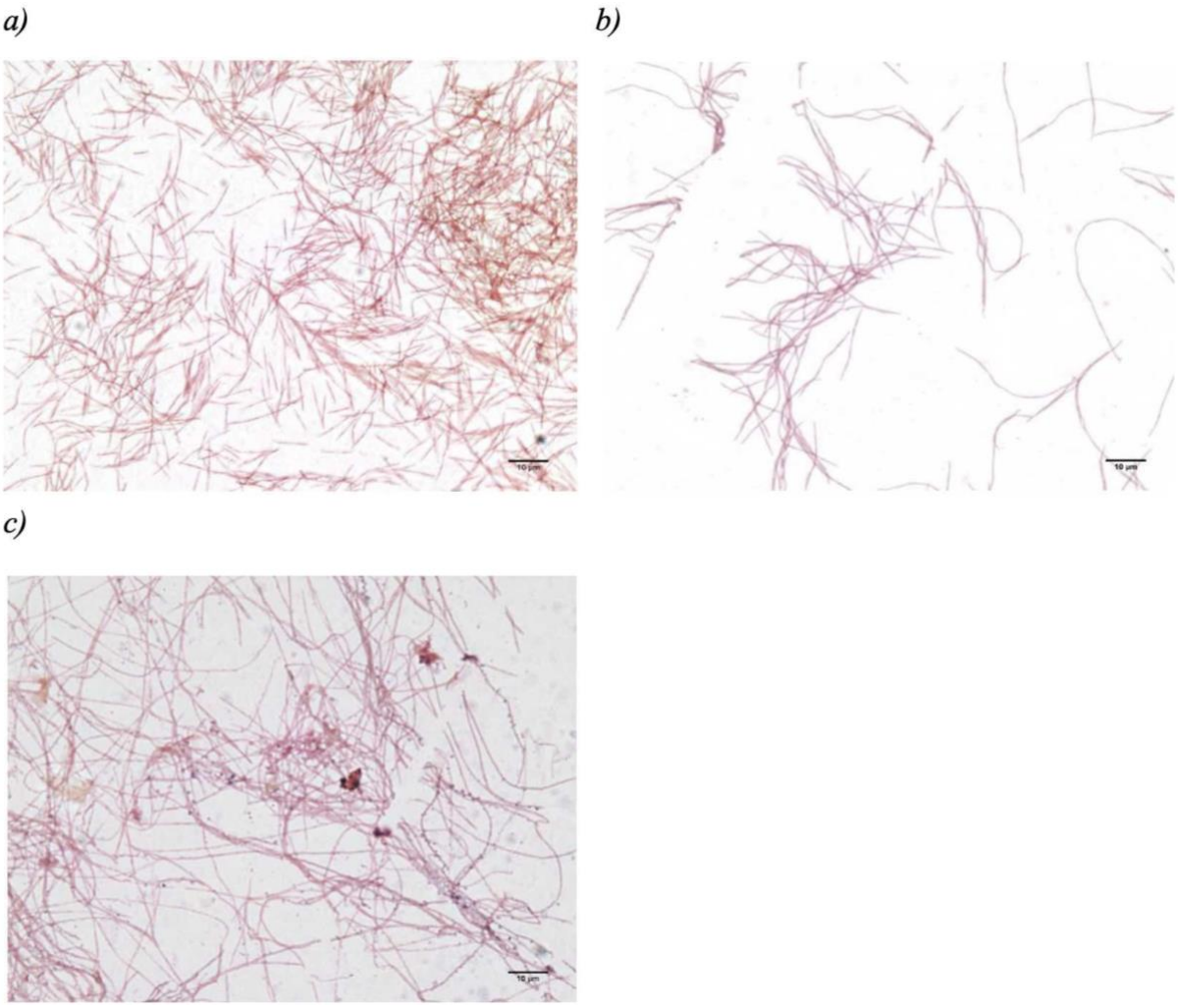
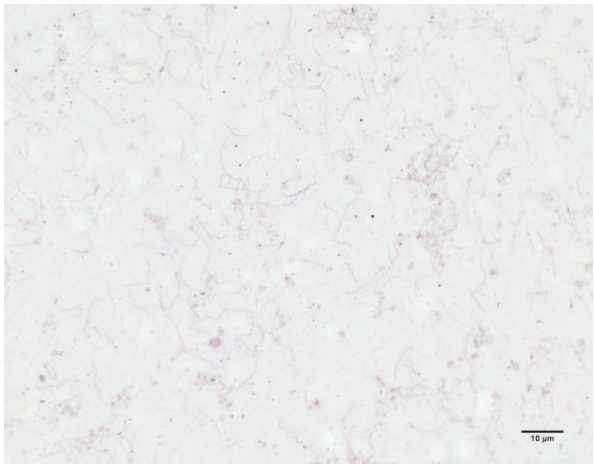
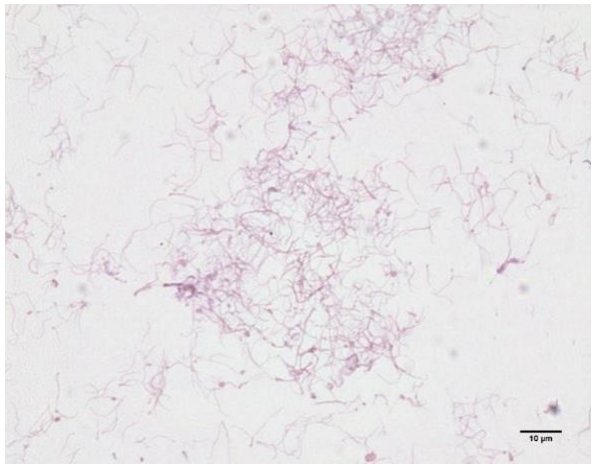



**Figure 3.10**: Representative Gram stain images of (a) live *F. nucleatum*, (b) heat-killed *F. nucleatum* and (c) oxygen-killed *F. nucleatum.* Bacterial cultures were emulsified in 50µl saline on glass slides. Heat and oxygen-killing resulted in increases in curvature to *F. nucleatums'* straight rigid rod structure.

*a)*



*b)*



*c)*

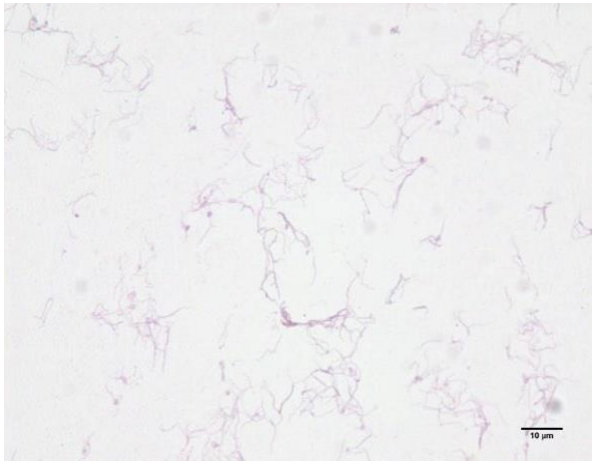


**Figure 3.11**: Representative Gram stain images of (a) live *T. denticola*, (b) heat-killed *T. denticola* and (c) oxygen-killed *T. denticola.* Bacterial cultures were emulsified in 50µl saline on glass slides. Heat-killing resulted in loss of *T. denticola* helical shaped structure whereas structure was maintained with oxygen-killing.

### 3.6 Effects of heat and oxygen-killing on pathogen morphology by scanning electron microscopy

As the effects of heat or oxygen killing were not clearly apparent following Gram staining, SEM was utilised to further explore the morphological changes brought about by these two methods of killing. SEM was performed on bacterial cultures grown on artificial saliva coated Thermanox® cover slips (explained further in section 2.5 and 2.5.1) and live bacteria were used as a control to compare differences after heat and oxygen-killing.

#### 3.6.1 Analysis of scanning electron microscope images after heat and oxygen-killing of pathogens

Analysis of SEM images showed that heat-killing of *P. gingivalis* appeared to produce additional background debris when compared with live and oxygen-killed *P. gingivalis* as shown in Figure 3.12. In addition, oxygen-killing of *P. gingivalis* caused clumping of bacterial cultures which was also shown by Gram staining (Figure 3.9c). However, clumping was not present in viable bacteria and after heat-killing of *P. gingivalis* and there was no visible effect on structural morphology in SEM images (Figure 3.12). Heat-killing of *F. nucleatum* also generated bacterial debris which was not visible in live and oxygen-killed *F. nucleatum* SEM images shown in Figure 3.13. The effects of heat-killing on bacteria morphology were however more apparent with *T. denticola* as shown in Figure 3.14, where heat-killing resulted in loss of *T. denticola* helical shaped morphology, but this structure was maintained after oxygen-killing, which further supports Gram stain results (Figure 3.11). In addition, heat-killing also resulted in bacterial debris when compared with live and oxygen-killed *T. denticola* which was also observed with *P. gingivalis* and *F. nucleatum*.

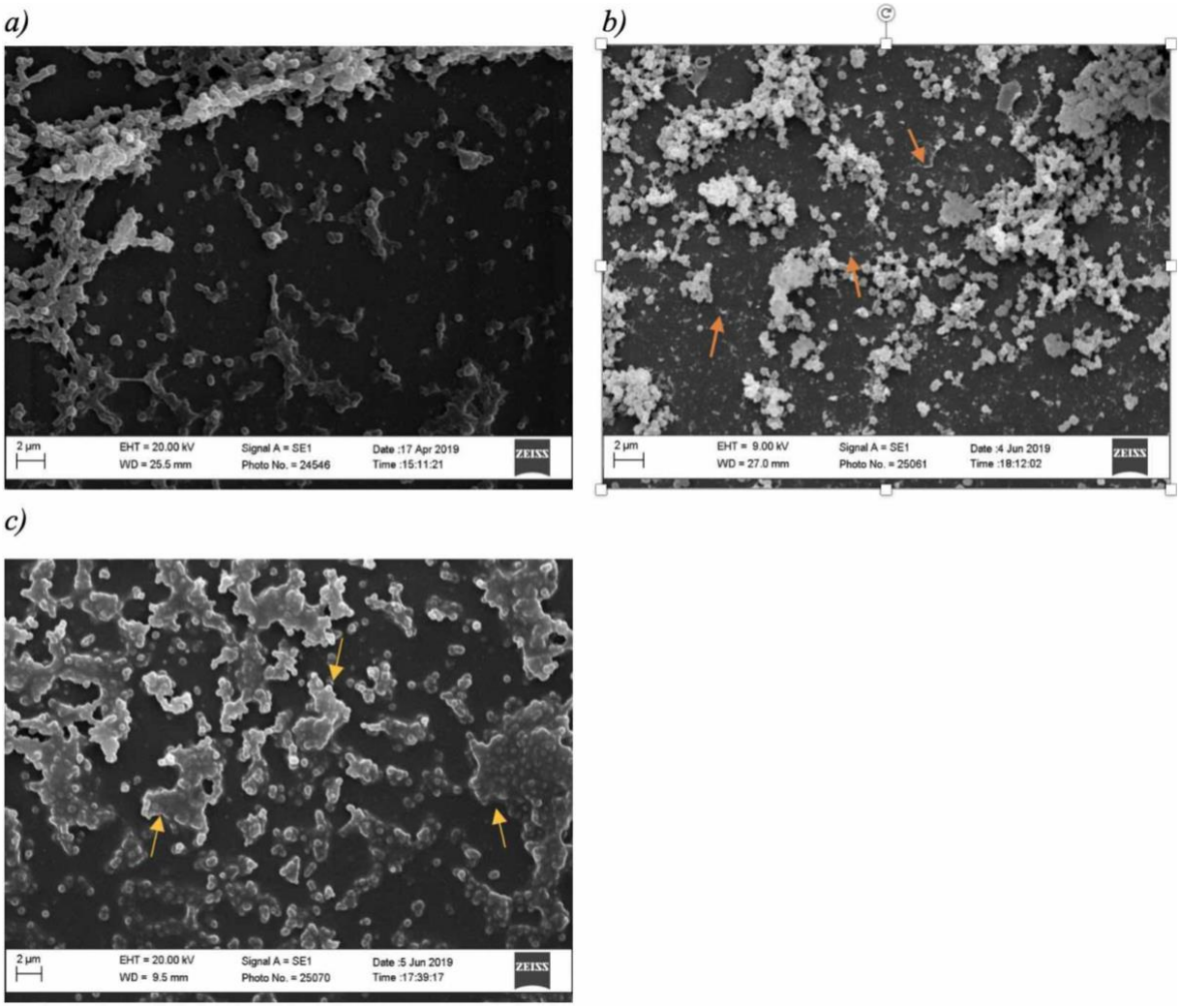



**Figure 3.12**: Representative SEM images captured of (a) live (b) heat-killed and (c) oxygen-killed *P. gingivalis*. Heat-killing of *P. gingivalis* resulted in bacterial debris (indicated by red arrows) as opposed to live and oxygen-killed *P. gingivalis.* Oxygen-killing of *P. gingivalis* resulted in clumping of bacteria (indicated by orange arrows) with no effect on morphology.

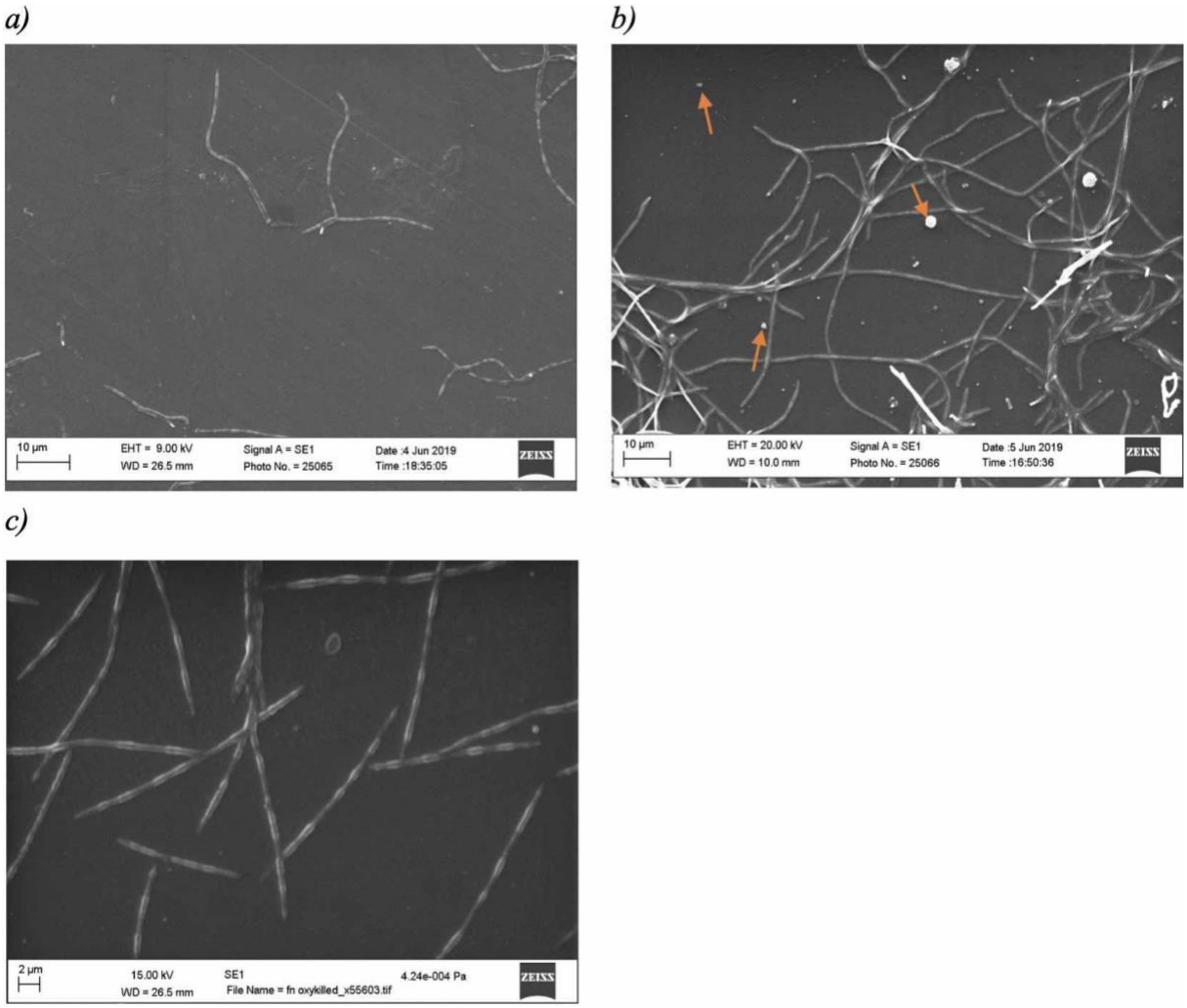



**Figure 3.13**: Representative SEM images captured of (a) live (b) heat-killed and (c) oxygen-killed *F. nucleatum*. Heat-killing of *F. nucleatum* resulted in bacterial debris (indicated by red arrows) as opposed to live and oxygen-killed *F. nucleatum.*

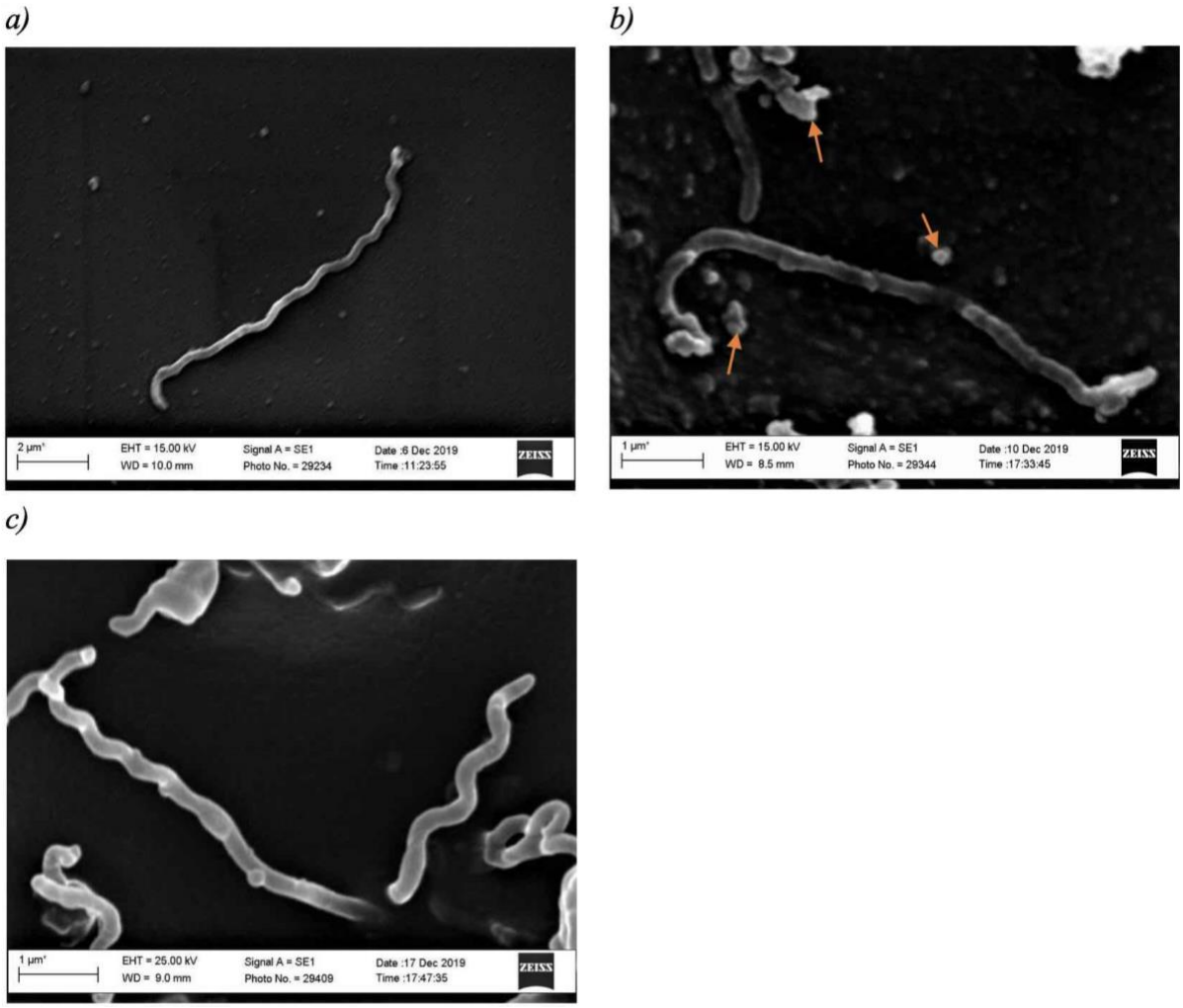



**Figure 3.14**: Representative SEM images captured of (a) live (b) heat-killed and (c) oxygen-killed *T. denticola*. Heat-killing of *T. denticola* resulted in bacterial debris (indicated by red arrows) and loss of its helical shaped morphology when compared with live and oxygen-killed *T. denticola.*

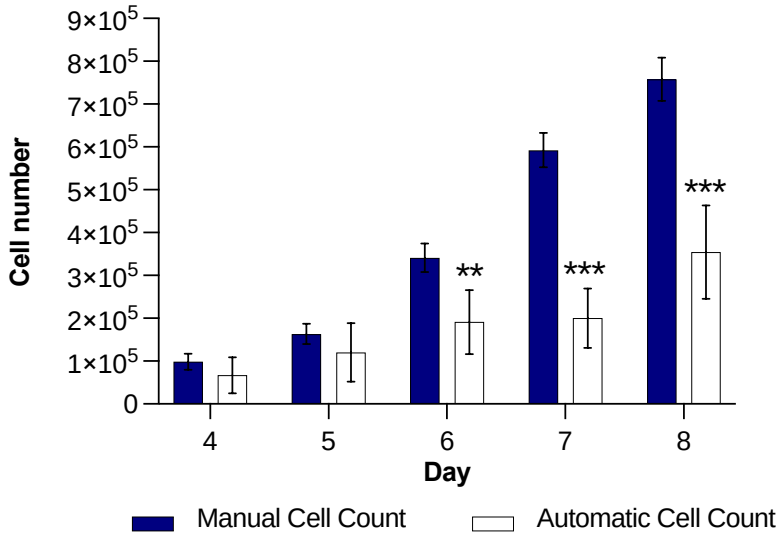
### 3.7 Manual (haemocytometer) vs Automatic (Tecan Spark) cell counts/viability

Automatic cell counting using the Tecan Spark® can offer a more time efficient method for high-throughput cell counts and for calculation of percentage cell viability in a sample when compared with manual cell counting, resulting in the ability to increase output of data. The consistency of cell counts and percent of viable cells readings using the automated method were initially determined by comparing against the conventional cell counting method of using a haemocytometer, to determine the validity of the automated method for use in subsequent studies. Cell counts and viability for both automated and manual approaches were attained using methods outlined in section 2.7.

#### 3.7.1 Analysis of manual and automatic counting on cell counts/viability

Cell number was significantly lower with the automated cell counting method when compared with manual counting on days 6 ($P<0.01$), 7 and 8 ($P<0.001$) after performing paired t-test statistical analysis (Figure 3.15a). In addition, percent of viable cells was significantly lower with the automated method compared with manual counting across all days ($P<0.001$) as shown in Figure 3.15b. The standard deviations (SD) with automatic cell counting were larger on each day when compared with manual cell counting when measuring both cell number and percentage cell viability. For example, the SD on day 8 with manual cell counting was 50,129 compared with 108,913 with automatic cell counting which is more than double the deviation. As a result of these data and the inaccuracies highlighted in cell counts and percentage cell viability, measurements were performed manually and the automatic method using the Tecan Spark® was not utilised in future experiments.

*a)*




*b)*

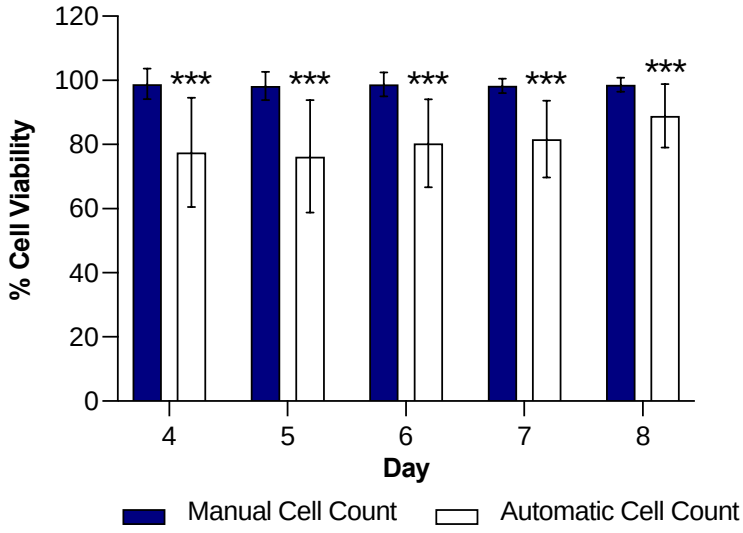



**Figure 3.15**: Comparison of the manual (haemocytometer) and automated (Tecan Spark®) methods to obtain (a) cell counts and (b) % cell viability. The automatic cell count method resulted in significantly lower cell counts on day 6, 7 and 8 compared with manual cell counting. Percentage cell viability was also significantly lower across all days with the automated method compared with manual. Significance was evaluated by paired t-test and error bars shown as SD. n=3, ** = $P<0.01$ and *** = $P<0.001$.

### 3.8 Development of a 2D oral epithelial model for EMT analysis

For ongoing experiments both heat and oxygen-killed bacteria were utilised to compare if the mode of killing used influenced induction of the EMT response in oral keratinocytes. Before this could be investigated, a suitable 8-day oral epithelial cell culture model that aimed to better represent the periodontal pocket epithelium environment was developed. An 8-day model originally proposed by Abdulkareem et al. (2017) was modified to better replicate the *in vivo* situation (see section 3.1). Initial experiments investigated the optimum cell seeding density needed in 6-well plates to reach a confluency of 85-90% after 8-days of incubation. Once the optimum cell seeding density was established, different cell growth models were developed with alterations to the cell culture media to determine effects on cell growth and to better mimic the subgingival environment.

#### 3.8.1 Optimising cell seeding density with percentage cell confluency

A suitable cell culture 6-well plate-based model for H400 cells was identified to optimise growth and survival conditions so a semi-confluent monolayer could be established. This approach would then provide the basis for initial pathogen challenge and further experimentation. It was important for cells to not reach full confluence and to avoid media exhaustion at day 8 as this would lead to changes in cell phenotype (Pavel et al., 2018) and media pH (Trajkovic et al., 2019). In addition, excessive cell growth would lead to build-up of metabolic waste products and less space for cells to grow. Ultimately, these factors would induce cellular stress and toxicity leading to cell death (Vis, Ito and Hofmann, 2020). It was also important to ensure sufficient viable cells were present at each time-point in order to identify EMT related changes. Therefore, the aim was to generate a cell monolayer with 85-

90% confluence after 8 days growth and to ensure media was not exhausted so cell viability was not affected.

#### 3.8.1.1 Effects of increasing cell density on cell confluency

Increasing the initial cell seeding density resulted in greater levels of cell confluency in 6-well plates across days 4-8 (see Figure 3.16). Wells that were seeded at 5000 cells in 2ml media and replaced every 2 days attained 81% cell confluency after 8-days growth, just below the optimal target range. However, doubling cell seeding density to 10,000 cells resulted in 90% confluency which was in the desired cell confluency range of 85-90% after 8-days. However, increasing cell seeding densities further results in excess levels of confluence on day 8 (15,000 and 20,000 resulted in confluency of 93% and 97%, respectively) which may suggest induction of cell stress and death. From the results obtained it was decided that an initial seeding density of 10,000 cells in 6 well plates would be utilised for subsequent EMT experiments.

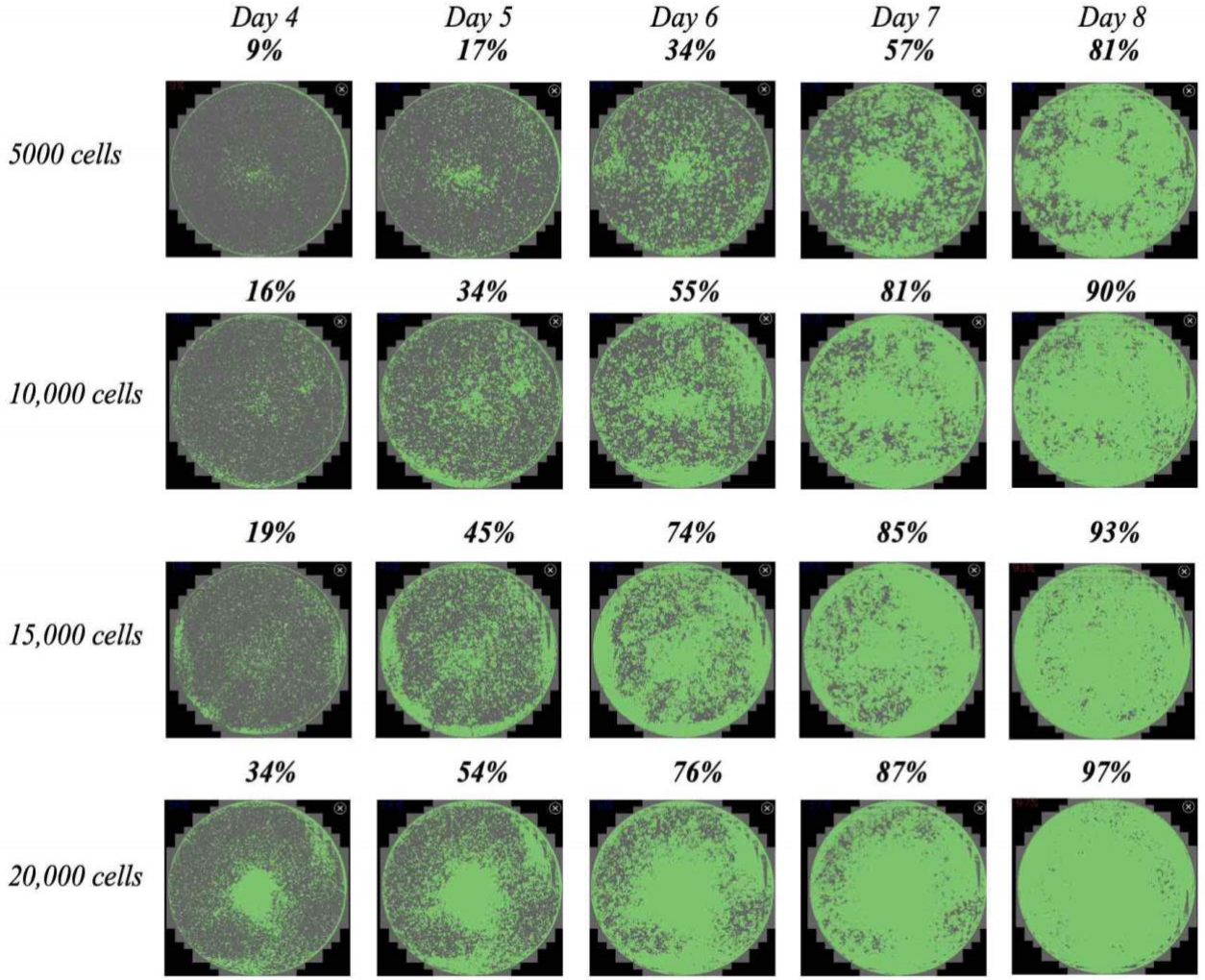



**Figure 3.16**: Representative well images showing cell confluence and % confluency values obtained using the Tecan Spark® multiplate reader. Six well plates were seeded with oral keratinocytes at 5000, 10000, 15000 and 20000 cells in 2ml supplemented DMEM media and media replenished every 2 days. Images were taken each day between day 4-8 and images displayed are representative of 3 images taken at each time point.

### 3.8.2 Cell growth models

After determining that 10,000 cells per well provided the optimum cell seeding density to generate the desired level of confluence on day 8, experiments were performed to measure cell number and viability over 8-days growth which were measured by performing manual cell counts and using the Trypan blue exclusion viability assay (see section 2.7.1). Cell growth and viability of cultures grown with media replacement every 2 days were initially investigated. However, as this would lead to an inaccurate representation of the sub-gingival pocket (see section 3.1), alterations to addition and amount of cell culture media used were made and cell growth and viability assessed.

#### 3.8.2.1 Effects of alterations to cell culture media on cell growth and viability

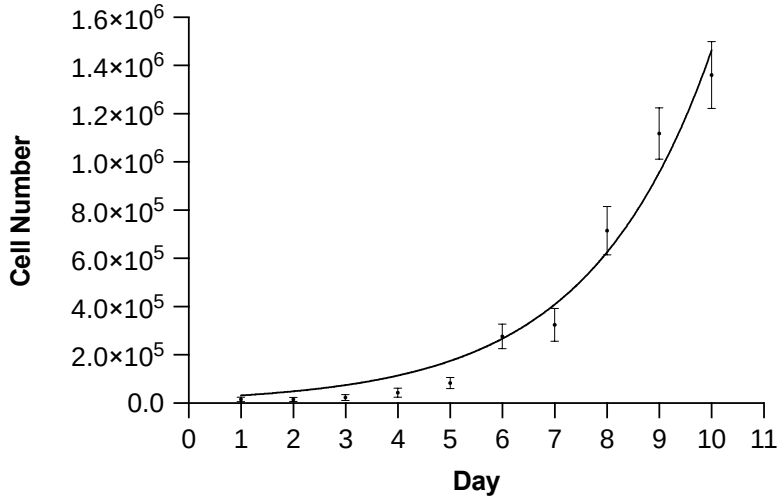
Cell growth curve and % cell viability of H400 cells over a 10-day period with 2ml media supplemented with 10% FBS and change of media every 2 days are shown in Figure 3.17. H400 cell number increased slowly from 10,000 +/- 500 to 83,000 +/- 22,000 cells from initial seeding to day 5 and then cells entered the log phase of growth where cell numbers increased exponentially from 83,000 +/- 22,000 to 1,361,000 +/- 140,000 cells from day 5 to day 10 (Figure 3.17a). The number of dead cells at each time-point were also obtained by using the Trypan blue exclusion viability assay to determine any effects on cell viability over the 10-day growth period. Percentage cell viability decreased from 100% on day 1 to its lowest at 95.37% +/- 3.86% on day 5 and then increased to 99.15% +/- 1.07% on day 10 (Figure 3.17b). However, this reduction in % cell viability was not significant when compared with day 1 after performing unpaired t-test statistical analysis.

Cell growth and viability was then investigated in another model that aimed to better mimic the clinical situation. In this model growth media was not changed during the 8 days of the study, rather additional media was added. This was to recreate the sub-gingival pocket environment of patients with chronic periodontitis where a local accumulation of cytokines is observed. To account for the nutritional requirements bought about by increase in cell number, 1ml of complete media was added every two days from the day of cell seeding. Cell number increased slowly from the day of seeding to day 5 (Figure 3.18a), which was similar to the model where media was replaced every two days. However, cell numbers increased at a slower rate from 10,000 +/- 500 to 44,000 +/- 19,000 cells which showed a reduction of 39,000 cells at day 5 when compared with the media replacement every 2 days approach. Cell numbers then increased exponentially from 44,000 +/- 19,000 to 562,000 +/- 45,000 cells from day 5 to day 8. However, there was 716,000 +/- 100,000 cells at day 8 for cells grown with media replacement which showed a reduction of 153,000 cells compared with those grown without media replacement but addition of media every two days. It was observed that % cell viability reduced to its lowest at 96.03% +/- 3.69% on day 5, however this reduction in cell viability was not significant after performing unpaired t-test statistical analysis (Figure 3.18b).

An initial volume of 2ml media and addition of 1ml media every two days resulted in reduced cell growth compared with replacing media every two days. Therefore, another model was investigated which used a greater starting volume of media in an attempt to remove the need for additional media change or supplementation whilst ensuring sufficient cell nutrition throughout the 8 days study period. The highest volume of media that is recommended for use in 6-well plates is 5ml, therefore this volume was selected for the eight-day cell growth

model. H400 cell number increased from 10,000 +/- 700 to 26,000 +/- 16,000 within 3 days, then cells entered the log phase of growth where cell number increased exponentially from 26,000 +/- 16,000 to 758,000 +/- 50,000 cells from day 3 to day 8 (Figure 3.19a). This is an increase of 42,000 cells when compared with the day 8 cell number of 716,000 +/- 100,000 in Figure 3.17a where media was replaced every two days. In addition, this cell number was also greater than the day 8 cell number of 562,000 +/- 45,000 cells in Figure 3.18a, where media was not replaced but 1ml was added every two days. The number of dead cells at each time-point were also determined to analyse whether there was any effect on % cell viability over the eight days. Percentage cell viability decreased from 100% on day 1 to its lowest at 96.67% +/- 3.91% on day 2, however this reduction in % cell viability was not significant when compared with the 100% cell viability observed on day 1 after performing unpaired t-test statistical analysis (Figure 3.19b). H400 cultures grown in 5ml supplemented DMEM media with no media change are shown at day 4 and 8 in Figure 3.20. As this model resulted in a greater final cell number compared with the other two models with no significant effect on % cell viability, it was used for downstream studies in which oral keratinocytes were challenged with periodontal pathogens and EMT-related changes assessed.

*a)*




*b)*

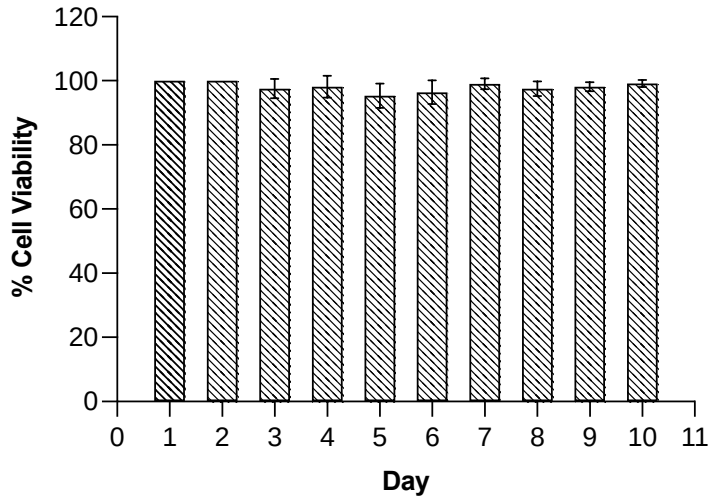
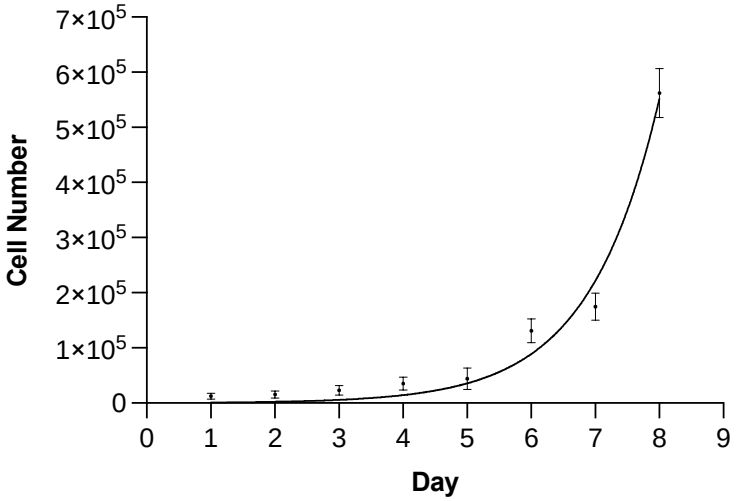



**Figure 3.17**: (a) Growth curve and (b) % cell viability of H400 cells over a 10-day period cultured in 2ml DMEM media supplemented with 10% FBS. Wells were seeded at an initial seeding density of $1x10^4$ and media was changed every 2 days. Cell number increased as the number of days increased and % cell viability was not significantly changed. Significance was evaluated by unpaired t-test and error bars shown as SD, n=3.

*a)*




*b)*

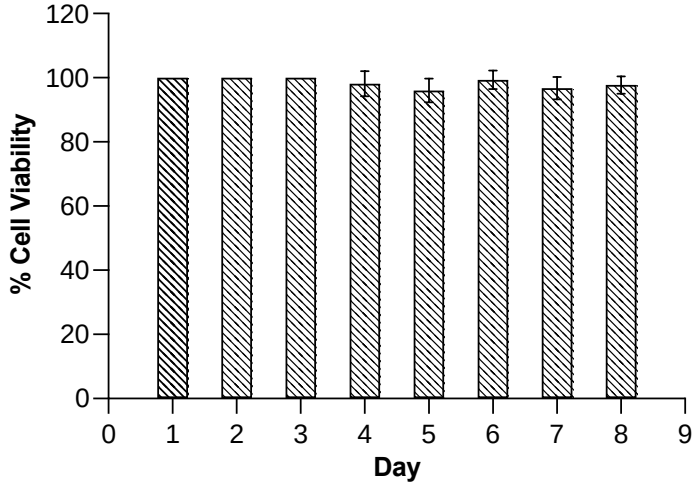
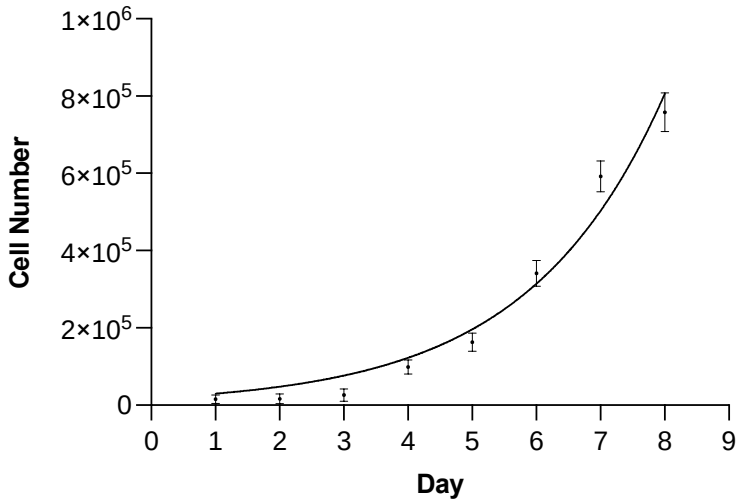



**Figure 3.18**: (a) Growth curve and (b) % cell viability of H400 cells over 8 days cultured in 2ml DMEM media supplemented with 10% FBS. Wells were seeded at an initial seeding density of $1x10^4$ and media was not changed every 2 days. However, 1ml of supplemented DMEM media was added every 2 days. The cell number increased with the days of culture and % cell viability was not significantly changed. Significance was evaluated by unpaired t-test and error bars shown as SD, n=3.

*a)*




*b)*

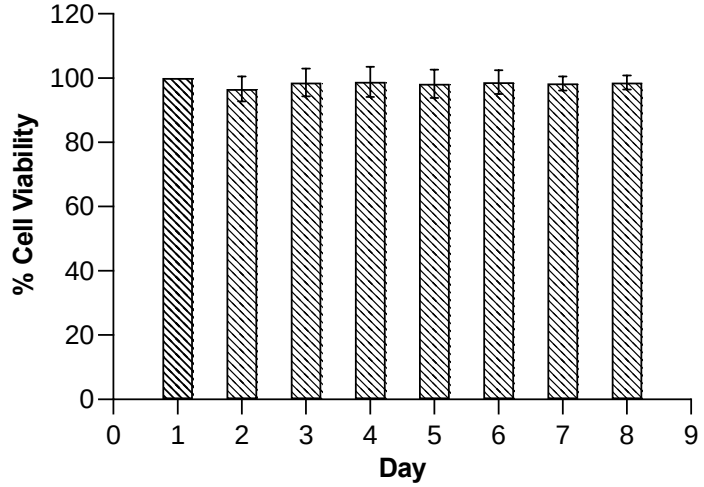



**Figure 3.19**: (a) Growth curve and (b) % cell viability of H400 cells over 8 days cultured in 5ml DMEM media supplemented with 10% FBS. Wells were seeded at an initial seeding density of $1x10^4$ and media was not changed during the 8 days. Cell number increased as the number of days increased and % cell viability was not significantly changed. Significance was evaluated by unpaired t-test and error bars shown as SD, n=3.

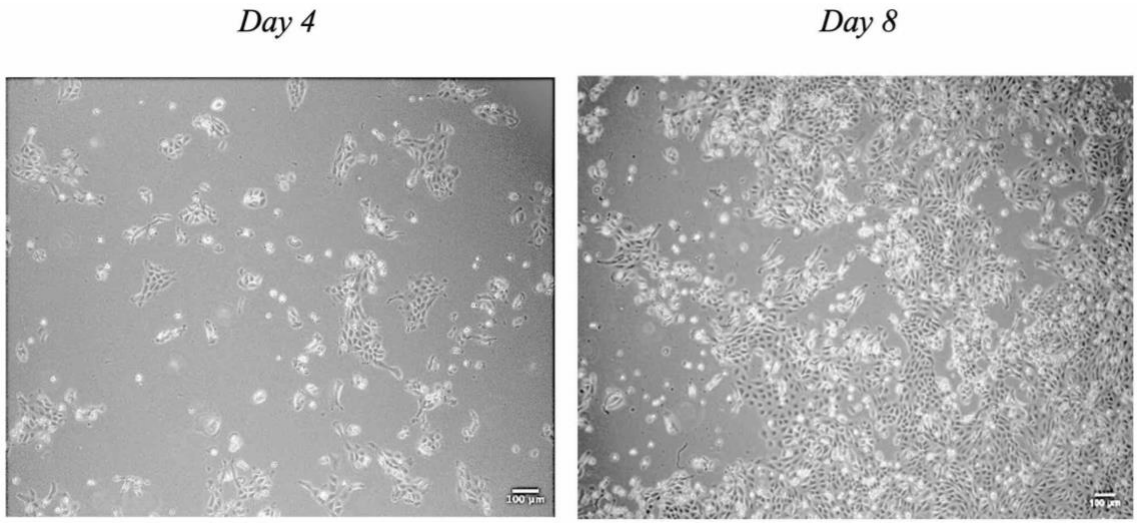



**Figure 3.20**: Representative light microscope images of H400 cells seeded at 10,000 cells in 6 well plates. Cells were grown in 5ml media supplemented with 10% FBS and images captured after 4 and 8 days growth. Media was not replaced every 2 days but kept the same throughout the 8-days. Day 4 image shows less degree of culture confluency when compared with the day 8 image which suggests an increase in cell number. Scale bars = 100μm.

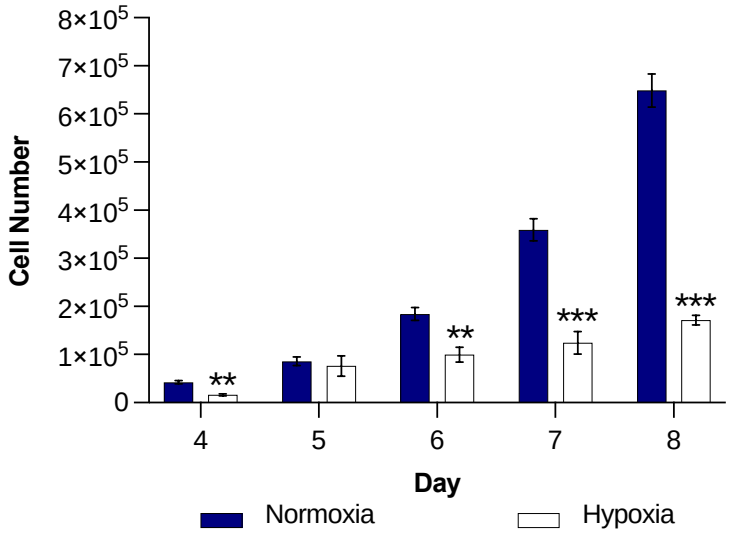
### 3.8.3 Using hypoxic conditions for H400 growth

The subgingival pocket is reported to be hypoxic where atmospheric oxygen concentration can be low as 1.8% (see section 3.1). Cell cultures were therefore grown in 1.8% oxygen to simulate conditions of the subgingival region providing a more relevant model. Cell growth and viability were measured by manual cell counting and using the Trypan blue exclusion cell viability assay and readings were compared to cultures grown in atmospheric oxygen (normoxia, 21% oxygen) which was used as the control.

#### 3.8.3.1 Effects of hypoxia on cell growth and viability

The effects of hypoxic and normoxic conditions on cell number and cell viability after 4-8 days growth are shown in Figure 3.21. Hypoxia significantly reduced cell number across days 4, 6 ($P<0.01$), 7 and 8 ($P<0.001$) when compared with cultures grown in normoxic conditions (Figure 3.21a). Cell viability was also significantly reduced in cultures grown in hypoxic conditions in comparison with normoxic conditions across all days ($P<0.05$ to $P<0.001$) and significance was tested using unpaired t-test (Figure 3.21b). This lower cell number was also evident in the representative light microscope images in Figure 3.22, where there was less confluency in cultures grown in hypoxic conditions compared with normoxic. As hypoxic conditions of 1.8% oxygen resulted in significant cellular death it was not appropriate for use in ongoing studies and therefore normoxic conditions were used in further experiments.

*a)*




*b)*

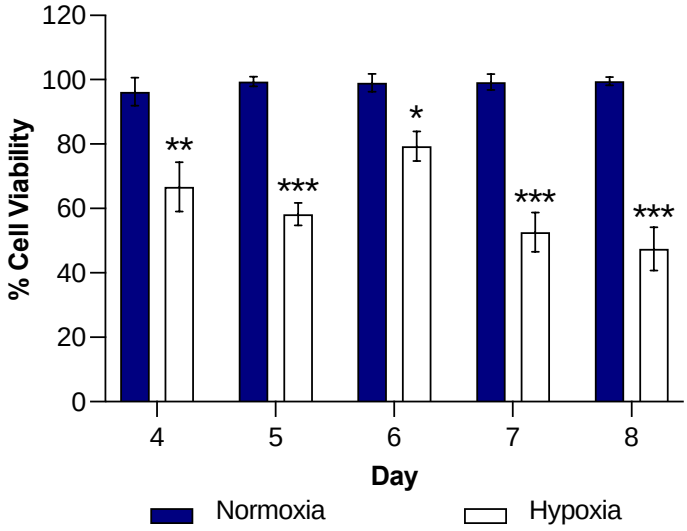



**Figure 3.21**: H400 cells grown in atmospheric oxygen (normoxic – 21% oxygen) and hypoxic conditions (1.8% oxygen) over 8 days and (a) cell number and (b) percent of viable cells assessed from day 4-8. Cell number was significantly lower in cultures grown in hypoxic conditions compared with normoxic on days 4, 6, 7 and 8. Also percent of viable cells was significantly lower in cultures grown in hypoxia compared with normoxia. Significance was evaluated by unpaired t-test and error bars shown as SD. n=3, * = $P<0.05$, ** = $P<0.01$ and *** = $P<0.001$.

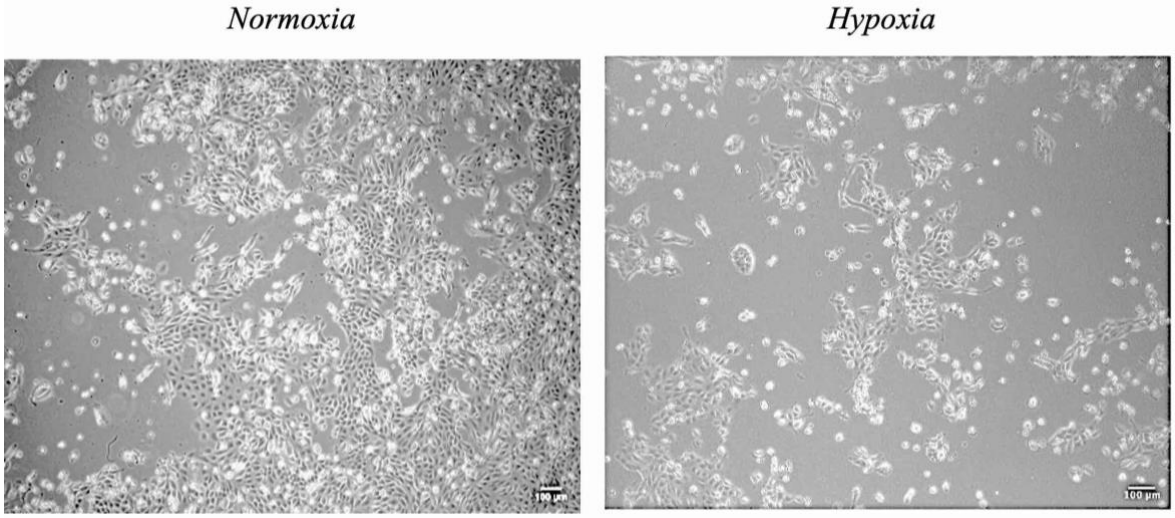



**Figure 3.22**: Representative light microscope images of H400 cells after 8-days growth in atmospheric conditions (normoxia – 21% oxygen) and hypoxia (1.8% oxygen). Cells were grown in 5ml media supplemented with 10% FBS and images captured using an inverted Zeiss Primovert microscope. Cultures in the normoxia image show a higher degree of confluency compared with cultures grown in hypoxic conditions. Images displayed are representative of 3 images captured. Scale bars = 100μm.

## 3.9 Discussion

### 3.9.1 Characterisation of periodontal pathogens by culture, Gram stain and PCR

The periodontal pathogen *P. gingivalis* produced typical black pigmented colonies on blood agar plates after 5-7 days growth (How, Song and Chan, 2016) in common with other strains of *P. gingivalis* such as the *W83* strain (Moreno and Contreras, 2013). In Figure 3.1b, *F. nucleatum* produced white translucent colonies as previously observed by Gharbia and Shah, (1990). The clouds of colonies observed after *T. denticola* growth is also consistent with findings observed by Chi, Limberger and Kuramitsu, (2002). As different strains of the same bacterial species share similar colony morphologies with each other, it was not sufficient to confirm correct bacterial strain by colony morphology only. Therefore, additional confirmatory investigations were required, Gram staining was performed to further distinguish between strains and to analyse for any contamination. *P. gingivalis* displayed a

coccobacilli morphology which was consistent with previous findings (Brunner et al., 2010), whilst *F. nucleatum* demonstrated typical morphology with long, spindle shaped rods (Nwaokorie et al., 2011). Morphologically, *T. denticola* are long helical-shaped rods typical of oral spirochetes (Ng et al., 2019). All three bacteria stained Gram negative and there were no bacteria which stained purple, suggesting that cultures were not contaminated with Gram-positive bacteria. A common environmental bacterial contaminant found in microbiology labs, that were not detected in the bacterial stocks used here, are *Staphylococci* (Ghayoor et al., 2015) which are Gram-positive facultative anaerobes, therefore the likelihood of this bacteria being present in cultures was high and identifying it was essential. The use of PCR on bacteria using species-specific primers is a widely used technique to confirm bacterial species, therefore it was used to further characterise bacteria. The PCR band present at 350bp for *P. gingivalis* (Figure 3.3a) are similar to previous findings (Lu et al., 2018). *F. nucleatum* showed bands at 300bp (Palmer, 2010) and *T. denticola* at 550bp (Külekçi et al., 2001) with no presence of contamination across all three bacteria. It is vital to correctly identify and characterise bacteria to check for contamination and ensure the right pathogen is used. *P. gingivalis*, *F. nucleatum* and *T. denticola* were successfully characterised by culture identification, Gram stain for morphological identification and PCR using species specific primers. Therefore, all three bacteria were used in ongoing experiments to challenge H400 cells and to assess for EMT-related changes.

### 3.9.2 Pathogen growth curves

Establishing the number of bacteria during growth is important so that the required volume of bacteria can be isolated for use in the tissue culture studies and to maintain the 100:1 bacterial oral epithelial cell ratio reported in the subgingival region. The growth of *P. gingivalis* in this

study showed similar growth patterns seen in a previous study where there was a lag phase of 12 hours and then a stationary phase of growth after 48 hours was achieved (Grenier et al., 2001). In addition, *F. nucleatum* showed similar growth (He et al., 2016), with a lag phase of 6 hours, but reached stationary phase of growth after 36 hours compared with the 24 hours seen in this study. This could be due to experimental differences *e.g.*, growth media used as *F. nucleatum* was grown in brain heart infusion as opposed to the TSB used in this study. *T. denticola* also demonstrated similar growth to published data (Abiko et al., 2014), however the lag phase of growth was 18 hours compared with 24 hours in this study. Again, this is most likely due to different experimental conditions, *e.g., T. denticola* was grown in mNOS medium supplemented with 10% rabbit serum as opposed to 2% used in this study and this increase in serum concentration may accelerate growth. It was also observed that *T. denticola* reached the stationary phase of growth after 96 hours in Abiko et al. (2014) study, but this could not be determined here as $OD_{600nm}$ values were still increasing and the experiment would need to be performed for longer than 72 hours. All three bacterial growth curves produced here showed similarities to those in the literature. Therefore, these growth curves were utilised to determine CFU/ml in cultures so that the correct number of bacteria could be isolated for use in on-going cell culture studies.

### 3.9.3 Oxygen killing of bacterial pathogens

The obligate anaerobes *P. gingivalis* and *T. denticola* were tolerant to oxygen between 8-24 hours of exposure whereas the facultative anaerobe, *F. nucleatum* was killed between 2-4hrs exposure to oxygen. This suggested that *F. nucleatum* is less tolerant to atmospheric oxygen than *P. gingivalis* and *T. denticola* as it is killed more rapidly. Previous studies have shown *F. nucleatum* tolerance to atmospheric oxygen to be 1 hour (Rolfe et al., 1978) as compared with

the 2-4 hours identified in this study. However, the present study used a higher bacterial concentration of 1 x $10^8$ when compared with 1 x $10^7$ used in the study of Rolfe et al. (1978). This may explain the longer oxygen tolerance observed here as there was a higher initial bacterial concentration. A previous study has also observed *T. denticola* to be viable for up to 80 mins exposure to atmospheric oxygen which is less than the tolerance of 8-24 hours reported here. However, the concentration of bacteria used was not stated and it may be due to the fact that a lower starting concentration of *T. denticola* was used (Loesche, 1969). The length of time *P. gingivalis* is tolerant to atmospheric oxygen has not been previously reported, therefore this data provides novel information for *P. gingivalis* oxygen tolerance.

It is expected that obligate anaerobes, such as *P. gingivalis* and *T. denticola,* would be less tolerant to oxygen than facultative anaerobes such as *F. nucleatum*, due to their strict requirements for an anaerobic environment (Johnson and Hug, 2019). This suggests possible oxidative stress resistance responses present in *P. gingivalis* and *T. denticola* that are not present in *F. nucleatum* which enable them to survive longer in oxygen. One mechanism which may be responsible for this in *P. gingivalis* involves a unique hemin layer present on the bacterial surface, which acts as a buffer against reactive oxygen species (ROS) such as hydrogen peroxide and it has been shown that hydrogen peroxide can damage bacterial proteins, lipids, RNA and DNA (Strand et al., 2010). The hemin layer of *P. gingivalis* produces μ-oxodimers which can initiate catalytic degradation of hydrogen peroxide enabling protection and longer survival in aerobic conditions (Smalley, Birss and Silver, 2000). One of these mechanisms in *T. denticola* involves Hydrogen Sulphide ($H_2S$) which is found in deep periodontal pockets and is a metabolic end-product of the *T. denticola* enzymes gamma-glutamyltransferase, cysteinylglycinase and cystalysin. It was observed that higher

concentrations of $H_2S$ decreased oxygen concentration in growth cultures generating a micro-anaerobic environment ideal for *T. denticola* growth and survival (Lai and Chu, 2008). As CFU/ml was kept the same for each bacterium, it further implies that the longer survival time of *P. gingivalis* and *T. denticola* in oxygen was due to oxidative stress resistance responses and not because of a higher concentration of bacteria.

Although it has been identified that a period of 8-24 hours is required to kill *P. gingivalis* and *T. denticola* by atmospheric oxygen, the introduction of more time points would determine the exact amount of time it takes to be killed. In conclusion, exposing *P. gingivalis*, *F. nucleatum* and *T. denticola* to atmospheric oxygen provides a suitable method to kill anaerobic bacteria and the exposure times observed here were used in later experiments.

### 3.9.4 Effects of heat and oxygen-killing on bacterial morphology

The effects of heat and oxygen-killing on *P. gingivalis* morphology were not clearly observable from Gram staining in Figure 3.9, however it was noted that oxygen-killing resulted in aggregation of colonies which was also further confirmed by SEM analysis in Figure 3.12c. A previous study has noted the effects of aggregation on oxygen concentration and it was shown that atmospheric oxygen concentration was lower in larger aggregated colonies of *Pseudomonas aeruginosa* compared with smaller aggregates (Wessel et al., 2014). Although *P. aeruginosa* is an aerobic bacterium the same concept of aggregation still applies to anaerobic bacteria. Therefore, this may provide evidence for a possible survival mechanism in *P. gingivalis* where colonies aggregate to try and recreate an anaerobic environment necessary for their survival.

Gram staining of *F. nucleatum* after heat and oxygen-killing showed a change of rod shape from its straight structure to visible increases in curvature. It has been previously noted that heat-killing can damage the bacterial lipid bilayer leading to rupturing of cells and loss of structure (Russell, 2003). However, the effects of oxygen-killing on *F. nucleatum* morphology have not been previously reported and the Gram stain here suggests that oxygen exposure can alter *F. nucleatum* morphology. Further analysis by SEM demonstrated no change in morphology when compared with live *F. nucleatum* suggesting that oxygen-killing did not alter the shape of every *F. nucleatum* cell but only a select few (Figure 3.13c).

*T. denticola* along with most other oral spirochetes have a helical-shaped structure which enables its motility (Ryan and Ray, 2003). As observed from the Gram stains in Figure 3.11 and SEM images in Figure 3.14, heat-killing results in loss of *T. denticola* helical shaped morphology. This may be due to the periplasmic flagella located between the outer membrane and the peptidoglycan layer in *T. denticola* which plays a significant role in maintaining its helical shape (Charon et al., 2012). Therefore, heat-killing may denature flagella which leads to loss of *T. denticola* helical structure observed here. Interestingly, oxygen-killing does not alter *T. denticola* morphology and it maintains its helical shape, suggesting that heat exposure is responsible for these alterations in morphology.

All three bacteria had more debris present after heat killing as evident in the SEM images when compared with live and oxygen-killed cultures (Figures 3.12, 3.13 and 3.14). Similar results have been noticed in a previous study which investigated the effects of heat-killing *Salmonella enterica* on bacterial morphology by transmission electron microscopy. There was increased formation of blebbing and vesicle formation and release of intracellular contents to

the surroundings. The lipid and cell envelope were also compromised leading to a loss of structural complexity and cell lysis (Correa et al., 2019). In addition, surface blebbing has also been observed with heat-killing of *E. coli* cells in another study (Katsui et al., 1982). Therefore, this may suggest that the debris present in all three heat-killed bacteria images are either external or internal constituents of bacteria which have fragmented due to thermal denaturation.

In conclusion oxygen-killing anaerobic bacteria appears to be preserving bacteria morphology more so than heat-killing and the data here provides an alternative method to kill anaerobic bacteria for use in cell culture models of periodontitis and to better simulate physiology. As heat-killed bacteria is the standard inactivated form of bacteria used in models of periodontitis, it was still used alongside oxygen-killed bacteria in ongoing studies to see how they compare.

### 3.9.5 Manual vs automatic cell counting

The automatic cell counting method using the Tecan Spark® and Cell chips™ provides faster result generation and reduces issues of subjectivity when compared with manual cell counting using an haemocytometer. Therefore, its potential use in providing cell count and % cell viability data were explored. Automatic cell counting resulted in significantly lower cell counts on days 6, 7 and 8 and significantly lower percentage cell viability across all days compared with manual cell counting. In addition, there was larger variance between readings obtained with the Tecan compared with manual readings (Figure 3.15). This contradicts the technical data supplied by the manufacturer which suggested comparable results to manual cell counting, alongside offering much higher reproducibility (Tecan, 2017). Although the

size of the cells needed to be detected were inputted (13 µm), the Tecan may still detect additional sample debris which are of similar size to H400 cells leading to false readings. This may explain the lower percentage cell viability readings observed with the Tecan compared with the manual counting method (Figure 3.15b). For these reasons, cell counts and % cell viability measurements were performed manually in all subsequent experiments.

### 3.9.6 Percentage cell confluency in different cell models

As the H400 cell line is well-characterised in our laboratory and widely reported in the literature, it was deemed unnecessary to re-characterise this cell line. H400 cells also have a doubling time of 24 - 48 hours, are generally easy to grow, express oral epithelial markers and are reported to be representative of gingival epithelium (Prime et al., 1990) making them suitable for use in the studies reported in this thesis. The desired percentage cell confluence of 85%-90% in 6 well plates after 8-days growth was achieved with a cell seeding density of 10,000 cells, therefore this seeding density was subsequently used in investigating different cell growth models. Figure 3.17 demonstrates a H400 growth curve with 2ml media and media replenishment every 2 days to compensate for media depletion and ensuring cultures receive the required nutritional requirements for optimal growth. Cultures were robust in this model with the rate of growth increasing up until day 10 and no significant effect on cell viability was observed. As media replacement would be an inaccurate representation of the sub gingival pocket during periodontitis (see section 3.1), a new model was explored where media was not replaced but 1ml media was added every 2 days (Figure 3.18) to compensate for nutritional demands brought on by increased cell growth. The decrease in cell growth observed with addition of 1ml media and no media replacement may be because 1ml media is not sufficient to meet demands of increased cell growth and addition of more volume of

media may overcome this issue. However, as handling and manipulation of cell culture plates every 2 days increases the risk of contamination, another model where media would not need to be replaced was explored to decrease this risk. As cells are grown for an extended period, they will also require high amounts of media to meet the demands of increased cell growth. The highest volume of media that is recommended for use in 6-well plates is 5ml, therefore growth and viability of cells grown in this amount of volume were explored. Cell cultures grown in 5ml (Figure 3.19) media grew similarly to cell cultures grown where media was replaced every 2 days. This approach showed no significant decrease in percentage cell viability, therefore providing a suitable model for use in downstream studies. The initial cell seeding density of 10,000 cells with 5ml media supplemented with 10% FBS and no media replacement was used in subsequent experiments where cell monolayers were challenged with periodontal pathogens and *E. coli* LPS.

### 3.9.7 Normoxia vs Hypoxia

The subgingival pocket is hypoxic with an $pO_2$ of 1.8% providing a suitable environment for anaerobic bacteria to grow and survive (Mettraux, Gusberti and Graf, 1983). Cell cultures were grown in these hypoxic conditions to better simulate physiological conditions and were compared with cultures grown in normoxic conditions. The decrease in cell number and % cell viability observed with hypoxia may be due to activation of hypoxia-inducible factor-1α (HIF-1α) which is the main transcription factor activated in hypoxic conditions (De lima et al., 2014). HIF-1α can initiate p53-independent apoptosis pathways including genes of the BCL-2 family (Vaupel and Mayer, 2007). This may explain the decrease in viable cells which ultimately leads to lower cell numbers observed in Figure 3.21. In conclusion, H400 cultures

grown in 1.8% oxygen resulted in cellular death, therefore normal atmospheric oxygen conditions of 21% were used in further experiments.

The following chapter investigated the potential of HK and OK *P. gingivalis*, *F. nucleatum* and *T. denticola* to induce EMT-related changes in oral keratinocytes using the 8-day model described here.

# 4. Epithelial-mesenchymal transition induction of H400 oral epithelial cells by heat and oxygen-killed periodontal pathogens

## 4.1 Introduction

This chapter focuses on the potential of HK and OK *P. gingivalis*, *F. nucleatum* and *T. denticola* to induce EMT in H400 cells after 8-day exposure. The periodontal pathogens used in this study were killed prior to epithelial cell stimulation. However, it is known that HK pathogens are still able to elicit similar cellular responses in epithelial cells as viable bacteria (Laheij et al., 2013). Some of these responses can be detrimental to epithelial cell growth (Shi et al., 2016) and viability (Basso et al., 2015) therefore, initial experiments investigated the impact of bacterial stimulation (HK and OK) on epithelial cell growth and viability.

It has been shown previously that HK *P. gingivalis* and *F. nucleatum* could induce EMT-related responses in OSCC cells (Abdulkareem et al., 2017). However, previous experiments here have shown heat-killing to be detrimental to bacterial morphology (see section 3.5.1 and 3.6.1). The changes as a result of heat killing may result in the loss of EMT induction potential. Conversely, oxygen-killing of anaerobes has been shown to preserve bacterial morphology (see section 3.5.1 and 3.6.1), therefore stimulating epithelial cells with OK pathogens would provide interactions that better simulate physiology and any subsequent EMT responses will be more clinically relevant. To investigate whether EMT-related responses changed, epithelial cells were stimulated with HK and OK bacteria and results compared to determine the EMT induction of respective stimulants.

EMT is a multi-faceted process which is implicated in a range of diseases including fibrosis of the liver, lung, heart and kidney, tumour metastasis and Crohn's disease (see section 1.3.1). Its progression is typically associated with a loss of epithelial phenotype and acquisition of mesenchymal characteristics. One of the hallmarks of EMT is the cadherin switch which

involves the replacement of epithelial adherens junction, including E-cadherin with N-cadherin (Loh et al., 2019). The gene expression of these markers and other EMT associated markers in epithelial cells after HK and OK pathogen challenge were therefore assessed by qRT-PCR analysis. IF staining was also performed to detect protein expression and localisation of these EMT-related markers specifically, E-cadherin, vimentin and snail-1. Another EMT associated feature is the loss of epithelial cell-cell adhesion allowing cells to detach and migrate into underlying tissues. A breakdown of epithelial integrity has been associated with initiation and propagation of periodontitis. A technique to determine this breakdown, widely reported in the literature is TEER, which was employed in this study to measure electrical resistance across epithelial monolayers as a surrogate marker of epithelial monolayer breakdown following stimulation with HK and OK pathogens.

As a result of EMT, cells gain migratory properties (explained further in section 1.3.2.2) and cell migration associated with gingival epithelial cells would lead to breakdown of the epithelium and loss of surrounding tissue. Therefore, migratory ability of H400 cells was initially assessed in cultures challenged to HK pathogens by scratch wound migration assay. However, traditional scratch wound assays have issues with reproducibility of the scratch wound producing variable wound areas. In order to mitigate against this the Ibidi 2-well insert method (refer to section 2.11.3) was used to perform migration assays in HK and OK pathogen exposed cultures.

In addition, any EMT-related responses after pathogen exposure in this study may be due to elevated levels of pro-inflammatory cytokines (explained further in section 1.3.5). For these

reasons, secreted levels of IL-1β, IL-8 and TGF-β1 in collected supernatants from H400 cultures exposed to HK and OK pathogens were measured by ELISA.

HK periodontal pathogens, *P. gingivalis* and *F. nucleatum,* have been shown to trigger host inflammatory responses and induce EMT in OSCC cells. This chapter therefore explores the potential of another periodontal pathogen, *T. denticola,* to induce EMT in OSCC cells and to identify whether OK bacteria offer a different stimulatory EMT potential compared with HK pathogens.

## 4.2 Effect of heat-killed and oxygen-killed periodontal pathogens on epithelial cell growth and viability

The effect of HK and OK pathogens on H400 growth and viability were assessed using the 8-day H400 growth model described in the previous chapter (see section 3.8). These were performed to identify any cytotoxic effects that HK and OK pathogens may generate in cell culture. Cell number and viability were determined using manual cell counts and Trypan blue (see section 2.7.1).

### 4.2.1 Analysis of heat-killed and oxygen-killed periodontal pathogens on epithelial cell growth and viability

Cell growth was significantly increased in cell cultures challenged with HK *P. gingivalis* on days 6) ($P<0.001$) and 7 ($P<0.01$) when compared with unstimulated cultures. Likewise, OK *P. gingivalis* also significantly increased cell growth on days 6 ($P<0.001$) and 7 ($P<0.001$) in comparison with media only control (Figure 4.1). However, HK and OK stimulants of *P. gingivalis* did not significantly affect cell growth in comparison with each other. Interestingly,

OK *P. gingivalis* exposure resulted in greatest final cell number after 8-days stimulation when compared with all other cultures. In addition, cell growth near the end of the experimental period (day 7 to 8) was declining in HK and OK *P. gingivalis* exposed cultures. Cell viability of all pathogen exposed cultures displayed non-significant decreases across all days.

OK *F. nucleatum* exposure significantly decreased cell number compared with cultures exposed to HK *F. nucleatum* ($P<0.01$) and media only cultures ($P<0.05$) on day 5 (Figure 4.2). It was observed that *E. coli* LPS, HK and OK *F. nucleatum* exposure resulted in lower final cell number in comparison with media only. In a similar manner to HK and OK *P. gingivalis*, HK and OK *F. nucleatum* did not significantly affect cell viability across all days in comparison with media only.

Cultures exposed to HK *T. denticola* ($P<0.05$) and OK *T. denticola* significantly increased cell number when compared with media only cultures after 8-days stimulation (Figure 4.3). HK *T. denticola* exposure resulted in the highest final cell number, although this was non-significant in comparison with cultures exposed to OK *T. denticola*. In addition, cell viability was non-significantly decreased with HK and OK *T. denticola* exposure across all days when compared with media only

Overall, HK and OK pathogens and *E. coli* LPS were non-toxic to oral keratinocytes as demonstrated by non-significant changes in cell viability, with HK and OK *P. gingivalis* significantly increasing cell growth after 6- and 7-days and HK and OK *T. denticola* after 8-days exposure. In addition, there was no significant differences in cell growth when

comparing HK and OK stimulants except on day 5, where OK *F. nucleatum* significantly decreased cell growth in comparison with HK *F. nucleatum*.

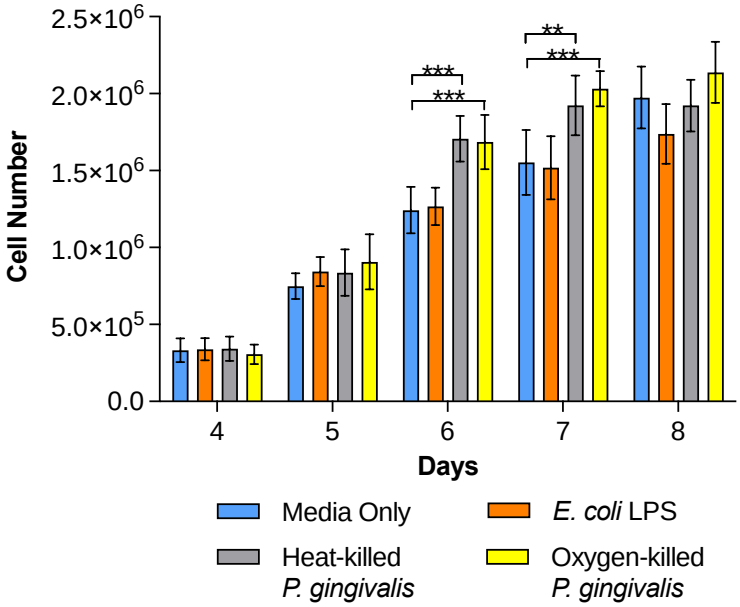



**Figure 4.1**: Cell growth of oral keratinocytes over 8-days incubation with media only or challenged with *E. coli* LPS and heat or oxygen-killed *P. gingivalis*. Significant increases in cell counts were observed in cultures challenged with heat and oxygen-killed *P. gingivalis* on days 6 and 7 in comparison with media only. Error bars shown as standard deviations and n=3, ** = P<0.01 and *** = P<0.001. Statistical analysis was ANOVA followed by a post-hoc Tukey Test.

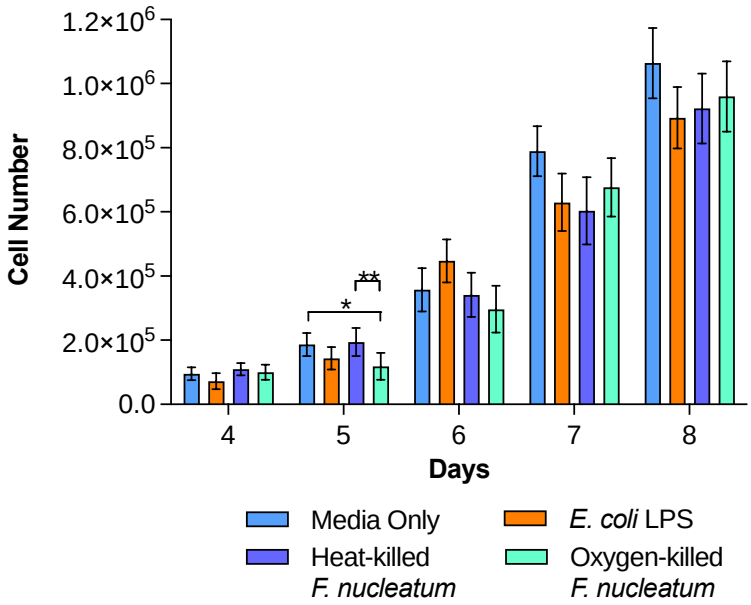



**Figure 4.2**: Cell growth of oral keratinocytes over 8-days incubation with media only or challenged with *E. coli* LPS and heat or oxygen-killed *F. nucleatum*. Results showed significant decreases in cell counts between media only and cultures challenged with oxygen-killed *F. nucleatum* on day 5. Cell counts significantly decreased in cultures challenged with oxygen-killed *F. nucleatum* compared with cultures exposed to heat-killed *F. nucleatum* on day 5. Error bars shown as standard deviations and n=3, * = $P<0.05$ and ** = $P<0.01$. Statistical analysis was ANOVA followed by a post-hoc Tukey Test.

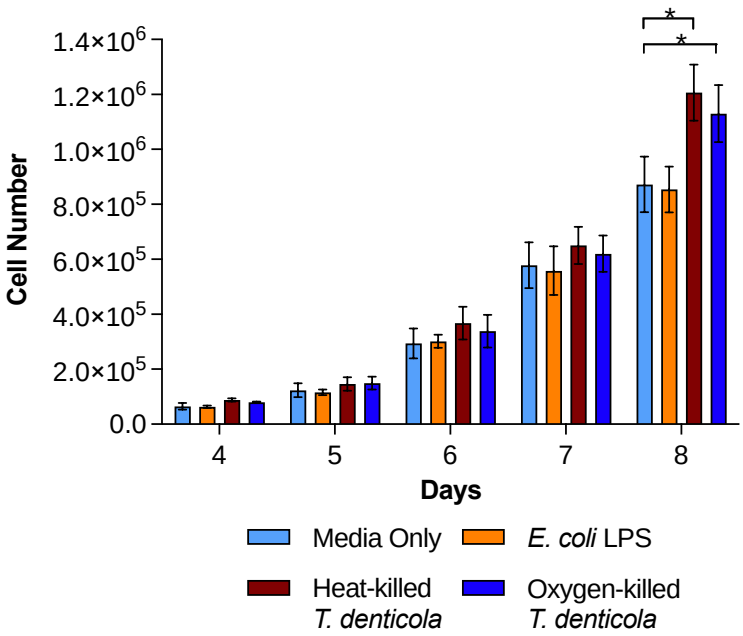



**Figure 4.3**: Cell growth of oral keratinocytes over 8-days incubation with media only or challenged with *E. coli* LPS and heat or oxygen-killed *T. denticola*. Significant increases in cell counts were observed in cultures exposed with heat and oxygen-killed *T. denticola* on day 8 in comparison with media only control. Error bars shown as standard deviations and n=3, * = $P<0.05$. Statistical analysis was ANOVA followed by a post-hoc Tukey Test.

## 4.3 Real-time PCR analysis of EMT related markers after heat and oxygen killed pathogen challenge

An efficient method to assess for induction of EMT was to perform gene expression analysis using qRT-PCR. qRT-PCR is a widely used sensitive technique that provides reproducible outcomes (Bustin, 2000). The induction of EMT after HK and OK pathogen exposure was assessed by gene expression profiling using genes characteristic of the epithelial and mesenchymal phenotype. In addition, gene expression of transcription factors and pro-inflammatory cytokines known to induce EMT were analysed. Analysis for each gene was performed on day-8 cultures separately for both HK and OK pathogens and results are displayed in separate graphs. A summary of gene expression ratios of the EMT related markers after heat and oxygen-killed pathogen exposure is provided in Table 4.1.

### 4.3.1 Gene expression of epithelial markers in oral keratinocytes

The down-regulation of adherens junction genes such as E-cadherin (and others associated with desmosome assembly such as desmoplakin-1) destabilises cell-cell epithelial attachments as is reported in the early stages of EMT. In addition, loss of cytoskeletal intermediate filaments, such as cytokeratins, are also associated with EMT (Huang, Guilford and Thiery, 2012), therefore the expression of these markers after HK and OK pathogen exposure were assessed by qRT-PCR analysis.

#### 4.3.1.1 Effects of pathogen exposure on epithelial marker gene expression

*E. coli* LPS presented significant down-regulation ($P<0.001$) of E-cadherin (0.17-fold) for both experiments (Figures 4.4a and 4.5a). HK *P. gingivalis* (0.39-fold) and *F. nucleatum* (0.51-fold) significantly down-regulated E-cadherin expression, but HK *T. denticola* (1.57-

fold) significantly increased expression in comparison with media only (P<0.001) (Figure 4.4a). However, all OK pathogens significantly decreased (P<0.001) E-cadherin expression with the greatest reduction associated with OK *F. nucleatum* (0.003-fold) exposure followed by *P. gingivalis* (0.05-fold) and OK *T. denticola* (0.13-fold) (Figure 4.5a). OK pathogens resulted in greater E-cadherin down-regulation in comparison with HK pathogen exposure.

Cytokeratin 5 expression was significantly down-regulated (P<0.01 and P<0.001) with *E. coli* LPS (0.67 - 0.71-fold) exposure (Figures 4.4b and 4.5b). Also, all HK pathogens significantly down-regulated (P<0.001) cytokeratin 5 expression (0.27 – 0.49-fold) with greatest reduction noted with HK *F. nucleatum* exposure in comparison with media only control (Figure 4.4b). Also, all OK pathogens (0.28 – 0.69-fold) significantly down-regulated (P<0.01 and P<0.001) cytokeratin 5 gene expression, with OK *T. denticola* resulting in greatest down-regulation compared with unstimulated cultures (Figure 4.5b).

Expression of desmoplakin-1 was also significantly decreased (P<0.01 and P<0.001) with *E. coli* LPS (0.22 - 0.31-fold) exposure in both experiments (Figures 4.4c and 4.5c). Exposure with all HK pathogens (0.27 – 0.7-fold) significantly decreased (P<0.001) desmoplakin-1 gene expression, with HK *F. nucleatum* (0.27-fold) causing greatest down-regulation of desmoplakin-1 in comparison with media only (Figure 4.4c). Similarly, all OK pathogen exposures (0.13 - 0.75-fold) significantly reduced (P<0.05, P<0.01 and P<0.001) desmoplakin-1 expression, however greatest down-regulation was associated with OK *T. denticola* exposure when compared with control (Figure 4.5c).

Overall, stimulation of oral keratinocytes with either HK or OK pathogens significantly down-regulated expression of EMT-related epithelial markers except for HK *T. denticola* which up-regulated E-cadherin expression. All OK pathogens induced early EMT-associated changes and could down-regulate E-cadherin expression more so than HK counterparts, therefore qRT-PCR analysis was continued for mesenchymal associated genes to further assess EMT induction.

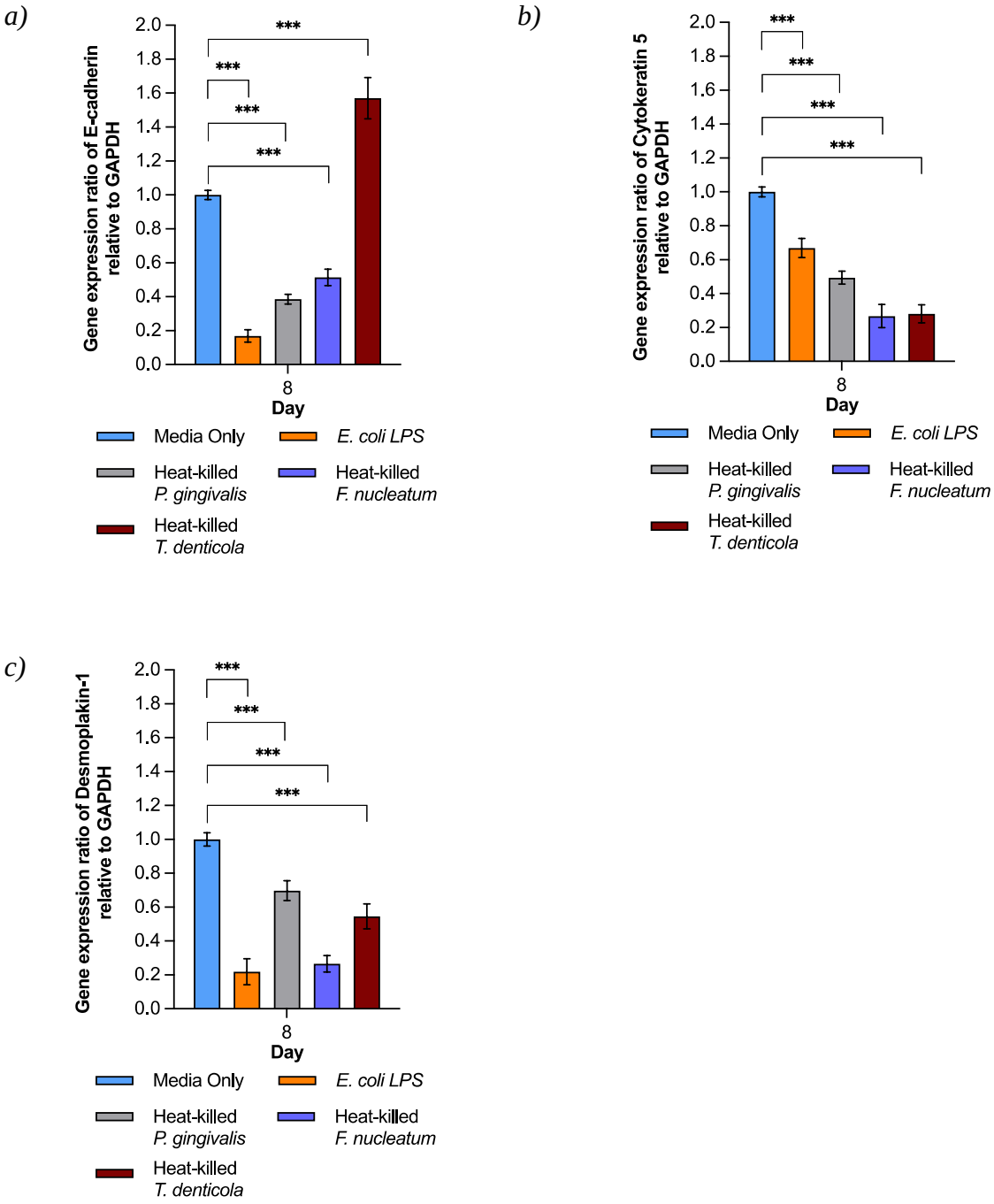



**Figure 4.4**: Gene expression ratios (relative to GAPDH) of epithelial markers for (a) E-cadherin, (b) Cytokeratin 5 and (c) Desmoplakin-1 as determined by quantitative real-time PCR on day-8 H400 cultures challenged with heat-killed *P. gingivalis*, *F. nucleatum* and *T. denticola*. The values obtained from each sample were normalised to GAPDH. All cultures challenged with heat-killed bacteria significantly down-regulated expression of epithelial markers E-cadherin, Cytokeratin 5 and Desmoplakin-1 when compared with unstimulated cultures. However, heat-killed *T. denticola* resulted in significantly increased E-cadherin expression. Error bars shown are standard deviations and experiments were performed in triplicate, *** = $P<0.001$.

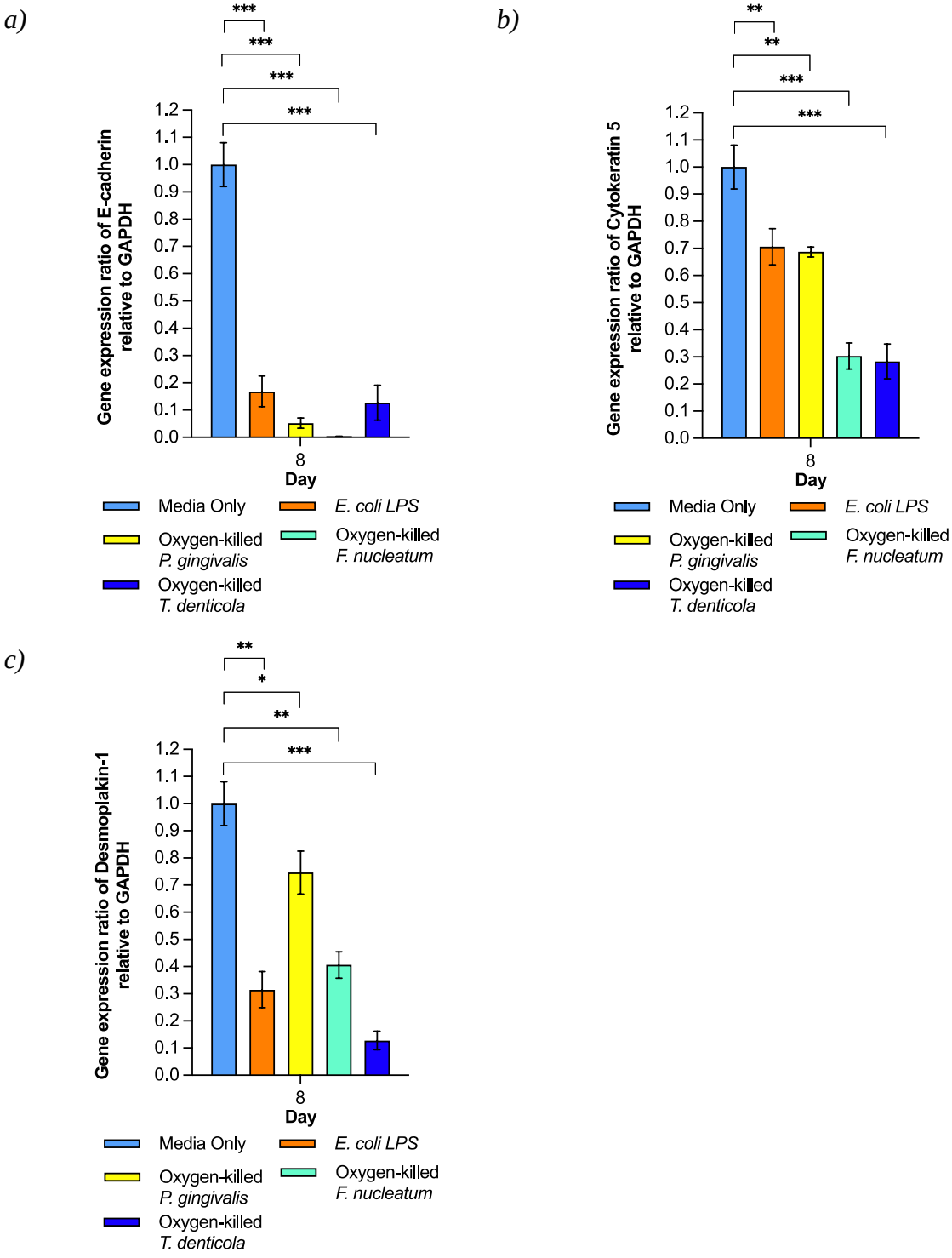



**Figure 4.5**: Gene expression ratios (relative to GAPDH) of epithelial markers for (a) E-cadherin, (b) Cytokeratin 5 and (c) Desmoplakin-1 as determined by quantitative real-time PCR on day-8 H400 cultures challenged with oxygen-killed *P. gingivalis*, *F. nucleatum* and *T. denticola*. All cultures challenged with oxygen-killed bacteria significantly down-regulated expression of epithelial markers E-cadherin, Cytokeratin 5 and Desmoplakin-1 when compared with unstimulated cultures. The values obtained from each sample were normalised to GAPDH and error bars shown are standard deviations and experiments were performed in triplicate. * = $P<0.05$, ** = $P<0.01$ and *** = $P<0.001$.

### 4.3.2 Gene expression of mesenchymal markers in oral keratinocytes

The up-regulated expression of N-cadherin and intermediate filament composition changes, where vimentin expression is increased enables cell motility and are key features of EMT (Huang, Guilford and Thiery, 2012). In addition, up-regulation of proteolytic enzymes such as MMP-9 can degrade extracellular matrix (ECM) components facilitating cell migration (Makela et al., 1994). Therefore, up-regulated expression of these markers would suggest induction of EMT and were therefore selected for qRT-PCR gene expression analysis after 8-day exposure to HK and OK pathogens.

#### 4.3.2.1 Effects of pathogen exposure on mesenchymal marker gene expression

Expression of N-cadherin was significantly up-regulated ($P<0.001$) with *E. coli* LPS (3.25 - 8.6-fold) exposure in both experiments in comparison with media only control (Figures 4.6a and 4.7a). HK pathogens (1.42 - 6.75-fold) also significantly up-regulated ($P<0.05$ and $P<0.001$) N-cadherin expression, with greatest increase associated with HK *F. nucleatum* exposure when compared with media only control (Figure 4.6a). N-cadherin was also significantly up-regulated ($P<0.05$ and $P<0.01$) after OK pathogen exposure (2.16 - 4.33-fold) with OK *T. denticola* causing the highest increase (Figure 4.7a).

Vimentin expression was also significantly up-regulated ($P<0.05$ and $P<0.001$) after *E. coli* LPS (1.6 - 1.74-fold) exposure in comparison with controls (Figures 4.6b and 4.7b). Similarly, vimentin was significantly up-regulated ($P<0.001$) with all HK pathogens (4.01 - 6.12-fold) with HK *F. nucleatum* stimulation resulting in the highest level of up-regulation (Figure 4.6b). OK pathogens (2.45 - 7.63-fold) also significantly increased ($P<0.05$, $P<0.01$

and P<0.001) vimentin expression, however OK *T. denticola* was responsible for greatest up-regulation in comparison with control (Figure 4.7b).

*E. coli* LPS exposure (5.41 - 7.75-fold) presented significant up-regulation (P<0.001) of MMP-9 in both experiments in comparison with media only control (Figure 4.6c and 4.7c). MMP-9 was also significantly up-regulated (P<0.001) after HK pathogen exposure (3.73 - 10.83-fold) with HK *F. nucleatum* being responsible for greatest up-regulation of MMP-9 (Figure 4.6c). Stimulation by OK pathogens (6.1 - 11.16-fold) also significantly (P<0.001) increased MMP-9 expression with OK *P. gingivalis* exposure resulting in greatest up-regulation in comparison with media only control (Figure 4.7c)

Amongst the HK pathogens, HK *F. nucleatum* caused the greatest up-regulation of mesenchymal genes, whilst OK *T. denticola* proved most effective in up-regulating both N-cadherin and vimentin amongst the OK pathogens. In conclusion, all HK and OK pathogens may induce EMT-associated phenotypic changes through up-regulated mesenchymal gene expression.

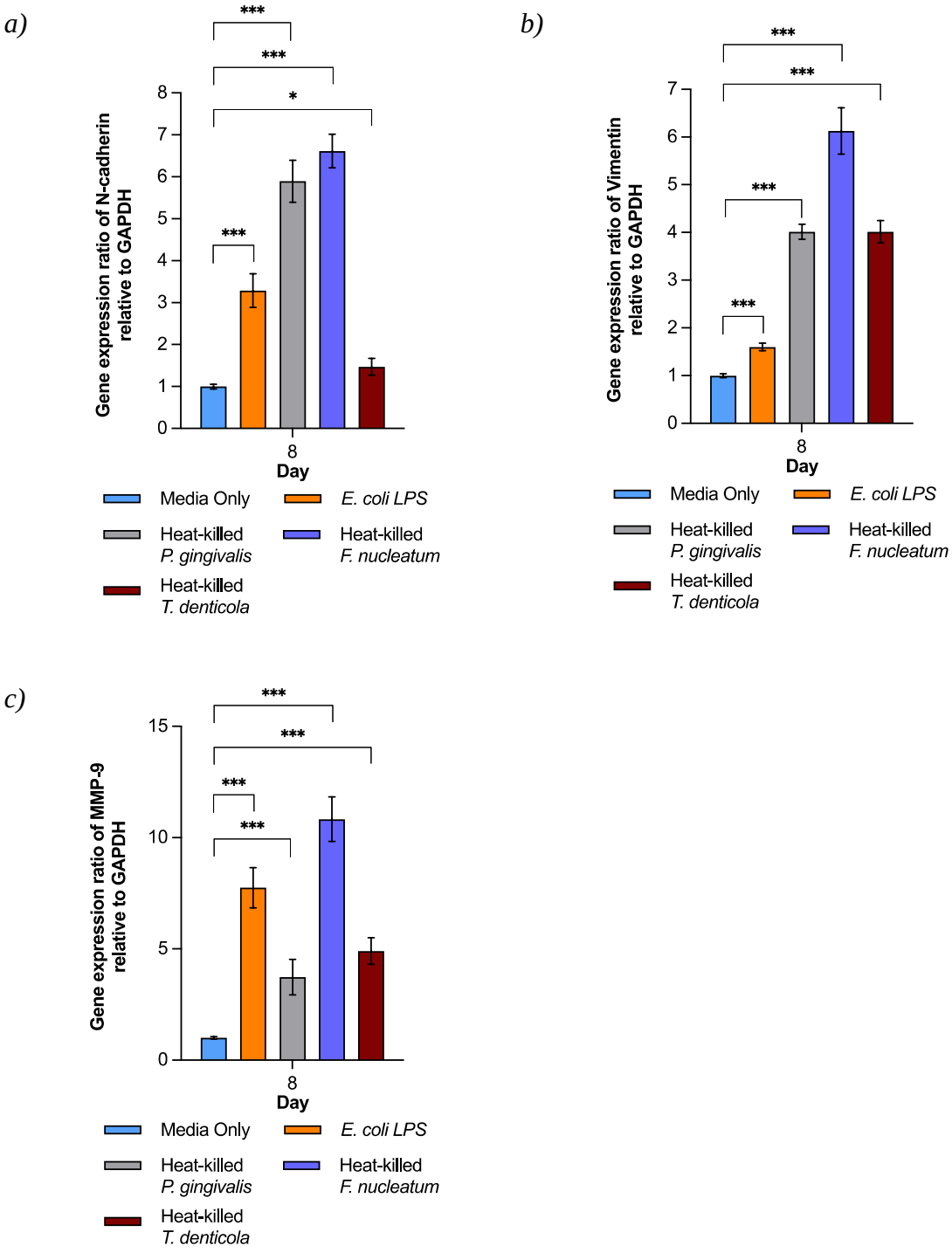



**Figure 4.6**: Gene expression ratios (relative to GAPDH) of mesenchymal markers for (a) N-cadherin, (b) vimentin and (c) MMP-9 as determined by quantitative real-time PCR on day-8 H400 cultures challenged with heat-killed *P. gingivalis*, *F. nucleatum* and *T. denticola*. All cultures challenged with heat-killed bacteria significantly up-regulated expression of mesenchymal markers N-cadherin, vimentin and MMP-9. The values obtained from each sample were normalised to GAPDH. Error bars shown are standard deviations and experiments were performed in triplicate. * = $P<0.05$ and *** = $P<0.001$.

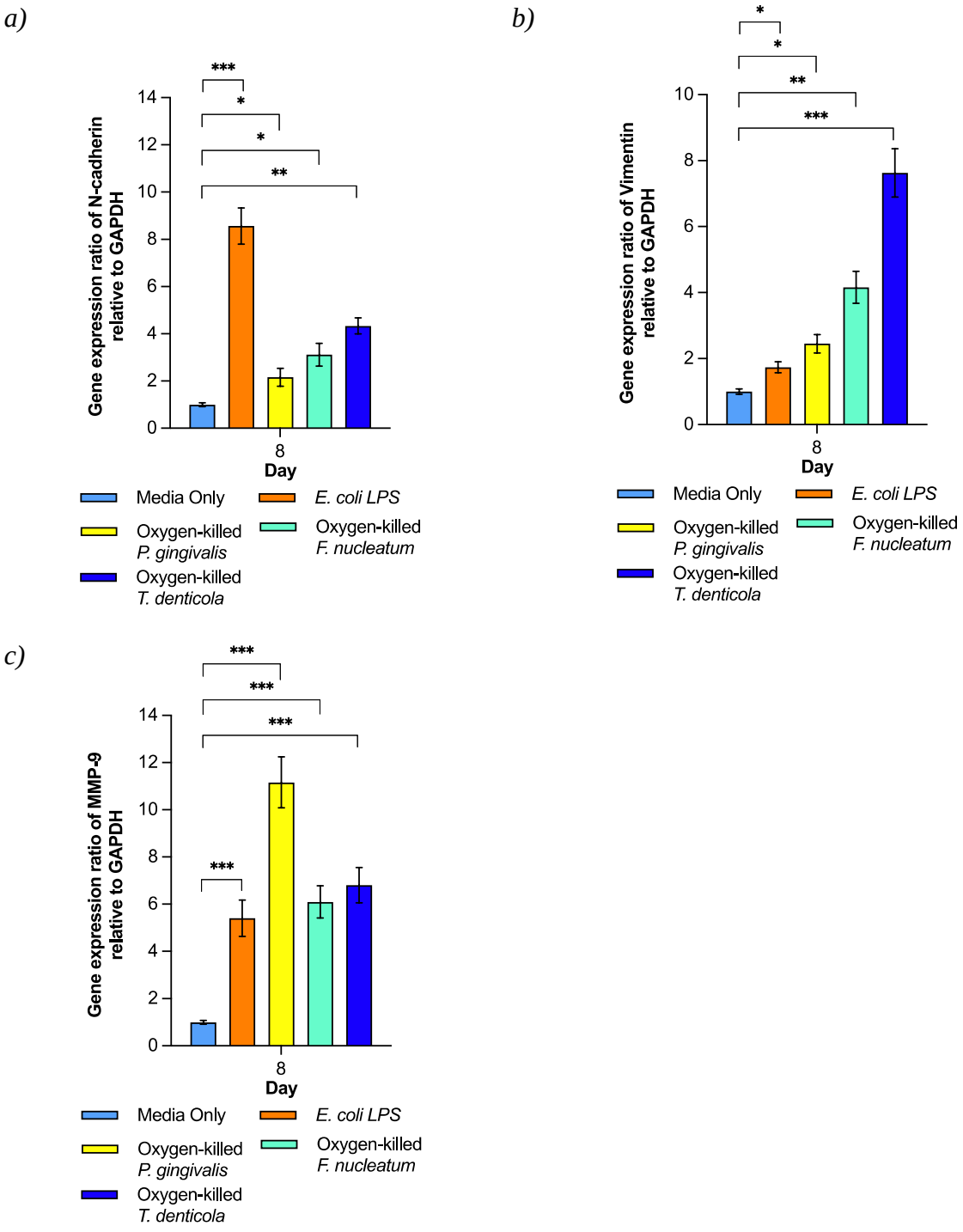



**Figure 4.7**: Gene expression ratios (relative to GAPDH) of mesenchymal markers for (a) N-cadherin, (b) vimentin and (c) MMP-9 as determined by quantitative real-time PCR on day-8 H400 cultures challenged with oxygen-killed *P. gingivalis*, *F. nucleatum* and *T. denticola*. All cultures challenged with oxygen-killed bacteria significantly up-regulated expression of mesenchymal markers N-cadherin, vimentin and MMP-9. The values obtained from each sample were normalised to GAPDH and error bars shown are standard deviations. Experiments were performed in triplicate. * = $P<0.05$, ** = $P<0.01$ and *** = $P<0.001$.

### 4.3.3 Gene expression of EMT-related transcription factors in oral keratinocytes

The regulation of epithelial and mesenchymal genes is controlled by the activation or inactivation of EMT-related transcription factors. The activation of transcription factors snail-1, snail-2 and twist-1 are commonly associated with regulating expression of many epithelial and mesenchymal related genes (Peinado, Olmeda and Cano, 2007). Therefore, these transcription factors were selected for qRT-PCR gene expression analysis in oral keratinocytes following HK and OK pathogen exposure.

#### 4.3.3.1 Effects of pathogen exposure on EMT-related transcription factor gene expression

Snail-1 was significantly up-regulated ($P<0.001$) after *E. coli* LPS (3.44 - 7.16-fold) exposure in both experiments when compared with controls (Figures 4.8a and 4.9a). In addition, the HK pathogens *T. denticola* (36.97-fold) and *F. nucleatum* (13.33-fold) significantly up-regulated ($P<0.001$) snail-1 expression, whilst exposure with HK *P. gingivalis* (0.22-fold) resulted in significant down-regulation of expression in comparison with media only control ($P<0.001$) (Figure 4.8a). However, all OK pathogens (3.11 - 4.54-fold) significantly up-regulated ($P<0.05$ and $P<0.01$) snail-1 expression with highest up-regulation associated with OK *F. nucleatum* (Figure 4.9a).

*E. coli* LPS exposure (1.64-fold) also significantly increased ($P<0.05$) snail-2 expression across both experiments in comparison with media only controls (Figures 4.8b and 4.9b). Snail-2 was significantly up-regulated ($P<0.01$ and $P<0.001$) with all HK pathogens (3.18 - 6.49-fold) with *P. gingivalis* exposure resulting in greatest up-regulation when compared with media only (Figure 4.8b). The OK stimulant of *T. denticola* (3.1-fold) also significantly up-

regulated (P<0.001) snail-2, whilst *F. nucleatum* exposure did not significantly up-regulate snail-2 when compared with control. However, OK *P. gingivalis* (0.53-fold) significantly down-regulated (P<0.05) snail-2 expression (Figure 4.9b).

Twist-1 gene expression was significantly up-regulated (P<0.01 and P<0.001) after *E. coli* LPS (5.74-fold) exposure in comparison with media only control (Figure 4.8c and 4.9c). Twist-1 was significantly up-regulated (P<0.01 and P<0.001) with all HK pathogen exposures (5.01 - 9.76-fold) with highest up-regulation as a result of HK *P. gingivalis* exposure (Figure 4.8c). All OK pathogens (1.02 - 9.3-fold) up-regulated twist-1 gene expression, however significant (P<0.001) and greatest up-regulation was associated with OK *T. denticola* exposure in comparison with media only control (Figure 4.9c).

Stimulation of oral keratinocytes with all HK and OK pathogens up-regulated expression of all EMT-related transcription factors, except HK and OK *P. gingivalis* which presented down-regulation of snail-1 and snail-2, respectively. In conclusion, HK and OK pathogens may induce EMT through up-regulated activity of key transcription factors.

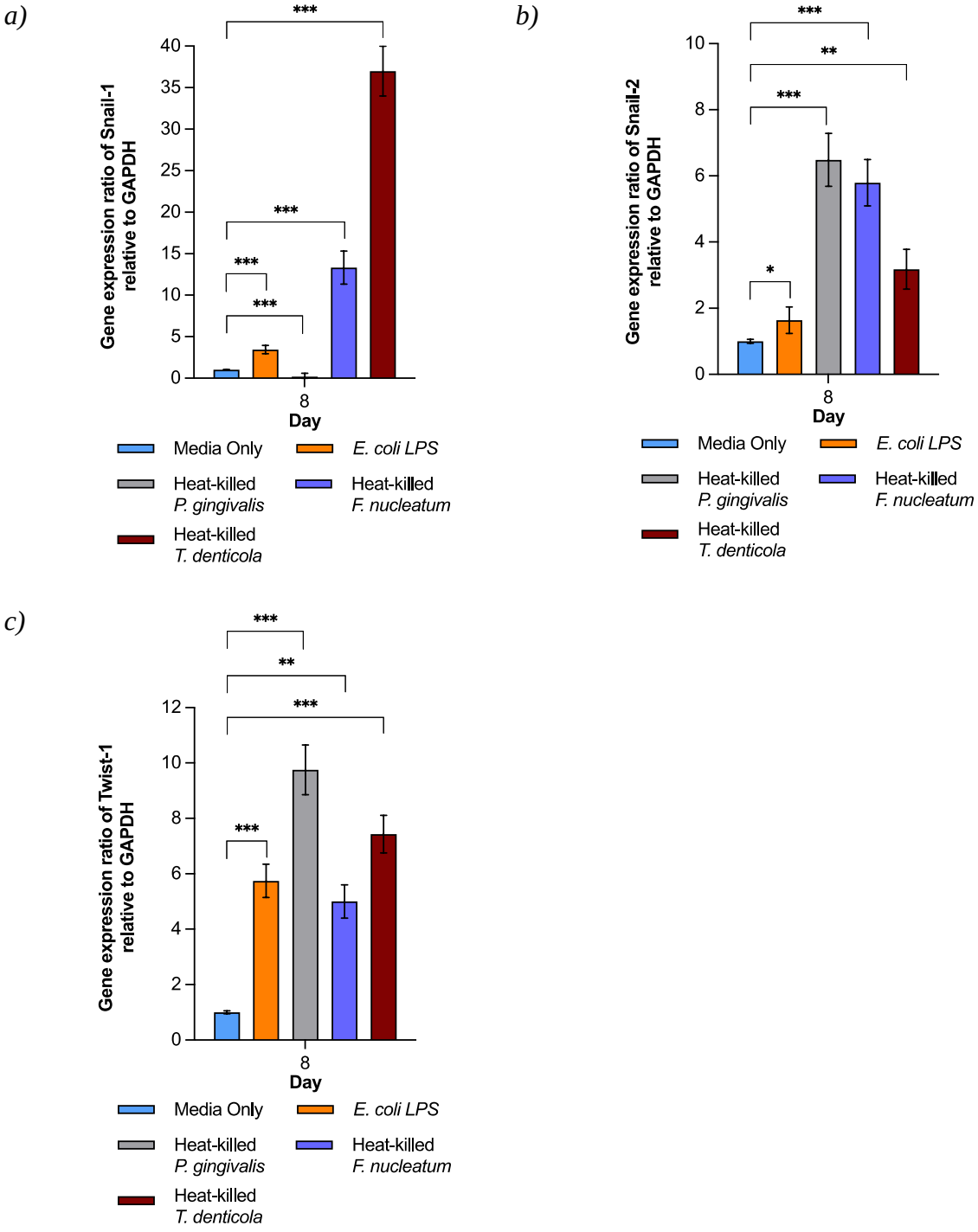



**Figure 4.8**: Gene expression ratios (relative to GAPDH) of EMT-related transcription factors for (a) snail-1, (b) snail-2 and (c) twist-1 as determined by quantitative real-time PCR on day-8 H400 cultures challenged with heat-killed *P. gingivalis*, *F. nucleatum* and *T. denticola*. The values obtained from each sample were normalised to GAPDH. All cultures challenged with heat-killed bacteria significantly up-regulated expression of snail-1, snail-2 and twist-1 when compared with unstimulated cultures. However, exposure with heat-killed *P. gingivalis* significantly decreased snail-1 expression. Error bars shown are standard deviations and experiments were performed in triplicate. * = P<0.05, ** = P<0.01 and *** = P<0.001.

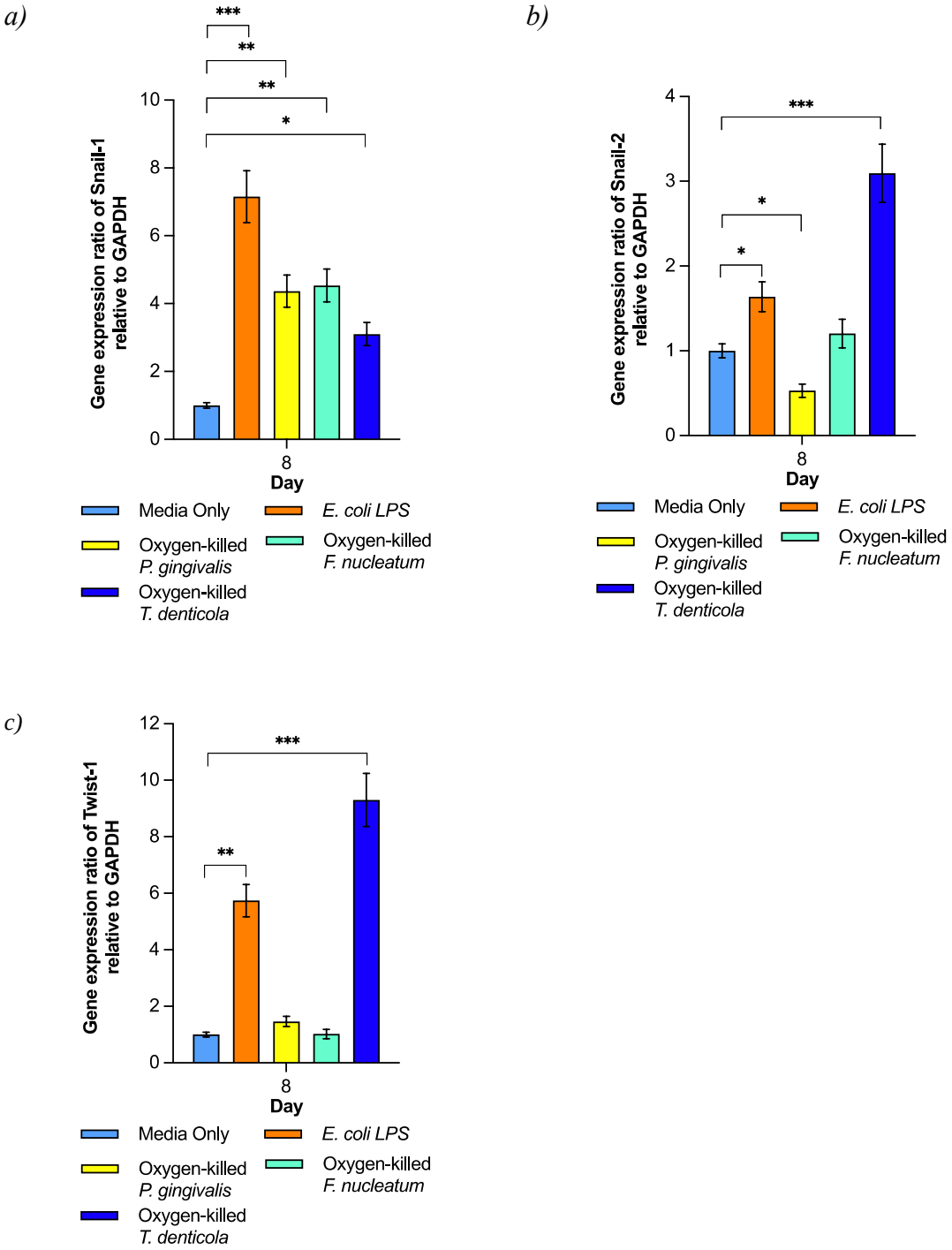



**Figure 4.9**: Gene expression ratios (relative to GAPDH) of EMT-related transcription factors for (a) snail-1, (b) snail-2 and (c) twist-1 as determined by quantitative real-time PCR on day-8 H400 cultures challenged with oxygen-killed *P. gingivalis*, *F. nucleatum* and *T. denticola*. All cultures challenged with oxygen-killed bacteria up-regulated expression of snail-1, snail-2 and twist-1 with *T. denticola* stimulation causing significant up-regulation of all three transcription factors in comparison with unstimulated cultures. However, exposure with oxygen-killed *P. gingivalis* significantly decreased snail-2 expression. The values obtained from each sample were normalised to GAPDH. Error bars shown are standard deviations and experiments were performed in triplicate. * = P<0.05, ** = P<0.01 and *** = P<0.001.

### 4.3.4 Gene expression of EMT-inducing pro-inflammatory cytokines in oral keratinocytes

Epithelial exposure to periodontal pathogens elicits a host-inflammatory response where pro-inflammatory cytokines are released. The pro-inflammatory cytokines IL-1β, IL-8 and TGF-β1 are associated with inducing EMT (see section 1.3.5), therefore gene expression of these cytokines was measured in oral keratinocytes after 8-day exposure to HK and OK pathogens.

#### 4.3.4.1 Effects of pathogen exposure on EMT- inducing pro-inflammatory cytokine gene expression

IL-1β was significantly up-regulated ($P<0.001$) with *E. coli* LPS (8.18 - 8.25-fold) exposure in both experimental studies when compared with media only control (Figures 4.10a and 4.11a). Exposure with all HK pathogens (3.63 - 5.99-fold) significantly up-regulated ($P<0.01$ and $P<0.001$) IL-1β expression after 8-days stimulation (Figure 4.10a) with greatest up-regulation associated with HK *F. nucleatum* exposure in comparison with media only control. Significant up-regulation ($P<0.01$) of IL-1β was also associated with OK *T. denticola* (3.67-fold) exposure (Figure 4.11a).

Expression of IL-8 after *E. coli* LPS (18.14 - 18.21-fold) exposure was significantly up-regulated ($P<0.001$) in comparison with media only control (Figures 4.10b and 4.11b). The HK stimulants (2.22 - 7.6-fold) also significantly increased ($P<0.05$ and $P<0.01$) IL-8 expression when compared with control and the greatest IL-8 increase amongst the HK pathogens was associated with *P. gingivalis* (Figure 4.10b). However, only the OK stimulant of *T. denticola* (25.11-fold) significantly increased ($P<0.001$) IL-8 gene expression (Figure 4.11b).

*E. coli* LPS (2.12 - 2.18-fold) exposure also significantly up-regulated ($P<0.05$ and $P<0.01$) expression of TGF-β1 after 8-days stimulation in comparison with control (Figures 4.10c and 4.11c). TGF-β1 was also significantly up-regulated ($P<0.05$, $P<0.01$ and $P<0.001$) with all HK pathogen exposures (1.26 - 2.94-fold) with greatest increase associated with HK *P. gingivalis* (Figure 4.10c). However, only OK pathogens *T. denticola* (6.58-fold) ($P<0.001$) and *F. nucleatum* (1.54-fold) ($P<0.05$) significantly up-regulated TGF-β1 expression in comparison with media only control (Figure 4.11c).

Gene expression of the pro-inflammatory cytokines IL-1β, IL-8 and TGF-β1 were all up-regulated in both HK and OK pathogen exposed cultures apart from OK *P. gingivalis* which down-regulated IL-1β and TGF-β1 expression. OK *T. denticola* was responsible for greatest up-regulation of IL-8 and TGF-β1 amongst all HK and OK pathogens. In conclusion, HK pathogens or OK *F. nucleatum* and *T. denticola* induced up-regulated pro-inflammatory cytokine gene expression possibly leading to increased pro-inflammatory cytokine release, which may have facilitated induction of EMT. To further confirm this, oral keratinocytes were exposed to HK and OK pathogens and amount of secreted IL-1β, IL-8 and TGF-β1 were measured by ELISAs.

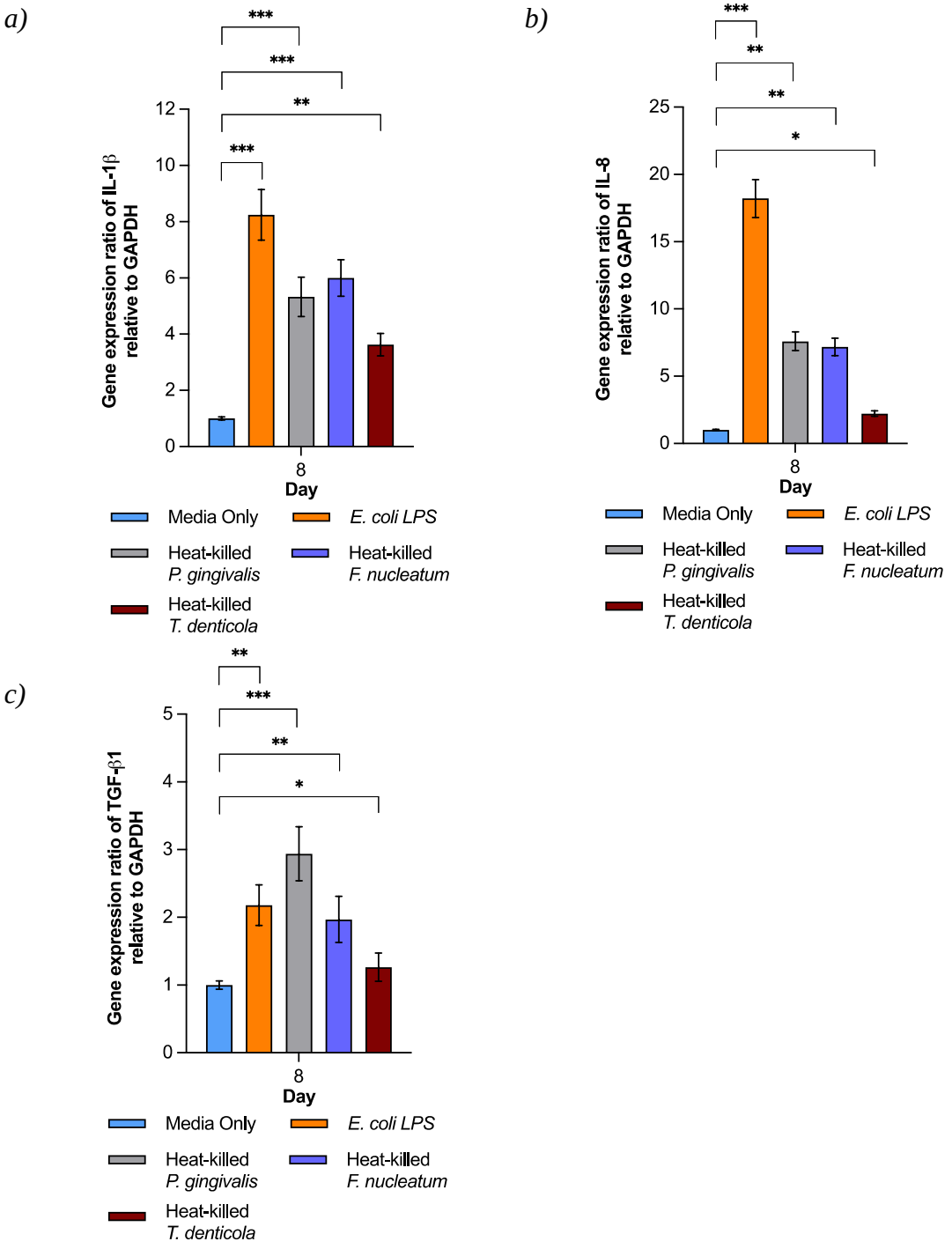



**Figure 4.10**: Gene expression ratios (relative to GAPDH) of pro-inflammatory cytokines for (a) IL-1β, (b) IL-8 and (c) TGF-β1 as determined by quantitative real-time PCR on day-8 H400 cultures challenged with heat-killed *P. gingivalis*, *F. nucleatum* and *T. denticola*. All cultures challenged with heat-killed bacteria significantly up-regulated expression of IL-1β, IL-8 and TGF-β1 when compared with unstimulated cultures. The values obtained from each sample were normalised to GAPDH. Error bars shown are standard deviations and experiments were performed in triplicate. * = P<0.05, ** = P<0.01 and *** = P<0.001.

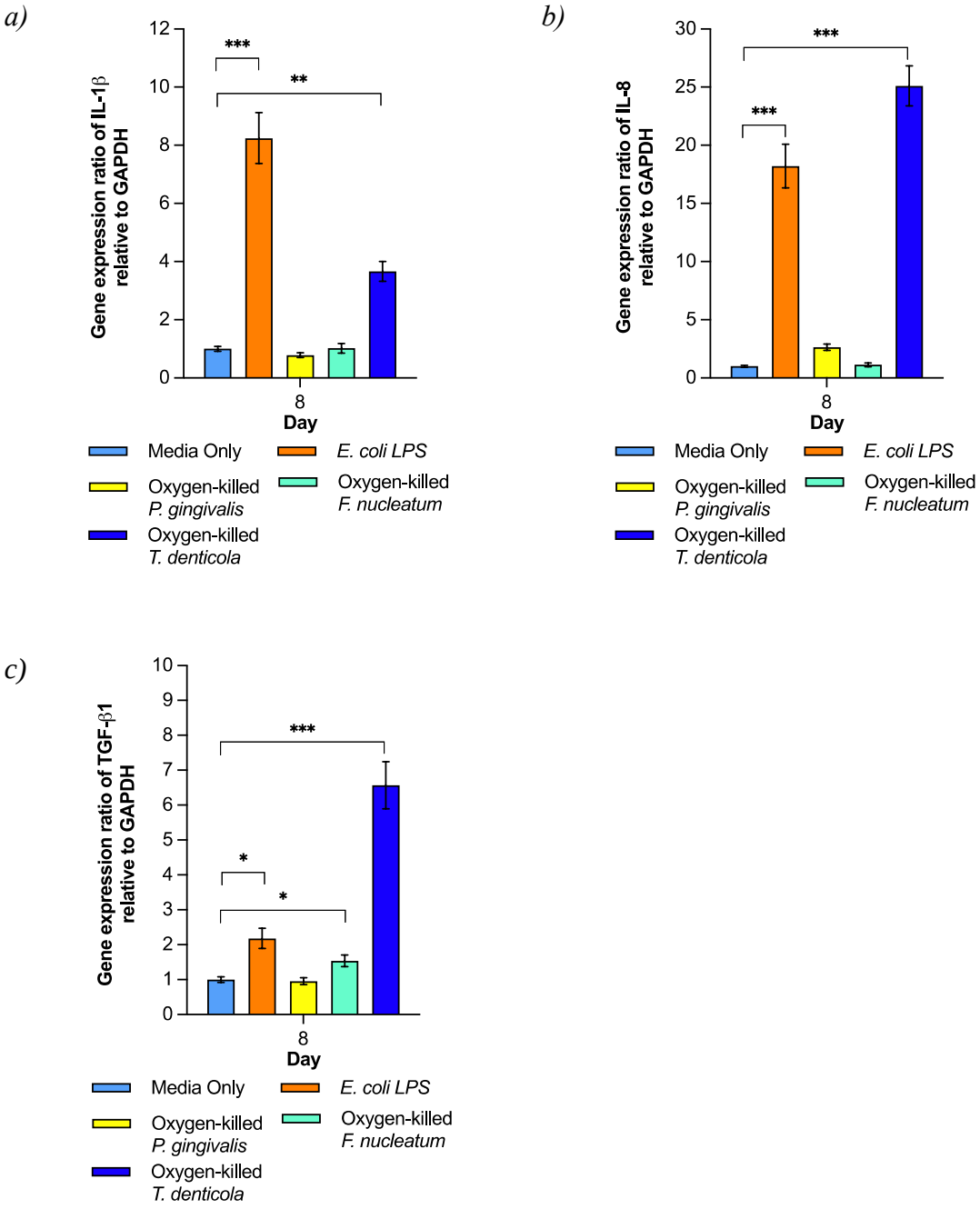



**Figure 4.11**: Gene expression ratios (relative to GAPDH) of pro-inflammatory cytokines for (a) IL-1β, (b) IL-8 and (c) TGF-β1 as determined by quantitative real-time PCR on day-8 H400 cultures challenged with oxygen-killed *P. gingivalis*, *F. nucleatum* and *T. denticola*. Cultures challenged with oxygen-killed *T. denticola* significantly up-regulated expression of IL-1β, IL-8 and TGF-β1 when compared with unstimulated cultures, whilst oxygen-killed *F. nucleatum* only significantly up-regulated TGF-β1 expression. The values obtained from each sample were normalised to GAPDH. Error bars shown are standard deviations and experiments were performed in triplicate. * = $P<0.05$, ** = $P<0.01$ and *** = $P<0.001$.

**Table 4.1**: Summary of gene expression ratios determined by quantitative real-time PCR of EMT related markers following 8-day exposure to heat and oxygen-killed pathogens

| | **Gene expression ratios of EMT related markers after pathogen exposure (heat and oxygen-killed)** | | | | | | |
|---|---|---|---|---|---|---|---|
| **Gene name** | *E. coli* LPS | *P. gingivalis* | | *F. nucleatum* | | *T. denticola* | |
| | | HK | OK | HK | OK | HK | OK |
| E-cadherin | 0.17 | 0.39 | 0.05 | 0.51 | 0.003 | 1.57 | 0.13 |
| Cytokeratin 5 | 0.67 | 0.49 | 0.69 | 0.27 | 0.3 | 0.28 | 0.28 |
| Desmoplakin-1 | 0.22 | 0.7 | 0.75 | 0.27 | 0.41 | 0.55 | 0.13 |
| N-cadherin | 8.6 | 5.82 | 2.16 | 6.75 | 3.12 | 1.42 | 4.33 |
| Vimentin | 1.74 | 4.01 | 2.45 | 6.12 | 4.16 | 4.02 | 7.63 |
| MMP-9 | 7.75 | 3.73 | 11.16 | 10.83 | 6.1 | 4.91 | 6.81 |
| Snail-1 | 7.16 | 0.22 | 4.37 | 13.33 | 4.54 | 36.97 | 3.11 |
| Snail-2 | 1.64 | 6.49 | 0.53 | 5.8 | 1.2 | 3.18 | 3.1 |
| Twist-1 | 5.74 | 9.76 | 1.47 | 5.01 | 1.02 | 7.44 | 9.3 |
| IL-1β | 8.25 | 5.31 | 0.78 | 5.99 | 1.02 | 3.63 | 3.67 |
| IL-8 | 18.21 | 7.6 | 2.63 | 7.18 | 1.13 | 2.22 | 25.11 |
| TGF-β1 | 2.18 | 2.94 | 0.95 | 1.97 | 1.54 | 1.26 | 6.58 |

Down-regulated  Up-regulated

### 4.4 Pro-inflammatory cytokine expression by Enzyme-linked immunosorbent assay

It has been noted that patients with periodontitis exhibit elevated levels of IL-1β, IL-8 and TGF-β1, which are key cytokines involved in the initiation of EMT (see section 1.3.5). Data here showed gene transcripts of these cytokines to be increased in epithelial cells after exposure to HK and OK pathogens (see section 4.3.4.1). This may have translated into increased cytokine secretion, therefore ELISAs were utilised to measure cytokine levels in collected supernatants from cultures stimulated by HK and OK pathogens. The cytokine levels presented for media only and *E. coli* LPS for each cytokine were kept constant, as ELISAs were performed collectively with all HK and OK pathogens.

#### 4.4.1 Analysis of IL-1β secretion

IL-1β secretion was significantly increased ($P<0.001$) in cultures exposed to HK *P. gingivalis* (4.19 pg/ml) after 1-day stimulation when compared with media only (3.73 pg/ml) and OK *P. gingivalis* (3.68 pg/ml) stimulated cultures (Figure 4.12a). On day 5, all stimulated cultures significantly up-regulated ($P<0.05$ and $P<0.001$) IL-1β secretion when compared with unstimulated cultures, with *E. coli* LPS (5.28 pg/ml) resulting in the highest level of IL-1β secretion followed by HK *P. gingivalis* (4.11 pg/ml) and OK *P. gingivalis* (4.05 pg/ml). This was also observed on day 8, where *E. coli* LPS (8.2 pg/ml), OK *P. gingivalis* (6.85 pg/ml) and HK *P. gingivalis* (5.35 pg/ml) exposure significantly increased ($P<0.001$) IL-1β secretion in comparison with media only (4.17 pg/ml). Also, OK *P. gingivalis* resulted in significantly increased IL-1β secretion when compared with its HK stimulant after 8-days exposure ($P<0.001$) (Figure 4.12a).

HK and OK *F. nucleatum* significantly induced IL-1β secretion on day 1 when compared with unstimulated cultures ($P<0.001$), with OK *F. nucleatum* resulting in 6.08 pg/ml secretion

compared with 6.06 pg/ml after HK *F. nucleatum* exposure (Figure 4.12b). On day 5 IL-1β levels ($P<0.001$) were still significantly greater in OK *F. nucleatum* (7.02 pg/ml) and HK *F. nucleatum* (6.75 pg/ml) exposed cultures in comparison with cultures in media only (3.81 pg/ml). Also, this secretion was significantly higher in cultures treated with OK *F. nucleatum* compared with its HK analogue ($P<0.05$). Significant levels ($P<0.001$) of IL-1β were also detected on day 8 after stimulation with HK (21.57 pg/ml) and OK *F. nucleatum* (17.04 pg/ml) when compared with unstimulated cultures (4.17 pg/ml). The HK stimulant of *F. nucleatum* however, resulted in significantly greater IL-1β secretion compared with its OK stimulant ($P<0.001$) (Figure 4.12b).

On day 1, cultures stimulated with HK (3.94 pg/ml) ($P<0.01$) and OK *T. denticola* (4.51 pg/ml) ($P<0.001$) significantly induced IL-1β secretion in comparison with cultures in media only (Figure 4.12c). This increased secretion was also significantly higher with OK *T. denticola* stimulation compared with its HK stimulant ($P<0.001$). After 5-days stimulation, IL-1β secretion was significantly reduced with HK *T. denticola* (3.3 pg/ml) ($P<0.001$) exposure and significantly increased with OK *T. denticola* (5.39 pg/ml) ($P<0.001$) exposure when compared with media only (3.81 pg/ml). Also, OK *T. denticola* exposure resulted in significantly higher IL-1β secretion in comparison with its HK stimulant ($P<0.001$). On day 8, IL-1β levels were significantly greater in OK *T. denticola* (19.52 pg/ml) challenged cultures compared with cultures in media only ($P<0.001$) and cultures exposed to HK *T. denticola* (4.29 pg/ml) ($P<0.001$) (Figure 4.12c).

All stimulated cultures increased IL-1β secretion after 8-days exposure with greatest secretion detected after HK *F. nucleatum* exposure and least after HK *P. gingivalis* exposure. OK

stimulants of *P. gingivalis* and *T. denticola* significantly increased IL-1β secretion when compared with their HK stimulants. In conclusion, oxygen-killed bacteria may stimulate greater IL-1β cytokine release when compared with heat-killed bacteria, possibly leading to greater induction of EMT.

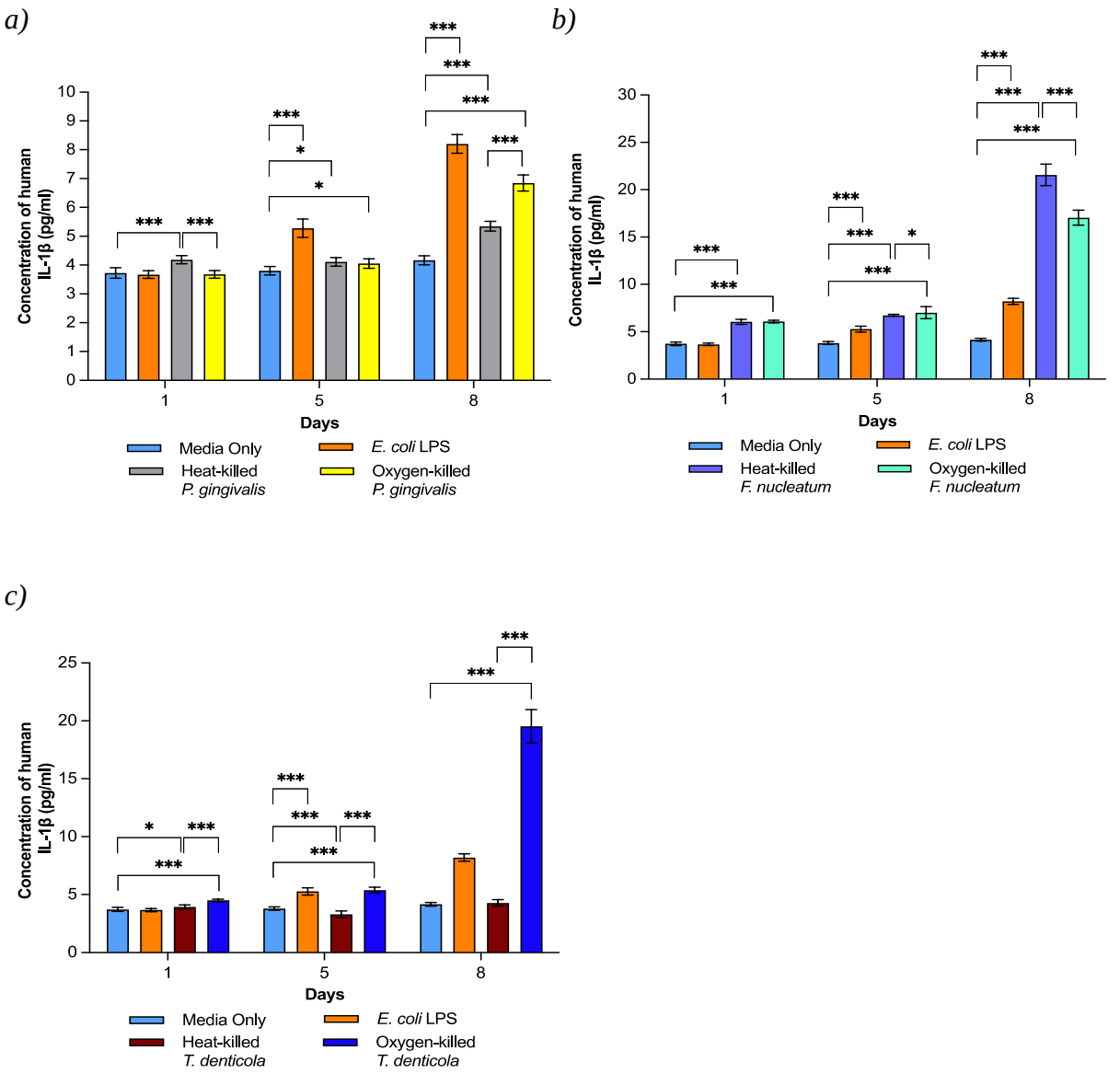



**Figure 4.12**: H400 cultures challenged with *E. coli* LPS, (a) heat and oxygen-killed *P. gingivalis*, (b) heat and oxygen-killed *F. nucleatum*, (c) heat and oxygen-killed *T. denticola* for IL-1β ELISA analysis on supernatants collected on day 1, 5 and 8. All cultures challenged with pathogens showed significantly increased IL-1β secretion after 8-days exposure except heat-killed *T. denticola* when compared with media only control. Error bars shown are standard deviations and n=9. * = P<0.05 and *** = P<0.001. Significance was tested using one-way ANOVA followed by a post-hoc Tukey test.

### 4.4.2 Analysis of IL-8 secretion

After 1 day stimulation *E. coli* LPS significantly increased IL-8 secretion when compared with unstimulated cultures (P<0.001) (Figure 4.13a). On day 5, *E. coli* LPS (7.54 µg/ml) and both HK *P. gingivalis* (5.39 µg/ml) and OK *P. gingivalis* (7.3 µg/ml) exposed cultures significantly increased IL-8 secretion (P<0.001) in comparison with unstimulated cultures. This secretion was significantly greater amongst cultures stimulated with OK *P. gingivalis* compared with its HK stimulant (P<0.001). After 8-days, *E. coli* LPS (8.66 µg/ml), HK (8.49 µg/ml) and OK *P. gingivalis* (7.34 µg/ml) exposure increased IL-8 secretion, with *E. coli* LPS and HK *P. gingivalis* resulting in significant release (P<0.001) when compared with cultures in media only (Figure 4.13a).

HK and OK *F. nucleatum* also significantly induced a greater IL-8 secretion on day 5 when compared with unstimulated cultures (P<0.001). IL-8 secretion was also significantly higher (P<0.001) in HK *F. nucleatum* challenged cultures (4.57 µg/ml) when compared with the OK stimulant (2.28 µg/ml) on day 5 (Figure 4.13b). However, on day 8 cultures stimulated with OK *F. nucleatum* resulted in greater IL-8 secretion of 6.91 µg/ml compared with 5.46 µg/ml secretion after HK *F. nucleatum* challenge.

On day 5, cultures stimulated with OK *T. denticola* (0.47 µg/ml) resulted in greater IL-8 secretion when compared with media only control (0.12 µg/ml), whereas HK *T. denticola* (0.11 µg/ml) exposure non-significantly decreased secretion. On day 8 however, IL-8 secretion was increased by both HK and OK *T. denticola* when compared with unstimulated cultures. Also, the HK analogue (7.98 µg/ml) resulted in significantly greater IL-8 secretion compared with the OK stimulant of *T. denticola* (5.53 µg/ml) (P<0.001) (Figure 4.13c).

In general, IL-8 release was increased after 8-days stimulation with pathogens, with HK *P. gingivalis* exposure resulting in greatest secretion and lowest after HK *F. nucleatum* challenge amongst the HK and OK pathogens used. Therefore, increased secretion of IL-8 after pathogen exposure may be responsible for triggering EMT-related responses in oral keratinocytes.

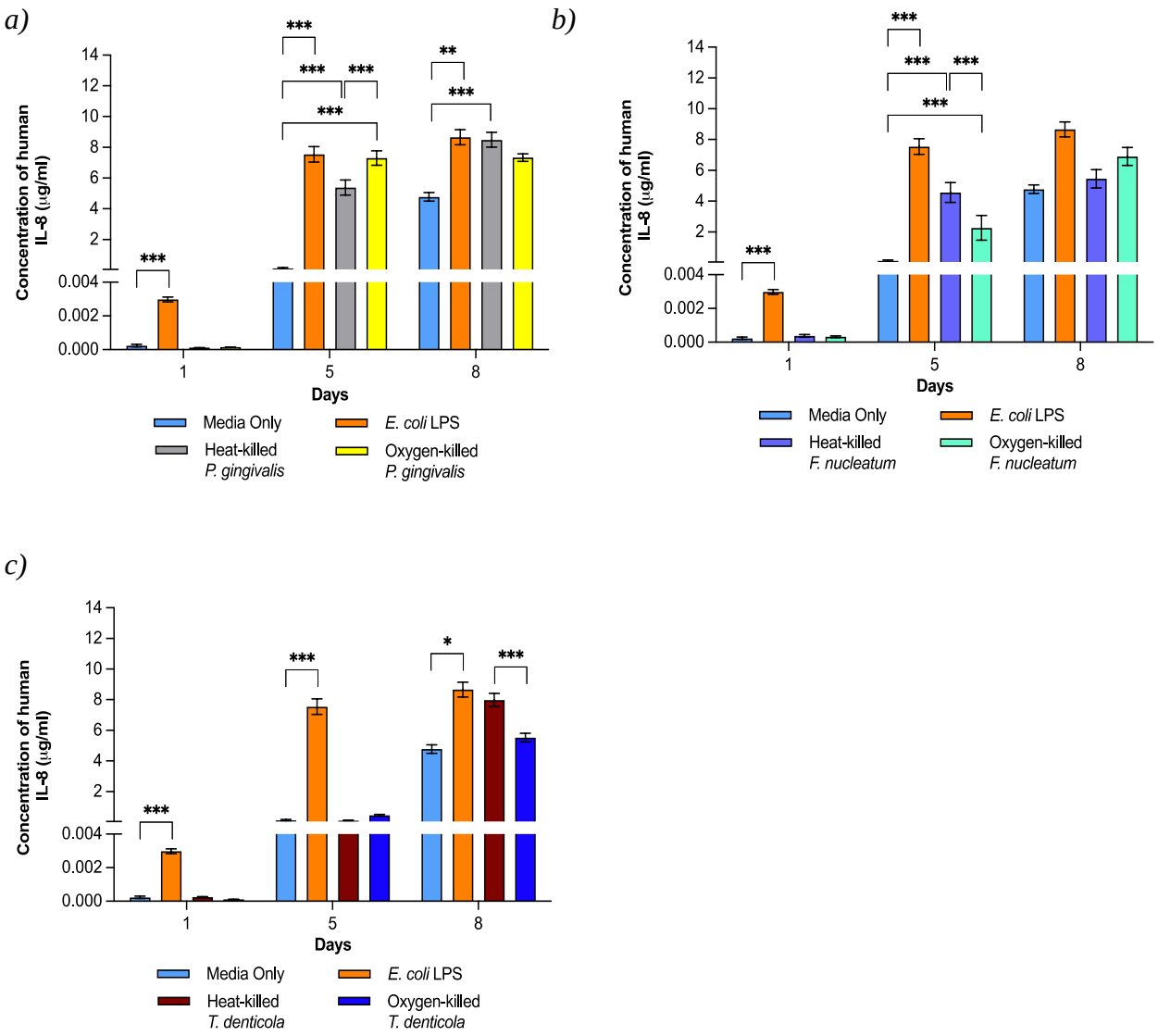



**Figure 4.13**: H400 cultures challenged with *E. coli* LPS, (a) heat and oxygen-killed *P. gingivalis*, (b) heat and oxygen-killed *F. nucleatum*, (c) heat and oxygen-killed *T. denticola* for IL-8 ELISA analysis on supernatants collected on day 1, 5 and 8. All pathogen stimulated cultures showed increased IL-8 secretion after 8-days when compared with media only control. Error bars shown are standard deviations and n=9. * = P<0.05 , ** = P<0.01 and *** = P<0.001. Significance was tested using one-way ANOVA followed by a post-hoc Tukey test.

### 4.4.3 Analysis of TGF-β1 secretion

TGF-β1 secretion was significantly increased (P<0.001) in cultures exposed to OK *P. gingivalis* (15.29 ng/ml) after 1 day stimulation when compared with media only (6.43 ng/ml) (Figure 4.14a). Also, detection of TGF-β1 in cultures exposed to the OK stimulant of *P. gingivalis* was significantly higher than its HK stimulant (4.68 ng/ml) (P<0.001). After 5-days, TGF-β1 levels were still significantly higher in OK *P. gingivalis* exposed cultures (13.52 ng/ml) (P<0.001) in comparison with control (P<0.001) and HK *P. gingivalis* (P<0.001). TGF-β1 levels were also still raised after *E. coli* LPS (13 ng/ml) exposure and significantly more than cultures in media only (P<0.001). HK *P. gingivalis* also raised TGF-β1 (6.36 ng/ml) levels in cultures after 5-day stimulation. Levels of TGF-β1 were still significantly raised (P<0.001) in cultures exposed to OK *P. gingivalis* (8.07 ng/ml) and *E. coli* LPS (5.83 ng/ml) after 8-days stimulation in comparison with media only (3.08 ng/ml). These TGF-β1 levels were also significantly higher in cultures exposed to the OK analogue of *P. gingivalis* when compared with its HK stimulant (3.42 ng/ml) (P<0.001) (Figure 4.14a).

TGF-β1 levels detected in cultures exposed to HK (9.04 ng/ml) and OK *F. nucleatum* (168.69 ng/ml) were significantly raised after 1 day exposure in comparison with media only (P<0.001) (Figure 4.14b). After 5-days these TGF-β1 levels were still significantly higher in cultures exposed to HK (10.98 ng/ml) (P<0.01) and OK *F. nucleatum* (126.57 ng/ml) (P<0.001) when compared with cultures in media only (4.91 ng/ml). On day 8, TGF-β1 levels were still significantly higher (P<0.001) in comparison with media only after HK (34.4 ng/ml) and OK *F. nucleatum* (187.17 ng/ml) exposure. In addition, exposure to the OK analogue of *F. nucleatum* resulted in significantly higher (P<0.001) TGF-β1 levels when compared with its HK stimulant across all days (Figure 4.14b).

Similarly, TGF-β1 levels were significantly raised (P<0.001) after exposure to HK (18.28 ng/ml) and OK *T. denticola* (61.76 ng/ml) in comparison with media only on day 1 (Figure 4.14c). After 5 days these levels were still significantly higher (P<0.001) in HK (45.68 ng/ml) and OK *T. denticola* (60.59 ng/ml) cultures compared with media only (4.91 ng/ml). The TGF-β1 levels detected after 8-days exposure showed similar findings where HK (48.48 ng/ml) and OK *T. denticola* (50.65 ng/ml) significantly raised levels compared with cultures in media only (3.08 ng/ml) (P<0.001). Like OK *P. gingivalis* and OK *F. nucleatum*, the OK stimulant of *T. denticola* significantly increased TGF-β1 levels when compared with its HK analogue for all days except day 8.

TGF-β1 levels were raised in all stimulated cultures after 8-days exposure in comparison with media only and greatest increase was associated with OK *F. nucleatum* exposure, whilst the least was with HK *P. gingivalis* exposure. OK analogues of *P. gingivalis* and *F. nucleatum* were able to significantly induce greater TGF-β1 secretion in comparison with HK stimulants across all days. This could have suggested greater EMT-related responses initiated by OK *P. gingivalis* and *F. nucleatum*, possibly through the activation of TGF-β mediated pathways.

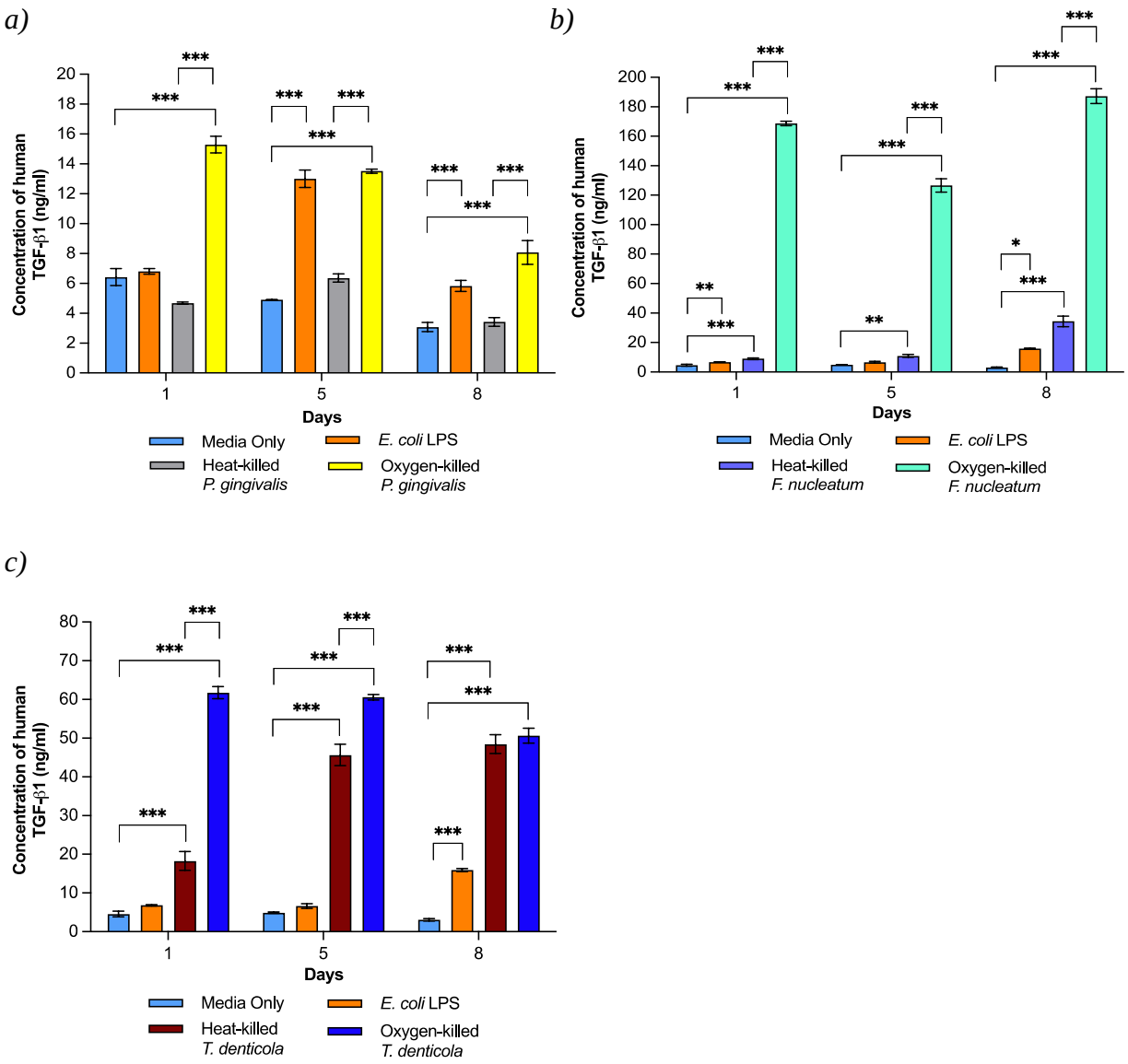



**Figure 4.14**: H400 cultures challenged with *E. coli* LPS, (a) heat and oxygen-killed *P. gingivalis*, (b) heat and oxygen-killed *F. nucleatum*, (c) heat and oxygen-killed *T. denticola* for TGF-β1 ELISA analysis on supernatants collected on day 1, 5 and 8. All cultures challenged with pathogens showed significantly increased TGF-β1 secretion after 8-days except HK *P. gingivalis* when compared with media only control. All oxygen-killed pathogens resulted in greater TGF-β1 secretion across all days when compared with cultures challenged by heat-killed stimulants. Error bars shown are standard deviations and n=9. * = P<0.05, ** = P<0.01 and *** = P<0.001. Significance was tested using one-way ANOVA followed by a post-hoc Tukey test.

### 4.5 Immunofluorescence for E-cadherin, Vimentin and Snail-1 proteins in oral keratinocytes after stimulation with heat and oxygen-killed pathogens

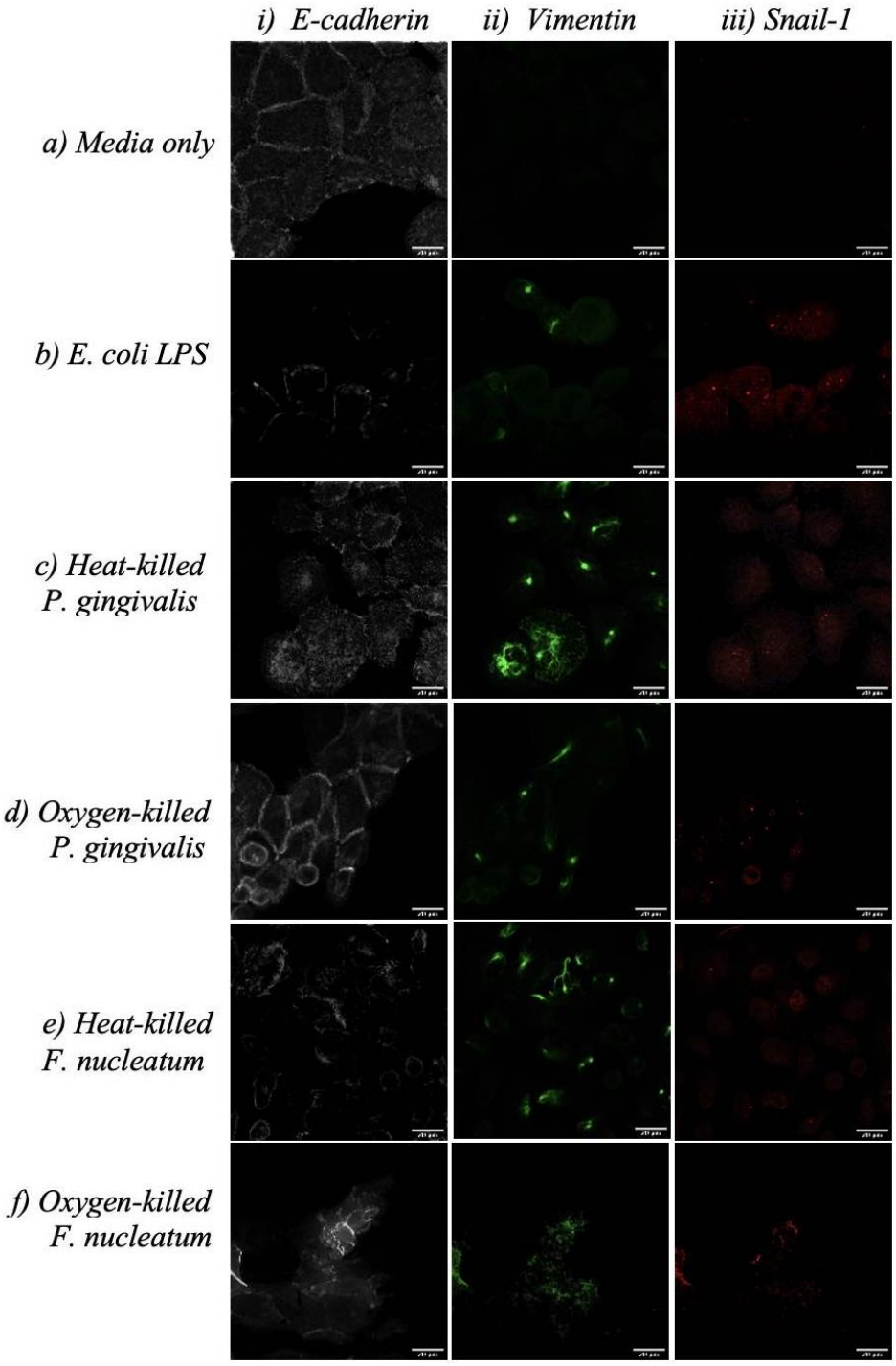
Previous data in the present study has shown that HK and OK periodontal pathogens can alter gene expression of E-cadherin (see section 4.3.1.1), vimentin (see section 4.3.2.1) and snail-1 (see section 4.3.3.1), in relation to EMT. As proteins affect cell function, immunofluorescence staining was utilised on oral keratinocytes cultures to detect protein expression and localisation of these markers after 8-day exposure to HK and OK pathogens.

#### 4.5.1 Effects of heat and oxygen-killed pathogens on E-cadherin, Vimentin and Snail-1 protein expression in oral keratinocytes

The epithelial marker E-cadherin was expressed in oral keratinocyte cultures in media only but lacked expression of the mesenchymal markers vimentin and snail-1 which is expected of epithelial cells (Figure 4.15a). However, *E. coli* LPS exposure caused decreased E-cadherin expression and increased expression of the mesenchymal markers vimentin and snail-1 (Figure 4.15b). In addition, both HK and OK analogues of *P. gingivalis*, *F. nucleatum* and *T. denticola* increased the expression of vimentin and snail-1 after 8-days exposure (Figure 4.15 c-h) ii) and iii)). Expression of E-cadherin was also down-regulated in all stimulated cultures, except for cultures exposed to HK and OK *P. gingivalis* and OK *F. nucleatum*. The 3T3 fibroblast cell line is a mesenchymal cell line which was used as an additional positive control in this study. IF staining of this cell line showed expression of vimentin covering the cytoplasm and snail-1 expression in the nucleus of all cells, however E-cadherin was not expressed (Figure 4.15j). The distribution of vimentin was similar in all challenged cultures except for OK *T. denticola* which had a vimentin distribution similar to 3T3 fibroblasts. Snail-1 distribution was similar in HK *P. gingivalis* and *F. nucleatum* stimulated cultures

where staining covered a large circular area and this was also observed in 3T3 fibroblasts. However, OK *P. gingivalis* and *F. nucleatum* exposure resulted in snail-1 being localised at multiple sites within a cell (Figure 4.15 d and f) iii)). However stimulation with *E. coli* LPS and OK *T. denticola* exhibited both snail-1 structures with snail-1 being localised at more sites after OK *T. denticola* exposure (Figure 4.15 b and h) iii)).

Data here indicated that exposure of epithelial cells to HK and OK periodontal pathogens could up-regulate expression of the cytoskeletal marker vimentin and also increase expression of the key EMT-related transcriptional factor snail-1. However, exposure to *E. coli* LPS, OK *P. gingivalis*, *F. nucleatum* and *T. denticola* showed snail-1 to be localised at multiple sites in comparison with the mesenchymal 3T3 cell line. Therefore, the location of snail-1 in oral keratinocytes after exposure to OK *T. denticola* was further explored.


i) E-cadherin
ii) Vimentin
iii) Snail-1
a) Media only
b) E. coli LPS
c) Heat-killed P. gingivalis
d) Oxygen-killed P. gingivalis
e) Heat-killed F. nucleatum
f) Oxygen-killed F. nucleatum

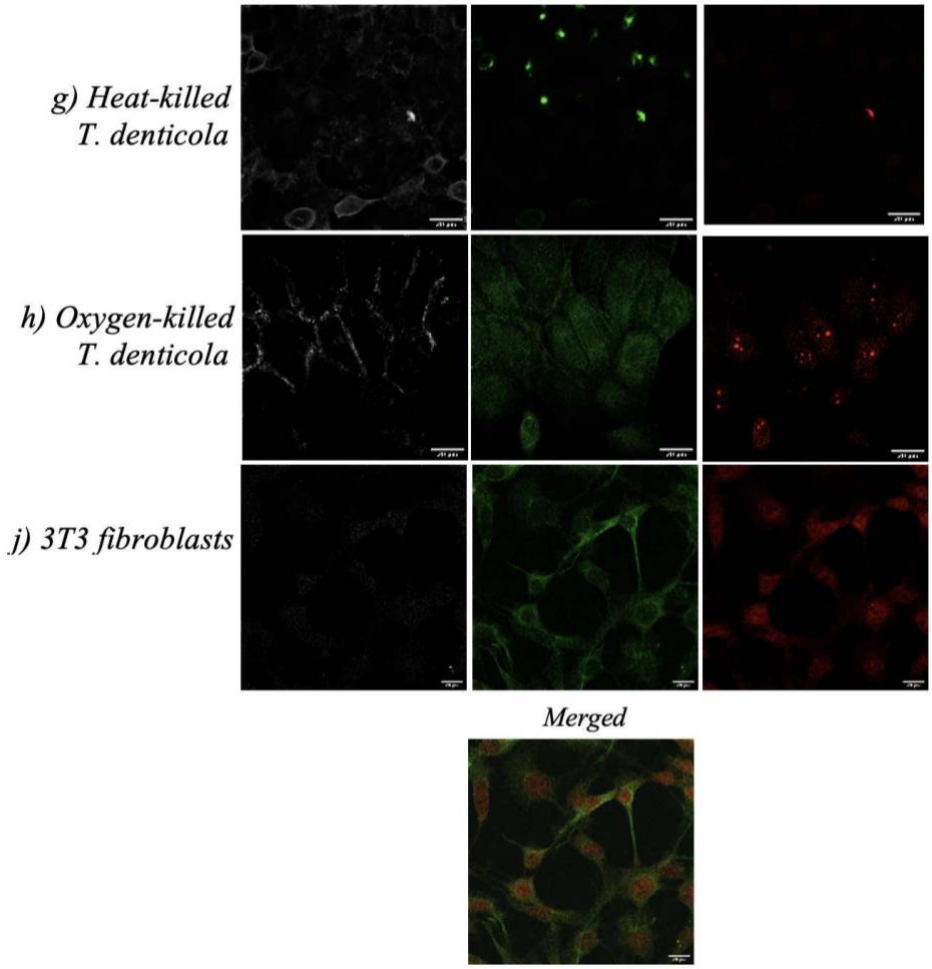



**Figure 4.15**: Representative IF images of day-8 H400 cell cultures stained for (i) E-cadherin, (ii) Vimentin and (iii) Snail-1 after exposure to (a) media only, (b) *E. coli* LPS, (c) – (d) heat and oxygen killed *P. gingivalis*, (e) – (f) *F. nucleatum* and (g) – (h) *T. denticola*. (j) 3T3 fibroblast cells were also stained and used as a positive control. E-cadherin expression was down-regulated in all stimulated cultures except after heat-killed and oxygen-killed *P. gingivalis* and oxygen-killed *F. nucleatum* exposure. Expression of the mesenchymal markers snail-1 and vimentin was greater in cell cultures challenged with heat and oxygen-killed bacteria when compared with media only control. Images displayed are representative of experiments performed in triplicate. Scale bars = 20 µm.

#### 4.5.1.1 Localisation of Snail-1 in oral keratinocytes after oxygen-killed *T. denticola* exposure

Snail-1 was expressed differently in oral keratinocytes after exposure to *E. coli* LPS, OK *P. gingivalis, F. nucleatum* and *T. denticola* where snail-1 was distributed in many localised sites within the cell (see Figure 4.15 iii)). This was more prevalent in cultures which were exposed to *T. denticola,* therefore the localisation of snail-1 in epithelial cells after OK *T. denticola* exposure was further investigated. Nuclear staining using DAPI with snail-1 staining of oral keratinocytes after OK *T. denticola* challenge revealed that snail-1 was localised in the nucleus. Interestingly, snail-1 seemed to be present in the nucleoli represented by the dark voids of the nuclei stained with DAPI. This was further confirmed by staining for upstream binding factor-1 (UBF-1) which stains the UBF protein found in nucleolar organizer regions (NORs) of the nucleolus. Staining with UBF-1 revealed that snail-1 was co-localised in the nucleolus of oral keratinocytes after exposure to OK *T. denticola* for 8-days (Figure 4.16).

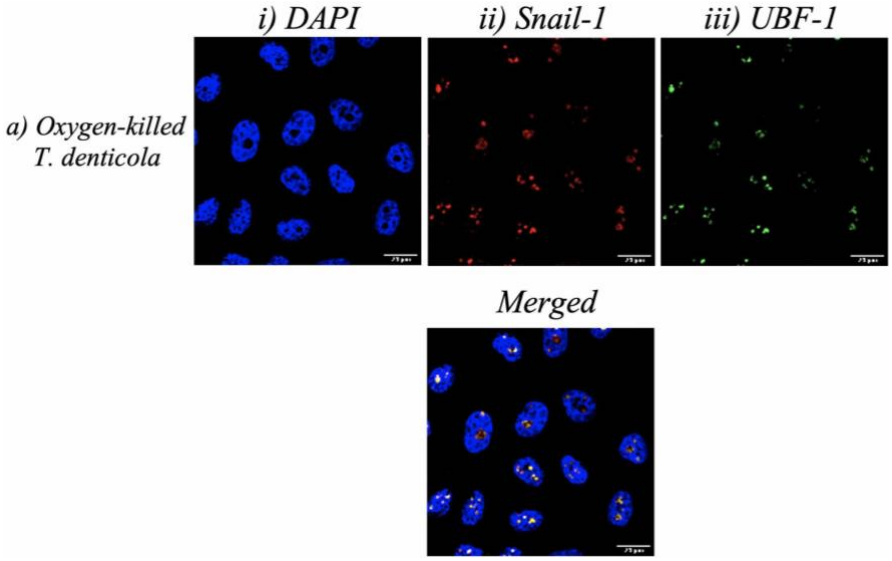



**Figure 4.16**: (i) DAPI, (ii) snail-1 and (iii) upstream binding factor-1 (UBF-1) immunofluorescent staining of H400 cells to determine localisation of snail-1 after 8 days challenge with (a) oxygen-killed *T. denticola*. Upstream binding factor-1 (UBF-1) stains the UBF protein which binds nucleolus organizer regions (NOR) which is key for nucleolus formation. Snail-1 and UBF-1 staining of oral keratinocytes shows that the key EMT transcription factor snail-1 was localised at NORs in the nucleolus after 8-days challenge with oxygen-killed *T. denticola.* Images displayed are representative of experiments performed in triplicate. Scale bars = 20 µm.

## 4.6 Cell migration of oral keratinocytes after exposure to heat and oxygen-killed periodontal pathogens

The down-regulation of cell-cell adhesion molecules, including E-cadherin and desmoplakin and replacement of keratin with vimentin aids cell motility, which is associated with EMT. As EMT advances, cells gain migratory properties, therefore the migratory ability of H400 cells was initially assessed in cultures challenged to HK *P. gingivalis* and *F. nucleatum* by utilising a scratch wound migration assay.

### 4.6.1 Optimising mitomycin C concentration for inhibition of proliferation

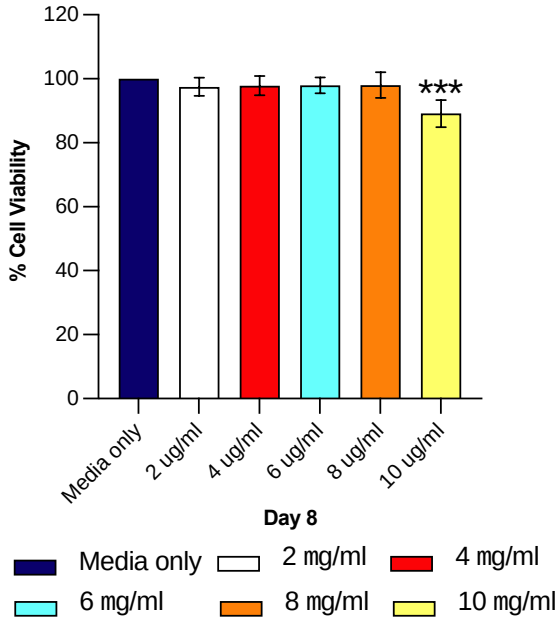
To measure wound migration, it is important to also inhibit cell proliferation as wound closure may also be caused by increased cell proliferation (Leoni et al., 2015). A commonly used inhibitor of proliferation is mitomycin C (MMC), which acts by inhibiting DNA synthesis (Grada et al., 2017), this was applied to oral keratinocytes prior to assessing the wound migratory ability of cells exposed to pathogens. However, the optimum MMC concentration for use on H400 cells needed to be established due to reported epithelial cell toxicity at higher concentrations (Kabiri et al., 2019; Varankar and Bapat, 2018). The MMC concentrations of 2, 4, 6, 8 and 10 µg/ml were initially selected and applied to H400 cells for 2 hours and cell toxicity assessed by measuring cell viability using the Trypan blue exclusion viability assay.

#### 4.6.1.1 Effects of increasing mitomycin C concentration on epithelial cell viability

Cell viability was not significantly decreased in cultures exposed to 2-8 µg/ml MMC (97.48% - 98.1%) but increasing to 10 µg/ml (89.11%) resulted in a significant decrease ($P<0.001$) of the percentage of viable cells in comparison with cultures in media only (Figure 4.17a). This

was further confirmed in representative light microscope images where there was increased presence of dead cells after 10 µg/ml MMC treatment as distinguished by rounded up morphology and detachment from cell culture substrate (Figure 4.17b). As 8 µg/ml was the highest MMC concentration identified that did not reduce oral keratinocyte viability, it was used in subsequent experiments to inhibit proliferation so cell migratory ability could be assessed in pathogen stimulated cultures.

*a)*




*b)*

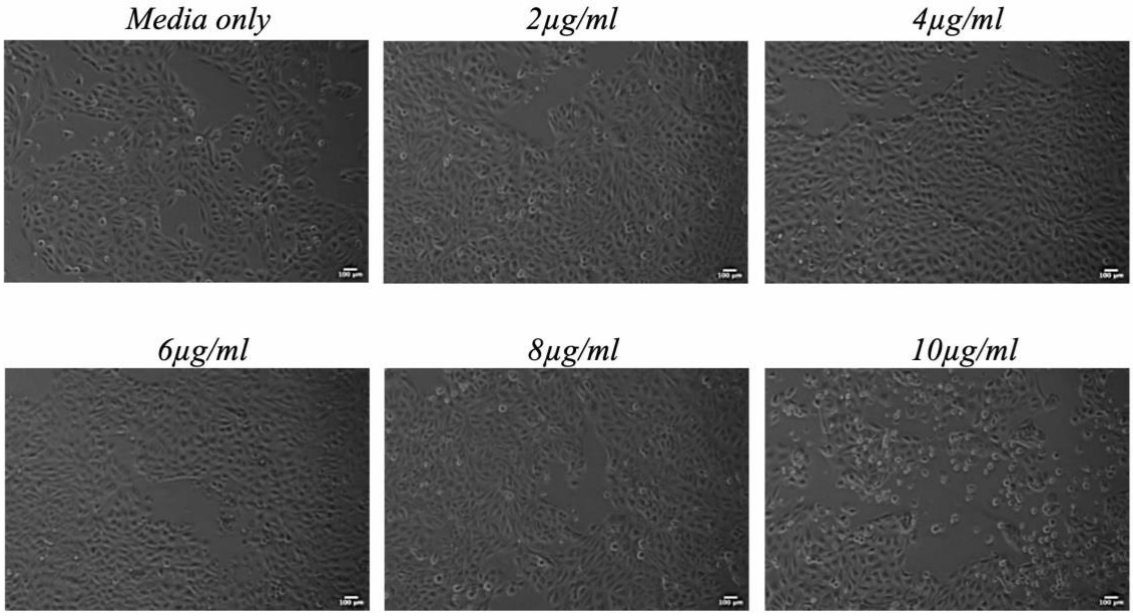



**Figure 4.17**: Oral keratinocyte cultures treated with 2, 4, 6, 8 and 10 µg/ml mitomycin C (MMC) for 2 hours and (a) percentage cell viability assessed to determine optimum MMC concentration to inhibit proliferation without causing cell toxicity. Cultures treated with 10 µg/ml resulted in significant decrease in % cell viability when compared with media only control. (b) Cell culture images captured after 2 hours treatment with varying concentration of MMC and images were captured using an inverted Zeiss Primovert microscope. Images displayed are representative of experiments performed in triplicate. *** = P<0.001 and scale bars = 100 µm.

### 4.6.2 Cell migration of oral keratinocytes after heat-killed *P. gingivalis* and *F. nucleatum* exposure using scratch wound assay

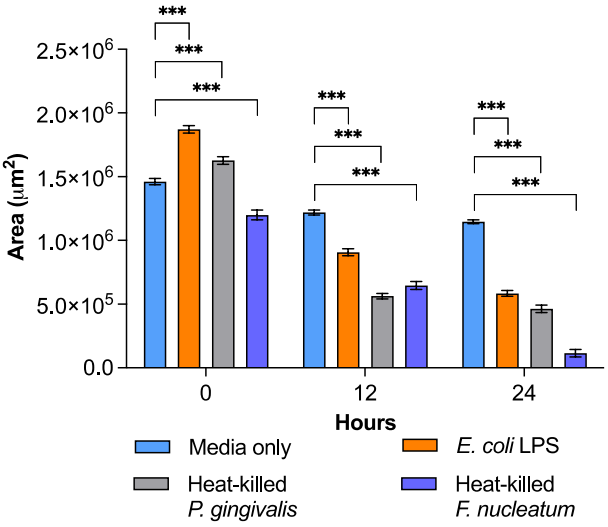
The scratch wound assay is a commonly used technique to measure the cell migratory ability of cells (Liang, Park and Guan, 2007). As the assay requires a mechanical scratch with a pipette tip it is a relatively resource-free method, however it necessitates the need for a steady hand to create a consistent equal sized gap. The assay is a straightforward and economical method to study cell migration and was therefore initially chosen to investigate cell migration of oral keratinocytes exposed to HK *P. gingivalis* and *F. nucleatum*.

#### 4.6.2.1 Analysis of oral keratinocyte wound gap closure after heat-killed pathogen exposure

The cell free gap areas at 0 hours showed varying measurements (1,199,000 – 1,872,000 square pixels) between cultures with significant differences ($P<0.001$) when compared with media only (1,461,000 square pixels) (Figure 4.18a) and these differences in wound areas were also visible in the scratch wound images (Figure 4.18b). This showed that producing a consistent cell free gap using the scratch method to assess cell migration was unreliable.

The scratch wound assay produced inconsistent initial cell-free gap areas in cultures, meaning it would be difficult to distinguish if changes in wound gap areas are due to increased cell migration brought on by pathogen stimulation or because of a smaller initial gap area. Therefore, another method to measure cell migration was investigated, where a consistent cell free gap area can be produced so any observed reductions in wound gap area would be due to increased cell migration.

*a)*




*b)*

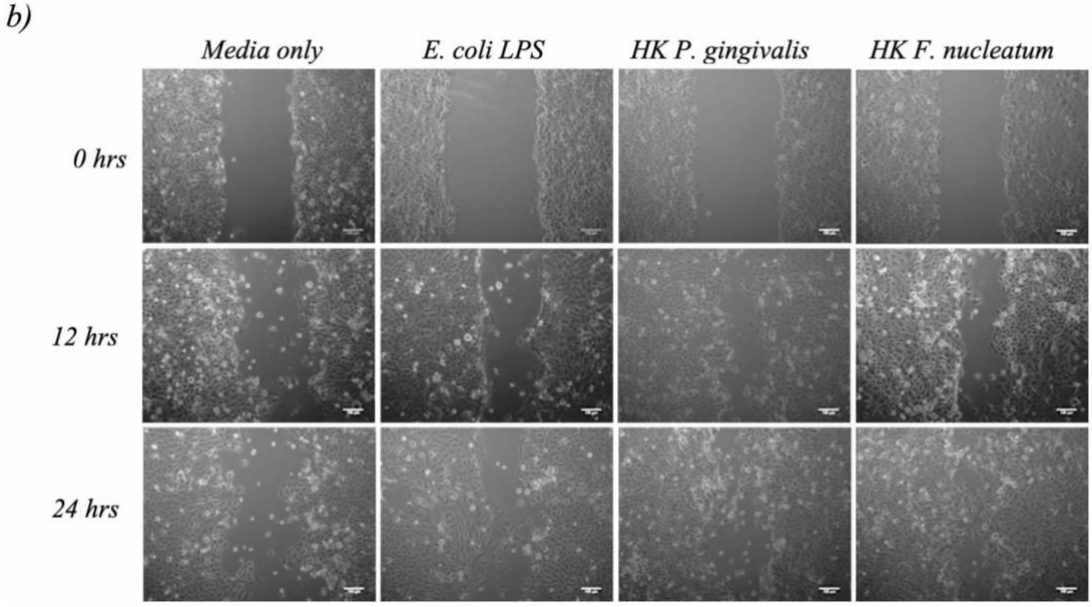



**Figure 4.18**: (a) Wound gap closure areas over 24 hours of H400 cell cultures after 8 days stimulation with heat-killed *P. gingivalis, F. nucleatum* and *E. coli* LPS. Cells were treated with mitomycin c (8ug/ml) for 2 hours before a scratch wound was introduced manually using a 10µl pipette tip and (b) images captured at 0, 12 and 24 hours. Initial wound gap areas at 0 hrs were significantly different in comparison with media only meaning that scratch wounds produced were inconsistent and any cell migration observed would be unreliable. Error bars shown are standard deviations and n=4. *** = P<0.001 and scale bars = 100 µm.

### 4.6.3 Cell migration of oral keratinocytes after heat and oxygen-killed pathogen exposure using Ibidi 2-well culture insert method

The Ibidi 2-well culture insert has been widely used to produce consistent wound gap areas for the analysis of cell migration (Fukuda et al., 2019; Liu et al., 2018; Mohan et al., 2018). Therefore, it was also employed in this study to overcome the inconsistency issue faced with producing wound gap areas by manual means of a scratch. Consistent wound gap areas were produced by Ibidi inserts and oral keratinocyte cell migration was assessed over 48 hours after being initially stimulated with *E. coli* LPS, HK or OK periodontal pathogens for 8-days.

#### 4.6.3.1 Analysis of oral keratinocyte wound gap closure after heat-killed and oxygen-killed pathogen exposure

The stimulation of oral keratinocyte cultures with pathogens increased the migratory ability of cells as seen by greater wound gap closure at all time points (Figure 4.19). The percentage wound gap area at 0 hours was calculated in relation to total area and values were similar to each other (18.51-20.43%) with non-significant differences indicating that the culture inserts produced consistent 500 µm gaps and any significant changes observed in gap closure would therefore be pathogen related. Wound closure at subsequent time points 12, 24 and 48 hours was greater in all stimulated cultures compared with media only control. After 48 hours, wound gap closure was significantly increased ($P<0.05$ and $P<0.001$) in all stimulated cultures (45% - 56.15%) except in OK *P. gingivalis* (42.81%) and HK *F. nucleatum* (39.53%) exposed cultures where wound gap closure was not significantly increased in comparison with media only control (32.92%). The greatest oral keratinocyte wound gap closure was associated with cultures exposed to OK *T. denticola* (56.15%) and least with HK *F. nucleatum* after 48 hours (Figure 4.19).

The wound gap closure between cultures stimulated with HK and OK stimulants of the same bacteria were then compared with cultures in media only and *E. coli* LPS controls to see if type of bacterial killing altered cell migratory ability. Wound gap closure values in media only cultures and *E. coli* LPS exposed cultures were the same in Figures 4.20, 4.21 and 4.22 as data was collected at the same time. Wound gap closure of cultures stimulated with HK *P. gingivalis* (54.45%) were significantly greater ($P<0.05$) in comparison with its OK stimulant (42.81%) 48 hours post insert removal (Figure 4.20b). However, wound gap closure in cultures exposed to OK *F. nucleatum* (45%) was not significantly greater after 48 hours in comparison with cultures exposed to its HK equivalent (39.53%) (Figure 4.21b). The OK stimulant (56.15%) of *T. denticola* however, significantly increased ($P<0.05$) wound gap closure after 48 hours in comparison with its HK equivalent (46.68%) (Figure 4.22b).

Oral keratinocyte migration increased after stimulation by HK and OK pathogens with greatest wound gap closure occurring following OK *T. denticola* stimulation in comparison with all HK and OK pathogens. The OK stimulant of *T. denticola* appeared to be more effective in promoting cell migration in comparison with its HK stimulant, but the converse was true for *P. gingivalis* where the HK stimulant was more effective than its OK equivalent. Overall, cell migration associated with EMT could be induced by HK and OK periodontal pathogens with the type of killed pathogen differentially inducing cell migration.

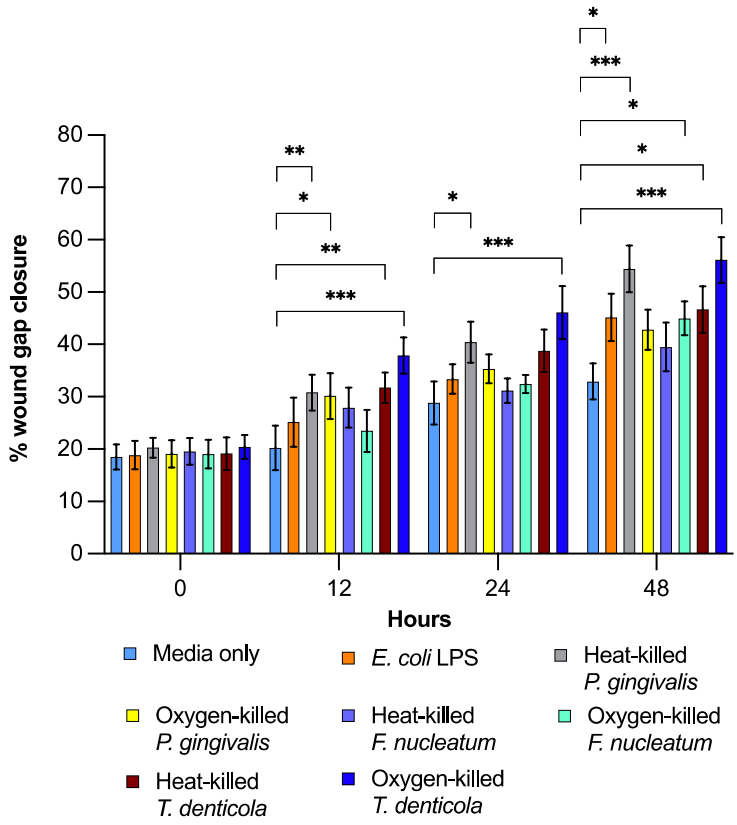



**Figure 4.19**: Percentage wound gap closure over 48 hours of H400 cells after 8 days stimulation with heat-killed and oxygen-killed *P. gingivalis, F. nucleatum*, *T. denticola* and *E. coli* LPS. Cultures stimulated with the heat-killed *P. gingivalis* and *T. denticola* and oxygen-killed *F. nucleatum* and *T. denticola* and *E. coli* LPS significantly increased wound gap closure, with oxygen-killed *T. denticola* resulting in greatest gap closure in comparison with media only after 48 hours. Error bars shown are standard deviations and n=3. * = P<0.05, ** = P<0.01 and *** = P<0.001.

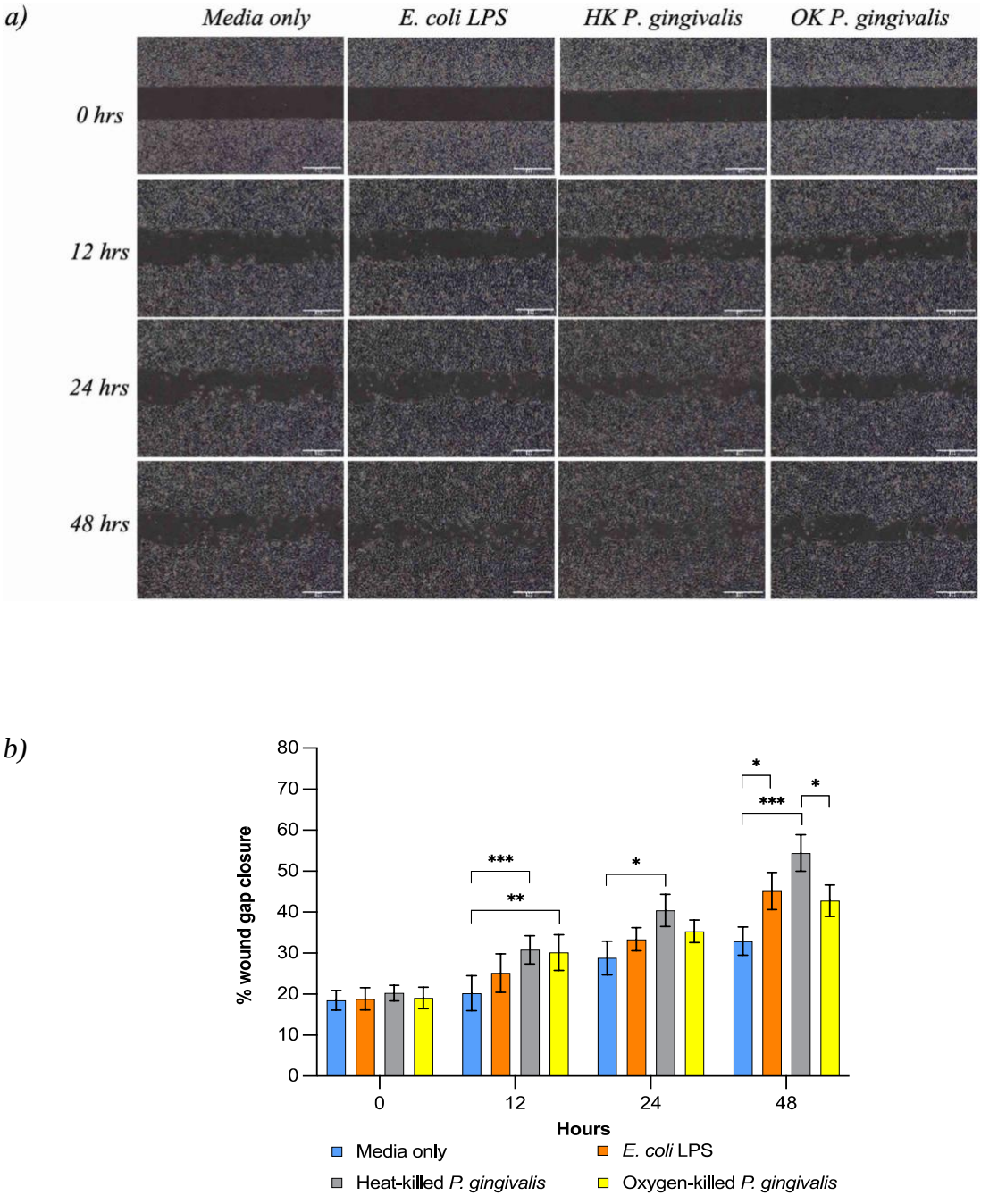
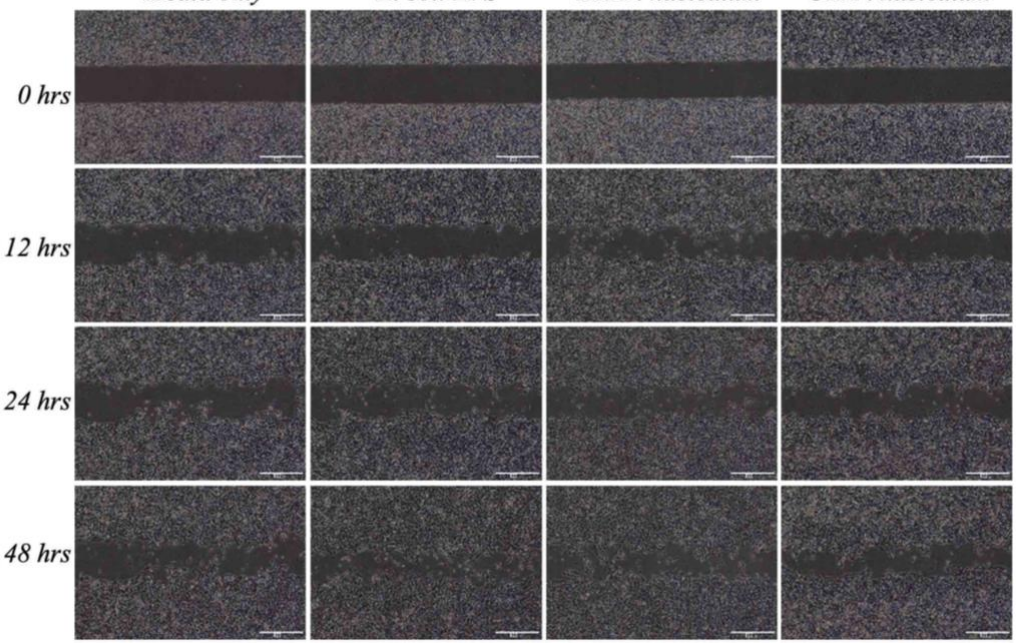



**Figure 4.20**: H400 cultures were stimulated for 8-days with heat-killed and oxygen-killed *P. gingivalis* and *E. coli* LPS prior to assessing cell migration. (a) Captured images of H400 cell migration at 0, 12, 24 and 48 hours post insert removal and (b) Percentage wound gap closure at 0, 12, 24 and 48 hours calculated by measuring wound gap area using ImageJ analysis. Heat-killed *P. gingivalis* challenged cultures resulted in significantly increased cell migration when compared with cultures challenged with oxygen-killed *P. gingivalis* after 48 hours. Error bars shown are standard deviations. Images displayed are representative of experiments performed in triplicate. * = P<0.05, ** = P<0.01 and *** = P<0.001 and scale bars = 500 µm.

a)




b)

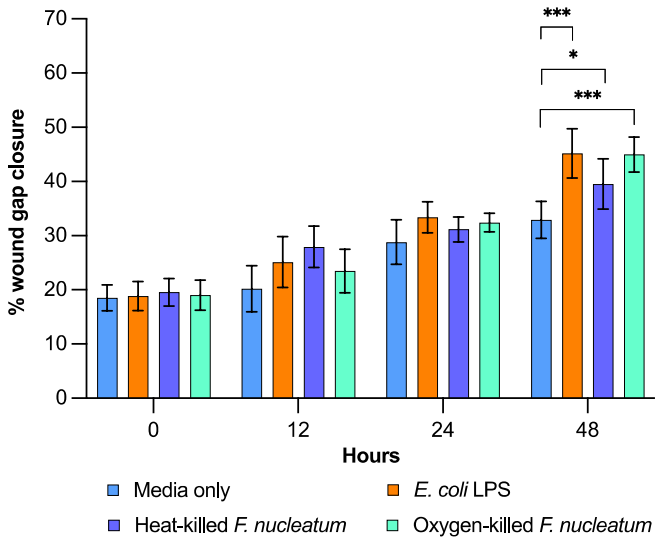
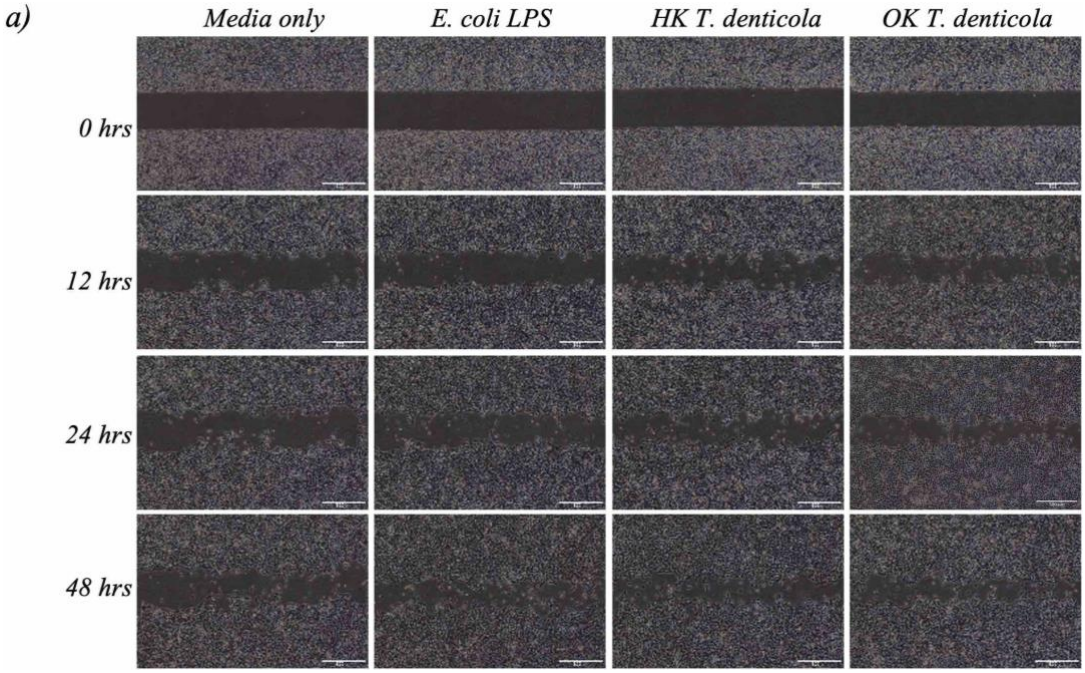



**Figure 4.21**: H400 cultures were stimulated for 8-days with heat-killed and oxygen-killed *F. nucleatum* and *E. coli* LPS prior to assessing cell migration. (a) Captured images of H400 cell migration at 0, 12, 24 and 48 hours post insert removal and (b) Percentage wound gap closure at 0, 12, 24 and 48 hours calculated by measuring wound gap area using ImageJ analysis. Oxygen-killed *F. nucleatum* challenged cultures resulted in non-significant increase in cell migration when compared with heat-killed *F. nucleatum* exposed cultures after 48 hours. Error bars shown are standard deviations. Images shown are representative of experiments performed in triplicate. * = P<0.05 and *** = P<0.001. Scale bars = 500 µm.

a)




b)

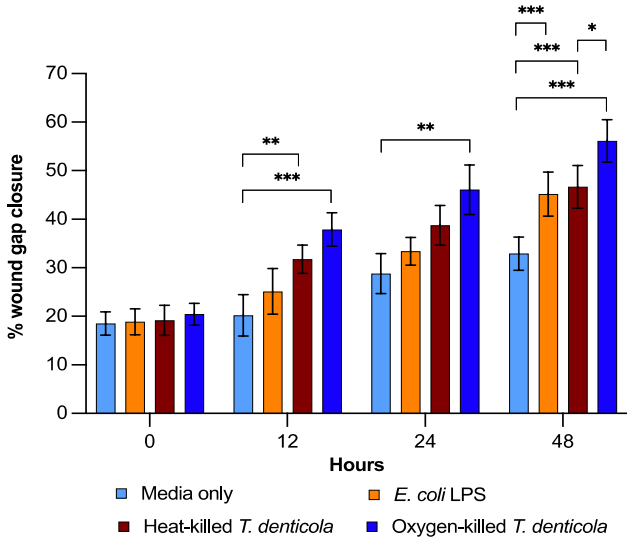



**Figure 4.22**: H400 cultures were stimulated for 8-days with heat-killed and oxygen-killed *T. denticola* and *E. coli* LPS prior to assessing cell migration. (a) Captured images of H400 cell migration at 0, 12, 24 and 48 hours post insert removal and (b) Percentage wound gap closure at 0, 12, 24 and 48 hours calculated by measuring wound gap area using ImageJ analysis. Oxygen-killed *T. denticola* stimulation resulted in increased cell migration across all time points, with significant increase occurring after 48 hours when compared with its heat-killed equivalent. Error bars shown are standard deviations. Images displayed are representative of experiments performed in triplicate. * = P<0.05, ** = P<0.01 and *** = P<0.001 and scale bars = 500 µm.

## 4.7 Trans-epithelial electrical resistance of oral keratinocyte monolayers after heat and oxygen-killed pathogen exposure

During EMT, epithelial cells lose cell-cell adhesions through down-regulation of tight junctions, adherens junctions and desmosomes (Lamouille, Xu and Derynck, 2014). This study has shown that most HK and OK pathogens could down-regulate the gene transcripts of E-cadherin and desmoplakin-1 (see section 4.3.1.1). TEER is a routinely employed technique to measure electrical resistance across an epithelial monolayer, with these values being strong indicators of epithelial barrier integrity (Srinivasan et al., 2015). Therefore, TEER was used to measure electrical resistance in oral keratinocyte monolayers stimulated with HK and OK pathogens for 8-days.

### 4.7.1 Effects of pathogen exposure on trans-epithelial electrical resistance in oral keratinocyte monolayers

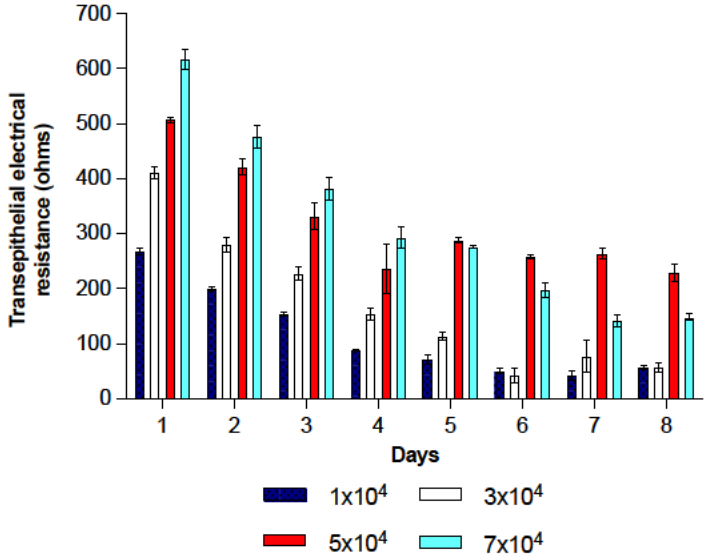
TEER analysis was initially performed on cultures using the model developed in this study where culture media was not changed throughout the 8-day period and was initially tested on a range of cell seeding densities. TEER decreased as the number of days increased in all cultures and greater TEER readings were associated with higher cell seeding densities across all days (Figure 4.23a). It was observed that media levels were reduced in all tissue culture inserts as the days progressed possibly due to media consumption by cells. This suggested that media levels affect TEER and levels needed to be kept constant to avoid disparity and to determine true effect of pathogens on TEER. Therefore, another model was investigated where media was replaced in the insert and wells every 2-days to keep media levels consistent. Replacing media every 2-days resulted in a general increase in TEER in all cultures which was expected due to increase in cell growth (Figure 4.23b). Therefore, for

ongoing experiments with HK and OK pathogen exposure, media was replaced and pathogens added simultaneously every 2 days.

Cell cultures challenged with HK pathogens decreased TEER across all days in comparison with media only, apart from HK *F. nucleatum* on day 4 and *E. coli* LPS on day 6, where an increase was noticed. Significant decrease in TEER readings were associated with HK *T. denticola* exposure (46 Ω) ($P<0.01$) on day 2 and HK *F. nucleatum* exposure (155.78 Ω) ($P<0.05$) on day 8 in comparison with media only (Figure 4.24a). Interestingly, lowest TEER in cultures was related to HK *T. denticola* exposure in 4 of the 7 days tested. Similarly, OK pathogens also reduced TEER at all days with all stimulated cultures significantly decreasing resistance on days 2 and 7 ($P<0.01$ and $P<0.001$) in comparison with media only. Interestingly, OK *F. nucleatum* was responsible for lowest TEER in 4 days of the 7 days tested. After 8-days stimulation, significant reductions in resistance were associated with OK *P. gingivalis* (306.61 Ω) ($P<0.05$) and *F. nucleatum* (258.78 Ω) ($P<0.001$) exposure when compared with cultures in media only (435.44 Ω) (Figure 4.24b).

Stimulation of oral keratinocytes with HK and OK pathogens decreased TEER in all cultures when compared with unstimulated cultures. This suggested that periodontal pathogens could have compromised epithelial barrier integrity possibly through loss of epithelial cell-cell contacts, which promoted EMT.

*a)*




*b)*

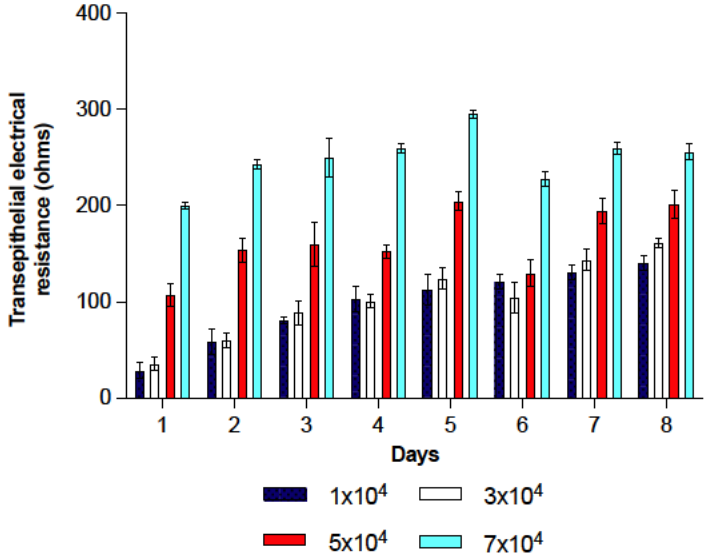
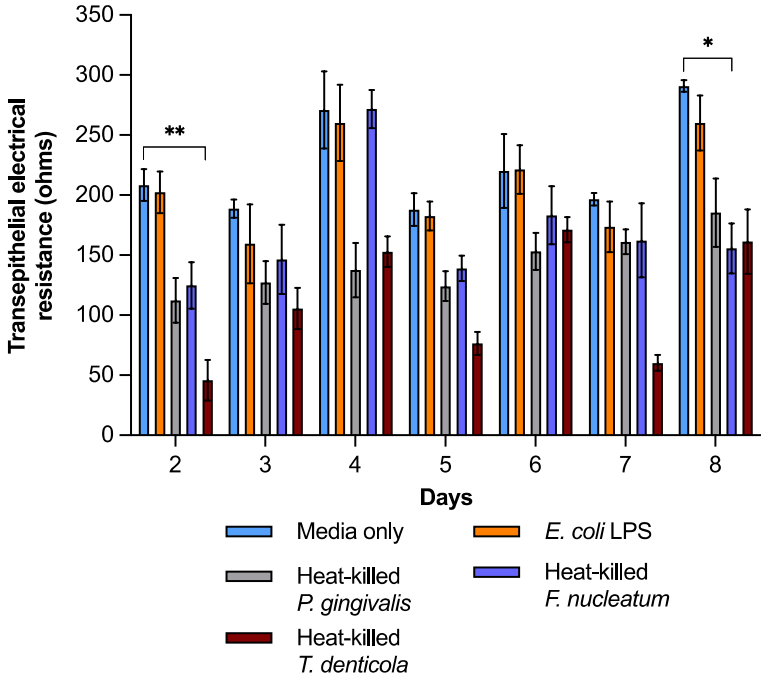



**Figure 4.23**: Trans-epithelial electrical resistance (TEER) readings of oral keratinocyte monolayers across 8-days with initial cell densities of $1x10^4$, $3x10^4$, $5x10^4$ and $7x10^4$. TEER was performed on cultures (a) without changing media and (b) with changing media every 2 days. TEER readings decreased as the days increased in the model without changing media, but changing media resulted in increased TEER readings and greater cell seeding densities were generally associated with higher TEER readings in both experiments. Error bars shown are standard deviations and n=4.

*a)*




*b)*

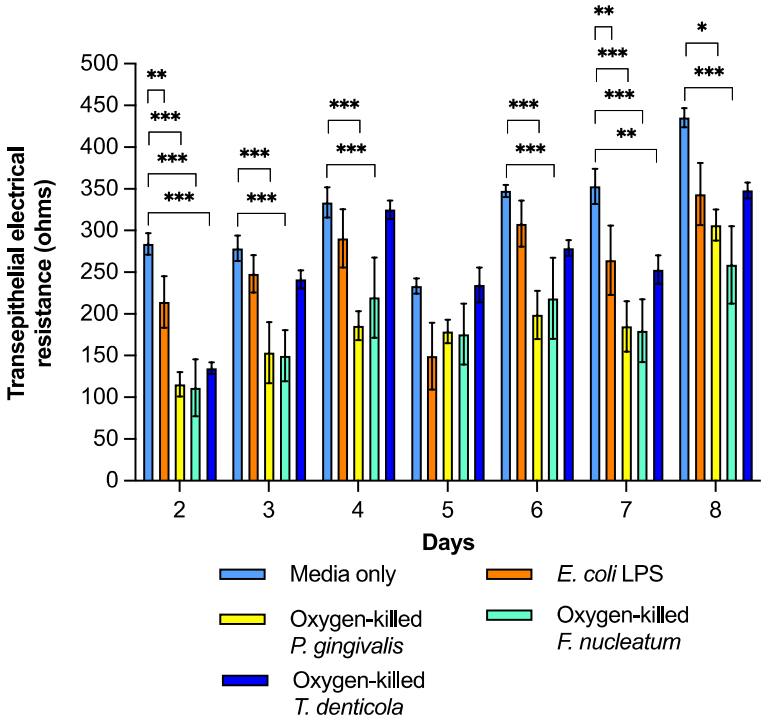



**Figure 4.24**: Trans-epithelial electrical resistance (TEER) readings from day 2-8 of oral keratinocyte monolayers challenged with (a) heat-killed *P. gingivalis*, *F. nucleatum* and *T. denticola* and (b) oxygen-killed *P. gingivalis*, *F. nucleatum* and *T. denticola.* TEER readings significantly decreased after heat-killed *T. denticola* exposure on day 2 and heat-killed *F. nucleatum* on day 8. All oxygen-killed bacteria resulted in decreased TEER readings across all days with significant decrease occurring with all pathogens on days 2 and 7 when compared with unstimulated cultures. Error bars shown are standard deviations and experiments performed in triplicate. * = P<0.05, ** = P<0.01 and *** = P<0.001.

## 4.8 Discussion

### 4.8.1 Effect of heat and oxygen-killed pathogens on epithelial cell growth and viability

As shown in Figures 4.1 and 4.2, HK and OK *P. gingivalis* and *F. nucleatum* did not significantly alter cell number after the 8-day experimental period, although there were significant increases in cell number on day 6 and 7 with HK and OK *P. gingivalis.* This may have been due to *P. gingivalis* enhancing cell division through the S-phase in epithelial cells which would lead to increased epithelial cell proliferation ultimately leading to greater cell number (Kuboniwa et al., 2008). However, these effects maybe be short-lived as cell numbers were not significantly higher at the end of the experimental period. It was also observed that cell number increase was less leading up to the end of the experimental period and this may be due to reduced area in the well brought about by increased cell number. This decrease in well area would mean there is not sufficient room for cells to grow and expand, therefore leading to reduced growth near the end of the experimental period.

The effects of OK *F. nucleatum* on cell growth have not been previously reported but HK *F. nucleatum* has previously shown to reduce cell number in oral keratinocytes after 5-days stimulation (Abdulkareem et al., 2018), which was also observed at days 6, 7 and 8 in this study (Figure 4.2). A previous study has also shown *F. nucleatum* to down-regulate cell cycle genes such as cyclin1, CDK2 and CDK4 (Bhattacharya et al., 2014). This would lead to decreased cell proliferation and division and it may provide an explanation for the reduced cell number seen in this study.

Out of the pathogens tested, both stimulants of *T. denticola* significantly increased cell number after 8-days stimulation (Figure 4.3). Previous studies have shown that exposure of epithelial cells to *T. denticola* activated MAP kinases ERK1 and ERK2 which are responsible

for controlling cell proliferation (Leung et al., 2002). Therefore, both HK and OK *T. denticola* may also have activated these kinases in oral keratinocytes leading to increased proliferation and the greater cell growth observed on day 8.

In conclusion this data provides novel information for the effects of OK pathogens on oral keratinocyte growth and viability. Overall, it was found that both HK and OK periodontal pathogens did not have any toxic effect on oral keratinocytes as cell viability was not negatively affected. As a result, both HK and OK periodontal pathogens were used in subsequent experiments to potentially induce EMT.

### 4.8.2 Heat and oxygen-killed periodontal pathogens compromise epithelial integrity

The down-regulated gene expression of E-cadherin with HK *P. gingivalis* and *F. nucleatum* exposure after real-time PCR analysis has been previously reported (Abdulkareem et al., 2017). This decreased E-cadherin expression after *P. gingivalis* exposure observed here may be due to virulence factors such as gingipains which have been shown to degrade E-cadherin expression (Katz et al., 2002). The *F. nucleatum* virulence factor, FadA, has also demonstrated its ability to internalise E-cadherin and it therefore may also play a role in down-regulating the E-cadherin gene expression seen here (Rubinstein et al., 2013). Interestingly, OK *P. gingivalis* and *F. nucleatum* elicited a similar response to HK equivalents suggesting that these virulence factors were still present and inducing these changes. The OK stimulant of *T. denticola* also down regulated E-cadherin gene expression, however the effects of *T. denticola* on E-cadherin expression have not been previously reported in the literature. This down-regulated E-cadherin expression may be due to the significantly increased secretion of IL-1β observed after OK *T. denticola* exposure, as it has been shown that IL-1β

can down-regulate expression of several epithelial markers including E-cadherin (Li et al., 2020). In addition, the *T. denticola* virulence factor dentilisin has demonstrated an ability to down-regulate expression of the tight junction protein, ZO-1, therefore it may also down-regulate expression of other junctional markers such as E-cadherin (Chi, Qi and Kuramitsu, 2003). Interestingly, HK *T. denticola* increased gene transcripts of E-cadherin, which may suggest that oxygen-killing is preserving certain proteins or virulence factors which may be responsible for down-regulating E-cadherin. Whilst heat-killing may be releasing components of *T. denticola* which can up-regulate E-cadherin expression. The effects of heat and oxygen killing on *T. denticola* will be explored later in this thesis (Chapter 6). In addition, reduction in E-cadherin gene expression after pathogen exposure was also supported by IF imaging of E-cadherin protein, where expression was reduced after HK *F. nucleatum* exposure. Similarly, E-cadherin protein expression has been shown to be down-regulated after live (Ma et al., 2018) and HK *F. nucleatum* (Abdulkareem et al., 2017) exposure. The protein expression of E-cadherin was also reduced in OK *T. denticola* exposed cultures in agreement with the gene expression data. However, gene expression of E-cadherin did not match protein expression levels after IF analysis in both stimulants of *P. gingivalis*, HK *T. denticola* and OK *F. nucleatum* exposed cultures. It is known that transcriptional levels do not always correlate with the amount of protein translation (de Sousa Abreu et al., 2009) and this could be due to regulatory systems such as post-transcriptional modifications (Vogel and Marcotte, 2012) and protein degradation (Koussounadis et al., 2015). These regulatory systems may be responsible for non-corresponding gene and protein expression data seen here.

Desmosomes connect to the intermediate filament, keratin, through desmoplakin and loss of either desmoplakin or keratin would lead to breakdown of epithelial cell-cell adhesion and

epithelial cytoskeletal structure (Lamouille, Xu and Derynck, 2014). Cytokeratin 5 gene transcripts were significantly down-regulated in all HK and OK pathogen stimulated cultures. Similarly, HK *P. gingivalis* has previously been shown to decrease cytokeratin 5 gene expression in H400 cells (Milward et al., 2007) although this was after 24 hours exposure in comparison with the 8-days used in this study. Cytokeratin 5 is highly expressed in squamous cell carcinoma cells (Chu and Weiss, 2002) and its down-regulation in some of these cultures may have been associated with increased gene expression of snail-1. Snail-1 has previously been shown to down-regulate expression of other cytokeratins such as cytokeratin 18 (Guaita et al., 2002) and it therefore may be responsible for the down-regulation of cytokeratin 5 seen in this study. Interestingly, gene transcripts of desmoplakin-1 were significantly down-regulated in HK and OK periodontal pathogen exposed cultures after qRT-PCR analysis. Desmoplakin is a major component of the desmosome structure and has two main isoforms, DPI and DPII (Green, Goldman and Chisholm, 1988). The N-terminal of desmoplakin is responsible for localisation to desmosomes whilst the C-terminal is associated with binding to intermediate filaments such as cytokeratin (Favre et al., 2018). It has been noted that the C-terminal of desomplakin-1 specifically binds to the head domain of cytokeratin 5 (Kouklis, Hutton and Fuchs, 1994), therefore down-regulation of either desmoplakin-1 or cytokeratin 5 after bacterial exposure would weaken this link leading to loss of cell-cell junctions and integrity of the epithelial barrier. Loss of cell-cell junctions was also supported by TEER data, where HK and OK periodontal pathogens decreased electrical resistance in epithelial monolayers when compared with unstimulated cultures. TGF-β1 was also detected at higher levels in stimulated cultures and TGF-β1 has previously shown to reduce TEER readings (Sume et al., 2010). Therefore, reduced TEER readings observed after HK and OK pathogen exposure may have been due to the increased TGF-β1 secretion that was observed across all

stimulated cultures. A supporting study has also reported that *T. denticola* can reduce TEER readings in epithelial cells through activity of its virulence factor, dentilisin (Chi, Qi and Kuramitsu, 2003). Although their study used live bacteria it could be interpreted that HK or OK *T. denticola* still maintain this virulence factor which may be responsible for the decreased TEER readings observed here.

### 4.8.3 Heat and oxygen-killed periodontal pathogens promote mesenchymal phenotype

The cadherin switch is considered a hallmark of EMT where the epithelial marker E-cadherin is replaced by the mesenchymal marker N-cadherin (Loh et al., 2019). This cadherin switch was observed in all stimulated cultures except after HK *T. denticola* exposure, which presented both high levels of E-cadherin and N-cadherin after real-time PCR analysis. It has been previously observed that HK *P. gingivalis* and *F. nucleatum* could promote this cadherin switch (Abdulkareem et al., 2017). Another study has reported this cadherin switch after *P. gingivalis* exposure mediated by TGF-β1, through activation of the TGF-β/Smad signalling pathway with the *P. gingivalis* virulence factor, fimbriae, playing an important role (Qi et al., 2020). Interestingly, the virulent outer membrane vesicles (OMVs) of *F. nucleatum* have shown to decrease E-cadherin whilst simultaneously increasing N-cadherin expression, suggesting that this may be responsible for the switch observed in this study (Munshi, 2017). However, the cadherin switch has not been previously reported in epithelial cells after OK *T. denticola* exposure. The increased N-cadherin gene expression after HK and OK *T. denticola* exposure may have been due to increased TGF-β1 secretion which has been reported to up-regulate N-cadherin expression (Araki et al., 2011). Interestingly, OK stimulants produced similar responses to HK stimulants with HK *T. denticola* being an exception as it increased E-cadherin expression, whilst OK *T. denticola* decreased expression. This may suggest that

heat-killing is denaturing or altering *T. denticola* protein and/or virulence factors responsible for causing E-cadherin down-regulation, whilst oxygen-killing preserves these structures.

Vimentin is a key cytoskeletal structure which replaces the epithelial intermediate filament keratin as EMT progresses (Liu et al., 2015). qRT-PCR analysis showed vimentins expression to be significantly up-regulated in cultures exposed to all pathogens. HK *P. gingivalis* and *F. nucleatum* have also previously been shown to increase vimentin expression after 8-day exposure (Abdulkareem et al., 2017) and data in the present study suggested that *T. denticola* could also induce vimentin expression. The transcription factor snail-1 has many gene regulatory targets and one of these is vimentin, therefore up-regulated gene expression of vimentin may be associated with the increased snail-1 expression observed here (Cano et al., 2000). IF analysis also showed increased vimentin protein expression across all stimulated cultures suggesting that the increased transcription of this gene was being translated to the protein level. IF staining was also performed on 3T3 fibroblasts which express mesenchymal markers such as vimentin (Feliksiak et al., 2020). Interestingly, OK *T. denticola* exposed cultures expressed vimentin distribution similarly to 3T3 fibroblasts and indeed mesenchymal stem cells (Mathews et al., 2017). This distribution of vimentin covered the cytoplasm of the cell, whereas cultures exposed to the other pathogens resulted in ball or knot-like structures which have been observed previously in cells at early stages of cell spreading (Terriac, Schütz and Lautenschläger, 2019), which may have suggested that vimentin in these cultures were in an early structural form, whilst vimentin in OK *T. denticola* exposed cultures were more mature. It can also be noted that vimentin gene expression (7.63-fold) was the greatest in OK *T. denticola* exposed cultures after real-time PCR analysis which suggested that the increased gene transcription was being translated to the protein level. Ultimately, OK *T. denticola* may

be progressing the formation of this cytoskeletal structure more rapidly than its HK stimulant and indeed the other periodontal pathogens.

MMP-9 gene expression was significantly up-regulated in cultures exposed to both HK and OK pathogens after qRT-PCR analysis. Similarly, increased expression of MMP-9 after HK *P. gingivalis* and *F. nucleatum* exposure has been previously observed (Abdulkareem et al., 2017). Interestingly, keratinocytes extracted from patients with periodontitis had up-regulated MMP-9 expression (Makela et al., 1994), suggesting that EMT-related responses may be occurring in these cells. The presence of *T. denticola* has also been linked with increased MMP-9 levels in gingival crevicular fluid (GCF) of patients with periodontitis (Yakob et al., 2013). In addition, the *T. denticola* virulence factor dentilisin has also shown to increase gene expression of the structurally similar MMP-2 in human periodontal ligament cells (Ganther et al., 2021), suggesting that dentilisin may be also causing increased MMP-9 gene expression observed here. Interestingly, the OK stimulant of *T. denticola* resulted in greater MMP-9 expression in comparison with its HK stimulant, suggesting that oxygen-killing is preserving virulence factors such as dentilisin more so than heat-killing, therefore resulting in greater MMP-9 gene up-regulation.

### 4.8.4 Heat or oxygen-killed pathogens can activate EMT related transcription factors

Snail-1 is a key EMT transcriptional factor which regulates many target genes associated with the progression of EMT. In this study, snail-1 gene expression was up-regulated in all exposed cultures except after HK *P. gingivalis* exposure in qRT-PCR analysis. This is in contrast with previous findings where live *P. gingivalis* (Lee et al., 2017) and HK *P. gingivalis* (Abdulkareem et al., 2017) exposure induced snail-1 up-regulation. The OK

analogue of *P. gingivalis* however increased snail-1 gene expression suggesting that heat-killing in this instance was proving detrimental to proteins or virulence factors responsible for snail-1 up-regulation. However, IF data shows the opposite effect with snail-1 protein expression present in all cultures even after HK *P. gingivalis* exposure. The pro-inflammatory cytokine TGF-β1 has been associated with inducing snail-1 expression (Peinado, Quintanilla and Cano, 2003) regulated via smad and non-smad pathways (Aomatsu et al., 2011) and may be responsible for the up-regulated snail-1 expression seen here. Interestingly, TGF-β1 levels were significantly lower after HK *P. gingivalis* exposure in comparison with its OK stimulant on day 8, suggesting that the HK stimulant was not consistently inducing TGF-β1 secretion resulting in down-regulated snail-1 gene expression. In addition, post-translational modifications or protein degradation may explain the differences between decreased snail-1 gene expression and increased protein expression observed here after HK *P. gingivalis* exposure. Interestingly, protein expression of snail-1 after HK *P. gingivalis* and *F. nucleatum* stimulation showed similarities to snail-1 expression in 3T3 fibroblasts, where snail-1 expression seemed to be covering the vicinity of the nucleus, although further nucleus staining with DAPI would be needed to confirm this. This type of snail-1 protein expression has been shown elsewhere in 3T3 cells (Francí et al., 2006) and indeed in epithelial cells which have undergone EMT (Singla et al., 2018), suggesting that these cells were possibly at a later stage of EMT. Snail-1 was localised at multiple sites in the nucleus in all other stimulated cultures and further co-staining with UBF-1 revealed snail-1 to be localised in the nucleoli. Ribosome biogenesis occurs in the nucleolus and is a key process involved in cell growth, proliferation and is involved in EMT. Snail-1 has shown to recruit to the nucleolus during ribosome biogenesis to assist with ribosomal RNA synthesis (Prakash et al., 2019), which may explain nucleolar localisation of snail-1 after pathogen exposure. *E. coli* LPS and

OK *T. denticola* presented both structures suggesting that snail-1 was being recruited to the nucleolus whilst still being expressed in the nucleus.

Another member of the snail family of transcription factors, snail-2 or slug has been implicated in regulating EMT (Assani and Zhou, 2018). Both HK and OK pathogens significantly up-regulated snail-2 gene expression, with the exception of OK *P. gingivalis* which down-regulated expression after qRT-PCR analysis. This is consistent with a previous study where HK *P. gingivalis* increased snail-2 gene expression (Abdulkareem et al., 2017) and live *P. gingivalis* was shown to increase snail-2 protein expression after Western blot analysis (Lee et al., 2017). In addition, HK *F. nucleatum* exposure for 8-days has also shown to up-regulate gene transcripts of snail-2 (Abdulkareem et al., 2017). Studies exploring the effect of *T. denticola* on snail-2 gene expression have yet to be performed, but a possible reason for snail-2 up-regulated gene expression may be connected with increased levels of secreted TGF-β1 observed after *T. denticola* exposure, as TGF-β1 has been shown to up-regulate snail-2 gene expression (Morita, Mayanagi and Sobue, 2007). In addition, up-regulated snail-2 transcription may be linked to the increased twist-1 activity as reported in this study, as twist-1 can bind to the snail-2 promoter to activate its transcription (Casas et al., 2011). Interestingly, OK *P. gingivalis* did not up-regulate snail-2 gene expression, suggesting that oxygen-killing maybe altering surface virulence factors responsible for snail-2 induction. One of these factors could be LPS which can up-regulate NF-kB expression (Diomede et al., 2017) which in turn activates snail-2 (Wang et al., 2013). Therefore, alterations to *P. gingivalis* LPS by oxygen-killing may be responsible for the lack of snail-2 gene expression observed here.

Twist-1 is part of the basic-helix-loop-helix (bHLH) family of transcription factors (Zhu et al., 2015) and its up-regulation is associated with inducing EMT (Wang et al., 2016). Interestingly, twist-1 gene expression was up-regulated in all stimulated cultures after qRT-PCR analysis. The up-regulation of twist-1 has also been previously observed after HK *P. gingivalis* and *F. nucleatum* exposure (Abdulkareem et al., 2017). This increased twist-1 gene expression after *F. nucleatum* exposure may be associated with *F. nucleatums'* virulent OMVs, which have shown to increase mRNA expression of twist-1 in epithelial cells (Munshi, 2017). Virulence factors of *P. gingivalis* may also be responsible for up-regulated twist-1 gene expression, as *P. gingivalis* LPS has shown to increase twist-1 gene expression in epithelial cells (Liu et al., 2021). As discussed in the previous paragraph, *P. gingivalis* LPS may be implicated in up-regulated snail-2 expression and changes to LPS, brought about by oxygen-killing may alter this response. Interestingly, both stimulants of *P. gingivalis* were able to up-regulate twist-1 gene expression, suggesting that oxygen-killing does not alter certain proteins or components on LPS that are responsible for inducing twist-1 expression. The effects of *T. denticola* on twist-1 gene expression have not been previously explored, but its up-regulation may be linked to the increased TGF-β1 secretion seen here after pathogen exposure, as it has been shown that TGF-β1 can induce twist-1 expression through the STAT3 signalling pathway (Cho et al., 2013).

### 4.8.5 Oxygen-killed pathogens promote greater expression of EMT-related pro-inflammatory cytokines

The pro-inflammatory cytokine, IL-1β has been associated with inducing EMT through changes in epithelial and mesenchymal marker expression (Li et al., 2020; Masola et al., 2019). The gene expression of IL-1β was up-regulated in all stimulated cultures after qRT-PCR analysis except in OK *P. gingivalis* exposed cultures. However, IL-1β ELISA data

shows that all stimulated cultures had increased IL-1β on day 8 in comparison with unstimulated cultures. Increased transcription and secretion of IL-1β has also been noted elsewhere, although this was after exposure with live cultures of *P. gingivalis* (Ding et al., 2020a) and *F. nucleatum* (Bui et al., 2016). In addition, HK *P. gingivalis* and *F. nucleatum* have also shown to increase the transcription of IL-1β in epithelial cells after 24 hours exposure (Milward et al., 2007). Furthermore, *T. denticola* has previously shown to increase the transcription and secretion of IL-1β after 24 hours exposure (Miyamoto, Ishihara and Okuda, 2006), therefore data here suggests that prolonged exposure up to 8-days of epithelial cells to *P. gingivalis*, *F. nucleatum* and *T. denticola* can still induce an IL-1β response. It was also interesting to see that OK stimulants resulted in greater IL-1β secretion compared with their HK stimulants, although this was the opposite with *F. nucleatum*. The significantly increased IL-1β secretion with OK *P. gingivalis* exposure compared with its HK stimulant may be associated with the actions of the surface virulence factor, fimbriae. The virulence factor fimbriae can induce IL-1β secretion (Amano et al., 2004) and heat-killing may be considerably altering the actions of this virulence factor, whilst oxygen-killing potentially maintains original fimbriae structure, leading to greater IL-1β secretion.

The pro-inflammatory cytokine IL-8 has shown to induce cell proliferation, migration, invasion and EMT which promotes tumour progression (Zhao et al., 2017). In this study, IL-8 gene transcripts were up-regulated in HK and OK pathogen exposed cultures after qRT-PCR analysis, which was also supported by ELISA analysis where levels of IL-8 were greater in all stimulated cultures. HK *P. gingivalis* has previously shown to up-regulate IL-8 gene transcripts (Milward et al., 2007), whilst both live and HK *P. gingivalis* have been shown to induce IL-8 secretion in epithelial cells and it was determined that *P. gingivalis* related IL-8

secretion was dependent on cell type (Yee et al., 2014). The IL-8 induction seen here by both HK and OK *P. gingivalis* may be associated with the proteinase Arg-gingipain, which has been shown to induce IL-8 gene transcription and secretion (Oido-Mori et al., 2001). The up-regulated transcripts (Milward et al., 2007) and secretion (Koike et al., 2020) of IL-8 after HK *F. nucleatum* exposure is in line with previous findings, however the effects of OK *F. nucleatum* on IL-8 have not been previously explored. The FadA virulence factor of *F. nucleatum* can up-regulate IL-8 gene expression (Rubinstein et al., 2013), therefore increased IL-8 transcripts observed here after HK and OK *F. nucleatum* exposure may be due to actions of FadA. It also suggests that both heat-killing and oxygen-killing does not alter this virulence factor as IL-8 was up-regulated in cultures exposed to both stimulants. In contrast to data here, *T. denticola* has been shown to not induce IL-8 transcription and secretion in epithelial cells (Brissette et al., 2008). However, cells were only stimulated by *T. denticola* for 24 hours when compared with the 8-day time point here, suggesting that longer exposure of epithelial cells to *T. denticola* induces up-regulated IL-8 gene expression and secretion. Interestingly it has also been noted that activation of twist-1 can up-regulate IL-8 production (Li et al., 2012) and twist-1 gene expression was up-regulated across all stimulated cultures here, suggesting that increased IL-8 gene transcripts and secretion observed here could have been due to activities of twist-1.

In this study, gene expression of TGF-β1 was up-regulated in all pathogen exposed cultures except after OK *P. gingivalis* exposure following qRT-PCR analysis. However, ELISA showed increased levels of secreted TGF-β1 across all HK and OK pathogen exposed cultures. This agreed with previous findings where gene transcripts and secretion of TGF-β1 were up-regulated after 8-day exposure to HK *P. gingivalis* and *F. nucleatum* exposure

(Abdulkareem et al., 2017). However, OK *P. gingivalis* and *F. nucleatums'* ability to induce TGF-β1 transcription and secretion have not been previously explored. The OK stimulants of pathogens stimulated greater TGF-β1 release compared with HK stimulants, with this being significantly greater after *P. gingivalis* and *F. nucleatum* exposure. This greater TGF-β1 response with OK *P. gingivalis* compared with its HK stimulant may be associated with cysteine proteases, as cysteine protease deficient *P. gingivalis* ($Kgp^-$ and $Rgp^-$) were unable to induce a TGF-β1 response like their wild-type counterparts (Bengtsson, Khalaf and Khalaf, 2015). Interestingly, live *P. gingivalis* can elicit a greater TGF-β1 response than HK *P. gingivalis* (Palm, Khalaf and Bengtsson, 2014), implying that heat-killing is denaturing these proteins or indeed other proteins responsible for inducing TGF-β1. The induction of TGF-β1 by *F. nucleatum* may be associated with its LPS, which has been shown to induce secretion of other pro-inflammatory cytokines such as: IL-6, IL-1β and TNF-α (Karpiński, 2019), although this needs to be confirmed with further studies. If *F. nucleatum* LPS role in inducing TGF-β1 is confirmed, then oxygen-killing may be preserving *F. nucleatum* LPS more so than heat-killing, leading to the greater TGF-β1 induction seen in the present study with the OK stimulant. TGF-β1 secretion after *T. denticola* exposure in epithelial cells has not been previously examined in human cells, although up-regulated gene expression (2.5-fold) has been reported in soft tissue and calvarial bone in mice (Bakthavatchalu et al., 2010). The up-regulated TGF-β1 detected in the present study may be associated with lipooligosaccharide (LOS) present on the surface of *T. denticola*, which has previously been shown the ability to activate secretion of other pro-inflammatory cytokines such as TNF-α (Rosen et al., 1999), however further studies are needed to confirm this.

### 4.8.6 Heat and oxygen-killed periodontal pathogens promote oral keratinocyte cell migration

As epithelial cells undergo EMT, motility is enhanced and an ability to migrate through the basement membrane is acquired (Aiello et al., 2018). The cell migratory ability of epithelial cells after periodontal pathogen exposure was measured using a 2-well insert wound migration assay. All stimulated cultures increased the rate of cell migration compared with unstimulated controls. Increased cell migration after HK *P. gingivalis* and *F. nucleatum* 8-day exposure of epithelial cells has also been previously observed (Abdulkareem et al., 2018). In addition, long term exposure (23-weeks) to live *P. gingivalis* at an MOI of 1:1 also increases epithelial cell migratory ability (Geng et al., 2017). The virulence factors gingipain of *P. gingivalis* have been shown to be involved in inducing cell migration in microglial cells (Nonaka and Nakanishi, 2020). Although this was in microglial cells, gingipains may still induce cell migration in epithelial cells leading to the increased cell migration observed in the present study. Exposure of colorectal cancer cells to live *F. nucleatum* for 24 hours has also been shown to increase cell migration in a scratch wound assay (Li et al., 2021). In addition, in another study, 2 hours exposure of oral squamous cell carcinoma (OSCC) cells to live *P. gingivalis, F. nucleatum* and *T. denticola* could increase cell migration via integrin/focal adhesion kinase (FAK) signalling. Furthermore, it was identified in this study that OSCC treatment with LOS and LPS derived from *T. denticola*, *P. gingivalis* and *F. nucleatum* promoted OSCC cell migration (Kamarajan et al., 2020), suggesting that the increased H400 cell migratory ability seen here could be due to these bacterial components. Interestingly, all stimulated cultures in the present study expressed higher levels of MMP-9 compared with the control and MMP-9 has been reported to breakdown epithelial cell-cell and cell-ECM contacts (Lin et al., 2011), possibly leading to the increased cell migration seen here. In this

study periodontal pathogen exposure decreased TEER readings, further suggesting breakdown of epithelial cell contacts which would facilitate cell migration.

It was also interesting to note that OK *F. nucleatum* and *T. denticola* had a greater effect on cell migratory ability than their HK equivalents and OK *P. gingivalis*. As TGF-β1 can promote cell migration (Xu, Lamouille and Derynck, 2009), increased migratory rate seen here may be due to higher levels of TGF-β1 secreted in OK *F. nucleatum* and *T. denticola* stimulated cultures, where 187.17 ng/ml and 50.65 ng/ml of TGF-β1 were detected compared with 8.07 ng/ml in OK *P. gingivalis* exposed cultures. Although OK *F. nucleatum* resulted in highest levels of TGF-β1 it did not result in greatest cell migration which was identified in cultures exposed to OK *T. denticola*. Therefore, this suggested there were other factors that resulted in this increased cell migratory ability in OK *T. denticola* exposed cultures and one of these factors may be increased snail-1 protein expression seen in Figure 4.15 h) iii). Snail-1 has been shown to increase cell migratory ability (Smith et al., 2014). In addition, gene transcripts of cytokeratin 5 and desmplakin-1 were less abundantly expressed in cultures after OK *T. denticola* exposure in comparison with the other OK pathogens. Therefore, greater down-regulation of these components that maintain epithelial cell-cell contacts, by OK *T. denticola* exposure may lead to the increased cell migration seen in this study. The mesenchymal markers N-cadherin (Wang et al., 2015) and vimentin (Battaglia et al., 2018) are also implicated in promoting cell migration. Interestingly, gene expression of these two markers was greatest after OK *T. denticola* exposure when compared with the other OK pathogens, therefore promoting the greater rate of cell migration identified in this study. In conclusion, a combination of down-regulated epithelial markers and up-regulated

mesenchymal markers results in a greater rate of cell migration observed in OK *T. denticola* exposed cultures.

Data in this chapter suggests that both HK and OK periodontal pathogens can differentially promote EMT-related changes in oral keratinocytes after 8-days exposure.

The following chapter looks at the potential of a known EMT inhibitor (Curcumin) to block EMT related changes in the oral keratinocyte model system presented in this thesis.

# 5. Inhibition of pathogen-induced epithelial-mesenchymal transition in oral keratinocytes

## 5.1 Introduction

Naturally derived and synthetic compounds have been widely used to inhibit EMT by targeting different mediators and pathways providing potential therapies for fibrosis and cancer (see section 1.7). Out of these EMT inhibitors, curcumin was selected to inhibit periodontal pathogen induced EMT as it is a naturally derived compound that possesses a wide array of anti-inflammatory properties (see section 1.7.1.1) and has been extensively used to inhibit EMT (see Table 1.4). Data presented in the previous chapter indicated that HK and OK periodontal pathogens could induce EMT-related changes in oral keratinocytes (H400 cells) after 8 days stimulation (Chapter 4). It was also established that oxygen-killing preserved bacterial structural morphology (see sections 3.5.1 and 3.6.1), suggesting that OK pathogens would provide disease relevant EMT-related responses. Therefore, the potential of curcumin to inhibit OK periodontal pathogen induced EMT was investigated. Initially, experiments focused on determining the most appropriate solute for curcumin and optimum curcumin concentration required which does not affect cell viability for use in the established 8-day EMT. Therefore, any effects on cell growth and toxicity were determined by manual cell counting and Trypan blue exclusion/Alamar blue viability assays.

It was observed that OK *T. denticola* significantly increased H400 cell number (see section 4.2.1) and this could have been due to increased cell proliferation (see section 4.8.1). Curcumin has been shown to inhibit epithelial cell proliferation in a number of studies (Liu et al., 2020; Sun and You, 2014; Zhou et al., 2017). Therefore, curcumins' potential to inhibit OK *T. denticola* induced cell growth was explored by cell counts and changes to cell viability due to both OK *T. denticola* and curcumin exposure.

As EMT progresses, cells gain migratory properties and all OK periodontal pathogens were found to induce oral keratinocyte cell migration (see section 4.6.3.1). Previous research has indicated that curcumin can inhibit cell migration (Deng et al., 2020; Gallardo et al., 2019 and Yang et al., 2012). Curcumin may also prevent EMT associated cell migration in gingival epithelial cells and this may be important in the maintenance of epithelial barrier function, thereby prevent bacterial invasion into the underlying connective tissue. Consequently, the potential of curcumin to inhibit OK pathogen induced oral keratinocyte migration was investigated after 8-days stimulation.

The exposure of oral keratinocytes to OK pathogens was shown to elicit EMT-associated gene expression changes (see section 4.3). These changes have been shown to be inhibited with curcumin treatment in a number of studies (Cao et al., 2017; Mukherjee et al., 2014; Ohnishi et al., 2020). Therefore, curcumins' potential to inhibit EMT-related gene expression changes brought about by OK pathogens after 8-days stimulation were explored by qRT-PCR analysis.

OK periodontal pathogens can induce a range of changes to gingival epithelial cells suggestive of EMT induction and this chapter reports how curcumin may impact on these changes.

### 5.2 Curcumin solubilised in DMSO for oral keratinocyte exposure

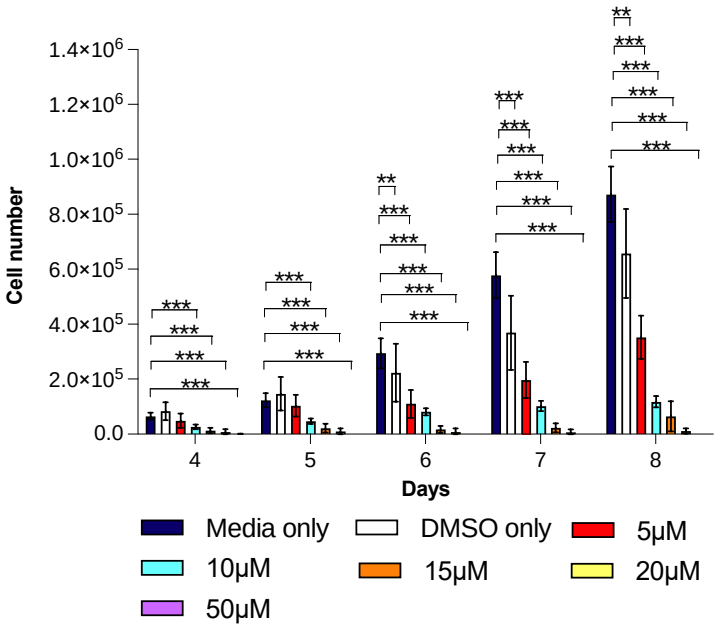
Curcumin has been shown to be dissolved in DMSO and successfully applied to epithelial cells at a final concentration of 0.5% (Kössler et al., 2012). Therefore, DMSO solubilisation was initially used to prepare a range of curcumin concentrations (5, 10, 15, 20 and 50µM) and applied to oral keratinocyte cultures with a 0.5% final DMSO concentration. DMSO only (vehicle control) and media only were used as controls. Cell growth and viability were assayed daily from day 4-8 using manual cell counts and Trypan blue exclusion cell viability analysis.

#### 5.2.1 Effects of DMSO and curcumin concentrations on cell growth and viability

Cell counts of cultures exposed to DMSO only ($P<0.01$) and all curcumin concentrations (5, 10, 15, 20 and 50µM) were significantly lowered ($P<0.001$) after 8-days exposure in comparison with media only control (Figure 5.1a). These lower cell numbers were associated with significantly decreased cell viability ($P<0.001$) in cultures exposed to DMSO only (71.7% cell viability) and all curcumin concentrations (0% - 48.3% cell viability) in comparison with media only (97.5% cell viability) (Figure 5.1b). Curcumin concentrations 10µM and higher significantly reduced cell number ($P<0.001$) from day 4 onwards, whereas DMSO only control and 5µM curcumin significantly reduced cell number ($P<0.01$ and $P<0.001$) from day 6 onwards when compared with media only. Cell viability was significantly reduced by 20 and 50µM curcumin ($P<0.001$) from day 4 onwards, whereas DMSO only control and all other curcumin concentrations significantly reduced cell viability from day 5 onwards ($P<0.001$) in comparison with media only control.

The DMSO only control at 0.5% final concentration, in which curcumin was dissolved, was toxic to H400 cells after 8-days incubation, with cell viability being significantly decreased ($P<0.001$) by 27.84%. For these reasons DMSO was not used to dissolve curcumin and an alternative option was investigated.

*a)*




*b)*

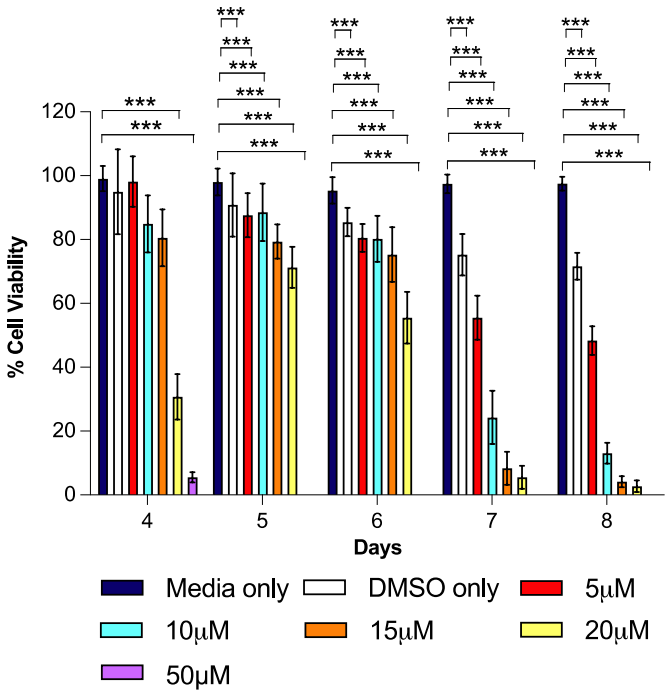



**Figure 5.1**: Effect of media only control, DMSO only (vehicle control), 5, 10, 15, 20 and 50μM concentrations of curcumin dissolved in DMSO on (a) H400 cell growth and (b) percentage cell viability after 4-8 days exposure. The vehicle control and all curcumin concentrations significantly decreased cell number on days 6-8 and percentage cell viability was significantly decreased from day 5-8. Error bars shown are standard deviations and n=3, ** = P<0.01 and *** = P<0.001. Statistical test was ANOVA followed by a post-hoc Tukey Test.

### 5.3 Curcumin solubilised in NaOH for oral keratinocyte exposure

As data indicated that DMSO showed toxicity to H400 cell cultures over 8-day exposure, an alternative solvent was used as a carrier for curcumin. A literature review identified that NaOH has been reported to successfully dissolve curcumin (Akkawi et al., 2019; Kurien et al., 2010; Kurien and Scofield, 2007). However, the optimum concentration of NaOH which doesn't affect H400 cell viability over 8-days needed to be initially determined, therefore cell viability of H400 cultures subjected to a range of NaOH concentrations were initially analysed using an Alamar blue assay after 8-days exposure.

#### 5.3.1 Effects of NaOH concentrations on oral keratinocyte cell viability

Cell cultures exposed to 0.45M (72.5% cell viability) and 0.5M (85.5% cell viability) NaOH significantly reduced the ($P<0.01$) percentage cell viability of oral keratinocytes after 8-day exposure in comparison with media only control (100%). The lower concentrations of 0.4M - 0.2M (93.9% - 95.4% cell viability) also significantly decreased ($P<0.05$) cell viability when compared with media only. However, cultures exposed to 0.15, 0.1 and 0.05M (99.4% - 99.8% cell viability) NaOH did not significantly decrease cell viability after 8-days (Figure 5.2). The highest concentration of NaOH which did not significantly reduce cell viability was 0.15M and curcumin was successfully dissolved in this concentration, therefore that concentration was used in further experiments to determine optimum curcumin concentration needed for use in the 8-day model.

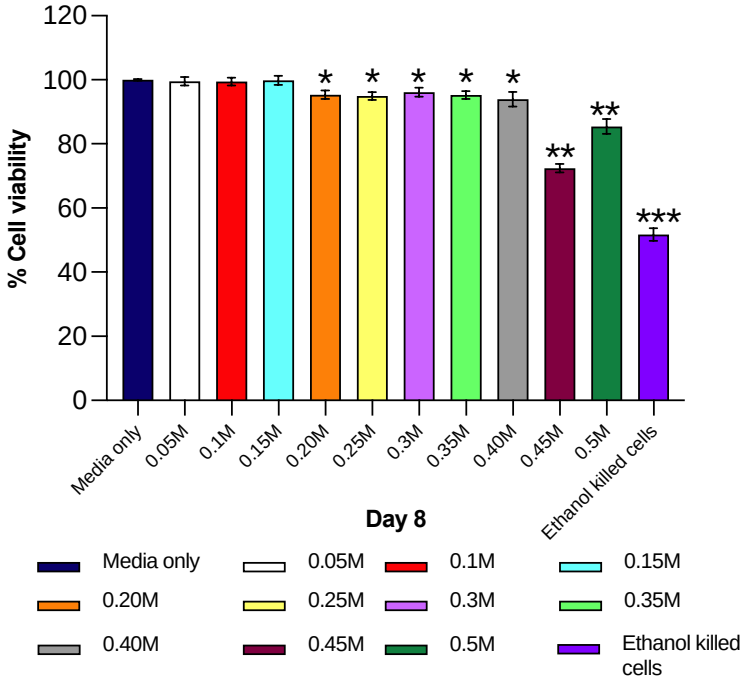



**Figure 5.2**: Percentage cell viability of day-8 H400 cultures exposed to increasing concentrations of sodium hydroxide (NaOH) determined by Alamar blue assay. H400 cell viability was significantly decreased in cultures exposed to concentrations of 0.2M NaOH and above when compared with media only control. Ethanol-killed cells were used as a positive control in this experiment. Error bars shown are standard deviations and n=3, * = $P<0.05$, ** = $P<0.01$ and *** = $P<0.001$. Statistical test was ANOVA followed by a post-hoc Tukey Test.

## 5.4 Optimising curcumin concentration for use on oral keratinocytes

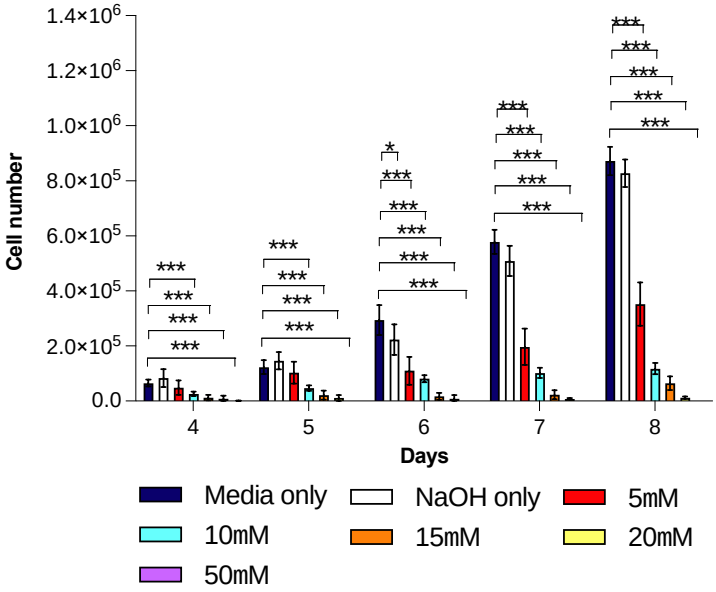
The optimum concentration of curcumin for use on oral keratinocytes over 8-days needed to be determined by establishing any adverse effects on cell viability. Therefore, the effects of a range of curcumin concentrations on epithelial cell growth were measured by cell counts and cell viability analysis using the Trypan blue exclusion cell viability assay from day 4-8. Alamar blue assay was also performed to further confirm any changes in cell viability.

### 5.4.1 Effects of increasing curcumin concentrations on H400 cell growth and viability

Cell cultures exposed to 10 - 50µM curcumin concentrations significantly reduced ($P<0.001$) cell number from day 4-8 when compared with media only controls (Figure 5.3a). This reduction in cell number was due to loss of cell viability in all cultures exposed to 10µM curcumin and above, with significant reduction ($P<0.001$) in number of viable cells observed on days 7 and 8 in comparison with media only controls (Figure 5.3a). Cell viability was significantly decreased ($P<0.001$) in these cultures on days 7 and 8 in comparison with media only control (Figure 5.3b). Significant reduction ($P<0.001$) in cell numbers were also observed in cultures exposed to 5µM curcumin from day 6 – 8 when compared with media only controls (Figure 5.3a). However, cell viability was not significantly reduced with exposure to 5µM curcumin at all days suggesting that this concentration was not resulting in loss of viability observed with higher concentrations (Figure 5.3b). Alamar blue assay of day 8 cultures exposed to all curcumin concentrations also confirmed significant loss ($P<0.001$) of cell viability with exposure to 10µM curcumin concentrations and above in comparison with media only controls (Figure 5.4). Also, similarly with Figure 5.3b, 5µM curcumin exposure did not significantly affect cell viability of H400 cells after performing Alamar blue assay (Figure 5.4)

In light of these data (sections 5.3.1 and 5.4.1) 5μM curcumin solubilised in 0.15M NaOH was selected for use with the 8-day H400 EMT model system developed to investigate the potential for inhibiting EMT in cells stimulated with OK periodontal pathogens.

*a)*




*b)*

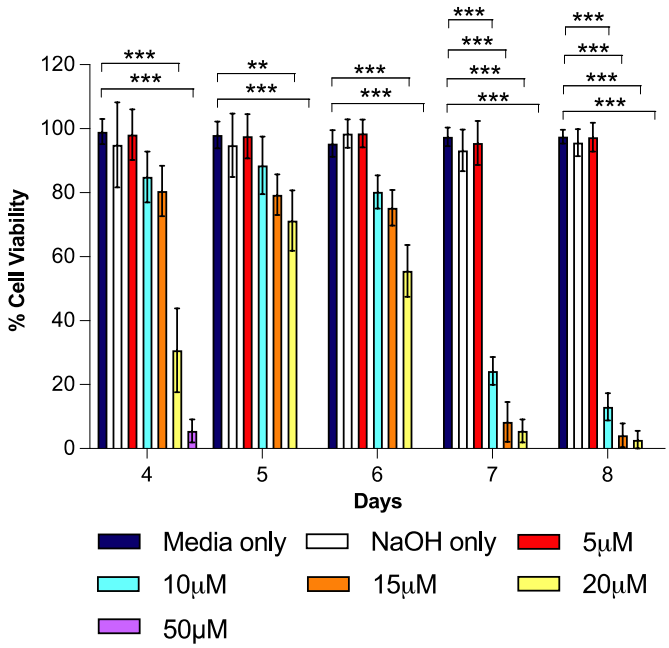



**Figure 5.3**: Effect of NaOH only (vehicle control), 5, 10, 15, 20 and 50µM concentrations of curcumin dissolved in NaOH on (a) H400 cell growth and (b) percentage cell viability after 4-8 days exposure. The vehicle control did not significantly decrease cell number at all days except day 6 and all curcumin concentrations significantly decreased cell number from day 6-8. Cell viability was significantly lowered after 20 and 50µM curcumin exposure at all days whilst 10 and 15µM curcumin significantly decreased cell viability on days 7 and 8. However, cell viability was not significantly affected by 5µM curcumin exposure at all days. Error bars shown are standard deviations and n=3, * = P<0.05, ** = P<0.01 and *** = P<0.001. Statistical test was ANOVA followed by a post-hoc Tukey Test.

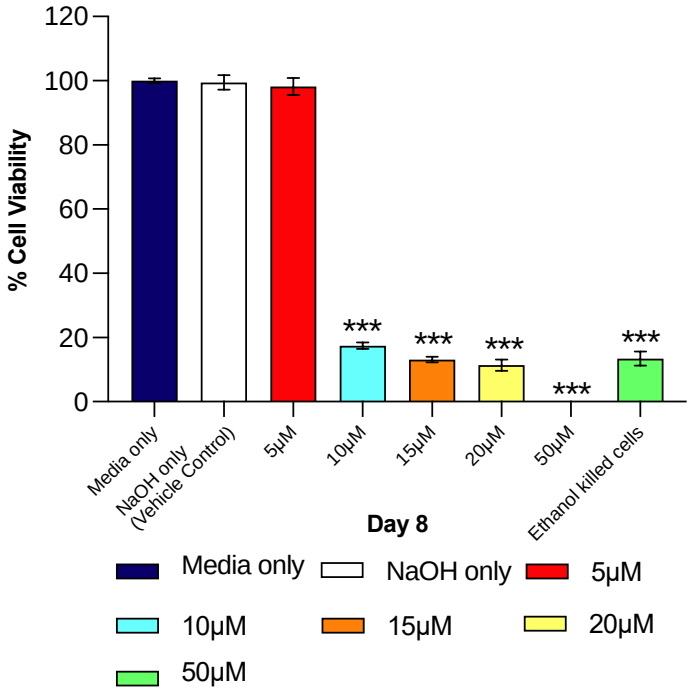



**Figure 5.4**: Percentage cell viability of day-8 H400 cultures exposed to increasing concentrations of curcumin dissolved in NaOH as determined by Alamar blue assay. Cell viability was significantly decreased in cultures exposed to curcumin concentrations of 10, 15, 20 and 50µM, whilst 5µM did not significantly affect H400 cell viability in comparison with media only control. Ethanol-killed cells were used as a positive control in this experiment. Error bars shown are standard deviations, n=3 and significance was tested in comparison with media only control (*** = P<0.001). Statistical test was ANOVA followed by post-hoc Tukey Test.

### 5.5 Curcumin and oxygen-killed *T. denticola* exposure of oral keratinocytes

Findings in section 4.2.1 showed that OK *T. denticola* stimulation significantly increased oral keratinocyte cell growth after 8-days exposure. Curcumin has previously been shown to inhibit epithelial cell proliferation which in turn can reduce cell growth (see section 5.1) Consequently, curcumin was applied at the same time as OK *T. denticola* and its potential to inhibit increased H400 cell growth was explored and any effects on cell viability were also determined.

#### 5.5.1 Effects of curcumin on oxygen-killed *T. denticola* induced oral keratinocyte cell growth and viability

After 8-days exposure to OK *T. denticola,* cell numbers significantly increased ($P<0.01$) in comparison with media only (Figure 5.5). However, cultures exposed to both OK *T. denticola* and curcumin resulted in significantly lower ($P<0.05$) cell numbers compared with cultures exposed to OK *T. denticola* only at day 8. In addition, cell number from these cultures was reduced and was similar to media only cell counts. Curcumin exposure resulted in lower cell number at all days except day 8 with significant reduction ($P<0.01$ and $P<0.001$) observed on days 5, 6 and 7 in comparison with media only. Cell viability of stimulated cultures was not significantly affected when compared with unstimulated cultures at all days.

The increased epithelial cell growth after OK *T. denticola* exposure was significantly decreased with 5μM curcumin after 8-days exposure, suggesting curcumins' ability to inhibit pathogen-induced oral keratinocyte cell growth whilst maintaining high levels of viability. In view of the results obtained the role of 5μM curcumin on EMT associated cell migration and marker expression was investigated.

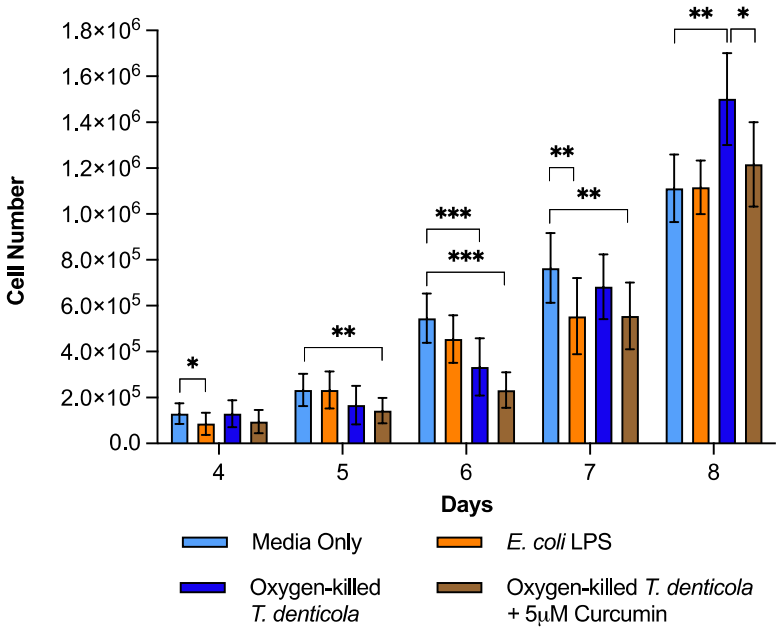



**Figure 5.5**: Cell growth of oral keratinocytes incubated with media only or challenged with *E. coli* LPS and oxygen-killed *T. denticola* +- 5μM curcumin from day 4-8. Cell growth was significantly increased after oxygen-killed *T. denticola* exposure on day 8. However, cultures exposed to oxygen-killed *T. denticola* and 5μM curcumin showed significantly lower cell number when compared with cultures exposed to oxygen-killed *T. denticola* on its own. Error bars shown are standard deviations and n=3, * = P<0.05, ** = P<0.01 and *** = P<0.001. Statistical test performed was ANOVA followed by a post-hoc Tukey Test.

## 5.6 Oxygen-killed pathogen induced cell migration of oral keratinocytes and curcumin

It was previously established that oral keratinocyte cell migration was increased after 8 days exposure to OK *P. gingivalis*, *F. nucleatum* and *T. denticola* (see section 4.6.3.1). Previous studies from the literature have shown curcumin to inhibit migratory ability of cells (see section 5.1), therefore its potential to inhibit OK pathogen induced cell migration was investigated using the 2-well insert wound migration assay as described in section 2.11.3.

### 5.6.1 Analysis of curcumin on oxygen-killed pathogen induced oral keratinocyte wound gap closure

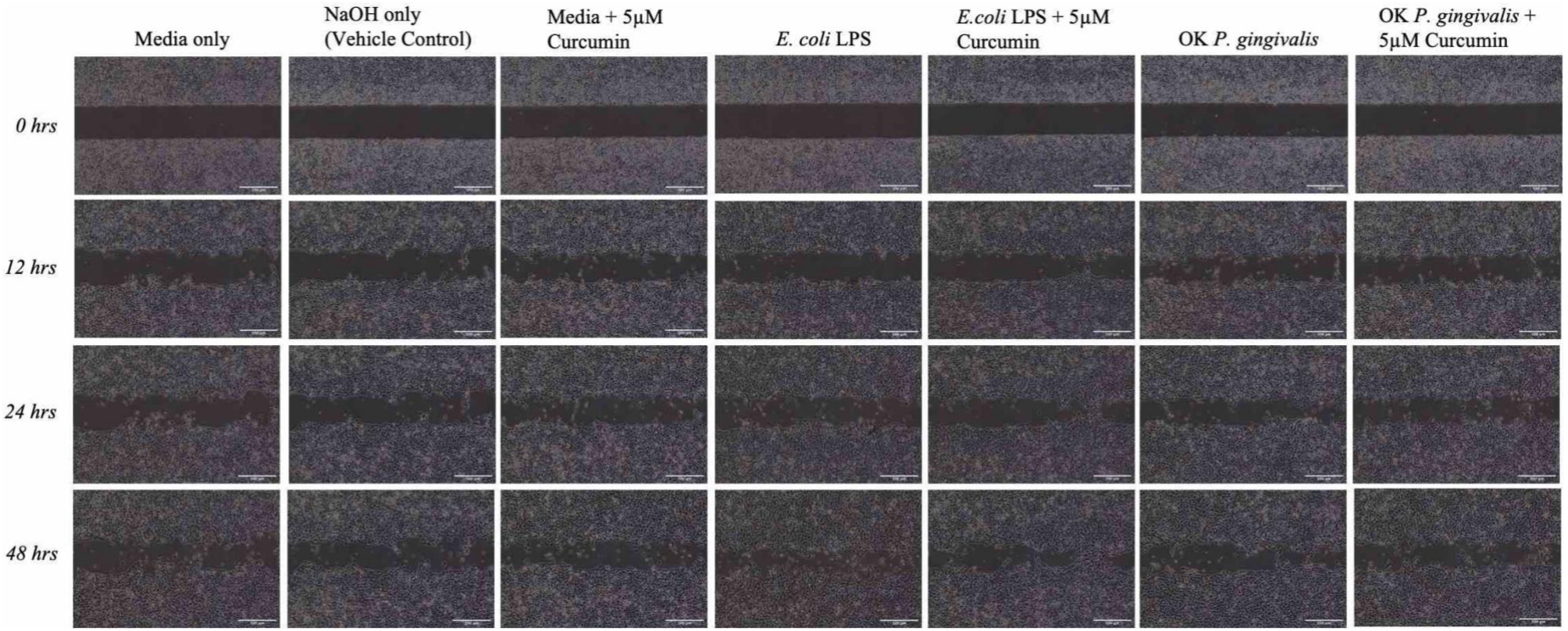
Wound gap closure data of cultures in media only +/- curcumin, *E. coli* LPS +/- curcumin and NaOH only (vehicle control) were the same in Figures 5.6, 5.7 and 5.8 as data was collected at the same time. Cultures exposed to NaOH only and 5μM curcumin only for 8-days did not significantly alter wound gap closure after 12, 24, and 48 hours post-insert removal (Figures 5.6, 5.7 and 5.8). Wound gap closure in cultures exposed to *E. coli* LPS (45.2%) was significantly increased ($P<0.05$) after 48 hours when compared with media only. The addition of curcumin non-significantly decreased *E. coli* LPS stimulated wound gap closure (42.7%) (Figures 5.6, 5.7 and 5.8).

OK *P. gingivalis* exposure significantly increased (30.1%) ($P<0.01$) wound gap closure when compared with media only controls (20.2%) after 12 hours post-insert removal. The presence of curcumin significantly reduced OK *P. gingivalis* induced wound gap closure at 12 hours to 22.7% ($P<0.05$) (Figure 5.6). OK *F. nucleatum* exposure significantly increased wound gap closure observed after 48 hours (to 45%) ($P<0.05$) when compared with media only controls. However, curcumin addition did not inhibit OK *F. nucleatum* induced wound gap closure

(Figure 5.7). Cultures exposed to OK *T. denticola* significantly increased ($P<0.01$ and $P<0.001$) wound gap closure at 12, 24 and 48 hours in comparison with media only. Curcumin addition significantly inhibited ($P<0.01$ and $P<0.001$) OK *T. denticola* induced wound gap closure after 12, 24 and 48 hours when compared with cultures exposed to OK *T. denticola* only (Figure 5.8).

Curcumin addition inhibited OK *P. gingivalis* and *T. denticola* induced wound gap closure, but it did not inhibit OK *F. nucleatum* induced wound gap closure. It was hypothesised that curcumin may have inhibited expression of genes associated with migration in OK *P. gingivalis* and *T. denticola* but not *F. nucleatum* exposed cultures. In order to investigate this possibility qRT-PCR was performed on cell cultures exposed to OK pathogens with curcumin for genes associated with migration and other EMT-related genes.

*a)*


Media only
NaOH only (Vehicle Control)
Media + 5µM Curcumin
E. coli LPS
E.coli LPS + 5µM Curcumin
OK P. gingivalis
OK P. gingivalis + 5µM Curcumin
0 hrs
12 hrs
24 hrs
48 hrs

*b)*

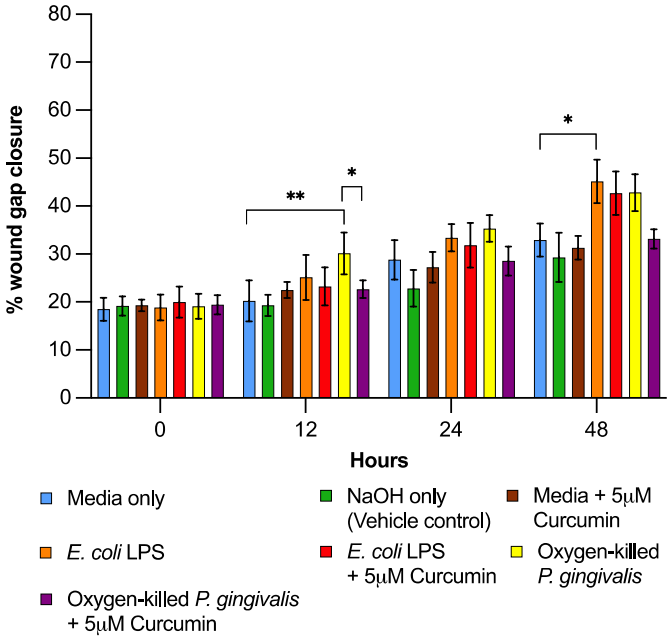
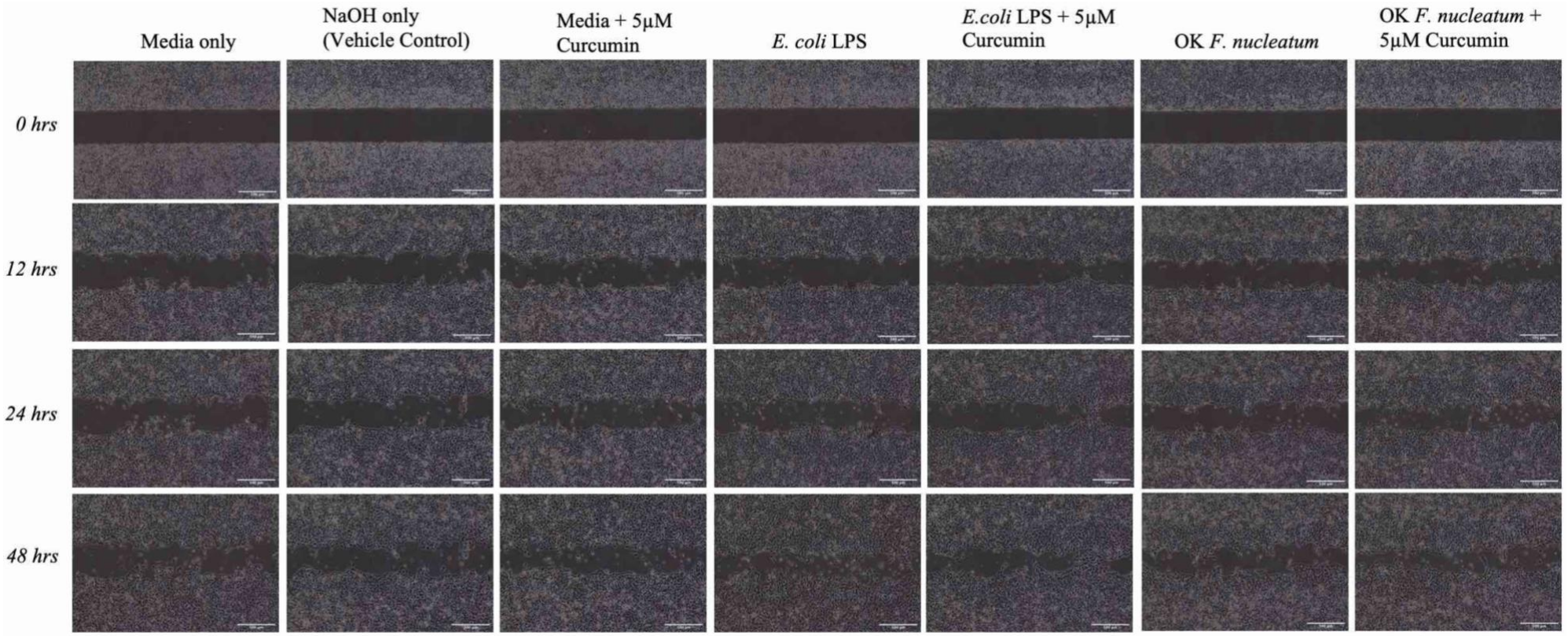



**Figure 5.6**: (a) Captured images at 0, 12, 24 and 48 hours post-insert removal of H400 cultures after 8 days challenge with NaOH only control (vehicle control), media only +/- 5μM curcumin, *E. coli* LPS +/- 5μM curcumin and oxygen-killed *P. gingivalis* +/- 5μM curcumin. (b) Percentage wound gap closure determined by measuring wound gap area using ImageJ analysis observed significantly increased wound gap closure with oxygen-killed *P. gingivalis* exposure after 12 hours. However, addition of curcumin significantly decreased wound gap closure in comparison with cultures exposed to oxygen-killed *P. gingivalis* only. *E. coli* LPS exposure significantly increased wound gap closure when compared with media only controls after 48 hours. Error bars shown are standard deviations. Images displayed are representative of experiments performed in triplicate. * = $P<0.05$, ** = $P<0.01$ and scale bars = 500 μm.

*a)*


Media only
NaOH only (Vehicle Control)
Media + 5µM Curcumin
E. coli LPS
E.coli LPS + 5µM Curcumin
OK F. nucleatum
OK F. nucleatum + 5µM Curcumin
0 hrs
12 hrs
24 hrs
48 hrs

*b)*

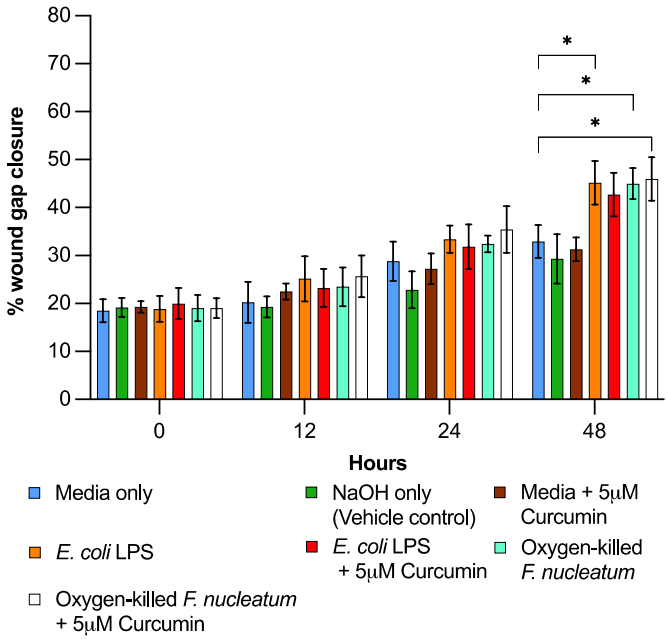
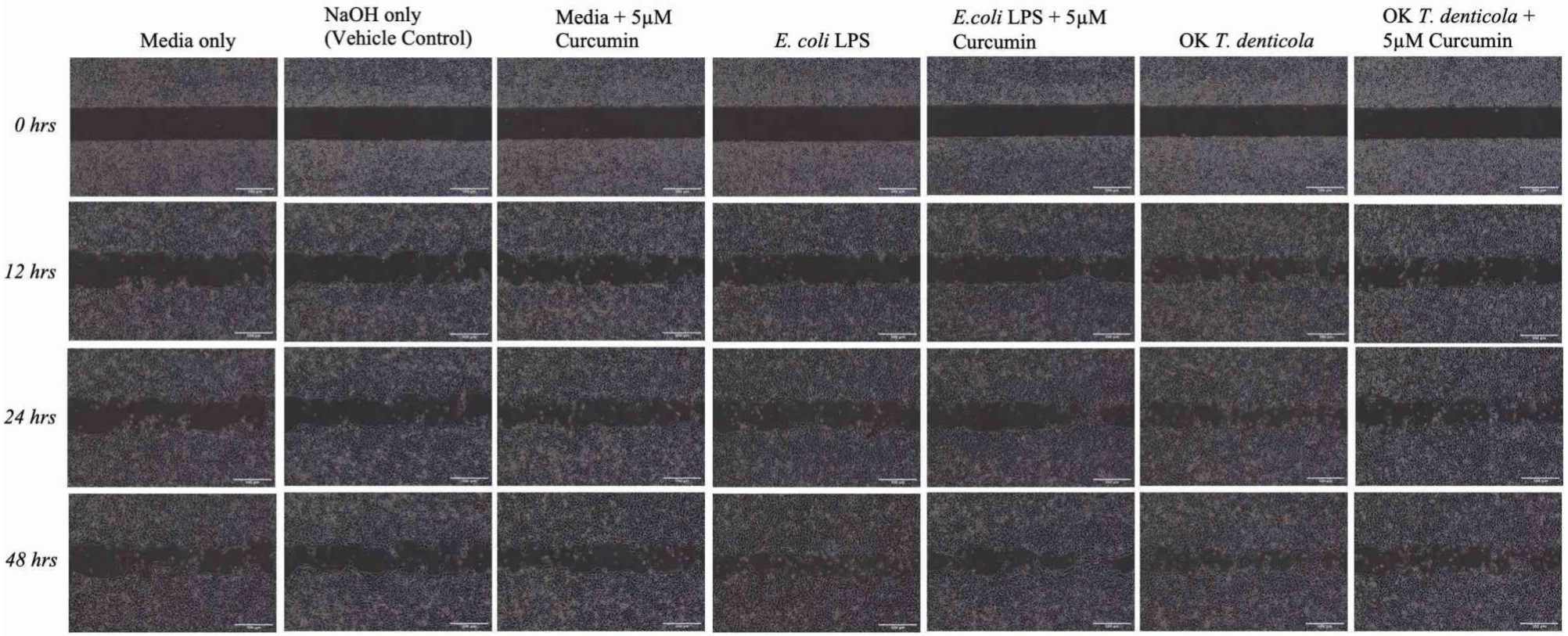



**Figure 5.7**: (a) Captured images at 0, 12, 24 and 48 hours post-insert removal of H400 cultures after 8 days challenge with NaOH only control (vehicle control), media only +/- 5µM curcumin, *E. coli* LPS +/- 5µM curcumin and oxygen-killed *F. nucleatum* +/- 5µM curcumin. (b) percentage wound gap closure determined by measuring wound gap area using ImageJ analysis observed significantly increased wound gap closure in *E. coli* LPS and oxygen-killed *F. nucleatum* +/- curcumin exposed cultures after 48 hours when compared with media only. Error bars shown are standard deviations. Images displayed are representative of experiments performed in triplicate. * = $P<0.05$ and scale bars = 500 µm.

*a)*


Media only
NaOH only (Vehicle Control)
Media + 5µM Curcumin
E. coli LPS
E.coli LPS + 5µM Curcumin
OK T. denticola
OK T. denticola + 5µM Curcumin
0 hrs
12 hrs
24 hrs
48 hrs

*b)*

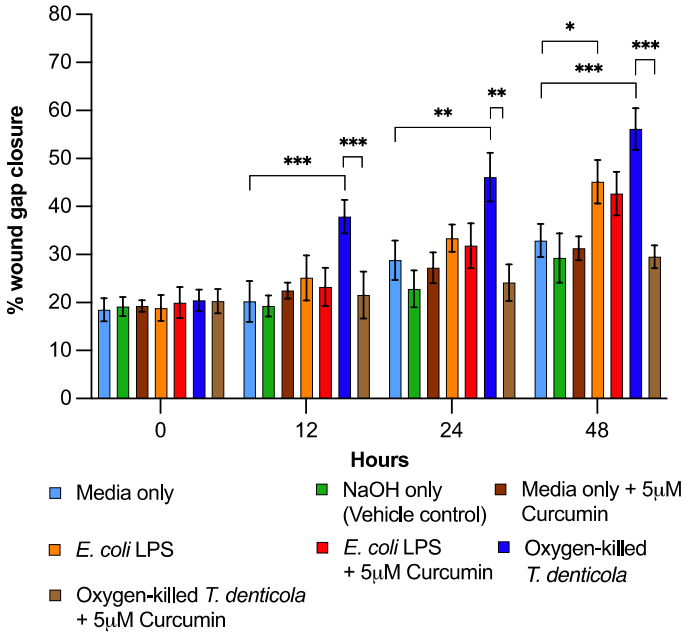



**Figure 5.8**: (a) Captured images at 0, 12, 24 and 48 hours post-insert removal of H400 cultures after 8 days challenge with NaOH only control (vehicle control), media only +/- 5μM curcumin, *E. coli* LPS +/- 5μM curcumin and oxygen-killed *T. denticola* +/- 5μM curcumin. (b) percentage wound gap closure determined by measuring wound gap area using ImageJ analysis observed significantly increased wound gap closure in cultures exposed to oxygen-killed *T. denticola* when compared with media only at 12, 24 and 48 hours. However, cultures exposed to both oxygen-killed *T. denticola* and curcumin significantly reduced wound gap closure when compared with cultures exposed to oxygen-killed *T. denticola* only at all time points. Error bars shown are standard deviations. Images displayed are representative of experiments performed in triplicate. * = P<0.05, ** = P<0.01, *** = P<0.001 and scale bars = 500 μm.

## 5.7 EMT-related gene expression changes in oral keratinocytes stimulated with oxygen-killed pathogens and curcumin

qRT-PCR was utilised on cultures challenged with OK pathogens with curcumin to assess whether curcumin can inhibit EMT-related gene expression changes and to better understand curcumins' differential effect in inhibiting OK pathogen induced cell migration (see section 5.6.1). Gene expression analysis was performed on day-8 cultures. A summary of gene expression ratios of the EMT related markers after oxygen-killed pathogen exposure with and without curcumin is provided in Table 5.1.

### 5.7.1 Gene expression of epithelial markers

The OK pathogens, *P. gingivalis*, *F. nucleatum* and *T. denticola* have previously demonstrated a capacity to down-regulate the expression of epithelial-related genes (see section 4.3.1.1). Exposure of epithelial cells to curcumin has been shown to inhibit this down-regulation (see section 5.1), therefore qRT-PCR was performed on cultures exposed to OK pathogens with or without curcumin.

#### 5.7.1.1 Effects of curcumin on oxygen-killed pathogen induced epithelial-related gene expression changes

The expression of E-cadherin was significantly down-regulated in all cultures exposed to *E. coli* LPS (0.17-fold) and OK pathogens (0.003 – 0.13-fold) after 8-days when compared with media only controls ($P<0.01$ and $P<0.001$). However, curcumin addition to pathogen exposed cultures significantly increased E-cadherin expression (5.1- 17.4-fold) in comparison with pathogens only ($P<0.001$) (Figure 5.9a). *E. coli* LPS (0.7-fold) and OK pathogens (0.28 – 0.69-fold) also significantly decreased expression of cytokeratin 5 compared with media only

exposure ($P<0.05$ and $P<0.001$). Similarly, to E-cadherin, curcumin addition (4.15 – 152.5-fold) significantly up-regulated cytokeratin-5 expression compared with pathogen exposure only ($P<0.01$ and $P<0.001$) (Figure 5.9b). In addition, expression of desmoplakin-1 was significantly down-regulated in all pathogen exposed cultures (0.13 – 0.41-fold) when compared with media only ($P<0.05$, $P<0.01$ and $P<0.001$), except for OK *P. gingivalis* exposure when it was not significantly down-regulated. Similar to the effects on E-cadherin and cytokeratin 5 expression, curcumin significantly up-regulated desmoplakin-1 expression (0.96 – 12.45-fold) when compared with cultures exposed to pathogens only ($P<0.05$, $P<0.01$ and $P<0.001$) (Figure 5.9c). Both vehicle control (12.45-fold) and curcumin only (4.48-fold) exposed cultures significantly up-regulated ($P<0.01$) cytokeratin 5 expression (Figure 5.9b). However, desmoplakin-1 expression was significantly down-regulated ($P<0.001$) with vehicle control (0.13-fold) (Figure 5.9c).

Overall, curcumin was able to inhibit OK pathogen induced down-regulation of the epithelial markers E-cadherin, cytokeratin 5 and desmoplakin-1 after 8 days incubation, therefore potentially preventing progression of EMT. To further confirm this, curcumins' potential in downregulating mesenchymal-related gene expression changes was investigated.

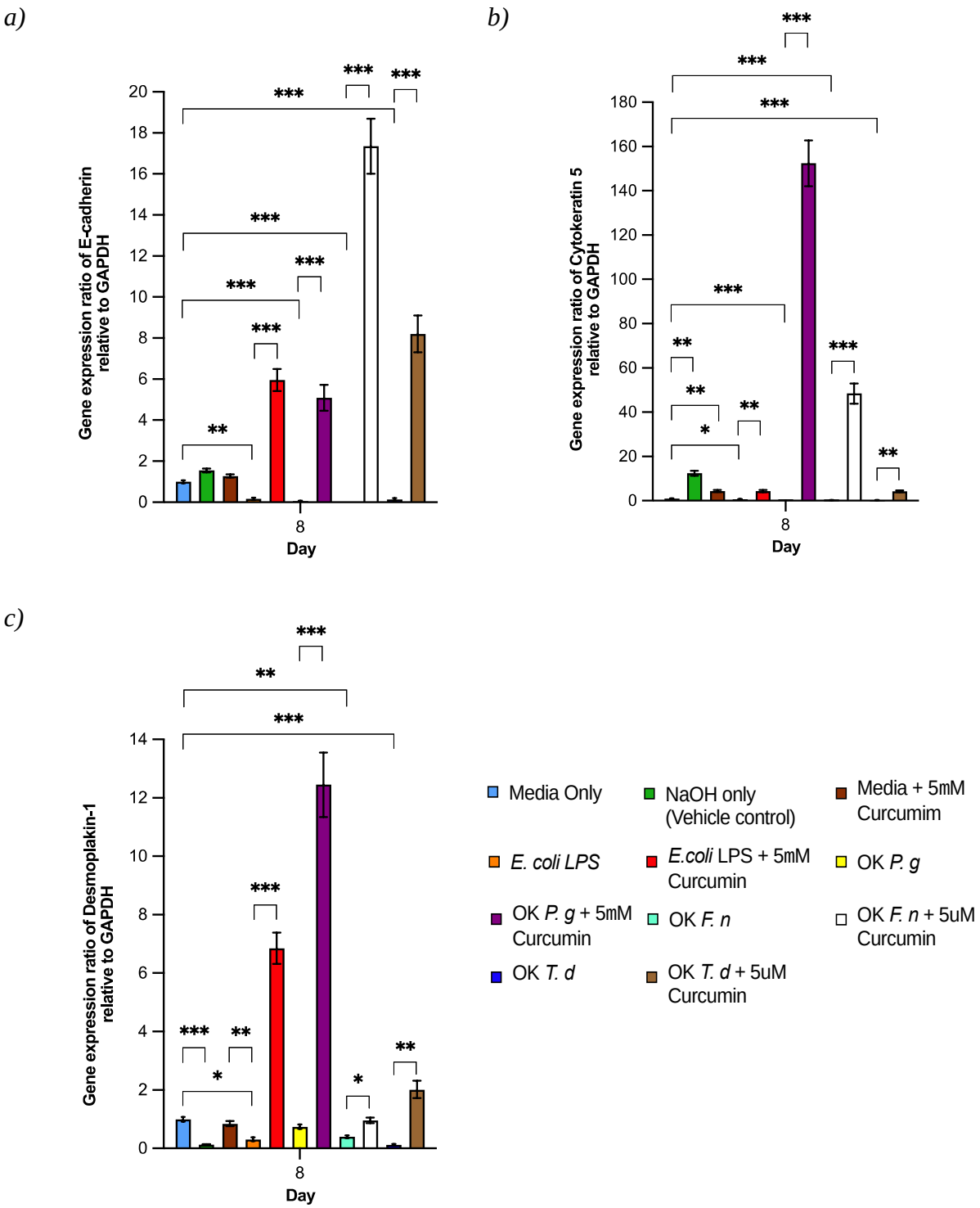



**Figure 5.9**: Gene expression ratios (relative to GAPDH) of epithelial markers for (a) E-cadherin, (b) Cytokeratin 5 and (c) Desmoplakin-1 determined by quantitative real-time PCR on day-8 H400 cultures challenged with *E. coli* LPS, oxygen-killed *P. gingivalis*, *F. nucleatum* and *T. denticola* +/- curcumin. The values obtained from each sample were normalised to GAPDH. All OK pathogens and *E. coli* LPS decreased epithelial marker expression however curcumin addition to pathogen stimulated cultures significantly increased expression above basal levels. Error bars shown are standard deviations and experiments were performed in triplicate. * = P<0.05, ** = P<0.01 *** = P<0.001.

### 5.7.2 Gene expression of mesenchymal markers

The mesenchymal markers N-cadherin, vimentin and MMP-9 all exhibited significantly increased gene expression after *E. coli* LPS and OK pathogen exposure (see section 4.3.2.1). These findings along with curcumins' potential to inhibit EMT (see section 5.1), suggested that curcumin may inhibit pathogen-induced mesenchymal marker expression. Therefore, gene expression of these markers was assessed in cultures exposed to OK pathogens with curcumin using qRT-PCR analysis.

#### 5.7.2.1 Effects of curcumin on oxygen-killed pathogen induced mesenchymal-related gene expression

Expression of N-cadherin was significantly up-regulated ($P<0.05$, $P<0.01$ and $P<0.001$) in *E. coli* LPS (8.57-fold) and OK pathogen (2.16 - 4.33-fold) exposed cultures in comparison with media only. However, cultures exposed to both pathogens and curcumin (0.06 – 5.37-fold) presented down-regulated expression, with curcumin significantly down-regulating N-cadherin expression following *E. coli* LPS ($P<0.01$) and OK *T. denticola* ($P<0.001$) exposure when compared with pathogen exposed cultures only (Figure 5.10a). Similarly, vimentin expression was significantly up-regulated ($P<0.05$ and $P<0.001$) in all pathogen exposed cultures (1.74 – 7.63-fold) compared with media only control. Curcumin significantly down-regulated ($P<0.05$ and $P<0.001$) vimentin expression (0.073 – 2.53-fold) for all cultures except OK *F. nucleatum* (Figure 5.10b). As observed with N-cadherin and vimentin expression, MMP-9 was significantly up-regulated for all OK pathogen stimulated cultures (5.41 – 11.16-fold) compared with media only ($P<0.01$ and $P<0.001$). However, curcumin treatment significantly decreased expression of MMP-9 (0.098 – 6.59-fold) in all cultures when compared with pathogen exposed cultures only ($P<0.05$, $P<0.01$ and $P<0.001$) (Figure

5.10c). Furthermore, the vehicle control significantly up-regulated ($P<0.01$) N-cadherin expression (3.43-fold) (Figure 5.10a) but significantly down-regulated ($P<0.05$) MMP-9 expression (0.27-fold) (Figure 5.10c) when compared with media only. In addition, curcumin only exposure significantly up-regulated vimentin expression (5.99-fold) (Figure 5.10b) in comparison with controls ($P<0.001$). Curcumin provided to be most effective in inhibiting up-regulated OK *T. denticola* induced N-cadherin, vimentin and MMP-9 expression by 4.28, 5.1 and 6.71-fold decreases, respectively.

In general, curcumin inhibited OK pathogen induced up-regulated gene expression of the mesenchymal markers N-cadherin, vimentin and MMP-9, with curcumin having significant effects on MMP-9 expression for all pathogen exposed cultures. Therefore, curcumin may have inhibited OK pathogen-induced EMT by supressing expression of mesenchymal-related genes. qRT-PCR was undertaken for EMT-related transcription factors to further deduce curcumins' downregulation of OK pathogen-induced EMT.

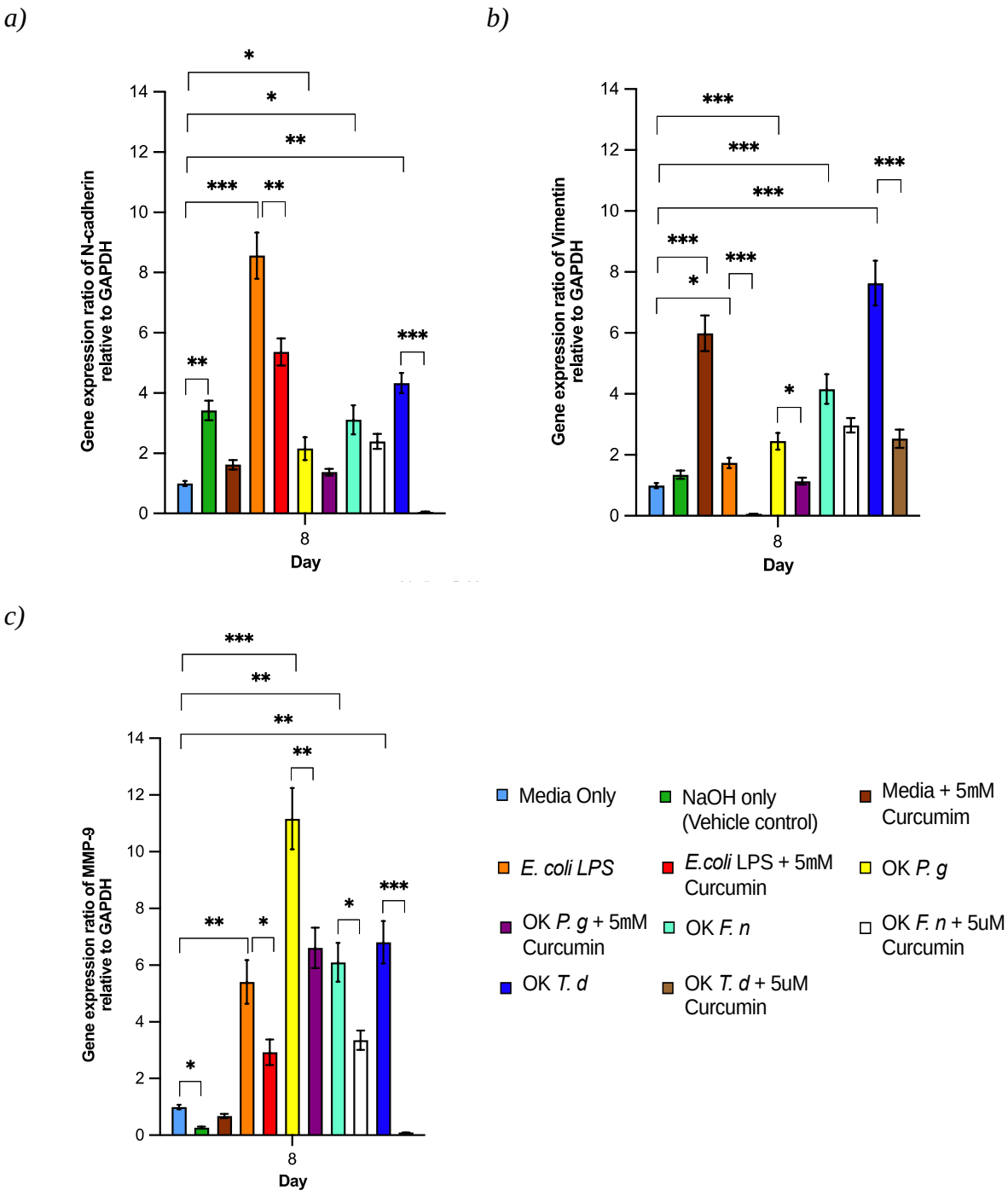



**Figure 5.10**: Gene expression ratios (relative to GAPDH) of mesenchymal markers for (a) N-cadherin, (b) Vimentin and (c) MMP-9 determined by quantitative real-time PCR on day-8 H400 cultures challenged with *E. coli* LPS, oxygen-killed *P. gingivalis*, *F. nucleatum* and *T. denticola* +/- curcumin. The values obtained from each sample were normalised to GAPDH. All cultures challenged with oxygen-killed pathogens significantly up-regulated expression of all mesenchymal markers and expression was decreased with curcumin addition. Curcumin significantly decreased *E. coli* LPS and oxygen-killed *T. denticola* induced up-regulation of all mesenchymal markers. Error bars shown are standard deviations and experiments were performed in triplicate. * = P<0.05, ** = P<0.01 and *** = P<0.001.

### 5.7.3 Gene expression of EMT-related transcription factors

The transcription factors snail-1, snail-2 and twist-1 are associated with regulating several genes associated with EMT (Peinado, Olmeda and Cano, 2007). Expression of these transcription factors in oral keratinocytes were generally up-regulated after OK pathogen exposure (see section 4.3.3.1) and curcumin has previously demonstrated its potential to inhibit EMT-related gene expression changes (see section 5.1). Therefore, qRT-PCR was performed on cultures exposed to OK pathogens with curcumin to assess curcumins' potential to inhibit pathogen-induced EMT transcription factor gene expression changes.

#### 5.7.3.1 Effects of curcumin on oxygen-killed pathogen induced expression of EMT-related transcription factors

Expression of snail-1 was significantly up-regulated ($P<0.001$) after exposure to all pathogens (3.11 – 7.16-fold) compared with media only controls. However, curcumin addition (0.18 – 4.23-fold) significantly down-regulated ($P<0.01$ and $P<0.001$) snail-1 expression when compared with cultures exposed to the pathogens only (Figure 5.11a). Snail-2 expression was up-regulated for all pathogen exposed cultures (1.2 – 3.1-fold) except OK *P. gingivalis* (0.53-fold) ($P<0.01$), with significant up-regulation ($P<0.01$) occurring with *E. coli* LPS and OK *T. denticola* exposure compared with media only. Curcumin significantly ($P<0.05$ and $P<0.01$) supressed *E. coli* LPS (1.16-fold) and OK *T. denticola* (2.3-fold) induced snail-2 expression. However, curcumin significantly up-regulated snail-2 expression (1.35-fold) in OK *P. gingivalis* stimulated cultures compared with cultures exposed to OK *P. gingivalis* only ($P<0.01$) (Figure 5.11b). Expression of twist-1 was up-regulated for all pathogen exposed cultures (1.02 – 9.3-fold) with *E. coli* LPS ($P<0.01$) and OK *T. denticola* ($P<0.001$) significantly up-regulating expression compared with media only. Curcumin significantly

(P<0.01 and P<0.001) reduced *E. coli* LPS (1.39-fold) and OK *T. denticola* (2.99-fold) induced twist-1 expression. In contrast, curcumin significantly up-regulated twist-1 expression in cultures exposed to OK *F. nucleatum* (3.11-fold) compared with cultures exposed to OK *F. nucleatum* only (P<0.05) (Figure 5.11c). The vehicle control significantly down-regulated (P<0.05 and P<0.001) snail-1 (0.13-fold) (Figure 5.11a) and twist-1 (0.4-fold) (Figure 5.11c) expression and expression of all genes was significantly down-regulated by curcumin only exposure (0.0002 - 0.21-fold) in comparison with media only control (P<0.001).

Overall, curcumin was able to significantly inhibit the expression of all three EMT transcription factors in cultures exposed to *E. coli* LPS and OK *T. denticola*, but curcumin differentially affected snail-2 and twist-1 gene expression in OK *P. gingivalis* and *F. nucleatum* exposed cultures, therefore possibly highlighting a mechanism through which curcumin exerted its EMT-inhibitory effects. Curcumins' potential to supress up-regulated gene expression of pro-inflammatory cytokines related to EMT induction was explored next.

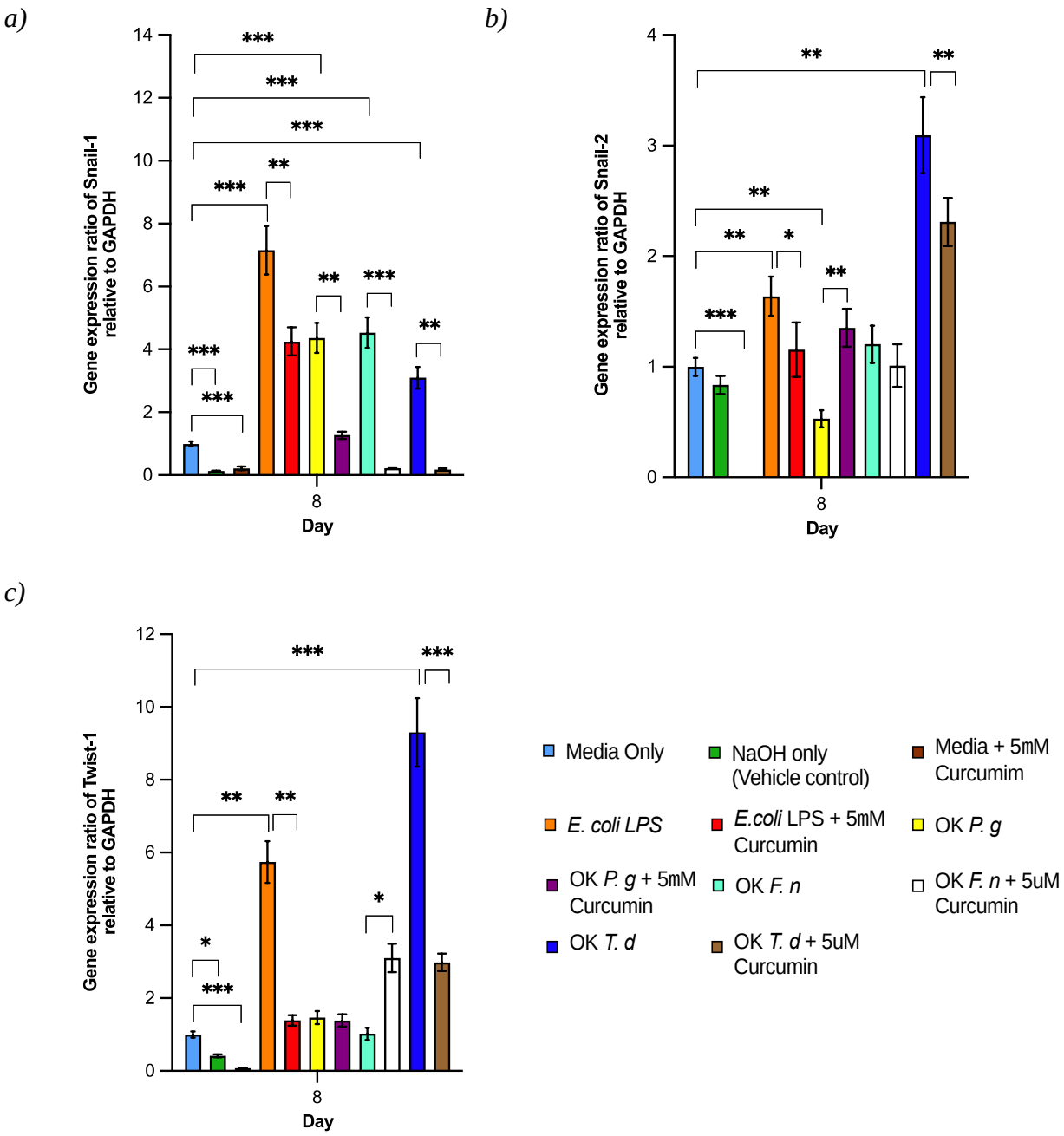



**Figure 5.11**: Gene expression ratios (relative to GAPDH) of EMT-related transcription factors for (a) snail-1, (b) snail-2 and (c) twist-1 determined by quantitative real-time PCR on day-8 H400 cultures challenged with *E. coli* LPS, oxygen-killed *P. gingivalis*, *F. nucleatum* and *T. denticola* +/- curcumin. The values obtained from each sample were normalised to GAPDH. All cultures challenged with oxygen-killed bacteria up-regulated expression of all genes except oxygen-killed *P. gingivalis* which decreased snail-2 expression in comparison with control. Curcumin significantly decreased *E. coli* LPS and oxygen-killed *T. denticola* induced expression of all mesenchymal markers. However, curcumin exposure resulted in differential responses in all genes after oxygen-killed *P. gingivalis* and *F. nucleatum* stimulation. Error bars shown are standard deviations and experiments were performed in triplicate. * = P<0.05, ** = P<0.01 and *** = P<0.001.

### 5.7.4 Gene expression of EMT-inducing pro-inflammatory cytokines

The pro-inflammatory cytokines IL-1β, IL-8 and TGF-β1 have been linked with inducing EMT (see section 1.3.5) and data here showed that *E. coli* LPS and OK pathogens could up-regulate gene expression of these cytokines (see section 4.3.4.1). Curcumin has been shown to possess anti-inflammatory properties (Cho, Lee and Kim, 2007; Mohankumar et al., 2015), therefore curcumin was supplemented into OK pathogen exposed cultures and its potential to inhibit pathogen-induced pro-inflammatory cytokine gene expression was analysed by qRT-PCR.

#### 5.7.4.1 Effects of curcumin on oxygen-killed pathogen induced EMT-related pro-inflammatory cytokine gene expression

IL-1β expression was significantly up-regulated in cultures exposed to *E. coli* LPS (8.25-fold) ($P<0.001$) and OK *T. denticola* (3.67-fold) ($P<0.01$) in comparison with media only controls. Curcumin significantly decreased *E. coli* LPS (3.91-fold) ($P<0.001$) and OK *T. denticola* (1.7-fold) ($P<0.05$) induced IL-1β gene expression compared with cultures exposed to pathogens only. Conversely, curcumin had the opposite effect in cultures exposed to *F. nucleatum* (2.65-fold) ($P<0.05$), where expression was significantly increased (Figure 5.12a). Expression of IL-8 however was increased in all pathogen stimulated cultures (1.13 – 25.11-fold) with *E. coli* LPS, OK *P. gingivalis* and *T. denticola* resulting in significant up-regulation compared with media only controls ($P<0.05$ and $P<0.001$). However, IL-8 expression was significantly decreased ($P<0.05$, $P<0.01$ and $P<0.001$) in these cultures with the addition of curcumin (0.017 – 8.2-fold) (Figure 5.12b). Cultures stimulated with *E. coli* LPS (2.18-fold), OK *F. nucleatum* (1.54-fold) and *T. denticola* (6.57-fold) significantly increased TGF-β1 expression in comparison with media only control ($P<0.05$, $P<0.01$ and $P<0.001$). Curcumin addition

(0.46 – 0.92-fold) significantly decreased all pathogen-induced TGF-β1 expression ($P<0.05$, $P<0.01$ and $P<0.001$), except in OK *P. gingivalis* (1.95-fold) exposed cultures where expression was significantly increased compared with cultures exposed to pathogens only ($P<0.05$) (Figure 5.12c). The vehicle control did not affect cytokine expression but curcumin only exposure (0.61-fold) significantly decreased TGF-β1 expression compared with media only ($P<0.05$) (Figure 5.12c).

Overall, curcumin significantly inhibited the expression of all three pro-inflammatory cytokines in cultures exposed to *E. coli* LPS and OK *T. denticola* but demonstrated differential responses in OK *P. gingivalis* and *F. nucleatum* stimulated cultures.

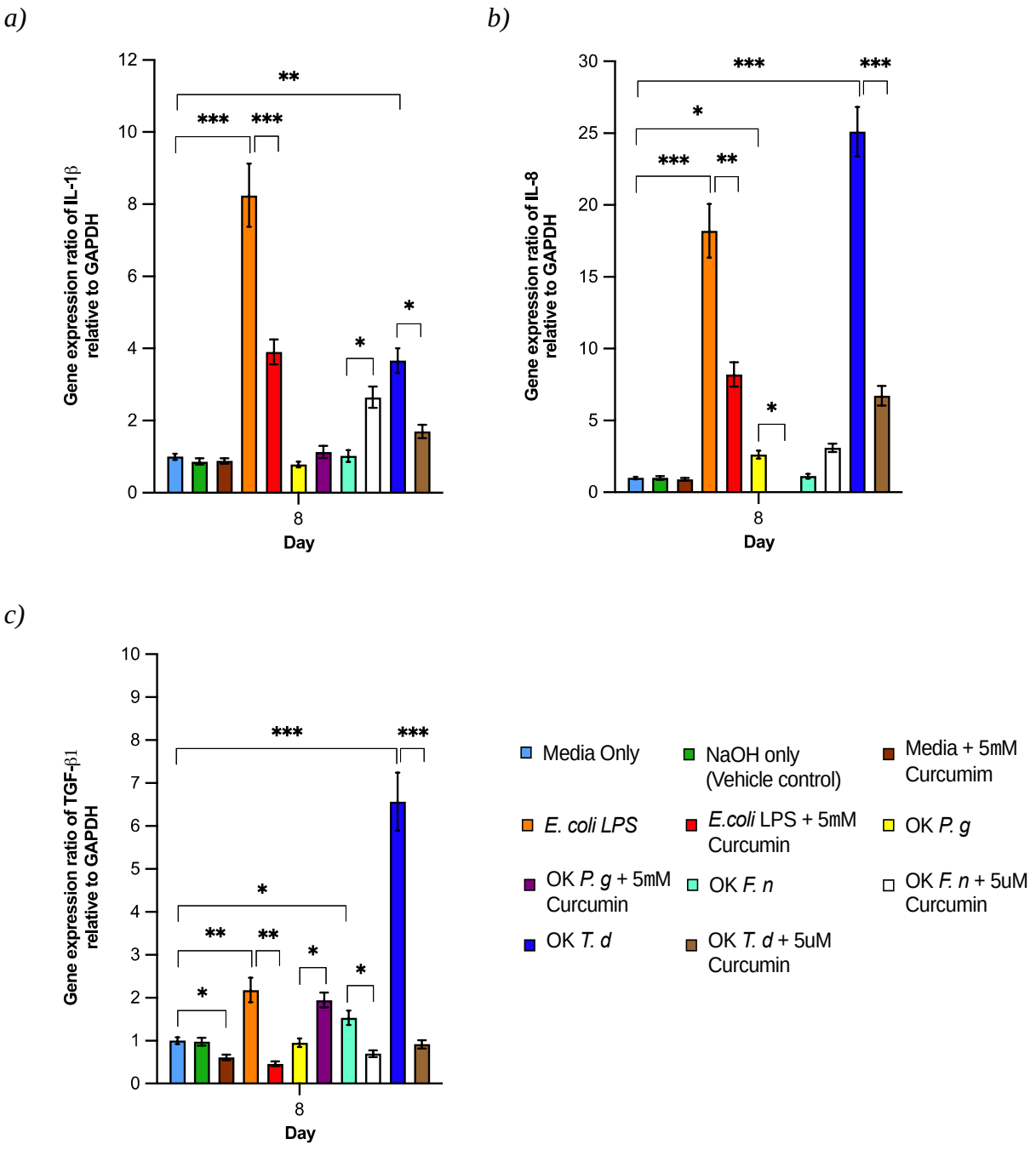



**Figure 5.12**: Gene expression ratios (relative to GAPDH) of pro-inflammatory cytokines for (a) IL-1β, (b) IL-8 and (c) TGF-β1 determined by quantitative real-time PCR on day-8 H400 cultures challenged with *E. coli* LPS, oxygen-killed *P. gingivalis*, *F. nucleatum* and *T. denticola* +/- curcumin. The values obtained from each sample were normalised to GAPDH. Expression of all cytokines were significantly increased after *E. coli* LPS and oxygen-killed *T. denticola* exposure in comparison with control, however addition of curcumin significantly decreased expression in these cultures. Curcumin addition in oxygen-killed *P. gingivalis* and *F. nucleatum* exposed cultures resulted in differential expression across all cytokines. Error bars shown are standard deviations and experiments were performed in triplicate. * = P<0.05, ** = P<0.01 and *** = P<0.001.

**Table 5.1**: Summary of gene expression ratios determined by quantitative real-time PCR of EMT related markers following 8-day exposure to oxygen-killed pathogens with and without curcumin.

| | **Gene expression ratios of EMT related markers after pathogen exposure (oxygen-killed) -/+ curcumin** | | | | | | | |
|---|---|---|---|---|---|---|---|---|
| **Curcumin** | - | + | - | + | - | + | - | + |
| **Gene name** | *E. coli* LPS | | *P. gingivalis* | | *F. nucleatum* | | *T. denticola* | |
| E-cadherin | 0.17 | 5.96 | 0.05 | 5.09 | 0.003 | 17.35 | 0.13 | 8.21 |
| Cytokeratin 5 | 0.71 | 4.41 | 0.69 | 152.5 | 0.3 | 48.34 | 0.28 | 4.15 |
| Desmoplakin-1 | 0.31 | 6.85 | 0.75 | 12.45 | 0.41 | 0.96 | 0.13 | 2.02 |
| N-cadherin | 8.57 | 5.37 | 2.16 | 1.38 | 3.12 | 2.4 | 4.33 | 0.06 |
| Vimentin | 1.74 | 0.07 | 2.45 | 1.14 | 4.16 | 2.97 | 7.63 | 2.53 |
| MMP-9 | 5.41 | 2.93 | 11.16 | 6.59 | 6.1 | 3.35 | 6.81 | 0.098 |
| Snail-1 | 7.16 | 4.23 | 4.37 | 1.28 | 4.54 | 0.23 | 3.11 | 0.18 |
| Snail-2 | 1.64 | 1.16 | 0.53 | 1.35 | 1.2 | 1.01 | 3.1 | 2.3 |
| Twist-1 | 5.74 | 1.39 | 1.47 | 1.39 | 1.02 | 3.11 | 9.3 | 2.99 |
| IL-1β | 8.25 | 3.91 | 0.78 | 1.14 | 1.02 | 2.65 | 3.67 | 1.7 |
| IL-8 | 18.21 | 8.2 | 2.63 | 0.017 | 1.13 | 3.11 | 25.11 | 6.73 |
| TGF-β1 | 2.18 | 0.46 | 0.95 | 1.95 | 1.54 | 0.7 | 6.57 | 0.92 |

Down-regulated  Up-regulated

### 5.8 Trans-epithelial electrical resistance of oral keratinocyte monolayers exposed to oxygen-killed *T. denticola* and *E. coli* LPS with curcumin

Previous findings here have shown decreased TEER readings after OK *T. denticola* and *E. coli* LPS exposure in oral keratinocyte cultures (see section 4.7.1). Curcumin has been shown to prevent loss of epithelial adhesion molecule gene expression in these cultures (see section 5.7.1.1), therefore TEER was performed on cultures exposed to OK *T. denticola* and *E. coli* LPS with curcumin, to further confirm whether curcumin may maintain epithelial integrity.

#### 5.8.1 Analysis of curcumin on trans-epithelial electrical resistance in oxygen-killed *T. denticola* and *E. coli* LPS exposed monolayers

TEER readings were not significantly different at all days in cultures exposed to *E. coli* LPS when compared with media only controls. The addition of curcumin to *E. coli* LPS stimulated cultures increased TEER for all days except day 3 where readings decreased in comparison with cultures stimulated with *E. coli* LPS only. OK *T. denticola* exposure significantly decreased TEER readings at all days except day 4 and 5 when compared with media only controls ($P<0.05$ and $P<0.01$). Curcumin exposure non-significantly decreased TEER values further for all days in OK *T. denticola* exposed cultures compared with cultures exposed to OK *T. denticola* only. TEER readings were significantly lower in OK *T. denticola* and curcumin exposed cultures in comparison with media only at all days except day 4 ($P<0.05$, $P<0.01$ and $P<0.001$) (Figure 5.13).

Overall, curcumin appeared to partially restore *E. coli* LPS induced loss of epithelial cell-cell adhesion as shown by increased TEER readings but, was ineffective in cultures exposed to OK *T. denticola*.

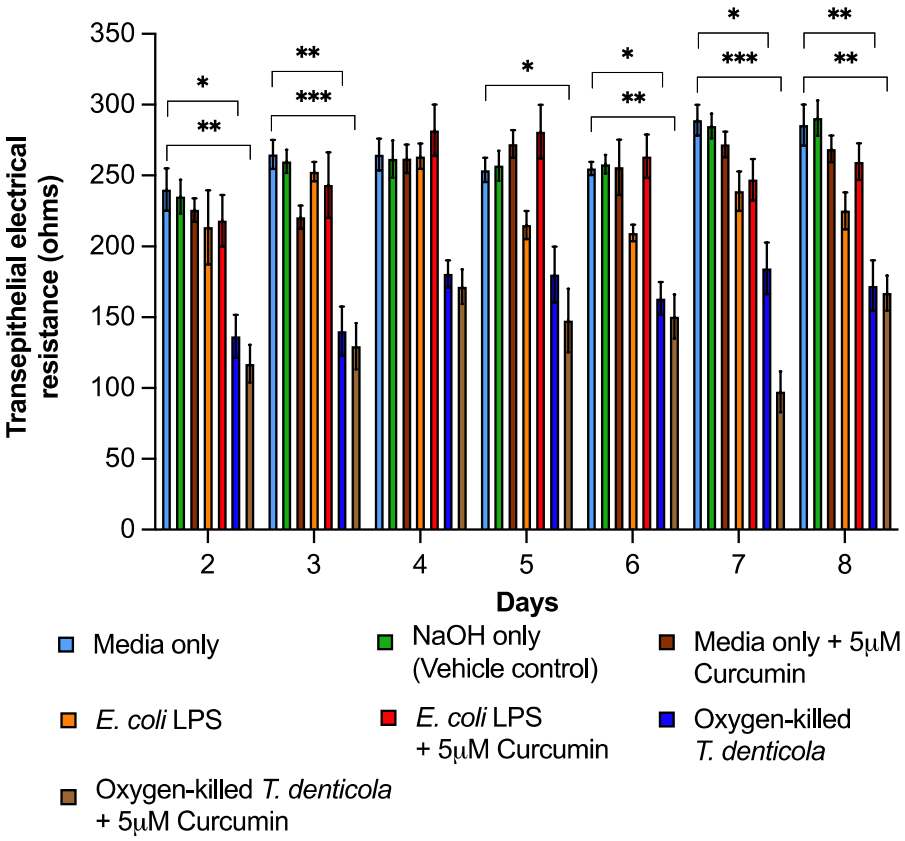



**Figure 5.13**: Trans-epithelial electrical resistance (TEER) readings of oral keratinocyte monolayers from day 2-8 challenged with *E. coli* LPS and oxygen-killed *T. denticola* +/- curcumin. *E. coli* LPS and oxygen-killed *T. denticola* exposure reduced TEER readings in comparison with media only control. *E. coli* LPS with curcumin resulted in greater TEER readings compared with *E. coli* LPS exposure only at all days except day 3. However, curcumin addition to oxygen-killed *T. denticola* stimulated cultures decreased TEER readings when compared with oxygen-killed *T. denticola* exposure only at all days. Error bars shown are standard deviations and experiments performed in triplicate. * = P<0.05, ** = P<0.01 and *** = P<0.001.

## 5.9 Discussion

### 5.9.1 Curcumin inhibits oxygen-killed *T. denticola* induced oral keratinocyte growth

Oral keratinocyte stimulation by OK *T. denticola* significantly increased cell growth and addition of curcumin was able to significantly inhibit this cell growth after 8-days exposure. Curcumin's inhibition of OK *T. denticola* induced cell growth has not been previously explored. It was determined from the literature that epithelial cell exposure to *T. denticola* activates cell proliferation pathways, MAP kinases ERK1 and ERK2, leading to increased cell division and growth (see section 4.8.1). Five-µM curcumin can decrease phosphorylation of ERK1/2 induced by TGF-β2 in epithelial cells after 48 hours exposure (Liu et al., 2020), therefore curcumin inhibition of OK *T. denticola* induced cell growth is potentially due to decreased activity of the cell proliferation pathways, ERK1/2.

A previous study has shown 5µM curcumin inhibited cell growth in normal and immortalized oral keratinocytes after 3-days exposure (Chakravarti et al., 2010). It was also observed in this study that protein levels of cyclin D1 were downregulated after curcumin exposure. Cyclin D1 binds to CDK4 and CDK6 to form active complexes that promote cell cycle progression through the G1 to S phase (Alao, 2007). Therefore, decreased cyclin D1 activity would decrease cell proliferation leading to the significantly lower cell number seen here after curcumin exposure. As cell growth was inhibited after 8-days exposure in the study, it was proposed that curcumin was able to exert its inhibitory effects over a longer period than 3-days. Further studies would be needed however to determine the exact mechanism through which curcumin inhibits OK *T. denticola* induced cell growth.

### 5.9.2 Curcumin inhibits oxygen-killed *P. gingivalis* and *T. denticola* induced oral keratinocyte cell migration

The exposure of oral keratinocytes to OK *P. gingivalis*, *F. nucleatum* and *T. denticola* significantly increased cell migration of oral keratinocytes, however the addition of curcumin was able to significantly inhibit OK *P. gingivalis* and *T. denticola* induced cell migration at some of the time points tested. The gingipains of *P. gingivalis* have been noted to induce cell migration in microglial cells (see section 4.8.6). Curcumin has been shown to significantly inhibit the activity of *P. gingivalis* gingipains in a dose-dependent manner (Singh et al., 2018), therefore curcumin inhibition of OK *P. gingivalis* induced cell migration observed here may be related to reduced activity of gingipains. The decreased OK *T. denticola* induced cell migration seen here with curcumin treatment may be associated with significant inhibition of N-cadherin gene expression. It is known that N-cadherin can promote cell motility (see section 4.8.6), however previous studies have not explored the ability of curcumin to inhibit N-cadherin gene up-regulation in oral epithelial cells. Interestingly, curcumin can inhibit N-cadherin gene expression in breast cancer cell lines (Gallardo and Calaf, 2016a) and N-cadherin protein expression in lung cancer cell lines (Deng et al., 2020). Data here may imply that curcumin was also able to inhibit N-cadherin gene up-regulation in oral epithelial cells, possibly leading to significant inhibition of OK *T. denticola* induced cell migration as was observed here. Interestingly, curcumin treatment did not inhibit OK *F. nucleatum* induced cell migration. This may have possibly related to vimentin gene expression which was significantly downregulated with curcumin addition in OK *P. gingivalis* and *T. denticola* stimulated cultures, but not in OK *F. nucleatum* stimulated cultures. Vimentin is a mesenchymal cytoskeletal structure that facilitates cell motility during EMT (Huang, Guilford

and Thiery, 2012), therefore findings here may suggest a role for vimentin in enabling cell motility for oral keratinocytes *in vitro*.

### 5.9.3 Curcumin inhibits oxygen-killed pathogen induced epithelial marker repression

The epithelial markers E-cadherin, cytokeratin 5 and desmoplakin-1 were all down-regulated with OK pathogen stimulation, however addition of curcumin to these pathogen exposed cultures inhibited and significantly up-regulated expression of these markers. Curcumin can up-regulate protein expression of E-cadherin in OSCC cells (Lee et al., 2015; Ohnishi et al., 2020) and E-cadherin gene expression in breast cancer cell lines (Mukherjee et al., 2014). In addition, curcumin significantly inhibited up-regulated EMT-related transcription factor, snail-1, for all OK pathogen stimulated cultures in the present study. Snail-1 is well known to directly repress E-cadherin expression (Kaufhold and Bonavida, 2014), therefore, curcumin may inhibit OK pathogen-induced E-cadherin gene expression through a snail-1 mediated pathway. Curcumins effects on cytokeratin 5 have not been previously explored however it has been shown to promote cytokeratin gene expression after TGF-β1 induced EMT in kidney epithelial cells, possibly through suppression of the Akt/mTOR pathway (Zhu et al., 2017). In addition, the ability of curcumin to restore desmoplakin-1 expression has not been previously investigated. Snail-1 can repress expression of other desmosomal components, such as plakophilin-2, in colorectal cells (De Craene et al., 2005), therefore snail-1 may potentially be involved in the repression of similar components such as desmoplakin-1. Consequently, the up-regulation of desmoplakin-1 gene expression observed here after curcumin addition maybe through repressed activity of snail-1. It would be expected that TEER would therefore increase with up-regulated expression of these epithelial cell adhesion markers after curcumin treatment. Interestingly, curcumin addition to pathogen stimulated cultures did not

significantly increase TEER readings, which suggested gene transcription was not being translated to the protein level possibly due to post-transcriptional regulatory systems as discussed in section 4.8.2.

### 5.9.4 Curcumin potentially inhibits oxygen-killed pathogen-induced mesenchymal gene expression

The addition of curcumin to *E. coli* LPS and OK *T. denticola* exposed cultures significantly inhibited N-cadherin gene expression and supporting data has shown curcumin to inhibit gene expression of N-cadherin in breast cancer cell lines (Gallardo and Calaf, 2016a). However, curcumin was ineffective at inhibiting OK *P. gingivalis* and *F. nucleatum* induced N-cadherin gene up-regulation and this may have been due to significantly up-regulated TGF-β1 and IL-1β gene expression observed in these cultures after curcumin addition when compared with pathogen only exposed cultures. Both TGF-β1 (Araki et al., 2011) and IL-1β (Li et al., 2020) have been shown to increase N-cadherin expression, therefore curcumin's ability to repress OK *P. gingivalis* and *F. nucleatum* induced N-cadherin gene up-regulation maybe counteracted by increased activity of these cytokines.

Curcumin significantly inhibited up-regulated gene expression of vimentin brought about by OK *P. gingivalis* and *T. denticola* stimulation. Curcumin has previously been shown to inhibit vimentin expression after hepatocyte growth factor induced EMT in OSCC cells, possibly through downregulation of the c-Met/ERK pathway (Ohnishi et al., 2020). In addition, another study observed repression of vimentin expression by curcumin, through suppression of the Akt/mTOR pathway after TGF-β1 induced EMT in kidney epithelial cells (Zhu et al., 2017). However, curcumin was ineffective in significantly inhibiting OK *F. nucleatum*

induced vimentin gene expression. Curcumin supplementation in OK *F. nucleatum* exposed cultures resulted in significantly increased gene expression of the EMT-related transcription factor twist-1. Overexpression of twist-1 has been implicated in inducing vimentin expression in previous investigations (Bulzico et al., 2018; Meng et al., 2018; Zhang et al., 2015b), therefore inhibition of OK *F. nucleatum* induced vimentin gene up-regulation by curcumin may be counteracted by twist-1 overexpression.

The up-regulated gene expression of MMP-9 after exposure with all OK pathogens was significantly inhibited by curcumin treatment. Curcumin has previously been shown to inhibit MMP-9 gene up-regulation in OSCC cells (Lee et al., 2015; Zhen et al., 2014) and gingival epithelial cells (Toraya et al., 2019). Urokinase-type plasminogen activator/receptor (uPA/R) signalling plays an important role in ECM destruction, which promotes EMT and it was previously observed that expression of uPA/R was simultaneously down-regulated along with MMP-9 expression after curcumin exposure in OSCC cells (Zhen et al., 2014). This may suggest that OK pathogen-induced MMP-9 gene expression observed here may be inhibited by curcumin potentially through uPA/R signalling.

### 5.9.5 Curcumin selectively inhibits oxygen-killed pathogen induced gene expression of EMT-related transcription factors

The up-regulated gene expression of snail-1 after OK pathogen exposure was significantly inhibited following curcumin treatment. A previous study has shown curcumin to down-regulate snail-expression in OSCC cells after 24 hours treatment in a dose dependent manner (Lee et al., 2015). Findings in the present study suggested that curcumin was still effective in inhibiting snail-1 expression over an extended period of 8-days. Another study has shown that

curcumin represses snail-1 expression via suppression of the Smad2 pathway in epithelial cells (Cao et al., 2017). Therefore, inhibition of OK pathogen-induced snail-1 gene up-regulation detected here after curcumin treatment, may possibly have been due to the activity of the Smad2 pathway, although further investigations are needed to confirm this.

Snail-2 upregulation by OK *T. denticola* exposure was significantly inhibited with curcumin supplementation. Curcumins' repression of snail-2 expression in oral epithelial cells has not been previously reported. Although, supporting studies have shown snail-2 (slug) gene (Gallardo and Calaf, 2016b) and protein expression (Deng et al., 2020; Thacker and Karunagaran, 2015) to be inhibited by curcumin in breast, cervical and lung cancer cell lines. Wnt/β-catenin is involved in activating snail-2 (Moon, Lee and Lim, 2021) and it was deduced that curcumin was able to repress β-catenin and inhibit the Wnt/β-catenin pathway leading to snail-2 down-regulation in epithelial cells (Thacker and Karunagaran, 2015). This pathway may be involved in curcumin inhibition of OK *T. denticola* induced snail-2 up-regulation observed here, however further investigations are needed to confirm this. In contrast, snail-2 was significantly up-regulated by curcumin addition in OK *P. gingivalis* stimulated cultures. This could have been related to the significantly increased gene transcript of TGF-β1 observed in these cultures after curcumin exposure, as TGF-β1 can up-regulate snail-2 gene transcription (Morita, Mayanagi and Sobue, 2007).

Curcumin also significantly inhibited the up-regulated twist-1 expression after OK *T. denticola* exposure. A study demonstrating curcumins' inhibition of EMT in OSCC cells showed twist-1 to be down-regulated by curcumin in a dose-dependent manner via a p53-dependent signalling pathway (Lee et al., 2015). It was also identified that TGF-β1 could up-

regulate twist-1 expression through the STAT3 signalling pathway (Cho et al., 2013). Curcumin inhibited OK *T. denticola* induced TGF-β1 gene expression here, which may potentially have indicated decreased TGF-β1 secretion, therefore leading to reduced STAT3 signalling and down-regulated twist-1 gene expression. However, curcumin had opposite effects on twist-1 gene expression in OK *F. nucleatum* stimulated cultures, where it significantly up-regulated expression. This outcome may have been associated with the increased IL-1β gene expression seen in these cultures after curcumin treatment, which could suggest increased IL-1β protein secretion. IL-1β is implicated in inducing twist-1 expression in epithelial cells (Jiménez-Garduño et al., 2017), therefore curcumins' inhibition of OK *F. nucleatum* induced twist-1 maybe counteracted by increased activity of IL-1β.

### 5.9.6 Curcumin selectively inhibits oxygen-killed pathogen induced gene expression of EMT promoting pro-inflammatory cytokines

Curcumin treatment was able to significantly prevent OK *T. denticola* induced IL-1β gene up-regulation. Curcumin has previously been shown to inhibit IL-1β secretion in epithelial cells (Wang, Ghosh and Ghosh, 2017a) and gene expression in human keratinocytes (Cho, Lee and Kim, 2007). In contrast, curcumin addition significantly increased expression of IL-1β in OK *F. nucleatum* stimulated cultures and this may have been associated with *F. nucleatums'* LPS which can induce IL-1β secretion (Martinho et al., 2016). Therefore, findings here suggested that curcumin may be ineffective or even promote the activity of *F. nucleatum* LPS resulting in increased IL-1β gene up-regulation.

Curcumin exposure significantly inhibited up-regulated gene transcripts of IL-8 after OK *P. gingivalis* and *T. denticola* exposure. Curcumin has been reported to down-regulate gene

expression of IL-8 in oesophageal epithelial cells (Rafiee et al., 2009) and OSCC cells (Cohen et al., 2009) and to initiate its effects via inhibition of Iκβ-kinase activity in the NF-κβ pathway (Cohen et al., 2009). Therefore, OK *P. gingivalis* and *T. denticola* induced IL-8 gene up-regulation may be inhibited by curcumin through NF-κβ signalling, although further studies are needed to confirm this.

TGF-β1 gene expression was significantly inhibited with curcumin addition in OK *F. nucleatum* and OK *T. denticola* exposed cultures. The effects of curcumin in supressing TGF-β1 gene up-regulation in oral epithelial cells has not been previously investigated. However, supporting data shows that curcumin can inhibit TGF-β1 secretion in breast epithelial cells via the NF-κB pathway (Mohankumar et al., 2015). The transcription factor snail-1 was significantly inhibited in the present study after curcumin addition and it is known that snail-1 can increase expression of TGF-β pathway genes via a positive feedback mechanism (Dhasarathy et al., 2011). Therefore, inhibition of the snail-1 transcription factor may lead to the down-regulation of TGF-β1 gene expression observed here. In contrast, curcumin significantly up-regulated TGF-β1 gene expression in OK *P. gingivalis* stimulated cultures. It was identified from the literature that cysteine proteases of *P. gingivalis* can induce a TGF-β1 response (Bengtsson, Khalaf and Khalaf, 2015), therefore curcumin may be promoting cysteine protease activity leading to the increased TGF-β1 gene expression observed here.

The next chapter focused on further understanding different EMT responses with HK and OK *T. denticola* stimulation by performing quantitative mass spectrometry-based proteomics on isolated *T. denticola* outer membrane proteins. These analyses may provide further insight

into the effects of heat and oxygen-killing on *T. denticola* and identify potential *T. denticola* membrane proteins which may promote EMT.

# 6. Mass spectrometry analysis of live, heat and oxygen-killed *T. denticola* proteins

## 6.1 Introduction

From the present study it was observed that oxygen-killing preserved *T. denticola* helical structure more so than heat-killing (see sections 3.5.1 and 3.6.1) and OK *T. denticola* generally stimulated greater EMT-related responses in oral keratinocytes when compared with HK *T. denticola* (see Chapter 4). It was hypothesised that heat-killing maybe denaturing proteins responsible for these changes. Therefore, quantitative mass spectrometry-based proteomics on isolated *T. denticola* outer membrane proteins was performed to further understand the effects of heat and oxygen-killing on *T. denticola* and identify potential *T. denticola* membrane proteins which may be important in stimulating EMT.

The database for annotation, visualization and integrated discovery (DAVID) knowledgebase (Dennis et al., 2003) was utilised to identify enriched biological themes of identified proteins based on gene ontology (GO) terms. GO is a bioinformatics attempt to organise knowledge about gene and gene products and allow functional analysis of data using term enrichment analysis (The Gene Ontology Consortium, 2016). Enriched GO terms were used to identify cellular components (location), biological processes (pathways and programs) and molecular functions of individual gene products. The Kyoto encyclopaedia of genes and genomes (KEGG) pathway database is an assortment of molecular pathway maps and it was utilised here to group genes into known pathways (Kanehisa et al., 2016). To further understand the relationships between proteins, the search tool for the retrieval of interacting genes/proteins (STRING) database was used to assess protein-protein interactions (Szklarczyk et al., 2016). These interactions were based on experimental evidence and information in curated databases.

## 6.2 Isolated *T. denticola* outer membrane proteins

Mass spectrometry analysis and searches of the reviewed UniProt knowledgebase (UniProtKb) protein database identified a total of 132 proteins in *T. denticola*, of which 10 were identified but not quantified (see appendices Table 9.1). These 10 proteins were not quantified because abundance levels were too low. Consequently, analysis of proteins was focused on the 122 identified and quantified proteins. To further understand the role of these 122 proteins, DAVID was utilised to perform GO term enrichment analysis to identify cellular components, biological processes and molecular functions of individual gene products. The genes were searched using existing data for *T. denticola* and any unrecognised genes after GO term enrichment analysis may be due to lack of available information for *T. denticola*.

### 6.2.1 Analysis of *T. denticola* outer membrane proteins

Using GO term enrichment analysis, it was found that the cellular component of 88 genes were enriched whilst 34 were not. From these 88 genes, 48 were identified to be located in the cytoplasm, 29 in the ribosome, 6 in the small ribosomal unit and 5 in the large ribosomal unit Table 6.1). GO analysis also revealed 49 genes which were attributed to biological processes whilst the remaining 73 genes were not identified with any biological processes. Out of these, 42 genes were involved in protein translation, 4 in glycolytic process and 3 in plasma membrane ATP synthesis coupled proton transport (Table 6.2). The molecular function of 85 genes were also identified whilst the remaining 37 genes were not. From the 85 genes, 39 were a structural ribosome constituent, 27 in rRNA binding, 9 in tRNA binding, 4 in translation elongation factor activity, 3 in proton-transporting ATP synthase activity and rotational mechanism and 3 in aminoacyl-tRNA editing activity (Table 6.3). DAVID also utilises the KEGG pathway database to identify pathways that proteins were involved in. Out

of the 122 genes, a total of 62 genes were recognised to be involved in pathways. Forty of these 62 were related with pathways involved in the ribosome function, 17 in aminoacyl-tRNA biosynthesis and 5 in RNA degradation (Table 6.4).

Further analysis by STRING was performed to establish interactions between proteins (Figure 6.1). The light blue lines (links or edges) between proteins (nodes) represented known interactions from curated databases whilst the pink lines represented known interactions from experimental results and were collectively known as protein associations. A total of 1022 protein associations were identified. The 44 nodes in red represented proteins in the network that were annotated with the search term ‘ribosome’ and most interactions between proteins were between ribosomal components signified by the density of light blue and pink lines between these red nodes (see Figure 6.1).

**Table 6.1**: Gene ontology (GO) term enrichment analysis of 122 *T. denticola* genes revealed the cellular component of 88 genes (shown by accession numbers). Refer to appendices Table 9.1 for protein description.

| **Cellular component** | **Accession numbers** |
|---|---|
| Cytoplasm/cytosol (n=48) | Q73K92, Q73QZ3, Q73NX6, Q73JR4, Q73M76, Q73NV3, Q73P70, Q73MV2, Q73MZ2, Q73M27, Q73P66, P61188, Q73J26, Q73MC2, Q73LG6, Q73R87, Q73RS4, Q73P28, Q73JM9, Q73PD8, Q73NH7, Q73RJ6, Q73NW1, Q73NB9, Q73RR5, P62221, Q73M39, Q73NT9, Q73Q56, Q73MP4, P62421, Q73P31, P62042, Q73JN2, Q73NR2, Q73RN8, Q73MD3, P62646, Q73QJ5, Q73KB2, Q73JB2, Q73KJ8, Q73QJ2, Q73KH5, Q73P19, P61339, P60920, Q73PN3 |
| Ribosome (n=29) | Q73PE7, Q73PK9, Q73KR3, P61070, Q73PM1, Q73PM0, Q73M02, Q73PK7, P62239, Q73P09, Q73PM3, Q73PB4, Q73PL9, Q73NW2, Q73LW1, Q73PL0, Q73PN2, Q73PN1, Q73N16, Q73PN0, P62443, Q73JJ0, Q73M34, Q73PL8, Q73PL7, Q73PL6, Q73JJ6, Q73JL8, Q73JJ5 |
| Small ribosomal unit (n=6) | Q73NV5, Q73NV4, Q73LC2, Q73PM6, Q73K75, Q73PL5 |
| Large ribosomal unit (n=5) | Q73JJ4, Q73PM9, Q73PM7, Q73PL3, Q73PM2 |

**Table 6.2**: A total of 49 genes (shown by accession numbers) were attributed to biological processes after gene ontology (GO) term enrichment analysis of 122 *T. denticola* genes. Refer to appendices Table 9.1 for protein description.

| **Biological process** | **Accession numbers** |
|---|---|
| Protein translation (n=42) | Q73PE7, Q73PK9, Q73NV4, Q73KR3, Q73K75, P61070, Q73PM1, Q73PM0, Q73Q68, Q73M02, Q73PK7, P62239, Q73PM9, Q73LC2, Q73PM7, Q73P09, Q73PM6, Q73PM3, Q73PM2, P61348, Q73PB4, Q73PL9, Q73NW2, Q73LW1, Q73PL0, Q73JJ4, Q73PN2, Q73PN1, Q73N16, Q73PN0, P62443, Q73JJ0, Q73M34, Q73NV5, Q73PL8, Q73PL7, Q73PL6, Q73PL5, Q73PL3, Q73JJ6, Q73JL8, Q73JJ5 |
| Glycolytic process (n=4) | P62421, Q73QV3, Q73P50, Q73NB9 |
| Plasma membrane ATP synthesis coupled transport (n=3) | Q73M29, Q73M28, Q73MX5 |

**Table 6.3**: The molecular function of 85 *T. denticola* genes (shown by accession numbers) were identified after gene ontology (GO) term enrichment analysis of 122 genes. Refer to appendices Table 9.1 for protein description.

| **Molecular function** | **Accession numbers** |
|---|---|
| Structural constituent of ribosome (n=39) | Q73PE7, Q73PK9, Q73NV4, Q73KR3, Q73K75, P61070, Q73PM1, Q73PM0, Q73M02, Q73PK7, P62239, Q73PM9, Q73LC2, Q73PM7, Q73P09, Q73PM6, Q73PM3, Q73PM2, Q73PB4, Q73PL9, Q73NW2, Q73LW1, Q73PL0, Q73JJ4, Q73PN2, Q73PN1, Q73N16, Q73PN0, P62443, Q73JJ0, Q73M34, Q73NV5, Q73PL8, Q73PL7, Q73PL6, Q73PL5, Q73PL3, Q73JJ6, Q73JL8 |
| rRNA binding (n=27) | Q73PK9, Q73NV4, Q73KR3, P61070, Q73PM1, Q73PM0, Q73M02, Q73PM9, Q73LC2, Q73PM7, Q73PM6, Q73PM3, Q73PM2, Q73PL9, Q73NW2, Q73LW1, Q73PL0, Q73JJ4, Q73PN1, Q73PN0, Q73M34, Q73NV5, Q73PL8, Q73PL7, Q73PL6, Q73PL5, Q73PL3 |
| tRNA binding (n=9) | Q73JJ4, Q73PL0, Q73PN2, Q73NT9, Q73PM0, Q73NV5, Q73NV4, Q73JB2, Q73R87 |
| Translation elongation factor activity (n=4) | Q73P31, Q73NV3, P61339, Q73PN3 |
| Proton-transporting ATP synthase activity, rotational mechanism (n=3) | Q73M29, Q73M28, Q73MX5 |
| aminoacyl-tRNA editing activity (n=3) | Q73JB2, Q73KJ8, Q73MZ2 |

**Table 6.4**: A total of 62 genes (shown by accession numbers) were recognised to be involved in molecular pathways out of the 122 *T. denticola* genes after searches in the KEGG pathway database. Refer to appendices Table 9.1 for protein description.

| **KEGG pathways** | **Accession numbers** |
|---|---|
| Ribosomal pathways (n=40) | Q73PE7, Q73PK9, Q73NV4, Q73KR3, Q73K75, P61070, Q73PM1, Q73PM0, Q73M02, Q73PK7, P62239, Q73PM9, Q73LC2, Q73PM7, Q73P09, Q73PM6, Q73PM3, Q73PM2, Q73PB4, Q73PL9, Q73NW2, Q73LW1, Q73PL0, Q73JJ4, Q73PN2, Q73PN1, Q73N16, Q73PN0, P62443, Q73JJ0, Q73M34, Q73NV5, Q73PL8, Q73PL7, Q73PL6, Q73PL5, Q73PL3, Q73JJ6, Q73JL8, Q73JJ5 |
| Aminoacyl-tRNA biosynthesis (n=17) | Q73PD8, Q73M65, Q73RJ6, Q73MZ2, Q73RR5, Q73NT9, Q73Q68, Q73NR2, Q73MC2, Q73KB2, Q73JB2, Q73KJ8, Q73P19, Q73R87, P60920, Q73P28 and P61348 |
| RNA degradation (n=5) | Q73NH7, Q73P50, Q73R54, Q73NW1, Q73Q16 |

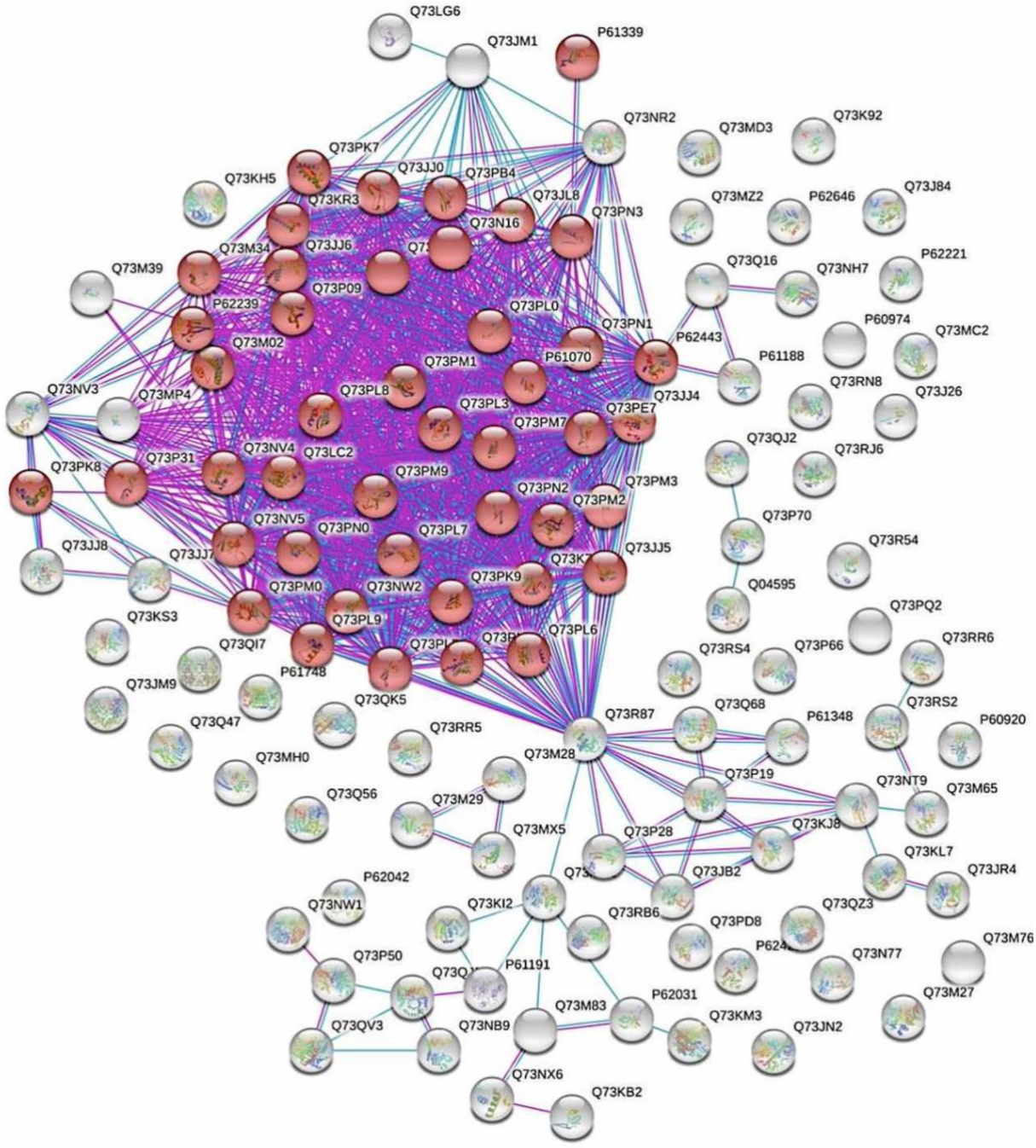



**Figure 6.1**: STRING visualization of 122 *T. denticola* proteins (shown by accession number) to establish interactions between proteins. The light blue lines between proteins (shown as nodes) represented known interactions from curated databases whilst the pink lines represented known interactions from experimental results and were collectively known as protein associations. A total of 1022 protein associations were identified and the 44 nodes in red represented proteins in the network that were annotated with the search term 'ribosome'. Most interactions occurred between ribosomal proteins as indicated by the density of light blue and pink, highlighting the complexity of interactions between these red nodes.

### 6.3 Analysis of *T. denticola* proteins

The abundance of *T. denticola* proteins after heat or oxygen killing was then compared with live *T. denticola* and presented using volcano plots. Proteins which were altered by a fold change of 2 or more (log2 = |1|) and above $p<0.05$ (-log10 p value = 1.3) were considered to be significantly altered and significance was tested using a paired t-test. These significantly altered proteins were outlined as red data points in the volcano plots with accession numbers present (see Figures 6.2 and 6.5).

#### 6.3.1 Live vs heat-killed *T. denticola* protein analysis

After plotting log2 fold change against -log10 p values, it was observed that the abundances of 26 proteins were significantly altered after heat-killing when compared with live *T. denticola* (Figure 6.2). From these 26, the abundance of 15 proteins were significantly decreased (Table 6.5) whilst 11 were significantly increased (Table 6.6). Out of these 15 significantly lower abundance proteins, 13 were located in the cytoplasm whilst 2 were transmembrane proteins as marked by † in Table 6.5. From these 13 cytoplasmic proteins, 8 were ribosomal proteins ‡ and 2 were nucleoid components ¥ and 3 in the cytosol §. The abundance of membrane protein insertase YidC (Q73JM1) (-2.079 - fold) was decreased the greatest after heat-killing *T. denticola*, whilst DNA-directed RNA polymerase subunit beta' (Q73JJ8) (-1.005 - fold) was decreased the least.

The 11 significantly higher abundance proteins consisted of 3 ribosomal proteins ‡ and 8 cytosolic proteins § and no proteins associated with the membrane were significantly increased after heat-killing. The protein abundance of 50S ribosomal protein L21 (Q73LW1)

(2.990 - fold) was increased the greatest after heat-killing, whilst elongation factor G 2 (Q73NV3) (1.170 - fold) was increased the least (Table 6.6).

STRING analysis of significantly lower abundance *T. denticola* proteins after heat-killing revealed that the membrane protein insertase YidC (Q73JM1) interacted with 50S ribosomal protein L3 (Q73PN1) and 50S ribosomal protein L2 (Q73PM9). Both these ribosomal proteins interact with each other and the other 6 ribosomal proteins. In addition, DNA-directed RNA polymerase subunit beta' (Q73JJ8) interacts with DNA-directed RNA polymerase subunit alpha (Q73PK8) and the alpha subunit also interacts with 50S ribosomal protein L2 (Q73PM9). The proteins glycerol-3-phosphate dehydrogenase [NAD(P)+] (P61748), ribonuclease Y (Q73R54), ornithine carbamoyltransferase, catabolic (Q73P70) and valine--tRNA ligase (Q73MZ2) were not recognised to have any known interactions with each other or the other lower abundance proteins (Figure 6.3).

STRING analysis for significantly higher abundance *T. denticola* proteins after heat-killing showed that the 50S ribosomal protein L21 (Q73LW1) interacts with elongation factor G 2 (Q73NV3). In addition, deoxyribose-phosphate aldolase (Q73QJ5) has been shown to interact with fructose-bisphosphate aldolase class 1 (Q73QV3). However, 7 proteins (accession numbers: P62421, Q73K92, Q73QI7, Q73RR5, Q73RS2, Q73M39 and Q73M83) did not have any known interactions with each other or the other higher abundance proteins (Figure 6.4).

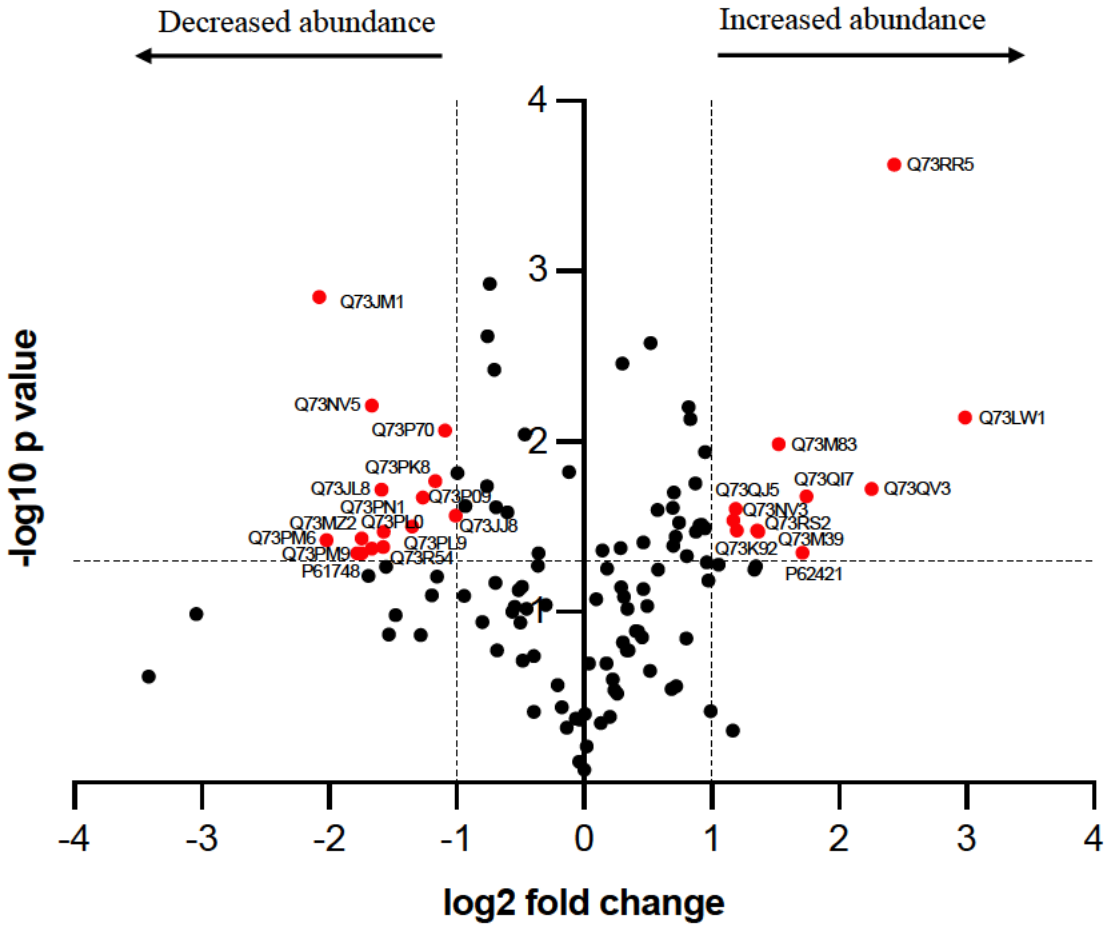



**Figure 6.2**: Liquid chromatography tandem mass spec (LC-MS/MS) analysis of tandem mass tags™ (TMT™) labelled live vs heat-killed *T. denticola* outer membrane proteins (shown by accession number) using Thermo orbitrap eclipse mass spectrometer and results were searched against the reviewed UniProt knowledgebase (UniProtKb) protein database. The horizontal dashed black line shows where $p = 0.05$ with points above the line having $p < 0.05$ (-log10 p value = 1.3) and points below the line having $p > 0.05$. Vertical dashed black lines represented a fold change of 2 (log2 = 1/-1). Proteins lying outside of these cut-off regions were considered significant and were outlined as red data points with accession numbers present. n=2. Abundances of 26 outer membrane proteins were significantly altered after heat-killing.

**Table 6.5**: The abundances of 15 proteins were significantly decreased ($p<0.05$) after heat-killing of *T. denticola* when compared with live *T. denticola*. From these proteins, 8 were ribosomal proteins ‡, 3 were cytosolic §, 2 were nucleoid components ¥ and 2 were transmembrane proteins †.

| Accession number | Protein description | Fold change |
|---|---|---|
| Q73JM1† | Membrane protein insertase YidC | -2.079 |
| Q73PM6 ‡ | 30S ribosomal protein S3 | -2.020 |
| Q73PM9 ‡ | 50S ribosomal protein L2 | -1.778 |
| Q73MZ2 § | Valine--tRNA ligase | -1.746 |
| P61748 § | Glycerol-3-phosphate dehydrogenase [NAD(P)+] | -1.743 |
| Q73PL0 ‡ | 30S ribosomal protein S13 | -1.664 |
| Q73NV5 ‡ | 30S ribosomal protein S12 | -1.664 |
| Q73JL8 ‡ | 50S ribosomal protein L34 | -1.588 |
| Q73R54† | Ribonuclease Y | -1.577 |
| Q73PN1 ‡ | 50S ribosomal protein L3 | -1.572 |
| Q73PL9 ‡ | 30S ribosomal protein S14 type Z | -1.349 |
| Q73P09 ‡ | 50S ribosomal protein L28 | -1.263 |
| Q73PK8 ¥ | DNA-directed RNA polymerase subunit alpha | -1.165 |
| Q73P70 § | Ornithine carbamoyltransferase, catabolic | -1.092 |
| Q73JJ8 ¥ | DNA-directed RNA polymerase subunit beta’ | -1.005 |

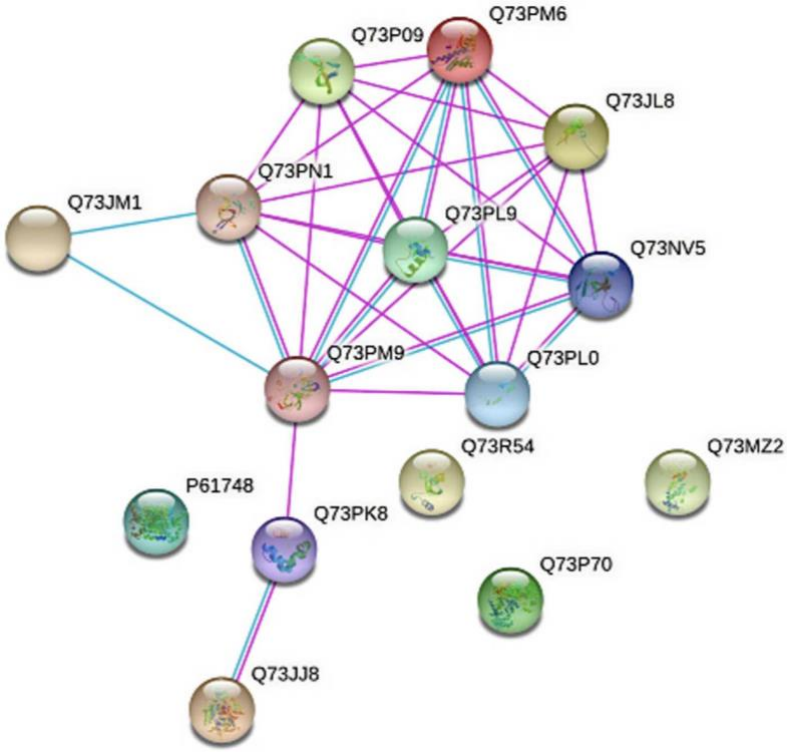



**Figure 6.3**: STRING visualization for protein interactions for the 15 significantly lower abundance *T. denticola* proteins (shown by accession number) affected by heat-killing. Light blue lines between proteins (shown as nodes) represented known interactions from curated databases whilst pink lines represented known interactions from experimental results. Membrane protein insertase YidC (Q73JM1) interacts with 50S ribosomal protein L3 (Q73PN1) and 50S ribosomal protein L2 (Q73PM9). All 8 ribosomal proteins (accession numbers: Q73PL0, Q73PN1, Q73NV5, Q73PL9, Q73PM9, Q73PM6, Q73P09, Q73JL8) interact with each other. Also, DNA-directed RNA polymerase subunit beta' (Q73JJ8) interacts with DNA-directed RNA polymerase subunit alpha (Q73PK8). This alpha subunit also interacts with 50S ribosomal protein L2 (Q73PM9).

**Table 6.6**: A total of 11 proteins abundance were significantly increased ($p<0.05$) after heat-killing of *T. denticola* when compared with live *T. denticola*. Out of these, 8 were cytosolic proteins § and 3 were ribosomal proteins ‡.

| **Accession number/*gene*** | **Protein description** | **Fold change** |
|---|---|---|
| Q73NV3 ‡ | Elongation factor G 2 | 1.170 |
| Q73QJ5 § | Deoxyribose-phosphate aldolase | 1.191 |
| Q73K92 § | Chaperone protein ClpB | 1.197 |
| Q73M39 ‡ | Trigger factor | 1.360 |
| Q73RS2 § | Bifunctional protein FolD | 1.368 |
| Q73M83 § | Glycine cleavage system H protein | 1.525 |
| P62421 § | Phosphoglycerate kinase | 1.714 |
| Q73QI7 § | Pyridoxal 5'-phosphate synthase subunit PdxS | 1.745 |
| Q73QV3 § | Fructose-bisphosphate aldolase class 1 | 2.256 |
| Q73RR5 § | Glycine-tRNA ligase | 2.432 |
| Q73LW1 ‡ | 50S ribosomal protein L21 | 2.990 |

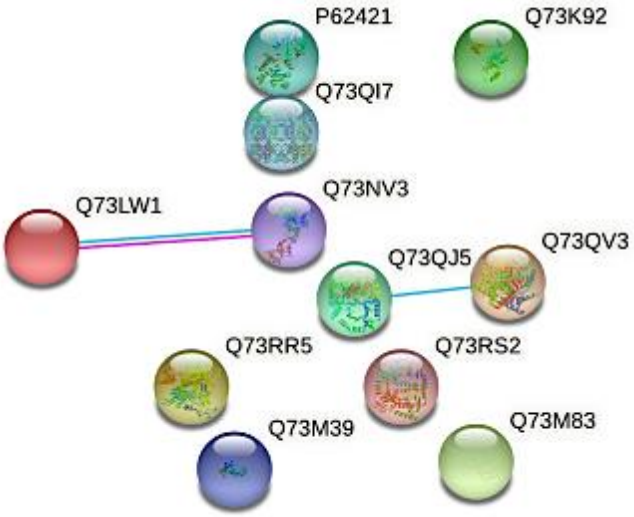



**Figure 6.4**: Eleven significantly higher abundance *T. denticola* proteins affected by heat-killing visualised by STRING analysis to identify protein-protein interactions. The 50S ribosomal protein L21 (Q73LW1) interacts with elongation factor G 2 (Q73NV3), whilst deoxyribose-phosphate aldolase (Q73QJ5) has shown to interact with fructose-bisphosphate aldolase class 1 (Q73QV3). Seven proteins (accession numbers: P62421, Q73K92, Q73QI7, Q73RR5, Q73RS2, Q73M39 and Q73M83) did not have any known interactions with each other or the other up-regulated proteins.

### 6.3.2 Live vs oxygen-killed *T. denticola* protein analysis

The abundances of 12 *T. denticola* proteins were significantly altered after oxygen-killing when compared with live *T. denticola* (Figure 6.5). Out of these 12, the membrane protein insertase YidC (Q73JM1) was the only significantly decreased protein. Whilst 11 proteins were significantly increased after oxygen-killing (Table 6.7). From these 11 increased proteins, 7 were cytosolic proteins [§] and 4 were ribosomal proteins [‡]. The highest increased *T. denticola* protein after oxygen-killing was DNA ligase (Q73MH0) (1.645 – fold), whilst D-alanine-D-alanine ligase (Q73JN2) (1.101 – fold) was increased the least (Table 6.7).

As only 1 protein, membrane protein insertase YidC (Q73JM1), was significantly decreased in *T. denticola* after oxygen-killing (-1.11 - fold), it was not possible to perform string analysis for this. However, STRING analysis for the significantly higher abundance proteins revealed that the 50S ribosomal protein L11 (P62443), 50S ribosomal protein L25 (Q73N16) and 50S ribosomal protein L5 (Q73PM0) all interact with each other. In addition, serine-tRNA ligase (Q73KB2) and acyl carrier protein (Q73NX6) have known interactions. However, it was evident that 6 proteins (accession numbers: Q73NT9, Q73NV3, Q73PD8, Q73MH0, Q73RR5 and Q73JN2) did not have any known interactions with each other or the other higher abundance proteins (Figure 6.6).

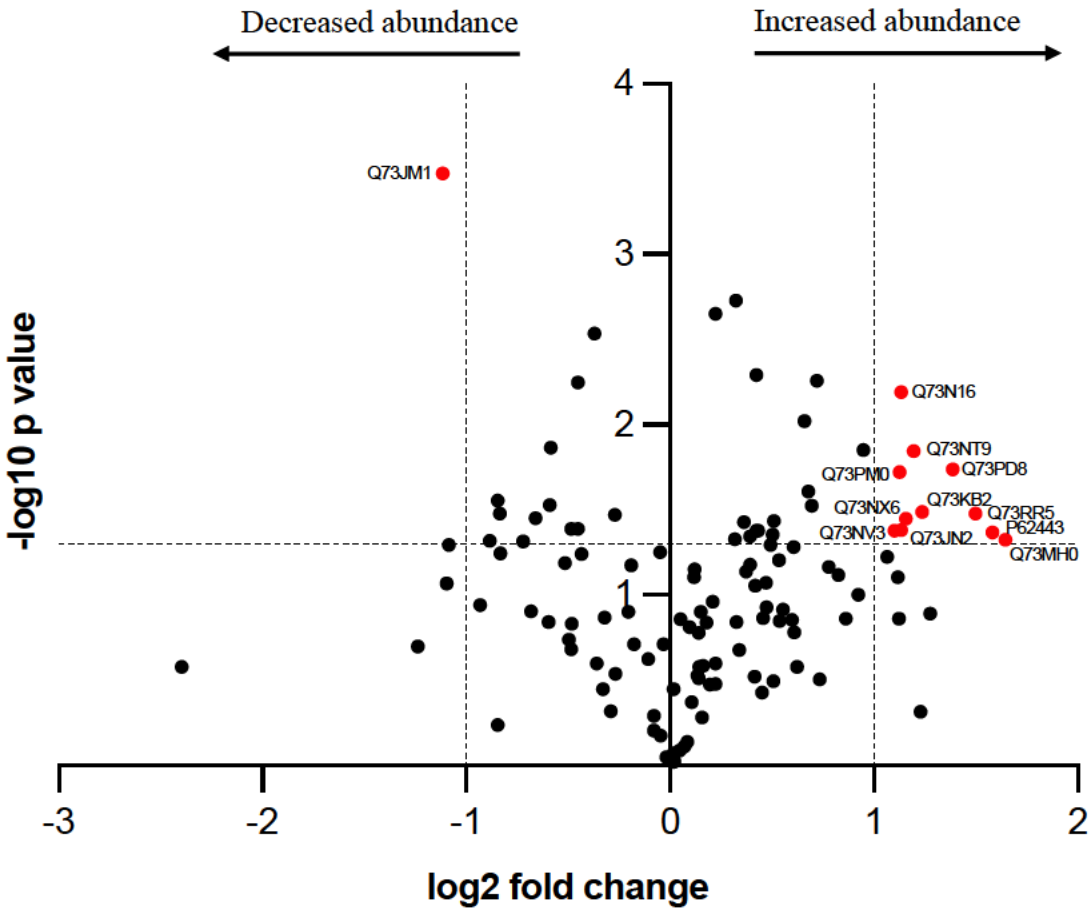



**Figure 6.5**: Liquid chromatography tandem mass spec (LC-MS/MS) analysis of TMT™ labelled live vs oxygen-killed *T. denticola* outer membrane proteins using Thermo orbitrap eclipse mass spectrometer and results were searched against the reviewed UniProt knowledgebase (UniProtKb) protein database. The horizontal dashed black line shows where p = 0.05 with points above the line having $p < 0.05$ (-log10 p value = 1.3) and points below the line having $p > 0.05$. Vertical dashed black lines represented a fold change of 2 (log2 = 1/-1. Proteins lying outside of these cut-off regions were considered significant and were outlined as red data points with accession numbers present. Abundances of 12 outer membrane proteins were significantly altered after oxygen-killing. n=2.

**Table 6.7**: The abundance of eleven proteins were significantly increased ($p<0.05$) after oxygen-killing *T. denticola* in comparison with live *T. denticola*. From these, 7 were cytosolic proteins § and 4 were ribosomal proteins ‡.

| Accession number | Protein description | Fold change |
|---|---|---|
| Q73JN2 § | D-alanine-D-alanine ligase | 1.101 |
| Q73PM0 ‡ | 50S ribosomal protein L5 | 1.126 |
| Q73N16 ‡ | 50S ribosomal protein L25 | 1.135 |
| Q73NV3 ‡ | Elongation factor G 2 | 1.136 |
| Q73NX6 § | Acyl carrier protein | 1.156 |
| Q73NT9 § | Methionine-tRNA ligase | 1.196 |
| Q73KB2 § | Serine-tRNA ligase | 1.238 |
| Q73PD8 § | Tyrosine-tRNA ligase | 1.386 |
| Q73RR5 § | Glycine-tRNA ligase | 1.498 |
| P62443 ‡ | 50S ribosomal protein L11 | 1.583 |
| Q73MH0 § | DNA ligase | 1.645 |

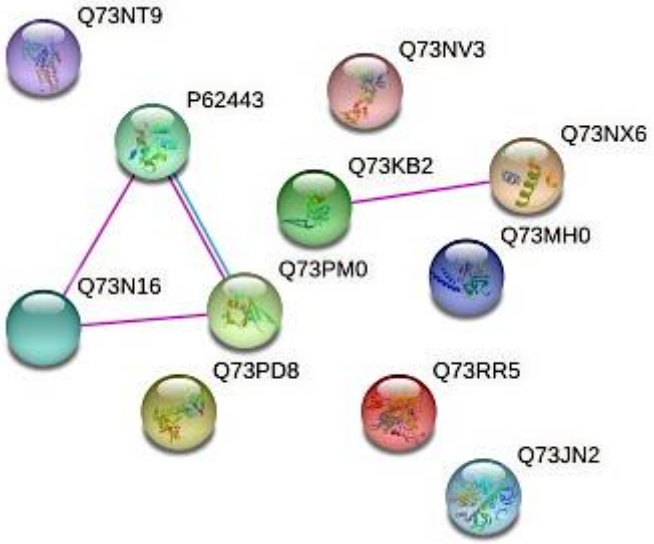



**Figure 6.6**: STRING was utilised to identify and visualise protein-protein interactions between the 11 significantly higher abundance proteins after oxygen-killing *T. denticola*. The 50S ribosomal protein L11 (P62443), 50S ribosomal protein L25 (Q73N16) and 50S ribosomal protein L5 (Q73PM0) all interact with each other. Also, serine-tRNA ligase (Q73KB2) and acyl carrier protein (Q73NX6) have known interactions. However, 6 proteins (accession numbers: Q73NT9, Q73NV3, Q73PD8, Q73MH0, Q73RR5 and Q73JN2) did not have any known interactions with each other or the other higher abundance proteins.

## 6.4 Discussion

The STRING analysis of identified and quantified proteins (Figure 6.1) revealed that most interactions occurred between the 44 ribosomal protein (red nodes) that were detected. It was interesting to see a number of ribosomal associated proteins even though only the membrane of *T. denticola* was isolated. The STRING analysis also revealed that the membrane protein YidC (Q73JM1) had interactions with many of these ribosomal proteins. It has been previously reported that YidC is able to interact with translating ribosomes forming a complex that enables protein insertion into the membrane (Kedrov et al., 2013; Wickles et al., 2014). Previous findings have also revealed that YidC binding to the ribosome is distributed over the large and small ribosomal subunits (Welte et al., 2012) and the C terminus of YidC is required for binding (Kohler et al., 2009). Therefore, presence of ribosomal proteins even after isolating the membrane maybe due to the C terminus of YidC which can bind to ribosomal components.

Data indicated that heat-killing of *T. denticola* resulted in significant changes in the abundance of 26 proteins, whereas oxygen-killing only significantly altered the abundance of 12 proteins, potentially revealing the damaging effects of heat-killing on *T. denticola* proteins. In addition, it also suggested that oxygen-killing was not as damaging to *T. denticola* proteins and preserved *T. denticola* components more than heat-killing. Heat-killing of *T. denticola* also resulted in decreased abundance of 15 proteins compared with only 1 after oxygen-killing. Previous findings have reported that high temperatures can result in protein denaturation in bacteria (Allwood and Russell, 1970; Harries and Russell, 1967) and this is due to breaking of hydrogen bonds (Cooper, 2005) which are key for protein folding and structure (Sheu et al., 2003). Therefore, decreased abundance of more proteins after heat-

killing is due to protein denaturation and findings also suggest that heat-killing was denaturing more proteins than oxygen-killing. Two of these proteins were membrane proteins whilst the rest were found in the cytoplasm which implied that heat-killing was damaging both surface and inner protein components of *T. denticola*. Eight of these lower abundance proteins after heat-killing consisted of ribosomal proteins. The ribosome is responsible for translating genetic information encoded in messenger RNAs (mRNA) into proteins (Korostelev, 2011). Therefore, this suggested that heat-killing was detrimental to *T. denticola* mRNA translational machinery possibly resulting in lack of protein synthesis essential for normal function and survival.

However, both heat and oxygen-killing resulted in the increased abundance of 11 cytoplasmic proteins each. Out of these, only 2 proteins (elongation factor G2 and glycine-tRNA ligase) were increased by both heat and oxygen-killing whilst the other 9 were different to each other, suggesting that the type of killing influenced the increased abundance of different *T. denticola* proteins.

### 6.4.1 Proteins involved in *T. denticola* structure

The inner membrane protein insertase YidC is a member of the evolutionary conserved YidC/Oxa1/Alb3 protein family (Saller et al., 2012) and its structure consists of five core transmembrane helices (Kumazaki et al., 2014). YidC plays key and versatile roles in the insertion of proteins into the inner membrane (Dalbey et al., 2014; Serek et al., 2004), folding of proteins (Nagamori, Smirnova and Kaback, 2004) and assembly of membrane protein complexes (van der Laan et al., 2003). The abundance of this essential structural membrane component was significantly decreased after both heat and oxygen-killing. However, heat-

killing (-2.079 – fold) resulted in greater decreases of YidC abundance in comparison with oxygen-killing (-1.11 - fold), suggesting that heat-killing was more damaging to YidC and therefore the structural integrity of *T. denticola*. The loss of *T. denticolas'* helical structure observed in SEM image analysis after heat-killing *T. denticola* (see section 3.6.1) may have been due to the denaturing of membrane structural components such as YidC. However, oxygen-killing maintained *T. denticolas'* helical structure (see section 3.6.1), suggesting the decrease in abundance of YidC after oxygen-killing was not sufficient to cause structural changes.

Another protein that was significantly decreased after heat-killing was Ribonuclease Y (RNase Y). RNase Y is a transmembrane protein bound to the inner membrane of *T. denticola* (Hamouche et al., 2020) and plays important roles in degradation of mRNA to regulate the amount of protein produced from each mRNA and to recycle ribonucleotides for use in new RNA molecules (Laalami, Zig and Putzer, 2013). This is an essential requirement for adapting to a rapidly changing environment where quick production of proteins is vital for survival (Hui, Foley and Belasco, 2014). Although RNase Y is not intrinsically linked with *T. denticola* structure, it may potentially be linked with other constituents of the membrane which maintain structure. Therefore, the loss of *T. denticolas'* helical shaped structure after heat-killing may be associated with the thermal denaturation of RNase Y.

### 6.4.2 Proteins involved in heat shock response

The accumulation of aggregated proteins brought about by heat stress can negatively affect cell machinery ultimately leading to cell death (Basta et al., 2020). In the present study, the abundance of chaperone protein ClpB (Q73K92) was significantly increased after heat-killing

of *T. denticola* in comparison with live *T. denticola*. ClpB is a highly conserved protein in bacteria that has been shown to provide protection against various forms of stress, in particular against heat shock (Alam et al., 2021). Findings in the present study agree with a previous study, where levels of *clpB* gene expression were increased at elevated temperatures in the *Campylobacter species, C. coli* and *C. lari* (Riedel et al., 2020). *ClpB* can facilitate the disaggregation of heat-stress damaged proteins to an aggregated state via its disaggregase activity (Lee et al., 2003). Studies investigating the activity of *ClpB* revealed that deletion of the *clpB* gene in *Francisella tularensis* resulted in lower bacterial survival rates at increased temperatures (Alam et al., 2018; Meibom et al., 2008). In addition, a *clpB* mutant of the pathogen *Pseudomonas putida* was unable to disaggregate aggregated proteins and was vital for cell survival after heat-stress (Ito et al., 2014). Therefore, this suggested that *T. denticola* responds to heat-stress by up-regulating *ClpB* production which plays a crucial role in disaggregating aggregated proteins and is essential in *T. denticolas'* survival.

The glycine cleavage system H protein (Q73M83) was significantly increased after heat-killing of *T. denticola* in comparison with live *T. denticola*. This protein is part of the glycine cleavage system which catalyses the synthesis of glycine in anaerobic bacteria (Kikuchi et al., 2008). The production of glycine is increased after heat-stress as it is needed for the synthesis of proteins responsible for the disaggregation of damaged proteins after heat-shock (Lüders, Fallet and Franco-Lara, 2009). One of these proteins may include glycine betaine which has previously been shown to protect against thermodenaturation in *E. coli* cells (Caldas et al., 1999). Therefore, significant increase of glycine system H protein after heat-killing of *T. denticola* may play a role in protecting *T. denticola* from heat stress.

### 6.4.3 Proteins potentially involved in oxidative stress response

D-alanine-D-alanine ligase is one of the key enzymes involved in the biosynthesis of peptidoglycan, catalysing the condensation of two D-Ala molecules using ATP (Kitamura et al., 2009). Peptidoglycans in *T. denticola* are responsible for cell architecture and for maintaining its coil configuration (Izard et al., 2008). It is known that exposure of bacterial cells to reactive oxygen species (ROS) can damage cellular components including membrane lipids and proteins. In addition, the peptidoglycan containing bacterial envelope is particularly prone to oxidative damage because of the outer membranes' high permeability to hydrophilic low-molecular-weight oxidants (Ezraty et al., 2017). D-alanine-D-alanine ligase was significantly increased after oxygen-killing of *T. denticola*, suggesting increased production of peptidoglycan to help repair damage imposed by oxygen exposure. Findings here may bring to light a potential oxidative stress response within *T. denticola* previously not reported.

### 6.4.4 Proteins potentially involved in EMT responses

RNase Y has been reported to play a key role in the activation of virulence genes in *Staphylococcus aureus* (Marincola et al., 2012). In addition, RNase Y has shown to affect the production of virulence factors in *S. aureus* through expression of the *agr* gene (global virulence regulator) or independently (Nagata, Kaito and Sekimizu, 2008). Furthermore, deletion of the RNase Y gene encoded by CfVA in *Streptococcus pyogenes* resulted in down-regulation of virulence genes and that RNase Y was necessary for the pathogenesis of *S. pyogenes* (Kang, Caparon and Cho, 2010). RNase Y may also be responsible for expression of virulence genes in *T. denticola* such as dentilisin. Dentilisin can stimulate EMT-associated changes by down-regulating expression of tight junction proteins such as ZO-1 (Chi, Qi and Kuramitsu, 2003) and up-regulating the expression of proteolytic enzymes such as MMP-2

(Ganther et al., 2021). The abundance of RNase Y was significantly decreased after heat-killing *T. denticola,* therefore possibly down-regulating virulence factors such as dentilisin and leading to the reduced EMT responses seen with HK *T. denticola* exposure in comparison with OK *T. denticola*.

D-alanine-D-alanine ligase has shown to activate NF-kB through the pathogen recognition receptor (PRR), Nod1 (Brandt et al., 2005). NF-kB activation has been shown to increase gene expression of EMT transcription factors such as snail-2 (Wang et al., 2013) and can induce the release of EMT-inducing pro-inflammatory cytokines IL-8 (Su et al., 2015b) and IL-1β (Milward et al., 2007; Lee et al., 2014). In addition, it has been shown that expression of the proteolytic enzyme MMP-9 can be promoted by IL-1β through NF-kB activation in epithelial cells (Tseng et al., 2013). Therefore, significant increases in D-alanine-D-alanine ligase after oxygen-killing of *T. denticola* may activate NF-kB. This may result in the production of EMT-inducing factors such as snail-2, IL-8 and IL-1β and may provide an explanation for the greater EMT responses observed after OK *T. denticola* exposure in comparison with HK *T. denticola*.

Ultimately, oxygen-killing preserved *T. denticola* proteins more so than heat-killing and the greater EMT responses observed in oral keratinocytes after OK *T. denticola* exposure in comparison with HK *T. denticola* may be associated with its structural integrity and the maintenance of EMT-inducing membrane proteins such as RNase Y and D-alanine-D-alanine ligase.

# 7. Conclusions and future work

## 7.1 Main conclusions

A key finding from the present study revealed that heat-killing was responsible for loss of *T. denticolas'* typical helical shaped structure, whilst oxygen-killing maintained *T. denticola* morphology following SEM analysis. Also, heat-killing resulted in increased bacterial debris (all pathogens) which would suggest loss of bacterial components due to thermal denaturation (Chapter 3). This is the first study to report the effects of heat and oxygen-killing on *P. gingivalis, F. nucleatum* and *T. denticola* structural morphology. Further elucidation of the effects of heat and oxygen-killing on *T. denticola* by quantitative mass spectrometry-based proteomics, revealed heat-killing resulted in significant alterations to 26 proteins whereas oxygen-killing had a less severe effect with 12 proteins altered. Novel data presented here also revealed a structural membrane protein, insertase YidC, to be less abundant after heat-killing than after oxygen-killing (Chapter 6). It was concluded that insertase YidC may play an integral part in maintaining the helical structure of *T. denticola*. Whilst previous authors have utilised proteomics on live *T. denticola* outer membrane proteins (Veith et al., 2019), the present study is the first to use and describe the effects of heat and oxygen-killing on the outer membrane proteins. Findings here now provide evidence for the potential benefits of using oxygen-killing to inactivate anaerobic pathogens rather than heat-killing for use in cell culture models of periodontitis that would better simulate the *in vivo* situation.

Preliminary investigations revealed novel evidence that both HK and OK *T. denticola* were able to significantly increase H400 cell number after 8-days exposure. Another key finding was that both HK and OK pathogens stimulated pro-inflammatory cytokine release (IL-1β, IL-8 and TGF-β1). Consequently, expression of EMT-related transcription factors (snail-1, snail-2 and twist-1) was increased in all stimulated cultures leading to down-regulated

expression of epithelial cell-cell adhesion and cytoskeletal markers (E-cadherin, desmoplakin-1 and cytokeratin 5). Molecular changes were confirmed with functional changes in the epithelial barrier, where electrical resistance (TEER data) in all stimulated epithelial monolayers was also decreased (Chapter 4). Novel data here provides evidence that OK *P. gingivalis*, OK *F. nucleatum* and both HK and OK *T. denticola* can induce relatively early EMT-associated changes and can compromise epithelial barrier integrity. This may translate clinically to the possible initiation and propagation of periodontitis by this mechanism.

Furthermore, data here showed that HK and OK periodontal pathogens can increase expression of mesenchymal-associated cell-surface (N-cadherin), cytoskeletal (vimentin) and ECM (MMP-9) components that can promote a migratory phenotype. Increased expression of mesenchymal markers may have been initiated by increased presence of pro-inflammatory cytokines which can activate EMT transcription factors that ultimately target these mesenchymal markers. Notably, EMT-associated molecular changes were affirmed by increased cell migration in all stimulated cultures (Chapter 4), providing evidence that periodontal pathogens may initiate EMT leading to epithelium breakdown, therefore possibly promoting the progression of periodontitis.

Initial studies showed that the naturally occurring EMT-inhibitor curcumin could suppress OK *T. denticola* induced cell growth after 8-days treatment. The present study is the first to demonstrate inhibition of OK *T. denticola* induced oral keratinocyte growth. Furthermore, findings here revealed that curcumin was able to inhibit OK pathogen induced down-regulation of epithelial markers (E-cadherin, desmoplakin-1 and cytokeratin 5) and inhibit up-regulated expression of mesenchymal markers (N-cadherin, vimentin and MMP-9). Curcumin

also inhibited expression of pro-inflammatory cytokines resulting in down-regulated snail-1 expression, therefore leading to attenuated EMT. Notably, curcumin inhibited OK *P. gingivalis* and *T. denticola* induced oral keratinocyte migration possibly through inhibition of vimentin and N-cadherin expression (Chapter 5). For the first time, it has now been shown that curcumin has the potential to inhibit OK periodontal pathogen induced EMT through associated changes to EMT-related markers in oral keratinocytes. Curcumin could theoretically be utilised as a therapeutic for the management of periodontitis by inhibiting EMT and maintaining the epithelial barrier, therefore preventing bacterial invasion into the underlying connective tissue and downstream inflammation of the periodontal tissues.

OK *T. denticola* generally stimulated greater EMT-related responses in oral keratinocytes in comparison with HK *T. denticola* (Chapter 4). Quantitative mass spectrometry-based proteomics on isolated *T. denticola* outer membrane proteins revealed two proteins, RNase Y (decreased abundance in HK *T. denticola*) and D-alanine-D-alanine ligase (increased abundance in OK *T. denticola*) to be implicated in promoting EMT (Chapter 6). Novel data here suggested that greater EMT responses observed in oral keratinocytes after OK *T. denticola* exposure in comparison with HK *T. denticola* may have been associated with membrane proteins such as RNase Y and D-alanine-D-alanine ligase. Findings here also provide evidence for the use of oxygen-killed anaerobic pathogens as opposed to heat-killed to better mimic the *in vivo* situation for EMT induction.

## 7.2 Limitations and future work

This thesis provides novel data on EMT induction by key periodontal pathogens in oral keratinocytes and the potential of curcumin to inhibit EMT. These findings provide a basis for future research however there are several limitations which are discussed below.

- One of the main limitations was the exposure of oral keratinocytes to only single pathogens to assess EMT. The subgingival biofilm consists of a multitude of pathogens which interact with each other and the epithelium, leading to an array of host cell responses. Therefore, exposing oral keratinocytes to a combination of periodontal pathogens or indeed multi-species biofilms would provide more relevant EMT responses. However, this would still be limited and further improvements to replicate physiology could be obtained by use of subgingival biofilms directly obtained from patients with periodontitis.

- In addition, the model developed here used killed pathogens to induce EMT. Although effects of heat killing on pathogens was mitigated by using oxygen-killing, interactions between epithelial cells and OK pathogens would not truly replicate physiology, as it is known that the subgingival biofilm consists of a combination of live and dead bacteria (Loesche et al., 1985). Therefore, future work could investigate the use of both live and killed periodontal pathogens to induce EMT to provide a more realistic model. As long-term exposure to live pathogens may result in cell culture infection and oxygen-killing can still alter proteins in pathogens, alternative methods to kill pathogens may provide better models and should be explored.

- The model developed here utilised an immortal cancer cell line and their continued culture can result in genotypic and phenotypic alterations (Burdall et al., 2003). Use of primary cells at an early stage of passage would likely provide a more realistic culture model. Furthermore, the cell culture model used here was based on an oral keratinocyte monolayer and was 2D in structure, therefore any EMT-related cell responses were restricted to bi-directional movements and this is not representative of the *in vivo* tissue architecture. The periodontium is a complex 3D structure which has many cellular layers and components, therefore models replicating this structure would provide a more clinically relevant situation. 3D organotypic cell culture models have been widely used (Hayden and Harbell, 2020) and may be utilised in future work to replicate the periodontium and periodontitis and to study more relevant EMT responses.

- This thesis describes EMT using published and accepted markers, *i.e.*, E-cadherin, N-cadherin, vimentin and snail-1. Although the genes analysed were integral to EMT induction, many other genes such as ZO-1, β-catenin, fibronectin and α-SMA are linked with EMT associated changes and future work could study these. This work could also shed light on mechanisms and pathways through which periodontal pathogens induce EMT. The ability of cells to gain invasive properties is a feature of EMT and can be measured by a transwell invasion assay (Justus et al., 2014). As the scope of investigations here did not cover oral keratinocyte tissue invasivity after periodontal pathogen exposure, further experiments could be performed to determine if oral keratinocytes acquire this property.

- Another limitation of this study was that multiple testing correction was not considered when performing multiple comparisons statistical analysis and correction may have affected the statistical significance reported for a number of comparisons. One of the simplest and most widely used multiple testing correction methods is the Bonferroni adjustment (Noble, 2009) which may have been used in the study here to further confirm significant results.

- Although curcumin was able to decrease some of the EMT responses brought about by OK periodontal pathogen exposure, further studies are needed to determine its ability to inhibit EMT-related protein expression and pro-inflammatory cytokine release. The use of curcumin therapeutically may provide challenges due to its strong colouration, solubility issues and low bioavailability (Lee et al., 2013). Other naturally occurring EMT inhibitors such as resveratrol (Zhang et al., 2015a; Choi et al., 2016; Dermani et al., 2016 and Xu et al., 2017a) and ergone (Hong et al., 2017) may provide better therapeutic solutions, depending on their efficacy in inhibiting periodontal pathogen induced EMT.

### 7.3 Concluding remarks

In conclusion, this thesis provides evidence for the benefits of using oxygen-killing to inactivate anaerobic pathogens rather than heat-killing for use in bacterial – cell stimulation models. It also provides evidence that periodontal pathogens can induce EMT in oral keratinocytes, through associated molecular and functional changes and lead to compromised epithelial barrier integrity. The naturally occurring EMT inhibitor curcumin can inhibit periodontal pathogen induced EMT-associated changes and maintenance of the epithelial

barrier. These findings offer the potential for further investigation of possible therapeutic use of EMT inhibitors in the management of periodontitis.

# 8. References

Aas, J. A., Paster, B. J., Stokes, L. N., Olsen, I. and Dewhirst, F. E., 2005. Defining the Normal Bacterial Flora of the Oral Cavity. *Journal of Clinical Microbiology*, 43(11), 5721-5732.

Abdulkareem, A. A., Shelton, R. M., Landini, G., Cooper, P. R. and Milward, M. R., 2017. Periodontal pathogens promote epithelial-mesenchymal transition in oral squamous carcinoma cells in vitro. *Cell Adhesion & Migration*, 12(2), 1-11.

Abdulkareem, A. A., Shelton, R. M., Landini, G., Cooper, P. R. and Milward, M. R., 2018. Potential role of periodontal pathogens in compromising epithelial barrier function by inducing epithelial-mesenchymal transition. *Journal of Periodontal Research*, 53(4), 65-574.

Abiko, Y., Nagano, K., Yoshida, Y. and Yoshimura, F., 2014. Major membrane protein TDE2508 regulates adhesive potency in *Treponema denticola*. *PLoS ONE*, 9(2), e89051.

Aggarwal, B. B., Deb, L. and Prasad, S., 2014. Curcumin differs from tetrahydrocurcumin for molecular targets, signaling pathways and cellular responses. Molecules, 20(1), 185-205.

Aggarwal, B. B., Gupta, S. C. and Sung, B., 2013. Curcumin: an orally bioavailable blocker of TNF and other pro-inflammatory biomarkers. *British Journal of Pharmacology*, 169(8), 1672-1692.

Ahmed, S., Goh, W. I. and Bu, W., 2010. I-BAR domains, IRSp53 and filopodium formation. *Seminars in Cell & Developmental Biology*, 21(4), 350-356.

Aiello, N. M., Maddipati, R., Norgard, R. J., Balli, D., Li, J., Yuan, S., Yamazoe, T., Black, T., Sahmoud, A., Furth, E. E., Bar-Sagi, D. and Stanger, B. Z., 2018. EMT subtype influences epithelial plasticity and mode of cell migration. *Developmental Cell*, 45(6), 681-695.

Akkawi, M., Lafi, S. A., Abu Remeleh, Q. A., Qutob, M. and Lutgen, P. 2019. Curcumin, a natural isolate from Curcuma longa (turmeric) with high β-hematin inhibitory potential. *Pharmacy & Pharmacology International Journal*, 7(1), 22-26.

Alam, A., Bröms, J. E., Kumar, R. and Sjöstedt, A., 2021. The Role of ClpB in Bacterial Stress Responses and Virulence. *Frontiers in Molecular Biosciences*, 8(1), 1-8.

Alam, A., Golovliov, I., Javed, E. and Sjöstedt, A., 2018. ClpB mutants of *Francisella tularensis* subspecies *holarctica* and *tularensis* are defective for type VI secretion and intracellular replication. *Scientific Reports*, 8(1), 11324-11334.

Alao, J. P., 2007. The regulation of cyclin D1 degradation: roles in cancer development and the potential for therapeutic invention. *Molecular Cancer*, 6(1), 1-16.

Albandar, J. M. and Rams, T. E., 2002. Global epidemiology of periodontal diseases: an overview. *Periodontology 2000*, 29(1), 7-10.

Aleksandrowicz, P., Brzezińska-Błaszczyk, E., Kozłowska, E., Żelechowska, P., Borgonovo, A. E. and Agier, J., 2021. Analysis of IL-1β, CXCL8, and TNF-α levels in the crevicular fluid of patients with periodontitis or healthy implants. *BMC Oral Health,* 21(120), 1-9.

Allwood, M. C. and Russell, A. D., 1970. Mechanisms of thermal injury in nonsporulating bacteria. *Advances in Applied Microbiology*, 1(12), 89–119.

Amalraj, A., Pius, A., Gopi, S. and Gopi, S., 2017. Biological activities of curcuminoids, other biomolecules from turmeric and their derivatives – A review. *Journal of Traditional and Complementary Medicine*, 7(2), 205-233.

Amano, A., Nakagawa, I., Okahashi, N. and Hamada, N., 2004. Variations of *Porphyromonas gingivalis* fimbriae in relation to microbial pathogenesis. *Journal of Periodontal Research*, 39(2), 136-142.

Amar, S., Gokce, N., Morgan, S., Loukideli, M., Van Dyke, T. E. and Vita, J. A., 2003. Periodontal disease is associated with brachial artery endothelial dysfunction and systemic inflammation. *Arteriosclerosis, Thrombosis, and Vascular Biology*, 23(7), 1245-1249.

Amar, S. and Han, X., 2003. The impact of periodontal infection on systemic diseases. *Med Sci Monit.*, 9(12), 291-299.

Aomatsu, K., Arao, T., Sugioka, K., Matsumoto, K., Tamura, D., Kudo, K., Kaneda, H., Tanaka, K., Fujita, Y., Shimomura, Y. and Nishio, K., 2011. TGF-β induces sustained upregulation of SNAI1 and SNAI2 through Smad and non-Smad pathways in a human corneal epithelial cell line. *Investigative Ophthalmology & Visual Science*, 52(5), 2437-2443.

Aplin, J. D. and Ruane, P. T., 2017. Embryo–epithelium interactions during implantation at a glance. *Journal of Cell Science*, 130(1), 15-22.

Araki, K., Shimura, T., Suzuki, H., Tsutsumi, S., Wada, W., Yajima, T., Kobayahi, T., Kubo, N. and Kuwano, H., 2011. E/N-cadherin switch mediates cancer progression via TGF-β-induced epithelial-to-mesenchymal transition in extrahepatic cholangiocarcinoma. *British Journal of Cancer*, 105(12), 1885-1893.

Araki, S., Omori, Y., Lyn, D., Singh, R. K., Meinbach, D. M., Sandman, Y., Lokeshwar, V. B. and Lokeshwar, B. L., 2007. Interleukin-8 Is a Molecular Determinant of Androgen Independence and Progression in Prostate Cancer. *Cancer Research*, 67(14), 6854-6862.

Assani, G. and Zhou, Y., 2018. Effect of modulation of epithelial-mesenchymal transition regulators Snail1 and Snail2 on cancer cell radiosensitivity by targeting of the cell cycle, cell apoptosis and cell migration/invasion (Review). *Oncology Letters*, 17(1), 23-30.

Avila-Carrasco, L., Majano, P., Sánchez-Toméro, J. A., Selgas, R., López-Cabrera, M., Aguilera, A. and González Mateo, G., 2019. Natural plants compounds as modulators of epithelial-to-mesenchymal transition. *Frontiers in Pharmacology*, 10(715), 1-24.

Baelum, V. and López, R., 2013. Periodontal disease epidemiology - learned and unlearned?. *Periodontology 2000*, 62(1), 37-58.

Bahekar, A. A., Singh, S., Saha, S., Molnar, J. and Arora, R., 2007. The prevalence and incidence of coronary heart disease is significantly increased in periodontitis: A meta-analysis. *American Heart Journal*, 154(5), 830-837.

Bahrami, A., Majeed, M. and Sahebkar, A., 2019. Curcumin: a potent agent to reverse epithelial-to-mesenchymal transition. *Cellular Oncology*, 42(4), 405-421.

Bai, X., Li, Y., Zhang, H., Wang, F., He, H., Yao, J., Liu, L. and Li, S., 2017. Role of matrix metalloproteinase-9 in transforming growth factor beta 1-induced epithelial-mesenchymal transition in esophageal squamous cell carcinoma. *OncoTargets and Therapy*, 10(1), 2837-2847.

Bakthavatchalu, V., Meka, A., Sathishkumar, S., Lopez, M. C., Verma, R. K., Wallet, S. M., Bhattacharyya, I., Boyce, B. F., Mans, J., Lamont, R. J., Baker, H. V., Ebersole, J. L. and Kesavalu, L., 2010. Molecular characterization of *Treponema denticola* infection-induced bone and soft tissue transcriptional profiles. *Molecular Oral Microbiology*, 25(4), 260-274.

Baron, S. and Hentges, D. J., 1996. *Anaerobes: General characteristics*. Medical Microbiology. 4th ed. Galveston, TX: University of Texas Medical Branch, pp. 337-357.

Bartold, P. M. and Narayanan, A. S., 2006. Molecular and cell biology of healthy and diseased periodontal tissues. *Periodontology 2000*, 40(1), 29-49.

Bartold, P. M., 1991. Connective tissues of the periodontium. Research and clinical implications. *Australian Dental Journal*, 36(4), 255-268.

Basso, F. G., Soares, D. G., Pansani, T. N., Turrioni, A. P. S., Scheffel, D. L., de Souza Costa, C. A. and Hebling, J., 2015. Effect of LPS treatment on the viability and chemokine synthesis by epithelial cells and gingival fibroblasts. *Archives of Oral Biology*, 60(8), 1117-1121.

Basta, D. W., Angeles-Albores, D., Spero, M. A., Ciemniecki, J. A. and Newman, D. K., 2020. Heat-shock proteases promote survival of Pseudomonas aeruginosa during growth arrest. *Proceedings of the National Academy of Sciences*, 117(8), 4358-4367.

Bates, R. C., Bellovin, D. I., Brown, C., Maynard, E., Wu, B., Kawakatsu, H., Sheppard, D., Oettgen, P. and Mercurio, A. M., 2005. Transcriptional activation of integrin β6 during the epithelial-mesenchymal transition defines a novel prognostic indicator of aggressive colon carcinoma. *Journal of Clinical Investigation*, 115(2), 339-347.

Battaglia, R. A., Delic, S., Herrmann, H. and Snider, N. T., 2018. Vimentin on the move: new developments in cell migration. *F1000Research*, 7(1796), 1-10.

Belcaro, G., Cesarone, M. R., Dugall, M., Pellegrini, L., Ledda, A., Grossi, M. G., Togni, S. and Appendino, G., 2010. Efficacy and safety of Meriva (R), a curcumin-phosphatidylcholine

complex, during extended administration in osteoarthritis patients. *Alternative Medicine Reviews*, 15(4), 337-344.

Belkin, A. M. and Stepp, M. A., 2000. Integrins as receptors for laminins. *Microscopy Research and Technique*, 51(3), 280-301.

Bengtsson, T., Khalaf, A. and Khalaf, H., 2015. Secreted gingipains from *Porphyromonas gingivalis* colonies exert potent immunomodulatory effects on human gingival fibroblasts. *Microbiological Research*, 178, 18-26.

Bergström, J., 2004. Tobacco smoking and chronic destructive periodontal disease. *Odontology*, 92(1), 1-8.

Berkovitz, B. K. B., Holland, G. R. and Moxham, B. J., 2009. *Oral Anatomy, Histology and Embryology*. 4th ed. Edinburgh: Elsevier, pp.237-238.

Bessède, E., Staedel, C., Acuña Amador, L. A., Nguyen, P. H., Chambonnier, L., Hatakeyama, M., Belleannée, G., Mégraud, F. and Varon, C., 2013. *Helicobacter pylori* generates cells with cancer stem cell properties via epithelial–mesenchymal transition-like changes. *Oncogene*, 33(32), 4123-4131.

Bhattacharya, R., Xu, F., Dong, G., Li, S., Tian, C., Ponugoti, B. and Graves, D. T., 2014. Effect of bacteria on the wound healing behavior of oral epithelial cells. *PLoS ONE*, 9(2), e89475.

Bhowmick, N. A., Ghiassi, M., Bakin, A., Aakre, M., Lundquist, C. A., Engel, M. E., Arteaga, C. L. and Moses, H. L., 2001. Transforming growth factor-β1 mediates epithelial to mesenchymal transdifferentiation through a RhoA-dependent Mechanism. *Molecular Biology of the Cell*, 12(1), 27-36.

Biga, L. M., Dawson, S., Harwell, A., Hopkins, R., Kaufmann, J., LeMaster, M., Matern, P., Morrison-Graham, K., Quick, D. and Runyeon, J., 2020. *Anatomy & Physiology*. 1st ed. Cornvalis, Oregon: Oregon State University, pp.168-177.

Bodet, C., Chandad, F. and Grenier, D., 2006. Inflammatory responses of a macrophage/epithelial cell co-culture model to mono and mixed infections with *Porphyromonas gingivalis*, *Treponema denticola*, and *Tannerella forsythia*. *Microbes and Infection*, 8(1), 27-35.

Borgnakke, W. S., Genco, R. J., Eke, P. I. and Taylor, G. W., 2018. *Oral health and diabetes*. Diabetes in America. 3rd ed. US: National Institutes of Health/National Institute of Diabetes and Digestive and Kidney Diseases (NIH/NIDDK), pp.1-51.

Borgnakke, W. S., Ylöstalo, P. V., Taylor, G. W. and Genco, R. J., 2013. Effect of periodontal disease on diabetes: systematic review of epidemiologic observational evidence. *Journal of Clinical Periodontology*, 40(4), S135-S152.

Borradori, L. and Sonnenberg, A., 1999. Structure and function of hemidesmosomes: more than simple adhesion complexes. *Journal of Investigative Dermatology*, 112(4), 411-418.

Bosshardt, D. D. and Lang, N. P., 2005. The Junctional Epithelium: from Health to Disease. *Journal of Dental Research*, 84(1), 9-20.

Boström, L., Linder, L. E. and Bergström, J., 1999. Smoking and crevicular fluid levels of IL-6 and TNF-a in periodontal disease. *Journal of Clinical Periodontology*, 26(6), 352-357.

Boyer, B., Tucker, G. C., Vallés, A. M., Gavrilovic, J. and Thiery, J. P., 1989. Reversible transition towards a fibroblastic phenotype in a rat carcinoma cell line. *International Journal of Cancer*, 44(S1), 69-75.

Brandt, S., Kwok, T., Hartig, R., Konig, W. and Backert, S., 2005. NF- B activation and potentiation of proinflammatory responses by the *Helicobacter pylori* CagA protein. Proceedings of the National Academy of Sciences, 102(26), 9300-9305.

Breljak, D., Ambriovic-Ristov, A., Kapitanovic, S., Cacev, T. and Gabrilovac, J., 2005. Comparison of three RT-PCR based methods for relative quantification of mRNA. *Food technology and biotechnology*, 43(4), 379-388.

Brissette, C. A., Pham, T. T., Coats, S. R., Darveau, R. P. and Lukehart, S. A., 2008. *Treponema denticola* does not induce production of common innate immune mediators from primary gingival epithelial cells. *Oral Microbiology and Immunology*, 23(6), 474-481.

Brizuela, M. and Winters, R., 2022. *Histology, Oral Mucosa*. 1st ed. Treasure Island, Florida: StatPearls, pp.1-10.

Brunner, J., Scheres, N., El Idrissi, N. B. E., Deng, D. M., Laine, M. L., van Winkelhoff, A. J. and Crielaard, W., 2010. The capsule of *Porphyromonas gingivalis* reduces the immune response of human gingival fibroblasts. *BMC Microbiology*, 10(5), 1-11.

Buccione, R., Caldieri, G. and Ayala, I., 2009. Invadopodia: specialized tumor cell structures for the focal degradation of the extracellular matrix. *Cancer and Metastasis Reviews*, 28(1-2), 137-149.

Bugueno, I. M., Batool, F., Korah, L., Benkirane-Jessel, N. and Huck, O., 2018. *Porphyromonas gingivalis* differentially modulates apoptosome apoptotic peptidase activating factor 1 in epithelial cells and fibroblasts. *The American Journal of Pathology*, 188(2), 404-416.

Bui, F. Q., Johnson, L., Roberts, J., Hung, S., Lee, J., Atanasova, K. R., Huang, P., Yilmaz, Ö. and Ojcius, D. M., 2016. *Fusobacterium nucleatum* infection of gingival epithelial cells leads to NLRP3 inflammasome-dependent secretion of IL-1β and the danger signals ASC and HMGB1. *Cellular Microbiology*, 18(7), 970-981.

Bulzico, D., Pires, B. R. B., De Faria, P. A. S., Neto, L. V. and Abdelhay, E., 2018. Twist1 correlates with epithelial-mesenchymal transition markers fibronectin and vimentin in adrenocortical tumors. *Anticancer Research*, 39(1), 173-175.

Burdall, S. E., Hanby, A. M., Lansdown, M. R. J. and Speirs, V., 2003. Breast cancer cell lines: friend or foe?. *Breast Cancer Research*, 5(2), 89-95.

Bustin, S. A., 2000. Absolute quantification of mRNA using real-time reverse transcription polymerase chain reaction assays. *Journal of Molecular Endocrinology*, 25(2), 169-193.

Bustin, S. A., Benes, V., Garson, J. A., Hellemans, J., Huggett, J., Kubista, M., Mueller, R., Nolan, T., Pfaffl, M. W., Shipley, G. L., Vandesompele, J. and Wittwer, C. T., 2009. The MIQE guidelines: Minimum information for publication of quantitative real-Time PCR experiments. *Clinical Chemistry*, 55(4), 611-622.

Cai, H., Zheng, Z., Sun, Y., Liu, Z., Zhang, M. and Li, C., 2015. The effect of curcumin and its nanoformulation on adjuvant-induced arthritis in rats. *Drug Design, Development and Therapy*, 60(5), 4931-4942.

Caldas, T., Demont-Caulet, N., Ghazi, A. and Richarme, G., 1999. Thermoprotection by glycine betaine and choline. *Microbiology*, 145(9), 2543-2548.

Cao, M., Liu, H., Liu, Z., Xiao, P., Chen, J., Tan, Y., Jiang, X., Jiang, Z., Qiu, Y., Huang, H., Zhang, Q. and Jiang, G., 2017. Curcumin downregulates the expression of Snail via suppressing Smad2 pathway to inhibit TGF-β1-induced epithelial-mesenchymal transitions in hepatoma cells. *Oncotarget*, 8(65), 108498-108508.

Camacho-Barquero, L., Villegas, I., Sánchez-Calvo, J., Talero, E., Sánchez-Fidalgo, S., Motilva, V. and Alarcón de la Lastra, C., 2007. Curcumin, a Curcuma longa constituent, acts on MAPK p38 pathway modulating COX-2 and iNOS expression in chronic experimental colitis. *International Immunopharmacology*, 7(3), 333-342.

Cano, A., Pérez-Moreno, M. A., Rodrigo, I., Locascio, A., Blanco, M. J., del Barrio, M. G., Portillo, F. and Nieto, M. A., 2000. The transcription factor Snail controls epithelial–mesenchymal transitions by repressing E-cadherin expression. *Nature Cell Biology*, 2(2), 76-83.

Carranza, F. A., Newman, M. G., Takei, H. H. and Klokkevold, P. R., 2006. *Carranza's clinical periodontology*. 10th ed. St. Louis: Elsevier Saunders, pp.10-250.

Casas, E., Kim, J., Bendesky, A., Ohno-Machado, L., Wolfe, C. J. and Yang, J., 2011. Snail2 is an essential mediator of Twist1-induced epithelial mesenchymal transition and metastasis. *Cancer Research*, 71(1), 245-254.

Caton, J. G., Armitage, G., Berglundh, T., Chapple, I. L. C., Jepsen, S., Kornman, K. S., Mealey, B. L., Papapanou, P. N., Sanz, M. and Tonetti, M. S., 2018. A new classification scheme for periodontal and peri-implant diseases and conditions - Introduction and key changes from the 1999 classification. *Journal of Periodontology*, 89(20), 1-8.

Cavallaro, U., Schaffhauser, B. and Christofori, G., 2002. Cadherins and the tumour progression: is it all in a switch? *Cancer Letters*, 176(2), 123-128.

Cekici, A., Kantarci, A., Hasturk, H. and Van Dyke, T. E., 2013. Inflammatory and immune pathways in the pathogenesis of periodontal disease. *Periodontology 2000*, 64(1), 57-80.

Cerajewska, T. L., Davies, M. and West, N. X., 2016. Periodontitis: a potential risk factor for Alzheimer's disease. *BDJ Team*, 3(4), 1-12.

Chakravarti, N., Kadara, H., Yoon, D., Shay, J. W., Myers, J. N., Lotan, D., Sonenberg, N. and Lotan, R., 2010. Differential inhibition of protein translation machinery by curcumin in normal, immortalized, and malignant oral epithelial cells. *Cancer Prevention Research*, 3(3), 331-338.

Chapple, I. L. C., Van der Weijden, F., Doerfer, C., Herrera, D., Shapira, L., Polak, D., Madianos, P., Louropoulou, A., Machtei, E., Donos, N., Greenwell, H., Van Winkelhoff, A. J., Eren Kuru, B., Arweiler, N., Teughels, W., Aimetti, M., Molina, A., Montero, E. and Graziani, F., 2015. Primary prevention of periodontitis: managing gingivitis. *Journal of Clinical Periodontology*, 42(16), S71-S76.

Charon, N. W., Cockburn, A., Li, C., Liu, J., Miller, K. A., Miller, M. R., Motaleb, M. and Wolgemuth, C. W., 2012. The Unique Paradigm of Spirochete Motility and Chemotaxis. *Annual Review of Microbiology*, 66(1), 349-370.

Chaudhary, V., Kishore, B., Rao, S. P., Kugaji, M. S. and Ingalagi, P., 2013. Detection of *Treponema denticola* by PCR in patients with different periodontal status. *International Journal of Current Microbiology and Applied Sciences*, 2(10), 172-178.

Chen, J., Ahmad, R., Li, W., Swain, M. and Li, Q., 2015. Biomechanics of oral mucosa. *Journal of The Royal Society Interface*, 12(109), 215-235.

Chen, L., Chen, D., Wang, M., Liu, D., Chen, H., Dou, F., Vaziri, N. D. and Zhao, Y., 2017a. Role of RAS/Wnt/β-catenin axis activation in the pathogenesis of podocyte injury and tubulo-interstitial nephropathy. *Chemico-Biological Interactions*, 273(4), 56-72.

Chen, Q., Yang, W., Wang, X., Li, X., Qi, S., Zhang, Y. and Gao, M., 2017b. TGF-β1 induces EMT in bovine mammary epithelial cells through the TGFβ1/Smad signaling pathway. *Cellular Physiology and Biochemistry*, 43(1), 82-93.

Chen, T., You, Y., Jiang, H. and Wang, Z. Z., 2017c. Epithelial-mesenchymal transition (EMT): A biological process in the development, stem cell differentiation, and tumorigenesis. *Journal of Cellular Physiology*, 232(12), 3261-3272.

Chen, X., Sun, R., Hu, J., Mo, Z., Yang, Z., Liao, D. and Zhong, N., 2008. attenuation of bleomycin-induced lung fibrosis by oxymatrine is associated with regulation of fibroblast proliferation and collagen production in primary culture. *Basic & Clinical Pharmacology & Toxicology*, 103(3), 278-286.

Chhunchha, B., Fatma, N., Bhargavan, B., Kubo, E., Kumar, A. and Singh, D. P., 2011. Specificity protein, Sp1-mediated increased expression of Prdx6 as a curcumin-induced antioxidant defense in lens epithelial cells against oxidative stress. *Cell Death & Disease*, 2(11), 1-13.

Chi, B., Limberger, R. J. and Kuramitsu, H. K., 2002. Complementation of a *Treponema denticola* flgE mutant with a novel coumermycin A1-resistant *T. denticola* shuttle vector system. *Infection and Immunity*, 70(4), 2233-2237.

Chi, B., Qi, M. and Kuramitsu, H. K., 2003. Role of dentilisin in *Treponema denticola* epithelial cell layer penetration. *Research in Microbiology*, 154(9), 637-643.

Cho, J., Lee, K. and Kim, C., 2007. Curcumin attenuates the expression of IL-1β, IL-6, and TNF-α as well as cyclin E in TNF-α-treated HaCaT cells; NF-κB and MAPKs as potential upstream targets. *International Journal of Molecular Medicine*, 19(1), 469-474.

Cho, K. H., Jeong, K. J., Shin, S. C., Kang, J., Park, C. G. and Lee, H. Y., 2013. STAT3 mediates TGF-β1-induced TWIST1 expression and prostate cancer invasion. *Cancer Letters*, 336(1), 167-173.

Cho, Y., Kim, K., Lee, Y., Ku, Y. and Seol, Y., 2021. Periodontal Wound Healing and Tissue Regeneration: A Narrative Review. *Pharmaceuticals*, 14(5), 456-473.

Choi, S. Y., Piao, Z. H., Jin, L., Kim, J. H., Kim, G. R., Ryu, Y., Lin, M. Q., Kim, H., Kee, H. J. and Jeong, M. H., 2016. Piceatannol attenuates renal fibrosis induced by unilateral ureteral obstruction via downregulation of histone deacetylase 4/5 or p38-MAPK signaling. *PLOS ONE*, 11(11), e0167340.

Christakis, N. A. and Fowler, J. H., 2007. The Spread of Obesity in a Large Social Network over 32 Years. *New England Journal of Medicine*, 357(4), 370-379.

Chu, P. G. and Weiss, L. M., 2002. Expression of cytokeratin 5/6 in epithelial neoplasms: An immunohistochemical study of 509 cases. *Modern Pathology*, 15(1), 6-10.

Cichon, M. A. and Radisky, D. C., 2014. Extracellular matrix as a contextual determinant of transforming growth factor-β signaling in epithelial-mesenchymal transition and in cancer. *Cell Adhesion & Migration*, 8(6), 588-594.

Cogoni, V., Morgan-Smith, A., Fenno, J. C., Jenkinson, H. F. and Dymock, D., 2012. *Treponema denticola* chymotrypsin-like proteinase (CTLP) integrates spirochaetes within oral microbial communities. *Microbiology*, 158(3), 759-770.

Cohen, A. N., Veena, M. S., Srivatsan, E. S. and Wang, M. B., 2009. Suppression of interleukin 6 and 8 production in head and neck cancer cells with curcumin via inhibition of Iκβ kinase. *Archives of Otolaryngology–Head & Neck Surgery*, 135(2), 190.

Cooper, A., 2005. Heat capacity effects in protein folding and ligand binding: a re-evaluation of the role of water in biomolecular thermodynamics. *Biophysical Chemistry*, 115(2-3), 89-97.

Correa, W., Brandenburg, J., Behrends, J., Heinbockel, L., Reiling, N., Paulowski, L., Schwudke, D., Stephan, K., Martinez-de-Tejada, G., Brandenburg, K. and Gutsmann, T., 2019. Inactivation of bacteria by γ-irradiation to investigate the interaction with antimicrobial peptides. *Biophysical Journal*, 117(10), 1805-1819.

Correa-Costa, M., Andrade-Oliveira, V., Braga, T. T., Castoldi, A., Aguiar, C. F., Origassa, C. S. T., Rodas, A. C. D., Hiyane, M. I., Malheiros, D. M. A. C., Rios, F. J. O., Jancar, S. and Câmara, N. O. S., 2014. Activation of platelet-activating factor receptor exacerbates renal inflammation and promotes fibrosis. *Laboratory Investigation*, 94(4), 455-466.

Cosseau, C., Devine, D. A., Dullaghan, E., Gardy, J. L., Chikatamarla, A., Gellatly, S., Yu, L. L., Pistolic, J., Falsafi, R., Tagg, J. and Hancock, R. E. W. (2008). The commensal *Streptococcus salivarius* K12 downregulates the innate immune responses of human epithelial cells and promotes host-microbe homeostasis. *Infection and Immunity*, 76(9), 4163-4175.

Creagh, E. M. and O'Neill, L. A. J., 2006. TLRs, NLRs and RLRs: a trinity of pathogen sensors that co-operate in innate immunity. *Trends in Immunology*, 27(8), 352-357.

Cross, M. L., Ganner, A., Teilab, D. and Fray, L. M., 2004. Patterns of cytokine induction by gram-positive and gram-negative probiotic bacteria. *FEMS Immunology & Medical Microbiology*, 42(2), 173-180.

Cutler, C. W., Machen, R. L., Jotwani, R. and Iacopino, A. M., 1999. Heightened gingival inflammation and attachment loss in type 2 diabetics with hyperlipidemia. *Journal of Periodontology*, 70(11), 1313-1321.

Dabija-Wolter, G., Cimpan, M., Costea, D. E., Johannessen, A. C., Sørnes, S., Neppelberg, E., Al-Haroni, M., Skaug, N. and Bakken, V., 2022. Fusobacterium nucleatum enters normal human oral fibroblasts. *Journal of Periodontology*, 80(7), 1174-1183.

Dalbey, R. E., Kuhn, A., Zhu, L. and Kiefer, D., 2014. The membrane protein insertase YidC. *Biochimica et Biophysica Acta*, 551843(8), 1489-1496.

Darrene, L. and Cecile, B., 2016. Experimental models of oral biofilms developed on inert substrates: A review of the literature. *BioMed Research International*, 2016(11), 1-8.

Darveau, R. P., 2010. Periodontitis: a polymicrobial disruption of host homeostasis. *Nature Reviews Microbiology*, 8(7), 481-490.

DaSilva-Arnold, S. C., Kuo, C., Davra, V., Remache, Y., Kim, P. C. W., Fisher, J. P., Zamudio, S., Al-Khan, A., Birge, R. B. and Illsley, N. P., 2018. ZEB2, a master regulator of the epithelial–mesenchymal transition, mediates trophoblast differentiation. *MHR: Basic science of reproductive medicine*, 25(2), 61-75.

Davis, F. M., Stewart, T. A., Thompson, E. W. and Monteith, G. R., 2014. Targeting EMT in cancer: opportunities for pharmacological intervention. *Trends in Pharmacological Sciences*, 35(9), 479-488.

Dawson, D. V., Drake, D. R., Hill, J. R., Brogden, K. A., Fischer, C. L. and Wertz, P. W., 2013. Organization, barrier function and antimicrobial lipids of the oral mucosa. *International Journal of Cosmetic Science*, 35(3), 220-223.

De Craene, B., Gilbert, B., Stove, C., Bruyneel, E., van Roy, F. and Berx, G., 2005. The transcription factor snail induces tumor cell invasion through modulation of the epithelial cell differentiation program. *Cancer Research*, 65(14), 6237-6244.

De Lima, P. O., Jorge, C. C., Oliveira, D. T. and Pereira, M. C., 2014. Hypoxic condition and prognosis in oral squamous cell carcinoma. *Anticancer Research*, 34(2), 605-612.

De Sousa Abreu, R., Penalva, L. O., Marcotte, E. M. and Vogel, C., 2009. Global signatures of protein and mRNA expression levels. *Molecular BioSystems*, 5(12), 1512-1526.

Deng, Q., Sun, X., Zhao, L., Geng, H., Liang, Z., Zhang, Z., Yu, D. and Zhong, C., 2016. Curcumin reverse cigarette smoke extract-induced human bladder epithelial-mesenchymal transition via suppresses NF-κB signaling in vitro. *Int J Clin Exp Med*, 9(2), 5031-5044.

Deng, X., Chen, C., Wu, F., Qiu, L., Ke, Q., Sun, R., Duan, Q., Luo, M. and Luo, Z., 2020. Curcumin inhibits the migration and invasion of non-small-cell lung cancer cells through radiation-induced suppression of epithelial-mesenchymal transition and soluble E-cadherin expression. *Technology in Cancer Research & Treatment*, 19(2), 1-11.

Dennis, G. J., Sherman, B. T., Hosack, D. A., Yang, J., Gao, W., Lane, H. C. and Lempicki, R. A., 2003. DAVID: Database for Annotation, Visualization, and Integrated Discovery. *Genome Biology*, 4(9), 3-5.

Deodhar, S. D., Sethi, R. and Srimar, R. C., 2013. Preliminary study on antirheumatic activity of curcumin (diferuloyl methane). *Indian Journal of Medical Research*, 138(1), 632-640.

Dermani, F. K., Saidijam, M., Amini, R., Mahdavinezhad, A., Heydari, K. and Najafi, R., 2016. Resveratrol inhibits proliferation, invasion, and epithelial–mesenchymal transition by increasing miR-200c expression in HCT-116 colorectal cancer cells. *Journal of Cellular Biochemistry*, 118(6), 1547-1555.

Devine, D. A., Marsh, P. D. and Meade, J., 2015. Modulation of host responses by oral commensal bacteria. *Journal of Oral Microbiology*, 7(1), 1-4.

Dhasarathy, A., Phadke, D., Mav, D., Shah, R. R. and Wade, P. A., 2011. The transcription factors snail and slug activate the transforming growth factor-beta signaling pathway in breast cancer. *PLoS ONE*, 6(10), 1-11.

Dierickx, K., Pauwels, M., Van Eldere, J., Cassiman, J. J., van Steenberghe, D. and Quirynen, M., 2002. Viability of cultured periodontal pocket epithelium cells and Porphyromonas gingivalis association. *Journal of Clinical Periodontology*, 29(11), 987-996.

Dinarello, C. A., 2017. Overview of the IL-1 family in innate inflammation and acquired immunity. *Immunological Reviews*, 281(1), 8-27.

Ding, P., Yang, M., Wang, N., Jin, L., Dong, Y., Cai, X. and Chen, L., 2020a. *Porphyromonas gingivalis*-induced NLRP3 inflammasome activation and its downstream interleukin-1β release depend on caspase-4. *Frontiers in Microbiology*, 11(1881), 1-15.

Ding, Z., Wu, X., Wang, Y., Ji, S., Zhang, W., Kang, J., Li, J. and Fei, G., 2020b. Melatonin prevents LPS-induced epithelial-mesenchymal transition in human alveolar epithelial cells via the GSK-3β/Nrf2 pathway. *Biomedicine & Pharmacotherapy*, 132(1), 110827-110842.

Diomede, F., Thangavelu, S. R., Merciaro, I., D'Orazio, M., Bramanti, P., Mazzon, E. and Trubiani, O., 2017. *Porphyromonas gingivalis* lipopolysaccharide stimulation in human periodontal ligament stem cells: role of epigenetic modifications to the inflammation. *European Journal of Histochemistry*, 61(3), 231-237.

Di Pierro, F., Bressan, A., Ranaldi, D., Rapacioli, G., Giacomelli, L. and Bertuccioli, A., 2015. Potential role of bioavailable curcumin in weight loss and omental adipose tissue decrease: preliminary data of a randomized, controlled trial in overweight people with metabolic syndrome. Preliminary study. *European Review for Medical and Pharmacological Sciences*, 19(21), 4195-4202.

Dongari-Bagtzoglou, A. and Kashleva, H., 2006. Development of a highly reproducible three-dimensional organotypic model of the oral mucosa. *Nature Protocols*, 1(4), 2012-2018.

Du, B. and Shim, J. S., 2016. Targeting epithelial–mesenchymal transition (EMT) to overcome drug resistance in cancer. *Molecules*, 21(7), 965-980.

Duband, J. L. and Thiery, J. P., 1982. Appearance and distribution of fibronectin during chick embryo gastrulation and neurulation. *Developmental Biology*, 94(2), 337-350.

Duffield, J. S., 2014. Cellular and molecular mechanisms in kidney fibrosis. *Journal of Clinical Investigation*, 124(6), 2299-2306.

Duval, K., Grover, H., Han, L., Mou, Y., Pegoraro, A. F., Fredberg, J. and Chen, Z., 2017. Modeling physiological events in 2D vs. 3D cell culture. *Physiology*, 32(4), 266-277.

Ebenman, B. and Jonsson, T., 2005. Using community viability analysis to identify fragile systems and keystone species. *Trends in Ecology & Evolution*, 20(10), 568-575.

Economist Intelligence Unit, 2021. *Time to take gum disease seriously: The societal and economic impact of periodontitis*. London: Economist, pp.31-33.

Engebretson, S. P., Hey-Hadavi, J., Ehrhardt, F. J., Hsu, D., Celenti, R. S., Grbic, J. T. and Lamster, I. B., 2004. Gingival crevicular fluid levels of interleukin-1β and glycemic control in patients with chronic periodontitis and type 2 diabetes. *Journal of Periodontology*, 75(9), 1203-1208.

Ezraty, B., Gennaris, A., Barras, F. and Collet, J., 2017. Oxidative stress, protein damage and repair in bacteria. *Nature Reviews Microbiology*, 15(7), 385-396.

Fadus, M. C., Lau, C., Bikhchandani, J. and Lynch, H. T., 2017. Curcumin: An age-old anti-inflammatory and anti-neoplastic agent. *Journal of Traditional and Complementary Medicine*, 7(3), 339-346.

Fan, D., Zhao, W., Wang, Y., Han, S. and Guo, S., 2012. Oxymatrine inhibits collagen synthesis in keloid fibroblasts via inhibition of transforming growth factor-β1/Smad signaling pathway. *International Journal of Dermatology*, 51(4), 463-472.

Fan, J. M., Huang, X. R., Ng, Y. Y., Nikolic-Paterson, D. J., Mu, W., Atkins, R. C. and Lan, H. Y., 2001. Interleukin-1 induces tubular epithelial-myofibroblast transdifferentiation through a transforming growth factor-β1-dependent mechanism in vitro. *American Journal of Kidney Diseases*, 37(4), 820-831.

Farooqui, T. and Farooqui, A. A., 2019. *Curcumin for neurological and psychiatric disorders*. 1st ed. Cambridge, Massachusetts: Academic Press, pp.23-44.

Fatima, I., El-Ayachi, I., Taotao, L., Lillo, M. A., Krutilina, R., Seagroves, T. N., Radaszkiewicz, T. W., Hutnan, M., Bryja, V., Krum, S. A., Rivas, F. and Miranda-Carboni, G. A., 2017. The natural compound Jatrophone interferes with Wnt/β-catenin signaling and inhibits proliferation and EMT in human triple-negative breast cancer. *PLOS ONE*, 12(12), e0189864.

Favre, B., Begré, N., Bouameur, J., Lingasamy, P., Conover, G. M., Fontao, L. and Borradori, L., 2018. Desmoplakin interacts with the coil 1 of different types of intermediate filament proteins and displays high affinity for assembled intermediate filaments. *PLOS ONE*, 13(10), e0205038.

Feliksiak, K., Witko, T., Solarz, D., Guzik, M. and Rajfur, Z., 2020. Vimentin association with nuclear grooves in normal MEF 3T3 cells. *International Journal of Molecular Sciences*, 21(20), 7478-7491.

Feng, Y., Chen, D., Vaziri, N. D., Guo, Y. and Zhao, Y., 2019. Small molecule inhibitors of epithelial-mesenchymal transition for the treatment of cancer and fibrosis. *Medicinal Research Reviews*, 40(1), 54-78.

Fernando, R. L., Castillo, M. D., Litzinger, M., Hamilton, D. H. and Palena, C., 2011. IL-8 signaling plays a critical role in the epithelial–mesenchymal transition of human carcinoma cells. *Cancer Research*, 71(15), 5296-5306.

Ferreira, V. H., Nazli, A., Dizzell, S. E., Mueller, K. and Kaushic, C., 2015. The anti-inflammatory activity of curcumin protects the genital mucosal epithelial barrier from disruption and blocks replication of HIV-1 and HSV-2. *PLOS ONE*, 10(4), 1-18.

Fintha, A., Gasparics, Á., Rosivall, L. and Sebe, A., 2019. Therapeutic targeting of fibrotic epithelial-mesenchymal transition–an outstanding challenge. *Frontiers in Pharmacology*, 10(388), 1-11.

Fisher, C., Meng, R., Bizouarn, F. and Scott, R., 2000. *High resolution melt parameter considerations for optimal data resolution.* California: Bio-rad laboratories, Inc., pp.1-24.

Fitzpatrick, S. G. and Katz, J., 2010. The association between periodontal disease and cancer: A review of the literature. *Journal of Dentistry*, 38(2), 83-95.

Fleisch, L. and Austin, J. C, 1978. A histologic study of the response of masticatory and lining mucosa to mechanical loading in the vervet monkey. *The Journal of Prosthetic Dentistry*, 39(2), 211-216.

Flemmig, T. F. and Beikler, T., 2010. Control of oral biofilms. *Periodontology 2000*, 55(1), 9-15.

Fragiadaki, M. and Mason, R. M., 2011. Epithelial-mesenchymal transition in renal fibrosis - evidence for and against. *International Journal of Experimental Pathology*, 92(3), 143-150.

Francí, C., Takkunen, M., Dave, N., Alameda, F., Gómez, S., Rodríguez, R., Escrivà, M., Montserrat-Sentís, B., Baró, T., Garrido, M., Bonilla, F., Virtanen, I. and García de Herreros, A., 2006. Expression of Snail protein in tumor–stroma interface. *Oncogene*, 25(37), 5134-5144.

Friedl, P. and Gilmour, D., 2009. Collective cell migration in morphogenesis, regeneration and cancer. *Nature Reviews Molecular Cell Biology*, 10(7), 445-457.

Fu, J., Ke, X., Tan, S., Liu, T., Wang, S., Ma, J. and Lu, H., 2015. The natural compound codonolactone attenuates TGF-β1-mediated epithelial-to-mesenchymal transition and motility of breast cancer cells. *Oncology Reports*, 35(1), 117-126.

Fukuda, S., Akiyama, M., Harada, H. and Nakahama, K., 2019. Effect of gap junction-mediated intercellular communication on TGF-β induced epithelial-to-mesenchymal transition. *Biochemical and Biophysical Research Communications*, 508(3), 928-933.

Gallardo, M. and Calaf, G. M., 2016a. Curcumin and epithelial-mesenchymal transition in breast cancer cells transformed by low doses of radiation and estrogen. *International Journal of Oncology*, 48(6), 2534-2542.

Gallardo, M. and Calaf, G. M., 2016b. Curcumin inhibits invasive capabilities through epithelial mesenchymal transition in breast cancer cell lines. *International Journal of Oncology*, 49(3), 1019-1027.

Gallardo, M., Kemmerling, U., Aguayo, F., Bleak, T. C., Muñoz, J. P. and Calaf, G. M., 2019. Curcumin rescues breast cells from epithelial-mesenchymal transition and invasion induced by anti-miR-34a. *International Journal of Oncology*, 56(2), 480-493.

Gallardo, M., Ponce-Cusi, R. and Calaf, G. M., 2017. Curcumin inhibits epithelial-mesenchymal transition and invasion in breast cancer cells by controlling miR-34a expression. *Cancer Res*, 77(2), 1478-1488.

Ganther, S., Radaic, A., Malone, E., Kamarajan, P., Chang, N. N., Tafolla, C., Zhan, L., Fenno, J. C. and Kapila, Y. L., 2021. *Treponema denticola* dentilisin triggered TLR2/MyD88 activation upregulates a tissue destructive program involving MMPs via Sp1 in human oral cells. *PLOS Pathogens*, 17(7), e1009311.

Garlet, G. P., 2010. Destructive and protective roles of cytokines in periodontitis: a re-appraisal from host defense and tissue destruction viewpoints. *Journal of Dental Research*, 89(12), 1349-1363.

Garrod, D. and Chidgey, M., 2008. Desmosome structure, composition and function. *Biochimica et Biophysica Acta (BBA) - Biomembranes*, 1778(3), 572-587.

Gaur, S. and Agnihotri, R., 2014. Alzheimer's disease and chronic periodontitis: Is there an association?. *Geriatrics & Gerontology International*, 15(4), 391-404.

Geerts, S. O., Legrand, V., Charpentier, J., Albert, A. and Rompen, E. H., 2004. Further evidence of the association between periodontal conditions and coronary artery disease. *Journal of Periodontology*, 75(9), 1274-1280.

Gehrig, J. S., Shin, D. E. and Willmann, D. E., 2020. *Microscopic anatomy of the periodontium*. Foundations of periodontics for the dental hygienist. 5th ed. Burlington, MA: Jones & Bartlett Learning, LLC, pp.35-36.

Geng, F., Liu, J., Guo, Y., Li, C., Wang, H., Wang, H., Zhao, H. and Pan, Y., 2017. Persistent exposure to *porphyromonas gingivalis* promotes proliferative and invasion capabilities, and tumorigenic properties of human immortalized oral epithelial cells. *Frontiers in Cellular and Infection Microbiology*, 7(57), 1-16.

Germano, F., Bramanti, E., Arcuri, C., Cecchetti, F. and Cicciù, M., 2013. Atomic force microscopy of bacteria from periodontal subgingival biofilm: Preliminary study results. *European Journal of Dentistry*, 7(2), 152-158.

Gharbia, S. E. and Shah, H. N., 1990. Heterogeneity within *Fusobacterium nucleatum*, proposal of four subspecies. *Letters in Applied Microbiology*, 10(2), 105-108.

Ghayoor, M., Qadoos, A., Bahadar, S., Hayat, A., Daud, M., Hassan, A., Ali, F., Zeb, A., Rahman, K. U., Wahab, A., Khattak, Z. F. and Khattak, B., 2015. Isolation and identification of common contaminants bacteria from working area in microbiology laboratory. *Journal of Bio-Molecular Sciences*, 3(2), 74-78.

Giacomelli, C., Daniele, S., Natali, L., Iofrida, C., Flamini, G., Braca, A., Trincavelli, M. L. and Martini, C., 2017. Carnosol controls the human glioblastoma stemness features through the epithelial-mesenchymal transition modulation and the induction of cancer stem cell apoptosis. *Scientific Reports*, 7(1), 1-17.

Giannopoulou, C., Kamma, J. J. and Mombelli, A., 2003. Effect of inflammation, smoking and stress on gingival crevicular fluid cytokine level. *Journal of Clinical Periodontology*, 30(2), 145-153.

Gibson, U. E., Heid, C. A. and Williams, P. M., 1996. A novel method for real time quantitative RT-PCR. *Genome Research*, 6(10), 995-1001.

Giepmans, B. N. G. and van IJzendoorn, S. C. D., 2009. Epithelial cell–cell junctions and plasma membrane domains. *Biochimica et Biophysica Acta (BBA) - Biomembranes*, 1788(4), 820-831.

Gilles, C., Newgreen, D.F, Sato H, Thompson, E. W., 2000-2013. *Matrix metalloproteases and epithelial-to-mesenchymal transition: implications for carcinoma metastasis*. In: Madame Curie Bioscience Database, Austin (TX): Landes Bioscience;. Available from: https://www.ncbi.nlm.nih.gov/books/NBK6387/

Girouard, M., Pool, M., Alchini, R., Rambaldi, I. and Fournier, A. E., 2016. RhoA proteolysis regulates the actin cytoskeleton in response to oxidative stress. *PLOS ONE*, 11(12), e0168641.

Glenn, H. L., Messner, J. and Meldrum, D. R., 2016. A simple non-perturbing cell migration assay insensitive to proliferation effects. *Scientific Reports*, 6(1), 1-12.

Goegan, P., Johnson, G. and Vincent, R., 1995. Effects of serum protein and colloid on the alamarBlue assay in cell cultures. *Toxicology in Vitro*, 9(3), 257-266.

Grabe, H. J., Schwahn, C., Völzke, H., Spitzer, C., Freyberger, H. J., John, U., Mundt, T., Biffar, R. and Kocher, T., 2009. Tooth loss and cognitive impairment. *Journal of Clinical Periodontology*, 36(7), 550-557.

Grada, A., Otero-Vinas, M., Prieto-Castrillo, F., Obagi, Z. and Falanga, V., 2017. Research techniques made simple: analysis of collective cell migration using the wound healing assay. *Journal of Investigative Dermatology*, 137(2), e11-e16.

Grant, M. M., Kolamunne, R. T, Lock, F. E., Matthews, J. B., Chapple, I. L. C. and Griffiths, H. R., 2010. Oxygen tension modulates the cytokine response of oral epithelium to periodontal bacteria. *Journal of Clinical Periodontology*, 37(12), 1039-1048.

Green, K. J., Goldman, R. D. and Chisholm, R. L., 1988. Isolation of cDNAs encoding desmosomal plaque proteins: evidence that bovine desmoplakins I and II are derived from two mRNAs and a single gene. *Proceedings of the National Academy of Sciences*, 85(8), 2613-2617.

Greenburg, G. & Hay, E.D., 1982. Epithelia suspended in collagen gels can lose polarity and express characteristics of migrating mesenchymal cells. *The Journal of cell biology*, 95(1), 333-339.

Grenier, D., Imbeault, S., Plamondon, P., Grenier, G., Nakayama, K. and Mayrand, D., 2001. Role of gingipains in growth of *Porphyromonas gingivalis* in the presence of human serum albumin. *Infection and Immunity*, 69(8), 5166-5172.

Guaita, S., Puig, I., Francí, C., Garrido, M., Domínguez, D., Batlle, E., Sancho, E., Dedhar, S., de Herreros, A. G. and Baulida, J., 2002. Snail induction of epithelial to mesenchymal transition in tumor cells is accompanied by muc1 repression and ZEB1 expression. *Journal of Biological Chemistry*, 277(42), 39209-39216.

Gupta, S. C., Patchva, S. and Aggarwal, B. B., 2013. Therapeutic roles of curcumin: lessons learned from clinical trials. The AAPS Journal, 15(1), 195-218.

Gupton, S. L. and Gertler, F. B., 2007. Filopodia: The Fingers That Do the Walking. *Science's STKE*, 400(5), 1-10.

Gürkan, A., Emingil, G., Çınarcık, S. and Berdeli, A., 2006. Gingival crevicular fluid transforming growth factor-β1 in several forms of periodontal disease. *Archives of Oral Biology*, 51(10), 906-912.

Guzman, S., Karima, M., Wang, H. and Dyke, T. E., 2003. Association between interleukin-1 genotype and periodontal disease in a diabetic population. *Journal of Periodontology*, 74(8), 1183-1190.

Hajam, I. A., Dar, P. A., Shahnawaz, I., Jaume, J. C. and Lee, J. H., 2017. Bacterial flagellin—a potent immunomodulatory agent. *Experimental & Molecular Medicine*, 49(9), e373-e373.

Hajishengallis, G., Liang, S., Payne, M. A., Hashim, A., Jotwani, R., Eskan, M. A., McIntosh, M. L., Alsam, A., Kirkwood, K. L., Lambris, J. D., Darveau, R. P. and Curtis, M. A., 2011. Low-abundance biofilm species orchestrates inflammatory periodontal disease through the commensal microbiota and complement. *Cell Host Microbe*, 10(5), 497-506.

Hamouche, L., Billaudeau, C., Rocca, A., Chastanet, A., Ngo, S., Laalami, S. and Putzer, H., 2020. Dynamic Membrane Localization of RNase Y in *Bacillus subtilis*. *mBio*, 11(1), 1-3.

Hao, Y., Baker, D. and ten Dijke, P., 2019. TGF-β-mediated epithelial-mesenchymal transition and cancer metastasis. *International Journal of Molecular Sciences*, 20(11), 2767-2801.

Haraszthy, V. I., Zambon, J. J., Trevisan, M., Zeid, M. and Genco, R. J., 2000. Identification of periodontal pathogens in atheromatous plaques. *Journal of Periodontology*, 71(10), 1554-1560.

Harries, D. and Russell, A., 1967. A note on some changes in the physical properties of *Escherichia coli* after heat treatment. *Journal of Pharmacy and Pharmacology*, 19(11), 740-743.

Hay, E. D. 1968. Organization and fine structure of epithelium and mesenchyme in the developing chick embryo. *Epithelial-Mesenchymal Interactions*, 1(2), 31-35.

Hay, E. D., 1995. An overview of epithelio-mesenchymal transformation. *Cells Tissues Organs*, 154(1), 8-20.

Hayden, P. J. and Harbell, J. W., 2020. Special review series on 3D organotypic culture models: Introduction and historical perspective. *In Vitro Cellular & Developmental Biology - Animal*, 57(2), 95-103.

Haynes, J., Srivastava, J., Madson, N., Wittmann, T. and Barber, D. L., 2011. Dynamic actin remodeling during epithelial–mesenchymal transition depends on increased moesin expression. *Molecular Biology of the Cell*, 22(24), 4750-4764.

He, Z., Huang, Z., Zhou, W., Tang, Z., Ma, R. and Liang, J., 2016. Anti-biofilm activities from resveratrol against *Fusobacterium nucleatum*. *Frontiers in Microbiology*, 79(1065), 1-9.

Hinz, B., 2021. Myofibroblasts. *Experimental Eye Research*, 142(1), 56-70.

Hollborn, M., Chen, R., Wiedemann, P., Reichenbach, A., Bringmann, A. and Kohen, L., 2013. Cytotoxic effects of curcumin in human retinal pigment epithelial cells. *PLoS ONE*, 8(3), 1-11.

Holt, S. C. and Ebersole, J. L., 2005. *Porphyromonas gingivalis*, *Treponema denticola*, and *Tannerella forsythia*: the 'red complex', a prototype polybacterial pathogenic consortium in periodontitis. *Periodontology 2000*, 38(1), 72-122.

Hong, D., Park, M., Jang, E. H., Jung, B., Kim, N. and Kim, J., 2017. Hispolon as an inhibitor of TGF-β-induced epithelial-mesenchymal transition in human epithelial cancer cells by co-regulation of TGF-β-Snail/Twist axis. *Oncology Letters*, 14(4), 4866-4872.

Hoving, J. C., Wilson, G. J. and Brown, G. D., 2014. Signalling C-Type lectin receptors, microbial recognition and immunity. *Cellular Microbiology*, 16(2), 185-194.

How, K. Y., Song, K. P. and Chan, K. G., 2016. *Porphyromonas gingivalis*: An overview of periodontopathic pathogen below the gum line. *Frontiers in Microbiology*, 7(53), 1-14.

Hsu, P., Chen, Y., Cheng, C., Kuo, C. and Sytwu, H., 2021. Interleukin-6 and interleukin-8 regulate STAT3 activation migration/invasion and EMT in chrysophanol-treated oral cancer cell lines. *Life*, 11(5), 423 – 434.

Hu, H., Lin, X., Liu, M., Fan, X. and Zou, W., 2015. Curcumin mediates reversion of HGF-induced epithelial-mesenchymal transition via inhibition of c-Met expression in DU145 cells. *Oncology Letters*, 11(2), 1499-1505.

Huang, R. Y., Guilford, P. and Thiery, J. P., 2012. Early events in cell adhesion and polarity during epithelial-mesenchymal transition. *Journal of Cell Science*, 125(19), 4417-4422.

Huang, S., Horng, C., Hsieh, Y., Hsieh, Y., Chu, S. and Chen, P., 2016. Epicatechin-3-gallate reverses TGF-β1-induced epithelial-to-mesenchymal transition and inhibits cell invasion and protease activities in human lung cancer cells. *Food and Chemical Toxicology*, 94(1), 1-10.

Huber, M. A., Kraut, N. and Beug, H., 2005. Molecular requirements for epithelial–mesenchymal transition during tumor progression. *Current Opinion in Cell Biology*, 17(5), 548-558.

Hui, M. P., Foley, P. L. and Belasco, J. G., 2014. Messenger RNA Degradation in Bacterial Cells. *Annual Review of Genetics*, 48(1), 537-559.

Humphrey, L. L., Fu, R., Buckley, D. I., Freeman, M. and Helfand, M., 2008. Periodontal disease and coronary heart disease incidence: A systematic review and meta-analysis. *Journal of General Internal Medicine*, 23(12), 2079-2086.

Ide, M. and Papapanou, P. N., 2013. Epidemiology of association between maternal periodontal disease and adverse pregnancy outcomes - systematic review. *Journal of Clinical Periodontology*, 84(4), S181-S194.

Ihara, H., Miura, T., Kato, T., Ishihara, K., Nakagawa, T., Yamada, S. and Okuda, K., 2003. Detection of *Campylobacter rectus* in periodontitis sites by monoclonal antibodies. *Journal of Periodontal Research*, 38(1), 64-72.

Ikenouchi, J., Matsuda, M., Furuse, M. and Tsukita, S., 2003. Regulation of tight junctions during the epithelium-mesenchyme transition: direct repression of the gene expression of claudins/occludin by Snail. *Journal of Cell Science*, 116(10), 1959-1967.

Ito, F., Tamiya, T., Ohtsu, I., Fujimura, M. and Fukumori, F., 2014. Genetic and phenotypic characterization of the heat shock response in *Pseudomonas putida*. *MicrobiologyOpen*, 3(6), 922-936.

Ito, R., Ishihara, K., Shoji, M., Nakayama, K. and Okuda, K., 2010. Hemagglutinin/Adhesin domains of *Porphyromonas gingivalis* play key roles in coaggregation with *Treponema denticola*. *FEMS Immunology & Medical Microbiology*, 60(3), 251-260.

Izard, J., Hsieh, C., Limberger, R. J., Mannella, C. A. and Marko, M., 2008. Native cellular architecture of *Treponema denticola* revealed by cryo-electron tomography. *Journal of Structural Biology*, 163(1), 10-17.

Jakubovics, N. S., Goodman, S. D., Mashburn-Warren, L., Stafford, G. P. and Cieplik, F., 2021. The dental plaque biofilm matrix. *Periodontology 2000*, 86(1), 32-56.

Jiang, H., Shen, J. and Ran, Z., 2017. Epithelial–mesenchymal transition in Crohn's disease. *Mucosal Immunology*, 11(2), 294-303.

Jiang, Q., Yu, Y., Ruan, H., Luo, Y. and Guo, X., 2014. Morphological and functional characteristics of human gingival junctional epithelium. *BMC Oral Health,* 14(30), 1-13.

Jiang, W. G., Sanders, A. J., Ruge, F. and Harding, K. G., 2011. Influence of interleukin-8 (IL-8) and IL-8 receptors on the migration of human keratinocytes, the role of PLC-γ and potential clinical implications. *Experimental and Therapeutic Medicine*, 3(2), 231-236.

Jiao, D., Wang, J., Lu, W., Tang, X., Chen, J., Mou, H. and Chen, Q., 2016. Curcumin inhibited HGF-induced EMT and angiogenesis through regulating c-Met dependent PI3K/Akt/mTOR signaling pathways in lung cancer. *Molecular Therapy - Oncolytics*, 3(1), 1-12.

Jiménez-Garduño, A. M., Mendoza-Rodríguez, M. G., Urrutia-Cabrera, D., Domínguez-Robles, M. C., Pérez-Yépez, E. A., Ayala-Sumuano, J. T. and Meza, I., 2017. IL-1β induced methylation of the estrogen receptor ERα gene correlates with EMT and chemoresistance in breast cancer cells. *Biochemical and Biophysical Research Communications*, 490(3), 780-785.

Jing, Y., Han, Z., Sun, K., Zhang, S., Hou, J., Liu, Y., Li, R., Gao, L., Zhao, X., Zhao, Q., Wu, M. and Wei, L., 2012. Toll-like receptor 4 signaling promotes epithelial-mesenchymal transition in human hepatocellular carcinoma induced by lipopolysaccharide. *BMC Medicine*, 10(98), 1-12.

Johnson, L. A. and Hug, L. A., 2019. Distribution of reactive oxygen species defense mechanisms across domain bacteria. *Free Radical Biology and Medicine*, 140(1), 93-102.

Joshipura, K. J., Wand, H. C., Merchant, A. T. and Rimm, E. B., 2004. Periodontal disease and biomarkers related to cardiovascular disease. *Journal of Dental Research*, 83(2), 151-155.

Julien, S., Puig, I., Caretti, E., Bonaventure, J., Nelles, L., van Roy, F., Dargemont, C., de Herreros, A. G., Bellacosa, A. and Larue, L., 2007. Activation of NF-κB by Akt upregulates Snail expression and induces epithelium mesenchyme transition. *Oncogene*, 26(53), 7445-7456.

Jung, H., Fattet, L., Tsai, J. H., Kajimoto, T., Chang, Q., Newton, A. C. and Yang, J., 2019. Apical–basal polarity inhibits epithelial–mesenchymal transition and tumour metastasis by PAR-complex-mediated SNAI1 degradation. *Nature Cell Biology*, 21(3), 359-371.

Justus, C. R., Leffler, N., Ruiz-Echevarria, M. and Yang, L. V., 2014. In vitro cell migration and invasion assays. *Journal of Visualized Experiments*, 88(51046), 1-8.

Kabiri, L., Irani, S., Nikpoor, A. R. and Afshari, J. T., 2019. Inhibitory and apoptotic effects of mannan-mitomycin c conjugate against transitional cell carcinoma and normal mouse fibroblasts. *Reports of Biochemistry and Molecular Biology*, 8(1), 63-71.

Kalluri, R., 2009. EMT: When epithelial cells decide to become mesenchymal-like cells. *Journal of Clinical Investigation*, 119(6), 1417-1419.

Kalluri, R. and Weinberg, R. A., 2009. The basics of epithelial-mesenchymal transition. *Journal of Clinical Investigation*, 119(6), 1420-1428.

Kamarajan, P., Ateia, I., Shin, J. M., Fenno, J. C., Le, C., Zhan, L., Chang, A., Darveau, R. and Kapila, Y. L., 2020. Periodontal pathogens promote cancer aggressivity via TLR/MyD88 triggered activation of Integrin/FAK signaling that is therapeutically reversible by a probiotic bacteriocin. *PLOS Pathogens*, 16(10), e1008881.

Kanehisa, M., Furumichi, M., Tanabe, M., Sato, Y. and Morishima, K., 2016. KEGG: new perspectives on genomes, pathways, diseases and drugs. *Nucleic Acids Research*, 45(D1), D353-D361.

Kang, S. O., Caparon, M. G. and Cho, K. H., 2010. Virulence Gene Regulation by CvfA, a Putative RNase: the CvfA-Enolase Complex in *Streptococcus pyogenes* Links Nutritional Stress, Growth-Phase Control, and Virulence Gene Expression. *Infection and Immunity*, 78(6), 2754-2767.

Karpiński, T. M., 2019. Role of oral microbiota in cancer development. *Microorganisms,* 7(1), 20-34.

Kasai, H., Allen, J. T., Mason, R. M., Kamimura, T. and Zhang, Z., 2005. TGF-β1 induces human alveolar epithelial to mesenchymal cell transition (EMT). *Respiratory Research*, 6(1), 20-34.

Katsui, N., Tsuchido, T., Hiramatsu, R., Fujikawa, S., Takano, M. and Shibasaki, I., 1982. Heat-induced blebbing and vesiculation of the outer membrane of *Escherichia coli*. *Journal of Bacteriology*, 151(3), 1523-1531.

Katz, J., Yang, Q., Zhang, P., Potempa, J., Travis, J., Michalek, S. M. and Balkovetz, D. F., 2002. Hydrolysis of epithelial junctional proteins by *Porphyromonas gingivalis* gingipains. *Infection and Immunity*, 70(5), 2512-2518.

Kaufhold, S. and Bonavida, B., 2014. Central role of Snail1 in the regulation of EMT and resistance in cancer: a target for therapeutic intervention. *Journal of Experimental & Clinical Cancer Research*, 33(1), 62-81.

Kedrov, A., Sustarsic, M., de Keyzer, J., Caumanns, J. J., Wu, Z. C. and Driessen, A. J. M., 2013. Elucidating the native architecture of the YidC: Ribosome complex. *Journal of Molecular Biology*, 425(22), 4112-4124.

Kikuchi, G., Motokawa, Y., Yoshida, T. and Hiraga, K., 2008. Glycine cleavage system: reaction mechanism, physiological significance, and hyperglycinemia. *Proceedings of the Japan Academy, Series B*, 84(7), 246-263.

Kilian, M., Chapple, I. L. C., Hannig, M., Marsh, P. D., Meuric, V., Pedersen, A. M. L., Tonetti, M. S., Wade, W. G. and Zaura, E., 2016. The oral microbiome – an update for oral healthcare professionals. *BDJ*, 221(10), 657-666.

Kim, H. J., Li, H., Collins, J. J. and Ingber, D. E., 2015. Contributions of microbiome and mechanical deformation to intestinal bacterial overgrowth and inflammation in a human gut-on-a-chip. *Proceedings of the National Academy of Sciences*, 113(1), E7-E15.

Kim, K. K., Kugler, M. C., Wolters, P. J., Robillard, L., Galvez, M. G., Brumwell, A. N., Sheppard, D. and Chapman, H. A., 2006. Alveolar epithelial cell mesenchymal transition develops in vivo during pulmonary fibrosis and is regulated by the extracellular matrix. *Proceedings of the National Academy of Sciences*, 103(35), 13180-13185.

Kim, J., Kong, J., Chang, H., Kim, H. and Kim, A., 2016. EGF induces epithelial-mesenchymal transition through phospho-Smad2/3-Snail signaling pathway in breast cancer cells. *Oncotarget*, 7(51), 85021-85032.

Kinane, D. F. and Chestnutt, I. G., 1997. Relationship of diabetes to periodontitis. *Curr Opin Periodontol.*, 4(2), 29-34.

Kinane, D. F., Galicia, J. C., Gorr, S., Stathopoulou, P. G. and Benakanakere, M., 2008. *P. gingivalis* interactions with epithelial cells. *Frontiers in Bioscience*, 13(13), 966-984.

Kitamura, Y., Ebihara, A., Agari, Y., Shinkai, A., Hirotsu, K. and Kuramitsu, S., 2009. Structure of D-alanine-D-alanine ligase from *Thermus thermophilus* HB8: cumulative conformational change and enzyme–ligand interactions. *Acta Crystallographica Section D Biological Crystallography*, 65(10), 1098-1106.

Knecht, A. K. and Bronner-Fraser, M., 2002. Induction of the neural crest: a multigene process. *Nature Reviews Genetics*, 3(6), 453-461.

Kohler, R., Boehringer, D., Greber, B., Bingel-Erlenmeyer, R., Collinson, I., Schaffitzel, C. and Ban, N., 2009. YidC and Oxa1 form dimeric insertion pores on the translating ribosome. *Molecular Cell*, 34(3), 344-353.

Koike, R., Cueno, M. E., Nodomi, K., Tamura, M., Kamio, N., Tanaka, H., Kotani, A. and Imai, K., 2020. Heat-Killed *Fusobacterium nucleatum* triggers varying heme-related inflammatory and stress responses depending on primary human respiratory epithelial cell type. *Molecules*, 25(17), 3839-3851.

Kolenbrander, P. E. and Andersen, R. N., 1989. Inhibition of coaggregation between *Fusobacterium nucleatum* and *Porphyromonas (Bacteroides) gingivalis* by lactose and related sugars. *Infection and Immunity*, 57(10), 3204-3209.

Kolenbrander, P. E., Andersen, R. N., Blehert, D. S., Egland, P. G., Foster, J. S. and Palmer, R. J., 2002. Communication among Oral Bacteria. *Microbiology and Molecular Biology Reviews*, 66(3), 486-505.

Koller, A. and Sapra, A., 2021. *Anatomy, Head and Neck, Oral Gingiva*. Ncbi.nlm.nih.gov. Available at: https://www.ncbi.nlm.nih.gov/books/NBK560662/#article-32174.s1 (Accessed 9 October 2021).

Kondo, Y., Higa-Nakamine, S., Noguchi, N., Maeda, N., Toku, S., Isohama, Y., Sugahara, K., Kukita, I. and Yamamoto, H., 2012. Induction of epithelial-mesenchymal transition by flagellin in cultured lung epithelial cells. *American Journal of Physiology-Lung Cellular and Molecular Physiology*, 303(12), L1057-L1069.

Korostelev, A. A., 2011. Structural aspects of translation termination on the ribosome. *RNA*, 17(8), 1409-1421.

Kössler, S., Nofziger, C., Jakab, M., Dossena, S. and Paulmichl, M., 2012. Curcumin affects cell survival and cell volume regulation in human renal and intestinal cells. *Toxicology*, 292(2-3), 123-135.

Kouklis, P. D., Hutton, E. and Fuchs, E., 1994. Making a connection: direct binding between keratin intermediate filaments and desmosomal proteins. *Journal of Cell Biology*, 127(4), 1049-1060.

Koussounadis, A., Langdon, S. P., Um, I. H., Harrison, D. J. and Smith, V. A., 2015. Relationship between differentially expressed mRNA and mRNA-protein correlations in a xenograft model system. *Scientific Reports*, 5(1), 1-9.

Krishnaswamy, K., 2020. Traditional Indian spices and their health significance. *Asia Pacific Journal of Clinical Nutrition*, 17(S1), 265-268.

Kuboniwa, M., Hasegawa, Y., Mao, S., Shizukuishi, S., Amano, A., Lamont, R. J. and Yilmaz, Ö., 2008. *P. gingivalis* accelerates gingival epithelial cell progression through the cell cycle. *Microbes and Infection*, 10(2), 122-128.

Kuboniwa, M. and Lamont, R. J., 2010. Subgingival biofilm formation. *Periodontology 2000*, 52(1), 38-52.

Külekçi, G., Çiftçi, S., Keskin, F., Kiliç, A. O., Türkoğlu, S., Badur, S., Develioğlu, Ö. N., Leblebicioğlu, B. and Külekçi, M., 2001. PCR analysis of *Actinobacillus actinomycetemcomitans, Porphyromonas gingivalis, Treponema denticola* and *Fusobacterium nucleatum* in middle ear effusion. *Anaerobe*, 7(5), 241-246.

Kumazaki, K., Kishimoto, T., Furukawa, A., Mori, H., Tanaka, Y., Dohmae, N., Ishitani, R., Tsukazaki, T. and Nureki, O., 2014. Crystal structure of *Escherichia coli* YidC, a membrane protein chaperone and insertase. *Scientific Reports*, 4(1), 1-6.

Kurien, B. T., Dillon, S. P., Dorri, Y., D'Souza, A. and Scofield, R. H., 2010. Curcumin does not bind or intercalate into DNA and a note on the gray side of curcumin. *International Journal of Cancer*, 128(1), 242-245.

Kurien, B. T. and Scofield, R. H., 2007. Curcumin/turmeric solubilized in sodium hydroxide inhibits HNE protein modification—An in vitro study. *Journal of Ethnopharmacology*, 110(2), 368-373.

Kuttan, R., Sudheeran, P. C. and Josph, C. D., 1987. Turmeric and curcumin as topical agents in cancer therapy. *Tumori Journal*, 73(1), 29-31.

Kyuno, D., Yamaguchi, H., Itu, T., Kono, T., Kimura, Y., Imamura, M., Konno, T., Hirata, K., Sawada, N. and Kojima, T., 2014. Targeting tight junctions during epithelial to mesenchymal transition in human pancreatic cancer. *World Journal of Gastroenterology*, 20(31), 10813-10824.

Laalami, S., Zig, L. and Putzer, H., 2013. Initiation of mRNA decay in bacteria. *Cellular and Molecular Life Sciences*, 71(10), 1799-1828.

Lagdive, S. S., Marawar, P. P., Byakod, G. and Lagdive, S. B., 2013. Evaluation and comparison of interleukin-8 (IL-8) level in gingival crevicular fluid in health and severity of periodontal disease: A clinico-biochemical study. *Indian Journal of Dental Research*, 24(2), 188-192.

Lahn, M. M., Herbertz, S., Sawyer, J. S., Stauber, A. J., Gueorguieva, I., Driscoll, K. E., Estrem, S. T., Cleverly, A. L., Desaiah, D., Guba, S. C., Benhadji, K. A. and Slapak, C. A., 2015. Clinical development of galunisertib (LY2157299 monohydrate), a small molecule inhibitor of transforming growth factor-beta signaling pathway. *Drug Design, Development and Therapy*, 9(4), 4479-4499.

Laheij, A. M. G. A., de Soet, J. J., Veerman, E. C. I., Bolscher, J. G. M. and van Loveren, C., 2013. The influence of oral bacteria on epithelial cell migration in vitro. *Mediators of Inflammation*, 2013(154532), 1-6.

Lai, Y. and Chu, L., 2008. Novel mechanism for conditional aerobic growth of the anaerobic bacterium *Treponema denticola*. *Applied and Environmental Microbiology*, 74(1), 73-79.

Lamouille, S., Xu, J. and Derynck, R., 2014. Molecular mechanisms of epithelial–mesenchymal transition. *Nature Reviews Molecular Cell Biology*, 15(3), 178-196.

Lasserre, J. F., Brecx, M. C. and Toma, S., 2018. Oral microbes, biofilms and their role in periodontal and peri-implant diseases. *Materials*, 11(10), 1802-1819.

Lee, A. Y., Fan, C., Chen, Y., Cheng, C., Sung, Y., Hsu, C. and Kao, T., 2015. Curcumin inhibits invasiveness and epithelial-mesenchymal transition in oral squamous cell carcinoma through reducing matrix metalloproteinase 2, 9 and modulating p53-e-cadherin pathway. *Integrative Cancer Therapies*, 14(5), 484-490.

Lee, C., Chang, J. S., Syu, S., Wong, T., Chan, J. Y., Tang, Y., Yang, Z., Yang, W., Chen, C., Lu, S., Tang, P., Yang, T., Chu, P., Hsiao, J. and Liu, K., 2014. IL-1β promotes malignant transformation and tumor aggressiveness in oral cancer. *Journal of Cellular Physiology*, 230(4), 875-884.

Lee, J. M., Dedhar, S., Kalluri, R. and Thompson, E. W., 2006. The epithelial–mesenchymal transition: new insights in signaling, development, and disease. *Journal of Cell Biology*, 172(7), 973-981.

Lee, J., Roberts, J. S., Atanasova, K. R., Chowdhury, N., Han, K. and Yilmaz, Ö., 2017. Human primary epithelial cells acquire an epithelial-mesenchymal-transition phenotype during long-term infection by the oral opportunistic pathogen, *Porphyromonas gingivalis*. *Frontiers in Cellular and Infection Microbiology*, 7(493), 1-15.

Lee, S. F. and Davey, L., 2017. Disulfide bonds: a key modification in bacterial extracytoplasmic proteins. *Journal of Dental Research*, 96(13), 1465-1473.

Lee, S., Sowa, M. E., Watanabe, Y., Sigler, P. B., Chiu, W., Yoshida, M. and Tsai, F. T. S., 2003. The Structure of ClpB. *Cell*, 115(2), 229-240.

Lee, W., Loo, C., Bebawy, M., Luk, F., Mason, R. S. and Rohanizadeh, R., 2013. Curcumin and its derivatives: Their application in neuropharmacology and neuroscience in the 21st century. *Current Neuropharmacology*, 11(4), 338-378.

Lee, W. Y, Park, Y. and Ahn, J. K., 2007. Improvement of ergone production from mycelial culture of *Polyporus umbellatus*. *Mycobiology*, 35(2), 82-86.

Leite, F. R. M., Peres, M. A. and Nascimento, G. G., 2019. Is the misinterpretation of association and causation a never-ending story?. *Australian Dental Journal*, 64(2), 201-202.

Leoni, G., Neumann, P. A., Sumagin, R., Denning, T. L. and Nusrat, A., 2015. Wound repair: role of immune–epithelial interactions. *Mucosal Immunology*, 8(5), 959-968.

Leung, W. K., Wu, Q., Hannam, P. M., McBride, B. C. and Uitto, V., 2002. *Treponema denticola* may stimulate both epithelial proliferation and apoptosis through MAP kinase signal pathways. *Journal of Periodontal Research*, 37(6), 445-455.

Li, C., Yang, D., Cao, X., Wang, F., Hong, D., Wang, J., Shen, X. and Chen, Y., 2017a. Fibronectin induces epithelial-mesenchymal transition in human breast cancer MCF-7 cells via activation of calpain. *Oncology Letters*, 13(5), 3889-3895.

Li, L., Lee, C., Lin, C., Chen, N., Chuang, L., Hung, C. and Liu, Y., 2017b. Trichostatin A attenuates ventilation-augmented epithelial-mesenchymal transition in mice with bleomycin-induced acute lung injury by suppressing the Akt pathway. *PLOS ONE*, 12(2), e0172571.

Li, R., Ong, S. L., Tran, L. M., Jing, Z., Liu, B., Park, S. J., Huang, Z. L., Walser, T. C., Heinrich, E. L., Lee, G., Salehi-Rad, R., Crosson, W. P., Pagano, P. C., Paul, M. K., Xu, S., Herschman, H., Krysan, K. and Dubinett, S., 2020. Chronic IL-1β-induced inflammation regulates epithelial-to-mesenchymal transition memory phenotypes via epigenetic modifications in non-small cell lung cancer. *Scientific Reports*, 10(377), 1-15.

Li, S., Kendall, S. E., Raices, R., Finlay, J., Covarrubias, M., Liu, Z., Lowe, G., Lin, Y., Teh, Y. H., Leigh, V., Dhillon, S., Flanagan, S., Aboody, K. S. and Glackin, C. A., 2012. TWIST1 associates with NF-κB subunit RELA via carboxyl-terminal WR domain to promote cell autonomous invasion through IL8 production. *BMC Biology*, 10(73), 1-16.

Li, S. and Luo, W., 2019. Matrix metalloproteinase 2 contributes to aggressive phenotype, epithelial-mesenchymal transition and poor outcome in nasopharyngeal carcinoma. *OncoTargets and Therapy*, 12(5), 5701-5711.

Li, W., Jiang, Z., Xiao, X., Wang, Z., Wu, Z., Ma, Q. and Cao, L., 2018. Curcumin inhibits superoxide dismutase-induced epithelial-to-mesenchymal transition via the PI3K/Akt/NF-κB pathway in pancreatic cancer cells. *International Journal of Oncology*, 52(5),1593-1602.

Li, W., Ma, J., Ma, Q., Li, B., Han, L., Liu, J., Xu, Q., Duan, W., Yu, S., Wang, F. and Wu, E., 2013. Resveratrol inhibits the epithelial-mesenchymal transition of pancreatic cancer cells via suppression of the PI-3K/Akt/NF-κB pathway. *Current Medicinal Chemistry*, 20(33), 4185-4194.

Li, X., Huang, J., Yu, T., Fang, X., Lou, L., Xin, S., Ji, L., Jiang, F. and Lou, Y., 2021. *Fusobacterium nucleatum* promotes the progression of colorectal cancer through Cdk5-activated Wnt/β-Catenin signaling. *Frontiers in Microbiology*, 11(545251), 1-13.

Li, Y., Wang, L., Pappan, L., Galliher-Beckley, A. and Shi, J., 2012. IL-1β promotes stemness and invasiveness of colon cancer cells through Zeb1 activation. *Molecular Cancer*, 11(1), 87-100.

Li, Z., Gou, J., Jia, J. and Zhao, X., 2015. MicroRNA-429 functions as a regulator of epithelial–mesenchymal transition by targeting Pcdh8 during murine embryo implantation. *Human Reproduction*, 30(3), 507-518.

Liang, C., Park, A. Y. and Guan, J., 2007. In vitro scratch assay: a convenient and inexpensive method for analysis of cell migration in vitro. *Nature Protocols*, 2(2), 329-333.

Lin, C., Tsai, P., Kandaswami, C. C., Lee, P., Huang, C., Hwang, J. and Lee, M., 2011. Matrix metalloproteinase-9 cooperates with transcription factor Snail to induce epithelial-mesenchymal transition. *Cancer Science*, 102(4), 815-827.

Lin, Y., Liu, J., Huang, Y., Liu, D., Zhang, G. and Kan, H., 2017. MicroRNA-489 plays an anti-metastatic role in human hepatocellular carcinoma by targeting matrix metalloproteinase-7. *Translational Oncology*, 10(2), 211-220.

Listgarten, M. A. and Hellden, L., 1978. Relative distribution of bacteria at clinically healthy and periodontally diseased sites in humans. *Journal of Clinical Periodontology*, 5(2), 115-132.

Liu, C., Lin, H., Tang, M. and Wang, Y., 2015. Vimentin contributes to epithelial-mesenchymal transition cancer cell mechanics by mediating cytoskeletal organization and focal adhesion maturation. *Oncotarget*, 6(18), 15966-15983.

Liu, H., Mao, Y., Xia, B., Long, C., Kuang, X., Huang, H., Ning, J., Ma, X., Zhang, H., Wang, R., Tang, H., Du, H., Yan, J., Zhang, Q., Zhang, X. and Shen, H., 2020. Curcumin inhibits proliferation and epithelial-mesenchymal transition in lens epithelial cells through multiple pathways. *BioMed Research International*, 2020, 1-11.

Liu, H., Zhang, X., Fan, T., Li, Y., Zhang, K., Ma, S., Song, Y., Xu, J., Wang, X., Wang, F. and Guan, F., 2018. Enhanced efficacy of combined tm with cisplatin targeting esophageal squamous cell carcinoma via suppressing stat3 signaling pathway. *SSRN Electronic Journal*, 11(1), 1-41.

Liu, M., Liu, Q., Fan, S., Su, F., Jiang, C., Cai, G., Wang, Y., Liao, G., Lei, X., Chen, W., Bi, J., Cheng, W., Zhao, L., Ruan, Y. and Li, J., 2021. LncRNA LTSCCAT promotes tongue squamous cell carcinoma metastasis via targeting the miR-103a-2-5p/SMYD3/TWIST1 axis. *Cell Death & Disease*, 12(144), 1-16.

Liu, W. and Saint, D. A., 2002. A new quantitative method of real time reverse transcription polymerase chain reaction assay based on simulation of polymerase chain reaction kinetics. *Analytical Biochemistry*, 302(1), 52-59.

Liu, L., Wang, Y., Yan, R., Li, S., Shi, M., Xiao, Y. and Guo, B., 2016a. Oxymatrine inhibits renal tubular EMT induced by high glucose via upregulation of SnoN and inhibition of TGF-β1/Smad signaling pathway. *PLOS ONE*, 11(3), e0151986.

Liu, S., Gao, M., Wang, X., Ding, S., Lv, J., Gao, D., Wang, Z. and Niu, Z., 2016b. Ubenimex attenuates acquired sorafenib resistance in renal cell carcinoma by inhibiting Akt signaling in a lipophagy associated mechanism. *Oncotarget*, 7(48), 79141-79153.

Lo, H., Hsu, S., Xia, W., Cao, X., Shih, J., Wei, Y., Abbruzzese, J. L., Hortobagyi, G. N. and Hung, M., 2007. Epidermal growth factor receptor cooperates with signal transducer and activator of transcription 3 to induce epithelial-mesenchymal transition in cancer cells via up-regulation of TWIST gene expression. *Cancer Res.*, 67(19), 9066-9076.

Lochter, A., Galosy, S., Muschler, J., Freedman, N., Werb, Z. and Bissell, M. J., 1997. Matrix metalloproteinase stromelysin-1 triggers a cascade of molecular alterations that leads to stable epithelial-to-mesenchymal conversion and a premalignant phenotype in mammary epithelial cells. *Journal of Cell Biology*, 139(7), 1861-1872.

Lockhart, P. B., Bolger, A. F., Papapanou, P. N., Osinbowale, O., Trevisan, M., Levison, M. E., Taubert, K. A., Newburger, J. W., Gornik, H. L., Gewitz, M. H., Wilson, W. R., Smith, S. C. and Baddour, L. M., 2012. Periodontal disease and atherosclerotic vascular disease: Does the evidence support an independent association?. *Circulation*, 125(20), 2520-2544.

LoConte, N. K., Razak, A. R. A., Ivy, P., Tevaarwerk, A., Leverence, R., Kolesar, J., Siu, L., Lubner, S. J., Mulkerin, D. L., Schelman, W. R., Deming, D. A., Holen, K. D., Carmichael, L., Eickhoff, J. and Liu, G., 2014. A multicenter phase 1 study of γ -secretase inhibitor RO4929097 in combination with capecitabine in refractory solid tumors. *Investigational New Drugs*, 33(1), 169-176.

Loesche, W. J., 1969. Oxygen sensitivity of various anaerobic bacteria. *Applied Microbiology*, 18(5), 723-727.

Loesche, W. J., Syed, S. A., Schmidt, E. and Morrison, E. C., 1985. Bacterial profiles of subgingival plaques in periodontitis. *Journal of Periodontology*, 56(8), 447-456.

Loh, C., Chai, J. Y., Tang, T. F., Wong, W. F., Sethi, G., Shanmugam, M. K., Chong, P. P. and Looi, C. Y., 2019. The E-Cadherin and N-Cadherin switch in epithelial-to-mesenchymal transition: signaling, therapeutic implications, and challenges. *Cells*, 8(10), 1118-1151.

Long, X., Ye, Y., Zhang, L., Liu, P., Yu, W., Wei, F., Ren, X. and Yu, J., 2015. IL-8, a novel messenger to cross-link inflammation and tumor EMT via autocrine and paracrine pathways (Review). *International Journal of Oncology*, 48(1), 5-12.

Loos, B. G., Craandijk, J., Hoek, F. J., Dillen, P. M. W. and Velden, U. V., 2000. Elevation of systemic markers related to cardiovascular diseases in the peripheral blood of periodontitis patients. *Journal of Periodontology*, 71(10), 1528-1534.

Lopez-Castejon, G. and Brough, D., 2011. Understanding the mechanism of IL-1β secretion. *Cytokine & Growth Factor Reviews*, 22(4), 189-195.

Lu, W., Gu, J., Zhang, Y., Gong, D., Zhu, Y. and Sun, Y., 2018. Tolerance induced by *Porphyromonas gingivalis* may occur independently of TLR2 and TLR4. *PLOS ONE*, 13(7), e0200946.

Luca, M., Huang, S., Gershenwald, J. E., Singh, R. K., Reich, R. and Bar-Eli, M., 1997. Expression of interleukin-8 by human melanoma cells up-regulates MMP-2 activity and increases tumor growth and metastasis. *The American Journal of Pathology*, 151(4), 1105-1113.

Lüders, S., Fallet, C. and Franco-Lara, E., 2009. Proteome analysis of the *Escherichia coli* heat shock response under steady-state conditions. *Proteome Science*, 7(1), 36-51.

Lynch, C. C., Vargo-Gogola, T., Matrisian, L. M. and Fingleton, B., 2010. Cleavage of E-cadherin by matrix metalloproteinase-7 promotes cellular proliferation in nontransformed cell lines via activation of RhoA. *Journal of Oncology*, 10(530745), 1-11.

Ma, C., Luo, H., Gao, F., Tang, Q. and Chen, W., 2018. *Fusobacterium nucleatum* promotes the progression of colorectal cancer by interacting with E-cadherin. *Oncology Letters*, 16(2), 2609-2610.

Mahendra, J., Mahendra, L., Felix, J. and Romanos, G., 2013. Prevelance of periodontopathogenic bacteria in subgingival biofilm and atherosclerotic plaques of patients undergoing coronary revascularization surgery. *Journal of Indian Society of Periodontology*, 17(6), 719-724.

Makela, M., Salo, T., Uitto, V. J. and Larjava, H., 1994. Matrix metalloproteinases (MMP-2 and MMP-9) of the oral cavity: Cellular origin and relationship to periodontal status. *Journal of Dental Research*, 73(8), 1397-1406.

Maldonado, R. F., Sá-Correia, I. and Valvano, M. A., 2016. Lipopolysaccharide modification in Gram-negative bacteria during chronic infection. *FEMS Microbiology Reviews*, 40(4), 480-493.

Manouchehr-Pour, M., Spagnuolo, P. J., Rodman, H. M. and Bissada, N. F., 1981. Comparison of neutrophil chemotactic response in diabetic patients with mild and severe periodontal disease. *Journal of Periodontology*, 52(8), 410-415.

Marincola, G., Schäfer, T., Behler, J., Bernhardt, J., Ohlsen, K., Goerke, C. and Wolz, C., 2012. RNase Y of *Staphylococcus aureus* and its role in the activation of virulence genes. *Molecular Microbiology*, 85(5), 817-832.

Markov, A. G., Aschenbach, J. R. and Amasheh, S., 2015. Claudin clusters as determinants of epithelial barrier function. *IUBMB Life*, 67(1), 29-35.

Martinho, F. C, Leite, F. R. M., Nóbrega, L. M. M., Endo, M. S., Nascimento, G. G., Darveau, R. P. and Gomes, B. P. F. A., 2016. Comparison of *Fusobacterium nucleatum* and *Porphyromonas gingivalis* lipopolysaccharides clinically isolated from root canal infection in the induction of pro-inflammatory cytokines secretion. *Brazilian Dental Journal*, 27(2), 202-207.

Maschler, S., Wirl, G., Spring, H., Bredow, D. V., Sordat, I., Beug, H. and Reichmann, E., 2005. Tumor cell invasiveness correlates with changes in integrin expression and localization. *Oncogene*, 24(12), 2032-2041.

Masola, V., Carraro, A., Granata, S., Signorini, L., Bellin, G., Violi, P., Lupo, A., Tedeschi, U., Onisto, M., Gambaro, G. and Zaza, G., 2019. In vitro effects of interleukin (IL)-1 beta inhibition on the epithelial-to-mesenchymal transition (EMT) of renal tubular and hepatic stellate cells. *Journal of Translational Medicine*, 17(12), 1-11.

Mathews, S., Prasad, T., Venugopa, B., Azad Palakkan, A., Kumar, A. P. R. and Kumary, T. V., 2017. Standardizing transdifferentiation of rabbit bone marrow mesenchymal stem cells to corneal lineage by simulating corneo-limbal cues. *Journal of Stem Cell Research and Medicine*, 2(2), 1-10.

Mathsyaraja, H. and Ostrowski, M. C., 2012. Setting Snail2's pace during EMT. *Nature Cell Biology*, 14(11), 1122-1123.

McHarg, S., Hopkins, G., Lim, L. and Garrod, D., 2014. Down-Regulation of desmosomes in cultured cells: the roles of PKC, microtubules and lysosomal/proteasomal degradation. *PLoS ONE*, 9(10), e108570.

Mealey, B. L. and Ocampo, G. L., 2007. Diabetes mellitus and periodontal disease. *Periodontology 2000*, 44(1), 127-153.

Medici, D. and Nawshad, A., 2010. Type I collagen promotes epithelial–mesenchymal transition through ILK-dependent activation of NF-κB and LEF-1. *Matrix Biology*, 29(3), 161-165.

Medzhitov, R. and Janeway, C., 2000. Innate immunity. *New England Journal of Medicine*, 343(5), 338-44.

Meibom, K. L., Dubail, I., Dupuis, M., Barel, M., Lenco, J., Stulik, J., Golovliov, I., Sjöstedt, A. and Charbit, A., 2008. The heat-shock protein ClpB of *Francisella tularensis* is involved in stress tolerance and is required for multiplication in target organs of infected mice. *Molecular Microbiology*, 67(6), 1384-1401.

Meng, J., Chen, S., Han, J., Qian, B., Wang, X., Zhong, W., Qin, Y., Zhang, H., Gao, W., Lei, Y., Yang, W., Yang, L., Zhang, C., Liu, H., Liu, Y., Zhou, H., Sun, T. and Yang, C., 2018. Twist1 regulates vimentin through Cul2 circular RNA to promote EMT in hepatocellular carcinoma. *Cancer Research*, 78(15), 4150-4162.

Mettraux, G. R., Gusberti, F. A. and Graf, H., 1983. Oxygen tension (pO2) in untreated human periodontal pockets. *Journal of Periodontology*, 55(9), 516-521.

Miles, A. A., Misra, S. S. and Irwin, J. O., 1938. The estimation of the bactericidal power of the blood. *Epidemiology and Infection*, 38(6), 732-749.

Millar, H. J., Nemeth, J. A., McCabe, F. L., Pikounis, B. and Wickstrom, E., 2008. Circulating human interleukin-8 as an indicator of cancer progression in a nude rat orthotopic human non–small cell lung carcinoma model. *Cancer Epidemiology Biomarkers & Prevention*, 17(8), 2180-2187.

Milward, M. R., Chapple, I. L. C., Wright, H. J., Millard, J. L., Matthews, J. B. and Cooper, P. R., 2007. Differential activation of NF-κB and gene expression in oral epithelial cells by periodontal pathogens. *Clinical & Experimental Immunology*, 148(2), 307-324.

Mintz, K. P. and Fives-Taylor, P. M., 1994. Adhesion of *Actinobacillus actinomycetemcomitans* to a human oral cell line. *Infection and Immunity*, 62(9), 3672-3678.

Mise, N., Savai, R., Yu, H., Schwarz, J., Kaminski, N. and Eickelberg, O., 2012. Zyxin is a transforming growth factor-β (TGF-β)/Smad3 target gene that regulates lung cancer cell motility via integrin α5β1. *Journal of Biological Chemistry*, 287(37), 31393-31405.

Miyamoto, M., Ishihara, K. and Okuda, K., 2006. The *Treponema denticola* surface protease dentilisin degrades interleukin-1β (IL-1β), IL-6, and tumor necrosis factor alpha. *Infection and Immunity*, 74(4), 2462-2467.

Mohan, A., Schlue, K. T., Kniffin, A. F., Mayer, C. R., Duke, A. A., Narayanan, V., Arsenovic, P. T., Bathula, K., Danielsson, B. E., Dumbali, S. P., Maruthamuthu, V. and Conway, D. E., 2018. Spatial proliferation of epithelial cells is regulated by E-cadherin force. *Biophysical Journal*, 115(5), 853-864.

Mohankumar, K., Sridharan, S., Pajaniradje, S., Singh, V. K., Ronsard, L., Banerjea, A. C., Somasundaram, D. B., Coumar, M. S., Periyasamy, L. and Rajagopalan, R., 2015. BDMC-A, an analog of curcumin, inhibits markers of invasion, angiogenesis, and metastasis in breast cancer cells via NF-κB pathway—A comparative study with curcumin. *Biomedicine & Pharmacotherapy*, 74, 178-186.

Moon, J. H., Lee, S. H. and Lim, Y. C., 2021. Wnt/β-catenin/Slug pathway contributes to tumor invasion and lymph node metastasis in head and neck squamous cell carcinoma. *Clinical & Experimental Metastasis*, 38(2), 163-174.

Moreno, S. and Contreras, A., 2013. Functional differences of *Porphyromonas gingivalis* fimbriae in determining periodontal disease pathogenesis: A literature review. *Colombia Medica*, 44(1), 48-56.

Morita, T., Mayanagi, T. and Sobue, K., 2007. Dual roles of myocardin-related transcription factors in epithelial–mesenchymal transition via slug induction and actin remodeling. *Journal of Cell Biology*, 179(5), 1027-1042.

Mukherjee, S., Mazumdar, M., Chakraborty, S., Manna, A., Saha, S., Khan, P., Bhattacharjee, P., Guha, D., Adhikary, A., Mukhjerjee, S. and Das, T., 2014. Curcumin inhibits breast cancer stem cell migration by amplifying the E-cadherin/β-catenin negative feedback loop. *Stem Cell Research & Therapy*, 5(5), 116-135.

Munshi, R. M., 2017. *The Association between Fusobacterium nucleatum Outer Membrane Vesicles and Colonic Cancer*. PhD Thesis, Trinity College Dublin, Dublin.

Mylavarapu, S., Kumar, H., Kumari, S., Sravanthi, L. S., Jain, M., Basu, A., Biswas, M., Mylavarapu, S. V. S., Das, A. and Roy, M., 2019. Activation of epithelial-mesenchymal transition and altered β-catenin signaling in a novel indian colorectal carcinoma cell line. *Frontiers in Oncology*, 9(54), 1-16.

Nagamori, S., Smirnova, I. N. and Kaback, H. R., 2004. Role of YidC in folding of polytopic membrane proteins. *Journal of Cell Biology*, 165(1), 53-62.

Nagase, H., Visse, R. and Murphy, G., 2006. Structure and function of matrix metalloproteinases and TIMPs. *Cardiovascular Research*, 69(3), 562-573.

Nagata, M., Kaito, C. and Sekimizu, K., 2008. Phosphodiesterase Activity of CvfA Is Required for Virulence in *Staphylococcus aureus*. *Journal of Biological Chemistry*, 283(4), 2176-2184.

Nakanishi, C. and Toi, M., 2005. Nuclear factor-κB inhibitors as sensitizers to anticancer drugs. *Nature Reviews Cancer*, 5(4), 297-309.

Nelson, C. M., Khauv, D., Bissell, M. J. and Radisky, D. C., 2008. Change in cell shape is required for matrix metalloproteinase-induced epithelial-mesenchymal transition of mammary epithelial cells. *Journal of Cellular Biochemistry*, 105(1), 25-33.

Ng, H., Slakeski, N., Butler, C. A., Veith, P. D., Chen, Y., Liu, S. W., Hoffmann, B., Dashper, S. G. and Reynolds, E. C., 2019. The role of *Treponema denticola* motility in synergistic biofilm formation with Porphyromonas gingivalis. *Frontiers in Cellular and Infection Microbiology*, 9(432), 1-15.

Nistico, P., Bissell, M. J. and Radisky, D. C., 2012. Epithelial-mesenchymal transition: general principles and pathological relevance with special emphasis on the role of matrix metalloproteinases. *Cold Spring Harbor Perspectives in Biology*, 4(2), 1-10.

Noble, W. S., 2009. How does multiple testing correction work?. *Nature Biotechnology*, 27(12), 1135-1137.

Nociti, F. H., Casati, M. Z. and Duarte, P. M., 2014. Current perspective of the impact of smoking on the progression and treatment of periodontitis. *Periodontology 2000*, 67(1), 187-210.

Nonaka, S. and Nakanishi, H., 2020. Secreted gingipains from *Porphyromonas gingivalis* induce microglia migration through endosomal signaling by protease-activated receptor 2. *Neurochemistry International*, 140(104840), 1-9.

Nwaokorie, F. O., Coker, A. O., Ogunsola, F. T., Avila-Campos, M. J., Jardim, E., Ayanbadejo, P. O., Umeizudike, K. A. and Taiwo, A. O., 2011. Isolation and molecular identification of *Fusobacterium nucleatum* from Nigerian patients with oro-facial infections. *West African journal of medicine*, 30(2), 125-129.

Ohbayashi, M., Kubota, S., Kawase, A., Kohyama, N., Kobayashi, Y. and Yamamoto, T., 2014. Involvement of epithelial-mesenchymal transition in methotrexate-induced pulmonary fibrosis. *The Journal of Toxicological Sciences*, 39(2), 319-330.

Ohnishi, Y., Sakamoto, T., Zhengguang, L., Yasui, H., Hamada, H., Kubo, H. and Nakajima, M., 2020. Curcumin inhibits epithelial-mesenchymal transition in oral cancer cells via c-Met blockade. *Oncology Letters*, 19(6), 4177-4182.

Oido-Mori, M., Rezzonico, R., Wang, P. L., Kowashi, Y., Dayer, J. M., Baehni, P. C. and Chizzolini, C., 2001. *Porphyromonas gingivalis* gingipain-R enhances interleukin-8 but decreases gamma interferon-inducible protein 10 production by human gingival fibroblasts in response to T-cell contact. *Infection and Immunity*, 69(7), 4493-4501.

Okuda, T., Kimizuka, R., Miyamoto, M., Kato, T., Yamada, S., Okuda, K. and Ishihara, K., 2007. *Treponema denticola* induces interleukin-8 and macrophage chemoattractant protein 1 production in human umbilical vein epithelial cells. *Microbes and Infection*, 9(7), 907-913.

Osterreicher, C. H., Penz-Osterreicher, M., Grivennikov, S. I., Guma, M., Koltsova, E. K., Datz, C., Sasik, R., Hardiman, G., Karin, M. and Brenner, D. A., 2010. Fibroblast-specific protein 1 identifies an inflammatory subpopulation of macrophages in the liver. *Proceedings of the National Academy of Sciences*, 108(1), 308-313.

Owusu-Akyaw, A., Krishnamoorthy, K., Goldsmith, L. T. and Morelli, S. S., 2018. The role of mesenchymal–epithelial transition in endometrial function. *Human Reproduction Update*, 25(1), 114-133.

Page, R. C. and Schroeder, H. E., 1976. Pathogenesis of inflammatory periodontal disease. A summary of current work. *Laboratory Investigation*, 34(3), 235-249.

Palm, E., Khalaf, H. and Bengtsson, T., 2014. Suppression of inflammatory responses of human gingival fibroblasts by gingipains from *Porphyromonas gingivalis*. *Molecular Oral Microbiology*, 30(1), 74-85.

Palmer, L. J., 2010. *Neutrophil extracellular traps in periodontitis*. PhD thesis, University of Birmingham, Birmingham.

Pan, Y., Teng, D., Burke, A. C., Haase, E. M. and Scannapieco, F. A., 2009. Oral bacteria modulate invasion and induction of apoptosis in HEp-2 cells by Pseudomonas aeruginosa. *Microbial Pathogenesis*, 46(2), 73-79.

Panahi, Y., Hosseini, M., Khalili, N., Naimi, E., Simental-Mendía, L. E., Majeed, M. and Sahebkar, A., 2016. Effects of curcumin on serum cytokine concentrations in subjects with metabolic syndrome: A post-hoc analysis of a randomized controlled trial. *Biomedicine & Pharmacotherapy*, 82(1), 578-582.

Park, J. and Schwarzbauer, J. E., 2013. Mammary epithelial cell interactions with fibronectin stimulate epithelial-mesenchymal transition. *Oncogene*, 33(13), 1649-1657.

Pavel, M., Renna, M., Park, S. J., Menzies, F. M., Ricketts, T., Füllgrabe, J., Ashkenazi, A., Frake, R. A., Lombarte, A. C., Bento, C. F., Franze, K. and Rubinsztein, D. C., 2018. Contact inhibition controls cell survival and proliferation via YAP/TAZ-autophagy axis. *Nature Communications*, 9(1), 1-17.

Peinado, H., Olmeda, D. and Cano, A., 2007. Snail, Zeb and bHLH factors in tumour progression: an alliance against the epithelial phenotype?. *Nature Reviews Cancer*, 7(6), 415-428.

Peinado, H., Quintanilla, M. and Cano, A., 2003. Transforming growth factor β-1 induces snail transcription factor in epithelial cell lines. *Journal of Biological Chemistry*, 278(23), 21113-21123.

Petersen, M., Thorikay, M., Deckers, M., van Dinther, M., Grygielko, E. T., Gellibert, F., de Gouville, A. C., Huet, S., ten Dijke, P. and Laping, N. J., 2008. Oral administration of GW788388, an inhibitor of TGF-β type I and II receptor kinases, decreases renal fibrosis. *Kidney International*, 73(6), 705-715.

Pfaffl, M. W., Tichopad, A., Prgomet, C. and Neuvians, T. P., 2004. Determination of stable housekeeping genes, differentially regulated target genes and sample integrity: BestKeeper – Excel-based tool using pair-wise correlations. *Biotechnology Letters*, 26(6), 509-515.

Pinnock, A., Murdoch, C., Moharamzadeh, K., Whawell, S. and Douglas, C. W. I., 2014. Characterisation and optimisation of organotypic oral mucosal models to study Porphyromonas gingivalis invasion. *Microbes and Infection*, 16(4), 310-319.

Pirola, L. and Fröjdö, S., 2008. Resveratrol: One molecule, many targets. *IUBMB Life*, 60(5), 323-332.

Platania, C. B. M., Fidilio, A., Lazzara, F., Piazza, C., Geraci, F., Giurdanella, G., Leggio, G. M., Salomone, S., Drago, F. and Bucolo, C., 2018. Retinal protection and distribution of curcumin in vitro and in vivo. *Frontiers in Pharmacology*, 9(670), 1-10.

Power, M. E., Tilman, D., Estes, J. A., Menge, B. A., Bond, W. J., Mills, L. S., Daily, G., Castilla, J. C., Lubchenco, J. and Paine, R. T., 1996. Challenges in the Quest for Keystones. *BioScience*, 46(8), 609-620.

Prakash, V., Carson, B. B., Feenstra, J. F., Dass, R. A., Sekyrova, P., Hoshino, A., Petersen, J., Guo, Y., Parks, M. M., Kurylo, C. M., Batchelder, J. E., Haller, K., Hashimoto, A., Rundqivst, H., Condeelis, J. S., Allis, C. D., Drygin, D., Nieto, M. A., Andäng, M., Percipalle, P., Bergh, J., Adameyko, I., Farrants, A. Ö., Hartman, J., Lyden, D., Pietras, K., Blanchard, S. C. and Vincent, C. T., 2019. Ribosome biogenesis during cell cycle arrest fuels EMT in development and disease. *Nature Communications*, 10(2110), 1-16.

Prasad, S. and Aggarwal, B. B., 2011. *Herbal medicine: Biomolecular and clinical aspects*. 2nd ed. Boca Raton (FL): CRC Press/Taylor & Francis, pp.263-285.

Preshaw, P. M., 2015. Detection and diagnosis of periodontal conditions amenable to prevention. *BMC Oral Health*, 15(S1), 1-11.

Preshaw, P. M., Alba, A. L., Herrera, D., Jepsen, S., Konstantinidis, A., Makrilakis, K. and Taylor, R., 2011. Periodontitis and diabetes: a two-way relationship. *Diabetologia*, 55(1), 21-31.

Presland, R. B. and Dale, B. A., 2000. Epithelial structural proteins of the skin and oral cavity: function in health and disease. *Critical Reviews in Oral Biology & Medicine*, 11(4), 383-408.

Prieto-García, E., Díaz-García, C. V., García-Ruiz, I. and Agulló-Ortuño, M. T., 2017. Epithelial-to-mesenchymal transition in tumor progression. *Medical Oncology*, 34(7), 122-130.

Prime, S. S., Nixon, S. V., Crane, I. J., Stone, A., Matthews, J. B., Maitland, N. J., Remnant, L., Powell, S. K., Game, S. M. and Scully, C., 1990. The behaviour of human oral squamous cell carcinoma in cell culture. *The Journal of Pathology*, 160(3), 259-269.

Priyadarsini, K. I., 2014. The chemistry of curcumin: from extraction to therapeutic agent. *Molecules*, 19(12), 20091-20112.

Prucksunand, C., Indrasukhsri, B., Leethochawalit, M. and Hungspreugs, K., 2001. Phase II clinical trial on effect of the long turmeric (Curcuma longa Linn.) on healing of peptic ulcer. *The Southeast Asian Journal of Tropical Medicine and Public Health*, 32(1), 208-215.

Qi, Y., Jiao, Y., Chen, P., Kong, J., Gu, B., Liu, K., Feng, D., Zhu, Y., Ruan, H., Lan, Z., Liu, Q., Mi, Y., Guo, X., Wang, M., Liang, G., Lamont, R. J., Wang, H., Zhou, F., Feng, X. and Gao, S., 2020. *Porphyromonas gingivalis* promotes progression of esophageal squamous cell cancer via TGFβ-dependent Smad/YAP/TAZ signaling. *PLOS Biology*, 18(9), e3000825.

Quan, J., Elhousiny, M., Johnson, N. W. and Gao, J., 2013. Transforming growth factor-β1 treatment of oral cancer induces epithelial-mesenchymal transition and promotes bone invasion via enhanced activity of osteoclasts. *Clinical & Experimental Metastasis*, 30(5), 659-670.

Rabinovitz, I., Toker, A. and Mercurio, A. M., 1999. Protein Kinase C–Dependent Mobilization of the α6β4 Integrin from Hemidesmosomes and Its Association with Actin-Rich Cell Protrusions Drive the Chemotactic Migration of Carcinoma Cells. *Journal of Cell Biology*, 146(5), 1147-1160.

Rafiee, P., Nelson, V. M., Manley, S., Wellner, M., Floer, M., Binion, D. G. and Shaker, R., 2009. Effect of curcumin on acidic pH-induced expression of IL-6 and IL-8 in human esophageal epithelial cells (HET-1A): role of PKC, MAPKs, and NF-κB. *American Journal of Physiology-Gastrointestinal and Liver Physiology*, 296(2), G388-G398.

Renner, G., Noulet, F., Mercier, M., Choulier, L., Etienne-Selloum, N., Gies, J., Lehmann, M., Lelong-Rebel, I., Martin, S. and Dontenwill, M., 2016. Expression/activation of α5β1 integrin is linked to the β-catenin signaling pathway to drive migration in glioma cells. *Oncotarget*, 7(38), 62194-62207.

Ricono, J. M., Huang, M., Barnes, L. A., Lau, S. K., Weis, S. M., Schlaepfer, D. D., Hanks, S. K. and Cheresh, D. A., 2009. Specific cross-talk between epidermal growth factor receptor and integrin v 5 promotes carcinoma cell invasion and metastasis. *Cancer Research*, 69(4), 1383-1391.

Ridley, A. J., 2011. Life at the leading edge. *Cell*, 145(7), 1012-1022.

Riedel, C., Förstner, K. U., Püning, C., Alter, T., Sharma, C. M. and Gölz, G., 2020. Differences in the Transcriptomic Response of *Campylobacter coli* and *Campylobacter lari* to Heat Stress. *Frontiers in Microbiology*, 11(523), 1-13.

Roche Diagnostics GmbH, 2011, *RealTime ready RT-qPCR assay development and qualification*. Available at: https://www.bionity.com/en/whitepapers/126309/realtime-ready-rt-qpcr-assay-development-and-qualification.html (Accessed: 07 January 2021).

Rofstad, E. K. and Halsør, E. F., 2000. Vascular endothelial growth factor, interleukin 8, platelet-derived endothelial cell growth factor, and basic fibroblast growth factor promote angiogenesis and metastasis in human melanoma xenografts. *Cancer Research*, 60(17), 4932-4938.

Rolfe, R. D., Hentges, D. J., Campbell, B. J. and Barrett, J. T., 1978. Factors related to the oxygen tolerance of anaerobic bacteria. *Applied and Environmental Microbiology*, 36(2), 306-313.

Rosen, G., Genzler, T. and Sela, M. N., 2008. Coaggregation of *Treponema denticola* with *Porphyromonas gingivalis* and *Fusobacterium nucleatum* is mediated by the major outer sheath protein of *Treponema denticola*. *FEMS Microbiology Letters*, 289(1), 59-66.

Rosen, G., Sela, M. N., Naor, R., Halabi, A., Barak, V. and Shapira, L., 1999. Activation of murine macrophages by lipoprotein and lipooligosaccharide of *Treponema denticola*. *Infection and Immunity*, 67(3), 1180-1186.

Rosenberg, B., Kemeny, G., Switzer, R. C. and Hamilton, T. C., 1971. Quantitative evidence for protein denaturation as the cause of thermal death. *Nature*, 232(5311), 471-473.

Rubinstein, M. R., Wang, X., Liu, W., Hao, Y., Cai, G. and Han, Y. W., 2013. *Fusobacterium nucleatum* promotes colorectal carcinogenesis by modulating E-cadherin/β-catenin signaling via its FadA adhesin. *Cell Host & Microbe*, 14(2), 195-206.

Russell, A. D., 2003. Lethal effects of heat on bacterial physiology and structure. *Science Progress*, 86(1-2), 115-137.

Russell, A. D. and Harries, D., 1967. Some aspects of thermal injury in *Escherichia coli*. *Applied Microbiology*, 15(2), 407-410.

Ryan, K. J. and Ray, C. G., 2003. *Spirochetes*. Sherris Medical Microbiology. 4th ed. New York, USA: McGraw-Hill Professional Publishing, pp.421-438.

Saito, A., Inagaki, S. and Ishihara, K., 2009. Differential ability of periodontopathic bacteria to modulate invasion of human gingival epithelial cells by Porphyromonas gingivalis. *Microbial Pathogenesis*, 47(6), 329-333.

Saller, M. J., Wu, Z. C., de Keyzer, J. and Driessen, A. J. M., 2012. The YidC/Oxa1/Alb3 protein family: common principles and distinct features. *Biological Chemistry*, 393(11), 1279-1290.

Salvi, G. E., Yalda, B., Collins, J. G., Jones, B. H., Smith, F. W., Arnold, R. R. and Offenbacher, S., 1997. inflammatory mediator response as a potential risk marker for periodontal diseases in insulin-dependent diabetes mellitus patients. *Journal of Periodontology*, 68(2), 127-135.

Samiei, M., Ahmadian, E., Eftekhari, A., Eghbal, M. A., Rezaie, F. and Vinken, M., 2019. Cell junctions and oral health. *EXCLI Journal*, 18(1), 317-330.

Sastrowijoto, S. H., Hillemans, P., Steenbergen, T. J., Abraham-Inpijn, L. and Graaff, J., 1989. Periodontal condition and microbiology of healthy and diseased periodontal pockets in type 1 diabetes mellitus patients. *Journal of Clinical Periodontology*, 16(5), 316-322.

Sauka-Spengler, T. and Bronner-Fraser, M., 2008. A gene regulatory network orchestrates neural crest formation. *Nature Reviews Molecular Cell Biology*, 9(7), 557-568.

Savagner, P., 2010. The epithelial-mesenchymal transition (EMT) phenomenon. *Annals of Oncology*, 21(S7), 89-92.

Scanlon, C. S., Van Tubergen, E. A., Inglehart, R. C. and D'Silva, N. J., 2012. Biomarkers of epithelial-mesenchymal transition in squamous cell carcinoma. *Journal of Dental Research*, 92(2), 114-121.

Scapoli, L., Girardi, A., Palmieri, A., Testori, T., Zuffetti, F., Monguzzi, R., Lauritano, D. and Carinci, F., 2012. Microflora and periodontal disease. *Dental Research Journal*, 9(s), 202-206.

Schaller, M., Zakikhany, K., Naglik, J. R., Weindl, G. and Hube, B., 2006. Models of oral and vaginal candidiasis based on in vitro reconstituted human epithelia. *Nature Protocols*, 1(6), 2767-2773.

Scheau, C., Badarau, I. A., Costache, R., Caruntu, C., Mihai, G. L., Didilescu, A. C., Constantin, C. and Neagu, M., 2019. The role of matrix metalloproteinases in the epithelial-mesenchymal transition of hepatocellular carcinoma. *Analytical Cellular Pathology*, 30(1), 1-10.

Schneider, C. A., Rasband, W. S. and Eliceiri, K. W., 2012. NIH image to ImageJ: 25 years of image analysis. *Nature Methods*, 9(7), 671-675.

Schroeder, H. E. and Listgarten, M. A., 1997. The gingival tissues: the architecture of periodontal protection. *Periodontology 2000*, 13(1), 91-120.

Schroeder, H. E., Münzel-Pedrazzoli, S. and Page, R. C., 1973. Correlated morphometric and biochemical analysis of gingival tissue in early chronic gingivitis in man. *Archives of Oral Biology*, 18(7), 899-923.

Serek, J., Bauer-Manz, G., Struhalla, G., van den Berg, L., Kiefer, D., Dalbey, R. and Kuhn, A., 2004. *Escherichia coli* YidC is a membrane insertase for Sec-independent proteins. *The EMBO Journal*, 23(2), 294-301.

Serrano-Gomez, S. J., Maziveyi, M. and Alahari, S. K., 2016. Regulation of epithelial-mesenchymal transition through epigenetic and post-translational modifications. *Molecular Cancer*, 15(1), 1-14.

Shah, P. P., Fong, M. Y. and Kakar, S. S., 2011. PTTG induces EMT through integrin αVβ3-focal adhesion kinase signaling in lung cancer cells. *Oncogene*, 31(26), 3124-3135.

Shahzad, M. M., Arevalo, J. M., Armaiz-Pena, G. N., Lu, C., Stone, R. L., Moreno-Smith, M., Nishimura, M., Lee, J. W., Jennings, N. B., Bottsford-Miller, J., Vivas-Mejia, P., Lutgendorf, S. K., Lopez-Berestein, G., Bar-Eli, M., Cole, S. W. and Sood, A. K., 2018. Stress effects on FosB and interleukin-8 (IL8)-driven ovarian cancer growth and metastasis. *Journal of Biological Chemistry*, 293(26), 35462-35470.

Shchipkova, A. Y., Nagaraja, H. N. and Kumar, P. S., 2010. Subgingival microbial profiles of smokers with periodontitis. *Journal of Dental Research*, 89(11), 1247-1253.

Shen, X., Yang, Y., Xiao, T., Peng, J. and Liu, X., 2011. Protective effect of oxymatrine on myocardial fibrosis induced by acute myocardial infarction in rats involved in TGF-β1-Smads signal pathway. *Journal of Asian Natural Products Research*, 13(3), 215-224.

Sheppard, D., 1996. Epithelial integrins. *BioEssays*, 18(8), 655-660.

Shetty, S. S., Sharma, M., Fonseca, F. P., Jayaram, P., Tanwar, A. S., Kabekkodu, S. P., Satyamoorthy, K. and Radhakrishnan, R., 2020. Signaling pathways promoting epithelial mesenchymal transition in oral submucous fibrosis and oral squamous cell carcinoma. *Japanese Dental Science Review*, 56(1), 97-108.

Sheu, S., Yang, D., Selzle, H. L. and Schlag, E. W., 2003. Energetics of hydrogen bonds in peptides. *Proceedings of the National Academy of Sciences*, 100(22), 12683-12687.

Shi, G. and Li, Q., 2005. Effects of oxymatrine on experimental hepatic fibrosis and its mechanismin vivo. *World Journal of Gastroenterology*, 11(2), 268-271.

Shi, H., Guo, Y., Liu, Y., Shi, B., Guo, X., Jin, L. and Yan, S., 2016. The in vitro effect of lipopolysaccharide on proliferation, inflammatory factors and antioxidant enzyme activity in bovine mammary epithelial cells. *Animal Nutrition*, 2(2), 99-104.

Shikatani, E. A., Trifonova, A., Mandel, E. R., Liu, S. T. K., Roudier, E., Krylova, A., Szigiato, A., Beaudry, J., Riddell, M. C. and Haas, T. L., 2012. Inhibition of proliferation, migration and proteolysis contribute to corticosterone-mediated inhibition of angiogenesis. *PLoS ONE*, 7(10), e46625.

Shungin, D., Cornelis, M. C., Divaris, K., Holtfreter, B., Shaffer, J. R., Yu, Y., Barros, S. P., Beck, J. D., Biffar, R., Boerwinkle, E. A., Crout, R. J., Ganna, A., Hallmans, G., Hindy, G., Hu, F. B, Kraft, P., McNeil, D. W., Melander, O., Moss, K. L., North, K. E., Orho-Melander, M., Pedersen, N. L., Ridker, P. M., Rimm, E. B., Rose, L. M., Rukh, G., Teumer, A., Weyant, R. J., Chasman, D. I., Joshipura, K., Kocher, T., Magnusson, P. K. E., Marazita, M. L., Nilsson, P., Offenbacher, S., Davey Smith, G., Lundberg, P., Palmer, T. M., Timpson, N. J., Johansson, I. and Franks, P. W., 2015. Using genetics to test the causal relationship of total adiposity and periodontitis: Mendelian randomization analyses in the Gene-Lifestyle Interactions and Dental Endpoints (GLIDE) Consortium. *International Journal of Epidemiology*, 44(2), 638-650.

Sigmaaldrich.com., 2021. *Lipopolysaccharides from Escherichia coli O26:B6 Ready Made solution, 1 mg/mL, 0.2 µm filtered | Sigma-Aldrich*. Available at: https://www.sigmaaldrich.com/GB/en/product/sigma/l5543# (Accessed 26 August 2021).

Singh, A. K., Yadav, S., Sharma, K., Firdaus, Z., Aditi, P., Neogi, K., Bansal, M., Gupta, M. K., Shanker, A., Singh, R. K. and Prakash, P., 2018. Quantum curcumin mediated inhibition of gingipains and mixed-biofilm of *Porphyromonas gingivalis* causing chronic periodontitis. *RSC Advances*, 8(70), 40426-40445.

Singh, A., Wyant, T., Anaya-Bergman, C., Aduse-Opoku, J., Brunner, J., Laine, M. L., Curtis, M. A. and Lewis, J. P., 2011. The capsule of *Porphyromonas gingivalis* leads to a reduction

in the host inflammatory response, evasion of phagocytosis, and increase in virulence. *Infection and Immunity*, 79(11), 4533-4542.

Singla, M., Kumar, A., Bal, A., Sarkar, S. and Bhattacharyya, S., 2018. Epithelial to mesenchymal transition induces stem cell like phenotype in renal cell carcinoma cells. *Cancer Cell International*, 18(57), 1-13.

Singhrao, S. K., Harding, A., Simmons, T., Robinson, S., Kesavalu, L. and Crean, S., 2014. Oral inflammation, tooth loss, risk factors, and association with progression of Alzheimer's disease. *Journal of Alzheimer's disease*, 42(3), 723-737.

Si-Tayeb, K., Monvoisin, A., Mazzocco, C., Lepreux, S., Decossas, M., Cubel, G., Taras, D., Blanc, J., Robinson, D. R. and Rosenbaum, J., 2006. Matrix metalloproteinase 3 is present in the cell nucleus and is involved in apoptosis. *The American Journal of Pathology*, 169(4), 1390-1401.

Skromne, I. and Stern, C. D., 2001. Interactions between Wnt and Vg1 signalling pathways initiate primitive streak formation in the chick embryo. *Development*, 128(15), 2915-2927.

Smalley, J. W., Birss, A. J. and Silver, J., 2000. The periodontal pathogen *Porphyromonas gingivalis* harnesses the chemistry of the μ-oxo bishaem of iron protoporphyrin IX to protect against hydrogen peroxide. *FEMS Microbiology Letters*, 183(1), 159-164.

Smith, B. N. and Bhowmick, N. A., 2016. Role of EMT in metastasis and therapy resistance. *Journal of Clinical Medicine*, 5(2), 1-17.

Smith, B. N., Burton, L. J., Henderson, V., Randle, D. D., Morton, D. J., Smith, B. A., Taliaferro-Smith, L., Nagappan, P., Yates, C., Zayzafoon, M., Chung, L. W. K. and Odero-Marah, V. A., 2014. Snail promotes epithelial mesenchymal transition in breast cancer cells in part via activation of nuclear ERK2. *PLoS ONE*, 9(8), e104987.

Socransky, S. S. and Haffajee, A. D., 1992. The bacterial etiology of destructive periodontal disease: current concepts. *Journal of Periodontology*, 63(4s), 322-331.

Socransky, S. S., Haffajee, A. D., Cugini, M. A., Smith, C. & Kent, R. L. Jr., 1998. Microbial complexes in subgingival plaque. *Journal of clinical periodontology*, 25(2), 134-144.

Souza, A. C. M. F., Souza, D. R. V., Sanabani, S. S., Giorgi, R. R. and Bendit, I., 2009. The performance of semi-quantitative differential PCR is similar to that of real-time PCR for the detection of the MYCN gene in neuroblastomas. *Brazilian Journal of Medical and Biological Research*, 42(9), 791-795.

Srinivasan, B., Kolli, A. R., Esch, M. B, Abaci, H. E., Shuler, M. L. and Hickman, J. J., 2015. TEER measurement techniques for in vitro barrier model systems. *Journal of Laboratory Automation*, 20(2), 107-126.

Stathopoulou, P. G., Benakanakere, M. R., Galicia, J. C and Kinane, D. F., 2010. Epithelial cell pro-inflammatory cytokine response differs across dental plaque bacterial species. *Journal of Clinical Periodontology*, 37(1), 24-29.

Stohs, S. J., Chen, O., Ray, S. D., Ji, J., Bucci, L. R. and Preuss, H. G., 2020. Highly bioavailable forms of curcumin and promising avenues for curcumin-based research and application: a review. *Molecules*, 25(6), 1397-1409.

Strand, K. R., Sun, C., Li, T., Jenney, F. E., Schut, G. J. and Adams, M. W. W., 2010. Oxidative stress protection and the repair response to hydrogen peroxide in the hyperthermophilic archaeon *Pyrococcus furiosus* and in related species. *Archives of Microbiology*, 192(6), 447-459.

Strutz, F., Okada, H., Lo, C. W., Danoff, T., Carone, R. L., Tomaszewski, J. E. and Neilson, E. G., 1995. Identification and characterization of a fibroblast marker: FSP1. *Journal of Cell Biology*, 130(2), 393-405.

Su, H., Jin, X., Zhang, X., Zhao, L., Lin, B., Li, L., Fei, Z., Shen, L., Fang, Y., Pan, H. and Xie, C., 2015a. FH535 increases the radiosensitivity and reverses epithelial-to-mesenchymal transition of radioresistant esophageal cancer cell line KYSE-150R. *Journal of Translational Medicine*, 13(104), 1-10.

Su, Y., Yang, J., Lee, H., Sheu, F., Hsu, C., Lin, S. and Chow, L., 2015b. The C-terminal disulfide bonds of *Helicobacter pylori* GroES are critical for IL-8 secretion via the TLR4-dependent pathway in gastric epithelial cells. *The Journal of Immunology*, 194(8), 3997-4007.

Sume, S. S., Kantarci, A., Lee, A., Hasturk, H. and Trackman, P. C., 2010. Epithelial to mesenchymal transition in gingival overgrowth. *The American Journal of Pathology*, 177(1), 208-218.

Sun, L., Liu, T., Zhang, S., Guo, K. and Liu, Y., 2017. Oct4 induces EMT through LEF1/β-catenin dependent WNT signaling pathway in hepatocellular carcinoma. *Oncology Letters*, 13(4), 2599-2606.

Sun, Y. and You, Z., 2014. Curcumin inhibits human retinal pigment epithelial cell proliferation. *International Journal of Molecular Medicine*, 34(4), 1013-1019.

Suzuki, N., Yoneda, M. and Hirofuji, T., 2013. Mixed red-complex bacterial infection in periodontitis. *International Journal of Dentistry*, 1(4), 1-6.

Szklarczyk, D., Morris, J. H., Cook, H., Kuhn, M., Wyder, S., Simonovic, M., Santos, A., Doncheva, N., Roth, A., Bork, P., Jensen, L. J. and von Mering, C., 2016. The STRING database in 2017: quality-controlled protein–protein association networks, made broadly accessible. *Nucleic Acids Research*, 45(D1), D362-D368.

Tang, D., Kang, R., Coyne, C. B., Zeh, H. J. and Lotze, M. T., 2012. PAMPs and DAMPs: signal 0s that spur autophagy and immunity. *Immunological Reviews*, 249(1), 158-175.

Tayebi, L. and Moharamzadeh, K., 2018. *Oral mucosa tissue engineering*. Biomaterials for Oral and Dental Tissue Engineering. 1st ed. Sheffield: Woodhead Publishing, pp.223-244.

Tecan, 2017. *Fast and accurate cell counting in a multimode microplate reader*. Mannedorf, Tecan Group Ltd., 1-4.

Terriac, E., Schütz, S. and Lautenschläger, F., 2019. Vimentin intermediate filament rings deform the nucleus during the first steps of adhesion. *Frontiers in Cell and Developmental Biology*, 7(106), 1-10.

Tervonen, T., Oliver, R. C, Wolff, L. F., Bereuter, J., Anderson, L. and Aeppli, D. M., 1994. Prevalence of periodontal pathogens with varying metabolic control of diabetes mellitus. *Journal of Clinical Periodontology*, 21(6), 375-379.

Thacker, P. C. and Karunagaran, D., 2015. Curcumin and emodin down-regulate TGF-β signaling pathway in human cervical cancer cells. *PLOS ONE*, 10(3), e0120045.

The gene ontology consortium, 2017. Expansion of the Gene Ontology knowledgebase and resources. *Nucleic Acids Research*, 45(D1), D331-D338.

The UniProt Consortium, UniProt: the universal protein knowledgebase in 2021. *Nucleic Acids Research*, 49 (D1), 480–489.

Tian, X., Liu, Z., Niu, B., Zhang, J., Tan, T. K., Lee, S. R., Zhao, Y., Harris, D. C. H. and Zheng, G., 2011. E-cadherin/β-catenin complex and the epithelial barrier. *Journal of Biomedicine and Biotechnology*, 2011, 1-6.

Todaro, G. J. and Green, H., 1963. Quantitative studies of the growth of mouse embryo cells in culture and their development into established lines. *Journal of Cell Biology*, 17(2), 299-313.

Toivola, D. M., Tao, G., Habtezion, A., Liao, J. and Omary, M. B., 2005. Cellular integrity plus: organelle-related and protein-targeting functions of intermediate filaments. *Trends in Cell Biology*, 15(11), 608-617.

Tomlins, R. I. and Ordal, Z. J., 1971. Precursor ribosomal ribonucleic acid and ribosome accumulation in vivo during the recovery of *salmonella typhimurium* from thermal injury. *Journal of Bacteriology*, 107(1), 134-142.

Toraya, S., Uehara, O., Hiraki, D., Harada, F., Neopane, P., Morikawa, T., Takai, R., Yoshida, K., Matsuoka, H., Kitaichi, N., Chiba, I. and Abiko, Y., 2019. Curcumin inhibits the expression of proinflammatory mediators and MMP-9 in gingival epithelial cells stimulated for a prolonged period with lipopolysaccharides derived from Porphyromonas gingivalis. *Odontology*, 108(1), 16-24.

Trajkovic, K., Valdez, C., Ysselstein, D. and Krainc, D., 2019. Fluctuations in cell density alter protein markers of multiple cellular compartments, confounding experimental outcomes. *PLOS ONE*, 14(2), e0211727.

Tran, S., Puhar, A., Ngo-Camus, M. and Ramarao, N., 2011. Trypan blue dye enters viable cells incubated with the pore-forming toxin hlyii of Bacillus cereus. *PLoS ONE*, 6(9), e22876.

Tribble, G. D. and Lamont, R. J., 2010. Bacterial invasion of epithelial cells and spreading in periodontal tissue. *Periodontology 2000*, 52(1), 68-83.

Tsai, C., Hayes, C. and Taylor, G. W., 2002. Glycemic control of type 2 diabetes and severe periodontal disease in the US adult population. *Community Dentistry and Oral Epidemiology*, 30(3), 182-192.

Tseng, H., Lee, I., Lin, C., Chi, P., Cheng, S., Shih, R., Hsiao, L. and Yang, C., 2013. IL-1β Promotes Corneal Epithelial Cell Migration by Increasing MMP-9 Expression through NF-κB- and AP-1-Dependent Pathways. *PLoS ONE*, 8(3), e57955.

van der Laan, M., Urbanus, M. L., ten Hagen-Jongman, C. M., Nouwen, N., Oudega, B., Harms, N., Driessen, A. J. M. and Luirink, J., 2003. A conserved function of YidC in the biogenesis of respiratory chain complexes. *Proceedings of the National Academy of Sciences*, 100(10), 5801-5806.

Varankar, S. S. and Bapat, S. A., 2018. Migratory metrics of wound healing: a quantification approach for in vitro scratch assays. *Frontiers in Oncology*, 8(633), 1-13.

Vaupel, P. and Mayer, A., 2007. Hypoxia in cancer: significance and impact on clinical outcome. *Cancer and Metastasis Reviews*, 26(2), 225-239.

Végran, F., Boidot, R., Michiels, C., Sonveaux, P. and Feron, O., 2011. Lactate influx through the endothelial cell monocarboxylate transporter MCT1 supports an NF-κB/IL-8 pathway that drives tumor angiogenesis. *Cancer Research*, 71(7), 2550-2560.

Veith, P. D., Glew, M. D., Gorasia, D. G., Chen, D., O'Brien-Simpson, N. M. and Reynolds, E. C., 2019. Localization of outer membrane proteins in *Treponema denticola* by quantitative proteome analyses of outer membrane vesicles and cellular fractions. *Journal of Proteome Research*, 18(4), 1567-1581.

Vesey, D. A., Cheung, C. W. Y., Cuttle, L., Endre, Z. A., Gobé, G. and Johnson, D. W., 2002. Interleukin-1β induces human proximal tubule cell injury, α-smooth muscle actin expression and fibronectin production1. *Kidney International*, 62(1), 31-40.

Vis, M. A. M., Ito, K. and Hofmann, S., 2020. Impact of culture medium on cellular interactions in in vitro co-culture systems. *Frontiers in Bioengineering and Biotechnology*, 8(1), 1-8.

Vleminckx, K., Vakaet, L. Jr., Mareel, M., Fiers, W. and Van Roy, F., 1991. Genetic manipulation of E-cadherin expression by epithelial tumor cells reveals an invasion suppressor role. *Cell*, 66(1), 107-119.

Vogel, C. and Marcotte, E. M., 2012. Insights into the regulation of protein abundance from proteomic and transcriptomic analyses. *Nature Reviews Genetics*, 13(4), 227-232.

Wang, J., Ghosh, S. S. and Ghosh, S., 2017a. Curcumin improves intestinal barrier function: modulation of intracellular signaling, and organization of tight junctions. *American Journal of Physiology-Cell Physiology*, 312(4), C438-C445.

Wang, M., Ren, D., Guo, W., Huang, S., Wang, Z., Li, Q., Du, H., Song, L. and Peng, X., 2015. N-cadherin promotes epithelial-mesenchymal transition and cancer stem cell-like traits via ErbB signaling in prostate cancer cells. *International Journal of Oncology*, 48(2), 595-606.

Wang, Q., Qu, C., Xie, F., Chen, L., Liu, L., Liang, X., Wu, X., Wang, P. and Meng, Z., 2017b. Curcumin suppresses epithelial-to-mesenchymal transition and metastasis of pancreatic cancer cells by inhibiting cancer-associated fibroblasts. *American Journal of Cancer Research*, 7(1), 125-133.

Wang, Y., Liu, J., Ying, X., Lin, P. C. and Zhou, B. P., 2016. Twist-mediated epithelial-mesenchymal transition promotes breast tumor cell invasion via inhibition of hippo pathway. *Scientific Reports*, 6(1), 1-10.

Wang, Y., Yue, B., Yu, X., Wang, Z. and Wang, M., 2013. SLUG is activated by nuclear factor kappa B and confers human alveolar epithelial A549 cells resistance to tumor necrosis factor-alpha-induced apoptosis. *World Journal of Surgical Oncology*, 11(12), 1-9.

Wang, Z., Li, Y., Kong, D. and H. Sarkar, F. H., 2010. The role of notch signaling pathway in epithelial-mesenchymal transition (EMT) during development and tumor aggressiveness. *Current Drug Targets*, 11(6), 745-751.

Wei, S. C., Fattet, L., Tsai, J. H., Guo, Y., Pai, V. H., Majeski, H. E., Chen, A. C., Sah, R. L., Taylor, S. S., Engler, A. J. and Yang, J., 2015. Matrix stiffness drives epithelial–mesenchymal transition and tumour metastasis through a TWIST1–G3BP2 mechanotransduction pathway. *Nature Cell Biology*, 17(5), 678-688.

Welte, T., Kudva, R., Kuhn, P., Sturm, L., Braig, D., Müller, M., Warscheid, B., Drepper, F. and Koch, H., 2012. Promiscuous targeting of polytopic membrane proteins to SecYEG or YidC by the *Escherichia coli* signal recognition particle. *Molecular Biology of the Cell*, 23(3), 464-479.

Wen, J., Zhao, Z., Huang, L., Wang, L., Miao, Y. and Wu, J., 2019. IL-8 promotes cell migration through regulating EMT by activating the Wnt/β-catenin pathway in ovarian cancer. *Journal of Cellular and Molecular Medicine*, 24(2), 1588-1598.

Wessel, A. K., Arshad, T. A., Fitzpatrick, M., Connell, J. L., Bonnecaze, R. T., Shear, J. B. and Whiteley, M., 2014. Oxygen limitation within a bacterial aggregate. *mBio*, 5(2), 1-9.

Wickles, S., Singharoy, A., Andreani, J., Seemayer, S., Bischoff, L., Berninghausen, O., Soeding, J., Schulten, K., van der Sluis, E. O. and Beckmann, R., 2014. A structural model of the active ribosome-bound membrane protein insertase YidC. *eLife*, 3(e03035), 1-17.

Winning, L. and Linden, G. J., 2015. Periodontitis and systemic disease. *BDJ Team*, 2(10), 7-10.

Winning, L. and Linden, G. J., 2017. Periodontitis and systemic Disease: Association or causality?. *Current Oral Health Reports*, 4(1), 1-7.

Winkelhoff, A. J., Bosch-Tijhof, C. J, Winkel, E. G. and Reijden, W. A., 2001. Smoking affects the subgingival microflora in periodontitis. *Journal of Periodontology*, 72(5), 666-671.

Woodcock, E. and Grigg, G. W., 1972. Repair of thermally induced DNA breakage in *Escherichia coli*. *Nature New Biology*, 237(72), 76-79.

World Health Organization, 2021. *Oral health*. Who.int. Available at: https://www.who.int/news-room/fact-sheets/detail/oral-health (Accessed 12 November 2021).

Wu, C., Yuan, Y., Liu, H., Li, S., Zhang, B., Chen, W., An, Z., Chen, S., Wu, Y., Han, B., Li, C. and Li, L., 2020. Epidemiologic relationship between periodontitis and type 2 diabetes mellitus. *BMC Oral Health*, 20(204), 1-15.

Wu, J. and Mlodzik, M., 2009. A quest for the mechanism regulating global planar cell polarity of tissues. *Trends in Cell Biology*, 19(7), 295-305.

Wu, Q., Hou, X., Xia, J., Qian, X., Miele, L., Sarkar, F. H. and Wang, Z., 2013. Emerging roles of PDGF-D in EMT progression during tumorigenesis. *Cancer Treatment Reviews*, 39(6), 640-646.

Wu, Y. I., Frey, D., Lungu, O. I., Jaehrig, A., Schlichting, I., Kuhlman, B. and Hahn, K. M., 2009. A genetically encoded photoactivatable Rac controls the motility of living cells. *Nature*, 461(7260), 104-108.

Wynn, T. A., 2008. Cellular and molecular mechanisms of fibrosis. *The Journal of Pathology*, 214(2), 199-210.

Wynn, T. A. and Ramalingam, T. R., 2012. Mechanisms of fibrosis: therapeutic translation for fibrotic disease. *Nature Medicine*, 18(7), 1028-1040.

Ximénez-Fyvie, L. A., Haffajee, A. D. and Socransky, S. S., 2000. Comparison of the microbiota of supra- and subgingival plaque in health and periodontitis. *Journal of Clinical Periodontology*, 27(9), 648-657.

Xu, J., Liu, D., Niu, H., Zhu, G., Xu, Y., Ye, D., Li, J. and Zhang, Q., 2017a. Resveratrol reverses Doxorubicin resistance by inhibiting epithelial-mesenchymal transition (EMT) through modulating PTEN/Akt signaling pathway in gastric cancer. *Journal of Experimental & Clinical Cancer Research*, 36(1), 1-14.

Xu, J., Lamouille, S. and Derynck, R., 2009. TGF-β-induced epithelial to mesenchymal transition. *Cell Research*, 19(2), 156-172.

Xu, J., Yang, H., Zhou, X., Wang, H., Gong, L. and Tang, C., 2015. Role of Wnt Inhibitory Factor-1 in inhibition of bisdemethoxycurcumin mediated epithelial-to-mesenchymal transition in highly metastatic lung cancer 95D cells. *Chinese Medical Journal*, 128(10), 1376-1383.

Xu, S., Jiang, B., Wang, H., Shen, C., Chen, H. and Zeng, L., 2017b. Curcumin suppresses intestinal fibrosis by inhibition of PPARγ-mediated epithelial-mesenchymal transition. *Evidence-Based Complementary and Alternative Medicine*, 2017(1), 1-12.

Xu, Y., Lou, Z. and Lee, S. H., 2017. Arctigenin represses TGF-β-induced epithelial mesenchymal transition in human lung cancer cells. *Biochemical and Biophysical Research Communications*, 493(2), 934-939.

Xue, C., Plieth, D., Venkov, C., Xu, C. and Neilson, E. G., 2003. The gatekeeper effect of epithelial-mesenchymal transition regulates the frequency of breast cancer metastasis. *Cancer Research*, 63(12), 3386-3394.

Xuebing, Y., Liguo, L., Hao, L., Huanlong, Q. and Zhenilang, S., 2017. Clinical significance of *Fusobacterium nucleatum*, epithelial–mesenchymal transition, and cancer stem cell markers in stage III/IV colorectal cancer patients. *OncoTargets and Therapy*, 10(1), 5031-5046.

Yadev, N. P., Murdoch, C., Saville, S. P. and Thornhill, M. H., 2011. Evaluation of tissue engineered models of the oral mucosa to investigate oral candidiasis. *Microbial Pathogenesis*, 50(6), 278-285.

Yakob, M., Meurman, J. H., Sorsa, T. and Söder, B., 2013. *Treponema denticola* associates with increased levels of MMP-8 and MMP-9 in gingival crevicular fluid. *Oral Diseases*, 19(7), 694-701.

Yang, C., Liu, Y., Ma, Y., Xue, Y., Liu, D., Ren, Y., Liu, X., Li, Y. and Li, Z., 2012. Curcumin blocks small cell lung cancer cells migration, invasion, angiogenesis, cell cycle and neoplasia through Janus Kinase-STAT3 signalling pathway. *PLoS ONE*, 7(5), e37960.

Yang, J., Antin, P., Berx, G., Blanpain, C., Brabletz, T., Bronner, M., Campbell, K. and Cano, A., 2020. Guidelines and definitions for research on epithelial–mesenchymal transition. *Nature Reviews Molecular Cell Biology*, 21(1), 341-352.

Yang, J., Mani, S. A., Donaher, J. L., Ramaswamy, S., Itzykson, R. A., Come, C., Savagner, P., Gitelman, I., Richardson, A. and Weinberg, R. A., 2004. Twist, a master regulator of morphogenesis, plays an essential role in tumor metastasis. *Cell*, 117(7), 927-939.

Yang, X., Wang, J., Guo, S., Fan, K., Li, J., Wang, Y., Teng, Y. and Yang, X., 2011. miR-21 promotes keratinocyte migration and re-epithelialization during wound healing. *International Journal of Biological Sciences*, 7(5), 685-690.

Yao, E. S., Lament, R. J., Leu, S. P. and Weinberg, A., 1996. Interbacterial binding among strains of pathogenic and commensal oral bacterial species. *Oral Microbiology and Immunology*, 11(1), 35-41.

Yao, Y., Li, Y., Zeng, X., Ye, Z., Li, X. and Zhang, L., 2018. Losartan alleviates renal fibrosis and inhibits endothelial-to-mesenchymal transition (EMT) under high-fat diet-induced hyperglycemia. *Frontiers in Pharmacology*, 9(1213), 1-12.

Yee, M., Kim, S., Sethi, P., Düzgüneş, N. and Konopka, K., 2014. *Porphyromonas gingivalis* stimulates IL-6 and IL-8 secretion in GMSM-K, HSC-3 and H413 oral epithelial cells. *Anaerobe*, 28, 62-67.

Yeung, K. T. and Yang, J., 2016. Epithelial–mesenchymal transition in tumor metastasis. *Molecular Oncology*, 11(1), 28-39.

Yilmaz, Ö., Young, P. A, Lamont, R. J. and Kenny, G. E., 2003. Gingival epithelial cell signalling and cytoskeletal responses to Porphyromonas gingivalis invasion. *Microbiology*, 149(9), 2417-2426.

Yin, J., Zeng, F., Wu, N., Kang, K., Yang, Z. and Yang, H., 2014. Interleukin-8 promotes human ovarian cancer cell migration by epithelial–mesenchymal transition induction in vitro. *Clinical and Translational Oncology*, 17(5), 365-370.

Yoshino, T., Saito, D., Atsuta, Y., Uchiyama, C., Ueda, S., Sekiguchi, K. and Takahashi, Y., 2014. Interepithelial signaling with nephric duct is required for the formation of overlying coelomic epithelial cell sheet. *Proceedings of the National Academy of Sciences*, 111(18), 6660-6665.

Yucel-Lindberg, T. and Båge, T., 2013. Inflammatory mediators in the pathogenesis of periodontitis. *Expert Reviews in Molecular Medicine*, 15(7), 1-22.

Zambruno, G., Marchisio, P. C., Marconi, A., Vaschieri, C., Melchiori, A., Giannetti, A. and De Luca, M., 1995. Transforming growth factor-beta 1 modulates beta 1 and beta 5 integrin receptors and induces the de novo expression of the alpha v beta 6 heterodimer in normal human keratinocytes: implications for wound healing. *Journal of Cell Biology*, 129(3), 853-865.

Zarco, M., Vess, T. and Ginsburg, G., 2011. The oral microbiome in health and disease and the potential impact on personalized dental medicine. *Oral Diseases*, 18(2), 109-120.

Zardawi, F., Gul, S., Abdulkareem, A., Sha, A. and Yates, J., 2021. Association between periodontal disease and atherosclerotic cardiovascular diseases: Revisited. *Frontiers in Cardiovascular Medicine*, 7(1), 1-17.

Zeng, X., Tu, M., Liu, D., Zheng, D., Zhang, J. and Leng, W., 2012. Periodontal disease and risk of chronic obstructive pulmonary disease: a meta-analysis of observational studies. *PLoS ONE*, 7(10), e46508.

Zeisberg, E. M., Tarnavski, O., Zeisberg, M., Dorfman, A. L., McMullen, J. R., Gustafsson, E., Chandraker, A., Yuan, X., Pu, W. T., Roberts, A. B., Neilson, E. G., Sayegh, M. H., Izumo, S. and Kalluri, R., 2007a. Endothelial-to-mesenchymal transition contributes to cardiac fibrosis. *Nature Medicine*, 13(8), 952-961.

Zeisberg, M. and Neilson, E. G., 2009. Biomarkers for epithelial-mesenchymal transitions. *Journal of Clinical Investigation*, 119(6), 1429-1437.

Zeisberg, M., Yang, C., Martino, M., Duncan, M. B., Rieder, F., Tanjore, H. and Kalluri, R., 2007b. Fibroblasts derive from hepatocytes in liver fibrosis via epithelial to mesenchymal transition. *Journal of Biological Chemistry*, 282(32), 23337-23347.

Zhang, L., Cheng, X., Gao, Y., Zhang, C., Bao, J., Guan, H., Yu, H., Lu, R., Xu, Q. and Sun, Y., 2016. Curcumin inhibits metastasis in human papillary thyroid carcinoma BCPAP cells via down-regulation of the TGF-β/Smad2/3 signaling pathway. *Experimental Cell Research*, 341(2), 157-165.

Zhang, N., Liu, Y., Wang, Y., Zhao, M., Tu, L. and Luo, F., 2017. Decitabine reverses TGF-β1-induced epithelial-mesenchymal transition in non-small-cell lung cancer by regulating miR-200/ZEB axis. *Drug Design, Development and Therapy*, 11(4), 969-983.

Zhang, P., Sun, Y. and Ma, L., 2015. ZEB1: At the crossroads of epithelial-mesenchymal transition, metastasis and therapy resistance. *Cell Cycle*, 14(4), 481-487.

Zhang, X., Liu, G., Kang, Y., Dong, Z., Qian, Q. and Ma, X., 2013. N-cadherin expression is associated with acquisition of EMT phenotype and with enhanced invasion in erlotinib-resistant lung cancer cell lines. *PLoS ONE*, 8(3), e57692.

Zhang, X., Wang, X., Xu, R., Ji, J., Xu, Y., Han, M., Wei, Y., Huang, B., Chen, A., Zhang, Q., Li, W., Wang, J., Li, X. and Qiu, C., 2018. YM155 decreases radiation-induced invasion and reverses epithelial–mesenchymal transition by targeting STAT3 in glioblastoma. *Journal of Translational Medicine*, 16(1), 1-11.

Zhang, Y., Liu, Y., Mao, Y., Dong, W., Zhu, X. and Jiang, L., 2015a. Resveratrol ameliorates lipopolysaccharide-induced epithelial mesenchymal transition and pulmonary fibrosis through suppression of oxidative stress and transforming growth factor-β1 signaling. *Clinical Nutrition*, 34(4), 752-760.

Zhang, Y., Wei, X., Liang, Y., Chen, W., Zhang, F., Bai, J., Qiu, S., Du, C., Huang, W. and Zhang, G., 2015b. Over-expressed twist associates with markers of epithelial mesenchymal transition and predicts poor prognosis in breast cancers via ERK and Akt activation. *PLOS ONE*, 10(8), e0135851.

Zhao, L., Yang, R., Cheng, L., Wang, M., Jiang, Y. and Wang, S., 2011. LPS-induced Epithelial-Mesenchymal Transition of intrahepatic biliary epithelial cells. *Journal of Surgical Research*, 171(2), 819-825.

Zhao, Z., Wang, S., Lin, Y., Miao, Y., Zeng, Y., Nie, Y., Guo, P., Jiang, G. and Wu, J., 2017. Epithelial-mesenchymal transition in cancer: Role of the IL-8/IL-8R axis. *Oncology Letters*, 13(6), 4577-4584.

Zhen, L., Fan, D., Yi, X., Cao, X., Chen, D. and Wang, L., 2014. Curcumin inhibits oral squamous cell carcinoma proliferation and invasion via EGFR signaling pathways. *International Journal of Clinical and Experimental Pathology*, 7(10), 6438–6446.

Zhou, M., Dong, J., Zha, L. and Liao, Y., 2021. Causal association between periodontal diseases and cardiovascular diseases. *Genes*, 13(1), 1-13.

Zhou, X., Kuang, X., Long, C., Liu, W., Tang, Y., Liu, L., Liu, H., He, J., Huang, Z., Fan, Y., Zhang, Q. and Shen, H., 2017. Curcumin inhibits proliferation and epithelial-mesenchymal transition of retinal pigment epithelial cells via multiple pathways. *Current Molecular Medicine*, 17(4), 312-319.

Zhu, F., Chen, M., Zhu, M., Zhao, R., Qiu, W., Xu, X., Liu, H., Zhao, H., Yu, R., Wu, X., Zhang, K. and Huang, H., 2017. Curcumin suppresses epithelial–mesenchymal transition of renal tubular epithelial cells through the inhibition of Akt/mTOR pathway. *Biological & Pharmaceutical Bulletin*, 40(1), 17-24.

Zhu, Q., Ma, C., Wang, Q., Song, Y. and Lv, T., 2015. The role of TWIST1 in epithelial-mesenchymal transition and cancers. *Tumor Biology*, 37(1), 185-197.

# 9. Appendices

## 9.1 List of proteins and abundances of isolated live, heat and oxygen-killed *T. denticola* outer membrane proteins

**Table 9.1**: Abundances of isolated *T. denticola* outer membrane proteins (live, heat and oxygen-killed) after performing quantitative mass spectrometry-based analysis using tandem mass tags (TMT™) and searched against the UniProt knowledgebase (UniProtKb) protein database. A total of 132 proteins were identified from which 10 were identified but not quantified and were highlighted in red at the bottom of the table. These 10 proteins were not quantified because abundance levels were too low.

| Accession | Description | Abundances (grouped): 126 (live *T. denticola*) | Abundances (grouped): 127 (live *T. denticola*) | Abundances (grouped): 128 (heat-killed *T. denticola*) | Abundances (grouped): 129 (heat-killed *T. denticola*) | Abundances (grouped): 130 (oxygen-killed *T. denticola*) | Abundances (grouped): 131 (oxygen-killed *T. denticola*) |
|---|---|---|---|---|---|---|---|
| Q73KH5 | Copper homeostasis protein CutC OS=Treponema denticola (strain ATCC 35405 / CIP 103919 / DSM 14222) OX=243275 GN=cutC PE=3 SV=1 | 31.8 | 36.5 | 68.1 | 66 | 21.5 | 21.1 |
| Q73QJ5 | Deoxyribose-phosphate aldolase OS=Treponema denticola (strain ATCC 35405 / CIP 103919 / DSM 14222) OX=243275 GN=deoC PE=3 SV=1 | 38.8 | 43.3 | 89.4 | 98 | 63.1 | 70 |
| Q73N77 | UPF0340 protein TDE_1278 OS=Treponema denticola (strain ATCC 35405 / CIP 103919 / DSM 14222) OX=243275 GN=TDE_1278 PE=3 SV=1 | 42.5 | 82.3 | 98.4 | 102.2 | 54.4 | 77.9 |
| P61748 | Glycerol-3-phosphate dehydrogenase [NAD(P)+] OS=Treponema denticola (strain ATCC 35405 / CIP 103919 / DSM 14222) OX=243275 GN=gpsA PE=3 SV=1 | 45.2 | 55.2 | 12.5 | 17.5 | 46.4 | 50.8 |
| Q73M65 | Methionyl-tRNA formyltransferase OS=Treponema denticola (strain ATCC 35405 / CIP 103919 / DSM 14222) OX=243275 GN=fmt PE=3 SV=1 | 50.9 | 55.1 | 32.8 | 32.7 | 67.6 | 79.5 |
| Q73MZ2 | Valine--tRNA ligase OS=Treponema denticola (strain ATCC 35405 / CIP 103919 / DSM 14222) OX=243275 GN=valS PE=3 SV=1 | 56.5 | 60.6 | 17.8 | 17.1 | 44.5 | 38.5 |

| | | | | | | | |
|---|---|---|---|---|---|---|---|
| Q73MV2 | Phosphoribosylformylglycinamidine synthase subunit PurQ OS=Treponema denticola (strain ATCC 35405 / CIP 103919 / DSM 14222) OX=243275 GN=purQ PE=3 SV=1 | 60.1 | 53.6 | 80 | 80.3 | 124.4 | 150.8 |
| Q73MH0 | DNA ligase OS=Treponema denticola (strain ATCC 35405 / CIP 103919 / DSM 14222) OX=243275 GN=ligA PE=3 SV=1 | 60.8 | 51.2 | 86 | 81.3 | 171 | 179.2 |
| Q73M29 | V-type ATP synthase beta chain OS=Treponema denticola (strain ATCC 35405 / CIP 103919 / DSM 14222) OX=243275 GN=atpB PE=3 SV=1 | 61.3 | 200.6 | 279.9 | 241.2 | 77.2 | 68.4 |
| Q73JM9 | ATP-dependent Clp protease proteolytic subunit 2 OS=Treponema denticola (strain ATCC 35405 / CIP 103919 / DSM 14222) OX=243275 GN=clpP2 PE=3 SV=1 | 67.6 | 67 | 163 | 180.1 | 104.8 | 90.5 |
| Q73NB9 | Triosephosphate isomerase OS=Treponema denticola (strain ATCC 35405 / CIP 103919 / DSM 14222) OX=243275 GN=tpiA PE=3 SV=1 | 70.8 | 82.1 | 140.8 | 145.6 | 130.3 | 105.2 |
| P62239 | 30S ribosomal protein S16 OS=Treponema denticola (strain ATCC 35405 / CIP 103919 / DSM 14222) OX=243275 GN=rpsP PE=3 SV=1 | 73.1 | 64.4 | 88.5 | 85.3 | 62.8 | 76.5 |
| P62042 | Probable transcriptional regulatory protein TDE_1487 OS=Treponema denticola (strain ATCC 35405 / CIP 103919 / DSM 14222) OX=243275 GN=TDE_1487 PE=3 SV=1 | 74.8 | 97.4 | 60.3 | 70.9 | 41.4 | 31.6 |
| Q73NV3 | Elongation factor G 2 OS=Treponema denticola (strain ATCC 35405 / CIP 103919 / DSM 14222) OX=243275 GN=fusA2 PE=3 SV=1 | 75 | 92.5 | 184.4 | 192.4 | 181.8 | 186.2 |
| Q73QK5 | Queuine tRNA-ribosyltransferase OS=Treponema denticola (strain ATCC 35405 / CIP 103919 / DSM 14222) OX=243275 GN=tgt PE=3 SV=1 | 77.7 | 72.9 | 154.7 | 138.4 | 152.3 | 163 |
| Q73PK7 | 50S ribosomal protein L17 OS=Treponema denticola (strain ATCC 35405 / CIP 103919 / | 77.7 | 76.9 | 59.6 | 61.2 | 116.7 | 89.5 |

| | | | | | | | |
|---|---|---|---|---|---|---|---|
| | DSM 14222) OX=243275 GN=rplQ PE=3 SV=1 | | | | | | |
| Q73JB2 | Isoleucine--tRNA ligase OS=Treponema denticola (strain ATCC 35405 / CIP 103919 / DSM 14222) OX=243275 GN=ileS PE=3 SV=1 | 78.4 | 56.5 | 46.1 | 37.9 | 91.2 | 100.6 |
| P60974 | Phosphatidylglycerol--prolipoprotein diacylglyceryl transferase OS=Treponema denticola (strain ATCC 35405 / CIP 103919 / DSM 14222) OX=243275 GN=lgt PE=3 SV=1 | 96.2 | 71.4 | 29.6 | 28.4 | 64.1 | 55.6 |
| Q73PN2 | 30S ribosomal protein S10 OS=Treponema denticola (strain ATCC 35405 / CIP 103919 / DSM 14222) OX=243275 GN=rpsJ PE=3 SV=1 | 97 | 110.3 | 96.5 | 105.8 | 245.9 | 205.6 |
| Q73KB2 | Serine--tRNA ligase OS=Treponema denticola (strain ATCC 35405 / CIP 103919 / DSM 14222) OX=243275 GN=serS PE=3 SV=1 | 97.2 | 114.9 | 169.5 | 179.4 | 248.6 | 251.6 |
| Q73LW1 | 50S ribosomal protein L21 OS=Treponema denticola (strain ATCC 35405 / CIP 103919 / DSM 14222) OX=243275 GN=rplU PE=3 SV=1 | 97.9 | 88.7 | 738.3 | 743.8 | 160 | 124.7 |
| Q73N16 | 50S ribosomal protein L25 OS=Treponema denticola (strain ATCC 35405 / CIP 103919 / DSM 14222) OX=243275 GN=rplY PE=3 SV=1 | 101.4 | 129.8 | 169.6 | 161.7 | 238.2 | 269.4 |
| Q73JJ0 | 50S ribosomal protein L33 OS=Treponema denticola (strain ATCC 35405 / CIP 103919 / DSM 14222) OX=243275 GN=rpmG PE=3 SV=1 | 103.7 | 113.1 | 61.5 | 71.4 | 110.2 | 104 |
| Q73PM2 | 50S ribosomal protein L14 OS=Treponema denticola (strain ATCC 35405 / CIP 103919 / DSM 14222) OX=243275 GN=rplN PE=3 SV=1 | 107.4 | 148.5 | 145.3 | 160.8 | 235.1 | 230.3 |
| Q73RJ6 | Cysteine--tRNA ligase OS=Treponema denticola (strain ATCC 35405 / CIP 103919 / DSM 14222) OX=243275 GN=cysS PE=3 SV=1 | 108.5 | 102.1 | 189.7 | 185.2 | 150.6 | 168.4 |

| | | | | | | | |
|---|---|---|---|---|---|---|---|
| Q73R87 | Glutamate--tRNA ligase OS=Treponema denticola (strain ATCC 35405 / CIP 103919 / DSM 14222) OX=243275 GN=gltX PE=3 SV=1 | 109.1 | 124 | 186.8 | 192.3 | 147.4 | 154.4 |
| P61348 | Aspartyl/glutamyl-tRNA(Asn/Gln) amidotransferase subunit B OS=Treponema denticola (strain ATCC 35405 / CIP 103919 / DSM 14222) OX=243275 GN=gatB PE=3 SV=1 | 110.5 | 126.6 | 218.6 | 238.7 | 125.3 | 199.1 |
| Q73PM7 | 50S ribosomal protein L22 OS=Treponema denticola (strain ATCC 35405 / CIP 103919 / DSM 14222) OX=243275 GN=rplV PE=3 SV=1 | 114.2 | 99 | 134.6 | 134.5 | 144.1 | 135.9 |
| Q73Q47 | Trans-2-enoyl-CoA reductase [NADH] OS=Treponema denticola (strain ATCC 35405 / CIP 103919 / DSM 14222) OX=243275 GN=fabV PE=1 SV=1 | 125.8 | 189.8 | 275.2 | 245.5 | 154.7 | 165.6 |
| Q73RR5 | Glycine--tRNA ligase OS=Treponema denticola (strain ATCC 35405 / CIP 103919 / DSM 14222) OX=243275 GN=glyQS PE=3 SV=1 | 134.5 | 169.7 | 803.5 | 838.2 | 426.4 | 432.6 |
| Q73PL0 | 30S ribosomal protein S13 OS=Treponema denticola (strain ATCC 35405 / CIP 103919 / DSM 14222) OX=243275 GN=rpsM PE=3 SV=1 | 135.7 | 120.7 | 42.1 | 38.8 | 178.6 | 157.9 |
| Q73KR3 | 50S ribosomal protein L20 OS=Treponema denticola (strain ATCC 35405 / CIP 103919 / DSM 14222) OX=243275 GN=rplT PE=3 SV=1 | 147.1 | 123.2 | 123.6 | 122.3 | 249.2 | 263.6 |
| Q73MC2 | Aspartate--tRNA(Asp/Asn) ligase OS=Treponema denticola (strain ATCC 35405 / CIP 103919 / DSM 14222) OX=243275 GN=aspS PE=3 SV=1 | 153.3 | 162.8 | 185.7 | 199.8 | 147.5 | 172.3 |
| Q73MD3 | tRNA-2-methylthio-N(6)-dimethylallyladenosine synthase OS=Treponema denticola (strain ATCC 35405 / CIP 103919 / DSM 14222) OX=243275 GN=miaB PE=3 SV=1 | 158.6 | 165.9 | 117.5 | 114.4 | 253.9 | 258.4 |

| | | | | | | | |
|---|---|---|---|---|---|---|---|
| P62443 | 50S ribosomal protein L11 OS=Treponema denticola (strain ATCC 35405 / CIP 103919 / DSM 14222) OX=243275 GN=rplK PE=3 SV=1 | 162.3 | 140.2 | 150.9 | 138.8 | 484.6 | 421.8 |
| Q73K92 | Chaperone protein ClpB OS=Treponema denticola (strain ATCC 35405 / CIP 103919 / DSM 14222) OX=243275 GN=clpB PE=3 SV=1 | 172 | 157 | 373.5 | 380.7 | 152.5 | 180.3 |
| Q73PD8 | Tyrosine--tRNA ligase OS=Treponema denticola (strain ATCC 35405 / CIP 103919 / DSM 14222) OX=243275 GN=tyrS PE=3 SV=1 | 184.7 | 163 | 151 | 150.1 | 473.3 | 435.5 |
| Q73KJ8 | Proline--tRNA ligase OS=Treponema denticola (strain ATCC 35405 / CIP 103919 / DSM 14222) OX=243275 GN=proS PE=3 SV=1 | 198.9 | 215.7 | 365.5 | 359.3 | 318.9 | 345.4 |
| Q73PK9 | 30S ribosomal protein S11 OS=Treponema denticola (strain ATCC 35405 / CIP 103919 / DSM 14222) OX=243275 GN=rpsK PE=3 SV=1 | 200.6 | 158.3 | 71.9 | 75.6 | 137.1 | 156.4 |
| P61339 | Elongation factor Ts OS=Treponema denticola (strain ATCC 35405 / CIP 103919 / DSM 14222) OX=243275 GN=tsf PE=3 SV=1 | 203.4 | 235.8 | 261.5 | 255.9 | 96.6 | 110.4 |
| Q73MP4 | SsrA-binding protein OS=Treponema denticola (strain ATCC 35405 / CIP 103919 / DSM 14222) OX=243275 GN=smpB PE=3 SV=1 | 205.5 | 253.4 | 160.5 | 167.7 | 247.9 | 234.1 |
| Q73M02 | 30S ribosomal protein S20 OS=Treponema denticola (strain ATCC 35405 / CIP 103919 / DSM 14222) OX=243275 GN=rpsT PE=3 SV=1 | 209.7 | 189.7 | 249.4 | 239.5 | 267.4 | 266 |
| Q73PM3 | 30S ribosomal protein S17 OS=Treponema denticola (strain ATCC 35405 / CIP 103919 / DSM 14222) OX=243275 GN=rpsQ PE=3 SV=1 | 211.2 | 196.9 | 154.2 | 141.5 | 325.2 | 274 |
| Q73Q68 | Glutamyl-tRNA(Gln) amidotransferase subunit A OS=Treponema denticola (strain | 231.8 | 210.8 | 98.2 | 101 | 158.1 | 194 |

| | | | | | | | |
|---|---|---|---|---|---|---|---|
| | ATCC 35405 / CIP 103919 / DSM 14222) OX=243275 GN=gatA PE=3 SV=1 | | | | | | |
| P62221 | Protein RecA OS=Treponema denticola (strain ATCC 35405 / CIP 103919 / DSM 14222) OX=243275 GN=recA PE=3 SV=1 | 234.5 | 276 | 350.9 | 349.6 | 249.3 | 314.2 |
| Q73R54 | Ribonuclease Y OS=Treponema denticola (strain ATCC 35405 / CIP 103919 / DSM 14222) OX=243275 GN=rny PE=3 SV=1 | 238.8 | 258.7 | 84.2 | 82.5 | 133.4 | 136 |
| Q73JR4 | S-adenosylmethionine synthase OS=Treponema denticola (strain ATCC 35405 / CIP 103919 / DSM 14222) OX=243275 GN=metK PE=3 SV=1 | 265.2 | 336.1 | 369 | 395.9 | 273.5 | 349.1 |
| Q73PL8 | 30S ribosomal protein S8 OS=Treponema denticola (strain ATCC 35405 / CIP 103919 / DSM 14222) OX=243275 GN=rpsH PE=3 SV=1 | 272.2 | 352 | 353.7 | 363.5 | 590.7 | 448.1 |
| Q73NW1 | Polyribonucleotide nucleotidyltransferase OS=Treponema denticola (strain ATCC 35405 / CIP 103919 / DSM 14222) OX=243275 GN=pnp PE=3 SV=1 | 277.9 | 293.1 | 509.4 | 537.7 | 183.2 | 216 |
| Q73MX5 | V-type ATP synthase subunit E OS=Treponema denticola (strain ATCC 35405 / CIP 103919 / DSM 14222) OX=243275 GN=atpE PE=3 SV=1 | 279.1 | 275 | 319.6 | 309 | 183.2 | 167.8 |
| Q73LC2 | 30S ribosomal protein S4 OS=Treponema denticola (strain ATCC 35405 / CIP 103919 / DSM 14222) OX=243275 GN=rpsD PE=3 SV=1 | 288.8 | 308.5 | 266.1 | 284.7 | 315 | 347.8 |
| Q73PM1 | 50S ribosomal protein L24 OS=Treponema denticola (strain ATCC 35405 / CIP 103919 / DSM 14222) OX=243275 GN=rplX PE=3 SV=1 | 310.1 | 337.4 | 223.1 | 220.3 | 384.5 | 357.1 |
| P60920 | Histidine--tRNA ligase OS=Treponema denticola (strain ATCC 35405 / CIP 103919 / DSM 14222) OX=243275 GN=hisS PE=3 SV=1 | 316 | 321.3 | 688 | 636.2 | 605.4 | 623.8 |
| P62646 | Protein-glutamate methylesterase/protein-glutamine glutaminase OS=Treponema | 327.1 | 381.7 | 916.2 | 874.6 | 792.7 | 744.9 |

| | | | | | | | |
|---|---|---|---|---|---|---|---|
| | denticola (strain ATCC 35405 / CIP 103919 / DSM 14222) OX=243275 GN=cheB PE=3 SV=1 | | | | | | |
| P61191 | Glutamate mutase sigma subunit OS=Treponema denticola (strain ATCC 35405 / CIP 103919 / DSM 14222) OX=243275 GN=glmS PE=3 SV=1 | 327.9 | 364.1 | 341.4 | 332.1 | 432.3 | 456.9 |
| Q73KS3 | UPF0597 protein TDE_2144 OS=Treponema denticola (strain ATCC 35405 / CIP 103919 / DSM 14222) OX=243275 GN=TDE_2144 PE=3 SV=1 | 332.6 | 336.7 | 198.7 | 202.3 | 444.2 | 482.7 |
| Q73J26 | GTPase HflX OS=Treponema denticola (strain ATCC 35405 / CIP 103919 / DSM 14222) OX=243275 GN=hflX PE=3 SV=1 | 350.6 | 389.1 | 459.1 | 455.3 | 351.2 | 349.4 |
| Q73NV4 | 30S ribosomal protein S7 OS=Treponema denticola (strain ATCC 35405 / CIP 103919 / DSM 14222) OX=243275 GN=rpsG PE=3 SV=1 | 356.1 | 325.9 | 360 | 1171.9 | 508.8 | 458.7 |
| Q73PB4 | 50S ribosomal protein L19 OS=Treponema denticola (strain ATCC 35405 / CIP 103919 / DSM 14222) OX=243275 GN=rplS PE=3 SV=1 | 376.5 | 435.5 | 235.3 | 231.9 | 483.5 | 464.5 |
| Q73PE7 | 50S ribosomal protein L13 OS=Treponema denticola (strain ATCC 35405 / CIP 103919 / DSM 14222) OX=243275 GN=rplM PE=3 SV=1 | 392.3 | 350.7 | 612.9 | 589 | 465 | 467 |
| Q73RB6 | Pyrrolidone-carboxylate peptidase OS=Treponema denticola (strain ATCC 35405 / CIP 103919 / DSM 14222) OX=243275 GN=pcp PE=3 SV=1 | 411.2 | 506.1 | 831.2 | 769.9 | 442.8 | 1709.5 |
| Q73M39 | Trigger factor OS=Treponema denticola (strain ATCC 35405 / CIP 103919 / DSM 14222) OX=243275 GN=tig PE=3 SV=1 | 415.4 | 443.1 | 1123 | 1080.5 | 447.2 | 483.9 |
| Q73NX6 | Acyl carrier protein OS=Treponema denticola (strain ATCC 35405 / CIP 103919 / DSM 14222) OX=243275 GN=acpP PE=3 SV=1 | 427.6 | 351.8 | 354.9 | 335.6 | 933.1 | 803.6 |
| Q73M76 | Citrate lyase acyl carrier protein OS=Treponema denticola (strain ATCC 35405 | 427.9 | 588.8 | 390.5 | 383.1 | 295.8 | 377.4 |

| | | | | | | | |
|---|---|---|---|---|---|---|---|
| | / CIP 103919 / DSM 14222) OX=243275 GN=citD PE=3 SV=1 | | | | | | |
| P61188 | Chaperone protein HtpG OS=Treponema denticola (strain ATCC 35405 / CIP 103919 / DSM 14222) OX=243275 GN=htpG PE=3 SV=1 | 430.2 | 371 | 435.8 | 440.9 | 328.8 | 336 |
| Q73LG6 | Protein translocase subunit SecA OS=Treponema denticola (strain ATCC 35405 / CIP 103919 / DSM 14222) OX=243275 GN=secA PE=3 SV=1 | 449.4 | 463.4 | 454.8 | 460.2 | 605.9 | 617.4 |
| Q73QJ2 | Arginine deiminase OS=Treponema denticola (strain ATCC 35405 / CIP 103919 / DSM 14222) OX=243275 GN=arcA PE=3 SV=1 | 491.9 | 525.8 | 579.9 | 570.7 | 613.5 | 521.4 |
| Q73NT9 | Methionine--tRNA ligase OS=Treponema denticola (strain ATCC 35405 / CIP 103919 / DSM 14222) OX=243275 GN=metG PE=3 SV=1 | 497.8 | 527.1 | 949.4 | 933.2 | 1144.5 | 1203.4 |
| Q73M28 | V-type ATP synthase alpha chain OS=Treponema denticola (strain ATCC 35405 / CIP 103919 / DSM 14222) OX=243275 GN=atpA PE=3 SV=1 | 502.3 | 537.7 | 766.8 | 782 | 710.2 | 771 |
| Q73PQ2 | Glycine/sarcosine/betaine reductase complex component A OS=Treponema denticola (strain ATCC 35405 / CIP 103919 / DSM 14222) OX=243275 GN=grdA PE=3 SV=2 | 518.2 | 491.4 | 397.1 | 389.1 | 341.1 | 381.7 |
| Q73P09 | 50S ribosomal protein L28 OS=Treponema denticola (strain ATCC 35405 / CIP 103919 / DSM 14222) OX=243275 GN=rpmB PE=3 SV=1 | 534.9 | 498.1 | 223.6 | 206.9 | 464.2 | 440.9 |
| Q73JN2 | D-alanine--D-alanine ligase OS=Treponema denticola (strain ATCC 35405 / CIP 103919 / DSM 14222) OX=243275 GN=ddl PE=3 SV=1 | 555.2 | 550.7 | 682.9 | 679.8 | 1229.9 | 1142.3 |
| Q73J84 | CTP synthase OS=Treponema denticola (strain ATCC 35405 / CIP 103919 / DSM 14222) OX=243275 GN=pyrG PE=3 SV=1 | 575.3 | 639.4 | 718.2 | 698.8 | 875 | 885.5 |
| Q73P19 | Asparagine--tRNA ligase OS=Treponema denticola (strain ATCC 35405 / CIP 103919 / | 598.5 | 607.2 | 594.8 | 628 | 872 | 782.6 |

| | | | | | | | |
|---|---|---|---|---|---|---|---|
| | DSM 14222) OX=243275 GN=asnS PE=3 SV=1 | | | | | | |
| Q73JJ4 | 50S ribosomal protein L1 OS=Treponema denticola (strain ATCC 35405 / CIP 103919 / DSM 14222) OX=243275 GN=rplA PE=3 SV=1 | 628.5 | 620.1 | 310.7 | 317.2 | 661 | 673.9 |
| Q73Q56 | Histidine ammonia-lyase OS=Treponema denticola (strain ATCC 35405 / CIP 103919 / DSM 14222) OX=243275 GN=hutH PE=3 SV=1 | 696.9 | 626.9 | 1281 | 1273.3 | 728.8 | 730 |
| Q73PL3 | 50S ribosomal protein L15 OS=Treponema denticola (strain ATCC 35405 / CIP 103919 / DSM 14222) OX=243275 GN=rplO PE=3 SV=1 | 703.8 | 737.3 | 711.2 | 738.5 | 541.4 | 573.4 |
| Q73PN0 | 50S ribosomal protein L23 OS=Treponema denticola (strain ATCC 35405 / CIP 103919 / DSM 14222) OX=243275 GN=rplW PE=3 SV=1 | 723.9 | 745.2 | 387.5 | 382.6 | 1139.1 | 1097.2 |
| Q73PL9 | 30S ribosomal protein S14 type Z OS=Treponema denticola (strain ATCC 35405 / CIP 103919 / DSM 14222) OX=243275 GN=rpsZ PE=3 SV=1 | 748.6 | 708.7 | 284 | 288.1 | 572.1 | 595 |
| Q73RN8 | Imidazolonepropionase OS=Treponema denticola (strain ATCC 35405 / CIP 103919 / DSM 14222) OX=243275 GN=hutI PE=3 SV=1 | 750.4 | 666.3 | 1183.1 | 1127 | 655 | 685.1 |
| Q73M34 | 30S ribosomal protein S18 OS=Treponema denticola (strain ATCC 35405 / CIP 103919 / DSM 14222) OX=243275 GN=rpsR PE=3 SV=1 | 802.1 | 738.2 | 1011 | 1056.6 | 596.6 | 504.4 |
| Q73JL8 | 50S ribosomal protein L34 OS=Treponema denticola (strain ATCC 35405 / CIP 103919 / DSM 14222) OX=243275 GN=rpmH PE=3 SV=1 | 825.7 | 864 | 278.8 | 283.1 | 488.4 | 460.3 |
| Q73PK8 | DNA-directed RNA polymerase subunit alpha OS=Treponema denticola (strain ATCC 35405 / CIP 103919 / DSM 14222) OX=243275 GN=rpoA PE=3 SV=1 | 866.7 | 894.3 | 391.9 | 393.4 | 585 | 585.1 |

| | | | | | | | |
|---|---|---|---|---|---|---|---|
| Q73JM1 | Membrane protein insertase YidC OS=Treponema denticola (strain ATCC 35405 / CIP 103919 / DSM 14222) OX=243275 GN=yidC PE=3 SV=1 | 873.8 | 886.5 | 200.5 | 216.2 | 400 | 413.2 |
| Q73PL6 | 50S ribosomal protein L18 OS=Treponema denticola (strain ATCC 35405 / CIP 103919 / DSM 14222) OX=243275 GN=rplR PE=3 SV=1 | 888.3 | 858.8 | 530.4 | 503.6 | 1207.1 | 1138.3 |
| Q73PM0 | 50S ribosomal protein L5 OS=Treponema denticola (strain ATCC 35405 / CIP 103919 / DSM 14222) OX=243275 GN=rplE PE=3 SV=1 | 901.1 | 974 | 1563.5 | 1577 | 2043 | 2049.9 |
| Q73RS4 | Peroxiredoxin OS=Treponema denticola (strain ATCC 35405 / CIP 103919 / DSM 14222) OX=243275 GN=TDE_0011 PE=3 SV=2 | 902.1 | 791.8 | 444.5 | 437.1 | 943.6 | 917.5 |
| Q73QV3 | Fructose-bisphosphate aldolase class 1 OS=Treponema denticola (strain ATCC 35405 / CIP 103919 / DSM 14222) OX=243275 GN=fda PE=3 SV=1 | 903.4 | 988.9 | 4584.1 | 4457.1 | 1654.2 | 1593.5 |
| Q73QI7 | Pyridoxal 5'-phosphate synthase subunit PdxS OS=Treponema denticola (strain ATCC 35405 / CIP 103919 / DSM 14222) OX=243275 GN=pdxS PE=3 SV=1 | 919.3 | 851.6 | 2933.4 | 3002.5 | 1005.8 | 1063.3 |
| Q73RS2 | Bifunctional protein FolD OS=Treponema denticola (strain ATCC 35405 / CIP 103919 / DSM 14222) OX=243275 GN=folD PE=3 SV=1 | 966.3 | 917 | 2376.7 | 2485.6 | 1319.5 | 1331.6 |
| Q73M27 | Adenine phosphoribosyltransferase OS=Treponema denticola (strain ATCC 35405 / CIP 103919 / DSM 14222) OX=243275 GN=apt PE=3 SV=1 | 969.2 | 912.4 | 617.3 | 656.1 | 675.8 | 791.7 |
| Q73NW2 | 30S ribosomal protein S15 OS=Treponema denticola (strain ATCC 35405 / CIP 103919 / DSM 14222) OX=243275 GN=rpsO PE=3 SV=1 | 983.2 | 1081.8 | 747.1 | 761.5 | 1158.5 | 1151.2 |
| Q73NV5 | 30S ribosomal protein S12 OS=Treponema denticola (strain ATCC 35405 / CIP 103919 / | 1004.3 | 992.2 | 314.5 | 315.6 | 721.7 | 756.5 |

| | | | | | | | |
|---|---|---|---|---|---|---|---|
| | DSM 14222) OX=243275 GN=rpsL PE=3 SV=1 | | | | | | |
| P61070 | 50S ribosomal protein L4 OS=Treponema denticola (strain ATCC 35405 / CIP 103919 / DSM 14222) OX=243275 GN=rplD PE=3 SV=1 | 1023.8 | 1110 | 674 | 730.4 | 1126.2 | 1191.9 |
| P62421 | Phosphoglycerate kinase OS=Treponema denticola (strain ATCC 35405 / CIP 103919 / DSM 14222) OX=243275 GN=pgk PE=3 SV=1 | 1025.5 | 1266.8 | 3823.7 | 3696.6 | 1435 | 1467.2 |
| Q73PM9 | 50S ribosomal protein L2 OS=Treponema denticola (strain ATCC 35405 / CIP 103919 / DSM 14222) OX=243275 GN=rplB PE=3 SV=1 | 1075.4 | 965.6 | 300.8 | 294.2 | 458.4 | 495.7 |
| Q73PL7 | 50S ribosomal protein L6 OS=Treponema denticola (strain ATCC 35405 / CIP 103919 / DSM 14222) OX=243275 GN=rplF PE=3 SV=1 | 1077.2 | 2269.4 | 157.9 | 155.3 | 321 | 315 |
| Q73JJ7 | DNA-directed RNA polymerase subunit beta OS=Treponema denticola (strain ATCC 35405 / CIP 103919 / DSM 14222) OX=243275 GN=rpoB PE=3 SV=1 | 1391.2 | 1315.6 | 855.2 | 818.9 | 1352.1 | 1295.2 |
| Q73K75 | 30S ribosomal protein S2 OS=Treponema denticola (strain ATCC 35405 / CIP 103919 / DSM 14222) OX=243275 GN=rpsB PE=3 SV=1 | 1446.5 | 1317 | 984.8 | 952.1 | 2350.2 | 2205.2 |
| Q73P31 | Elongation factor P OS=Treponema denticola (strain ATCC 35405 / CIP 103919 / DSM 14222) OX=243275 GN=efp PE=3 SV=1 | 1462.4 | 1212.1 | 615.1 | 553.9 | 711 | 692.1 |
| Q73JJ8 | DNA-directed RNA polymerase subunit beta' OS=Treponema denticola (strain ATCC 35405 / CIP 103919 / DSM 14222) OX=243275 GN=rpoC PE=3 SV=1 | 1634.6 | 1719.7 | 829.2 | 842.3 | 1212.3 | 1239.4 |
| Q73JJ5 | 50S ribosomal protein L10 OS=Treponema denticola (strain ATCC 35405 / CIP 103919 / DSM 14222) OX=243275 GN=rplJ PE=3 SV=1 | 1755.6 | 2026.4 | 575.4 | 594.1 | 2035.8 | 1876.4 |

| | | | | | | | |
|---|---|---|---|---|---|---|---|
| Q73PN1 | 50S ribosomal protein L3 OS=Treponema denticola (strain ATCC 35405 / CIP 103919 / DSM 14222) OX=243275 GN=rplC PE=3 SV=1 | 1792.7 | 1651.1 | 589.5 | 569.1 | 1335.2 | 1185.4 |
| Q73P28 | Arginine--tRNA ligase OS=Treponema denticola (strain ATCC 35405 / CIP 103919 / DSM 14222) OX=243275 GN=argS PE=3 SV=1 | 1861.7 | 1387.5 | 201.3 | 192.6 | 1604.2 | 1215.7 |
| Q73P50 | Enolase OS=Treponema denticola (strain ATCC 35405 / CIP 103919 / DSM 14222) OX=243275 GN=eno PE=3 SV=1 | 1936.5 | 2096.9 | 2821.1 | 2974.2 | 2214.8 | 2129.4 |
| Q73PL5 | 30S ribosomal protein S5 OS=Treponema denticola (strain ATCC 35405 / CIP 103919 / DSM 14222) OX=243275 GN=rpsE PE=3 SV=1 | 2099.6 | 1888.3 | 671.8 | 686.1 | 1796.6 | 1730.6 |
| Q73M83 | Glycine cleavage system H protein OS=Treponema denticola (strain ATCC 35405 / CIP 103919 / DSM 14222) OX=243275 GN=gcvH PE=3 SV=1 | 2157.8 | 2159.6 | 6276 | 6146.5 | 3623.5 | 4026.6 |
| Q73P66 | Acetate kinase OS=Treponema denticola (strain ATCC 35405 / CIP 103919 / DSM 14222) OX=243275 GN=ackA PE=3 SV=1 | 2444.4 | 2430.7 | 4286.2 | 4309.1 | 3058.8 | 3041.5 |
| Q73NR2 | Threonine--tRNA ligase OS=Treponema denticola (strain ATCC 35405 / CIP 103919 / DSM 14222) OX=243275 GN=thrS PE=3 SV=1 | 2506.3 | 2411.1 | 1470.2 | 1432.7 | 2918.3 | 2826 |
| Q73QZ3 | Probable cytosol aminopeptidase OS=Treponema denticola (strain ATCC 35405 / CIP 103919 / DSM 14222) OX=243275 GN=pepA PE=3 SV=1 | 2524.4 | 2354.7 | 3038.7 | 3020.9 | 2704.9 | 2667.3 |
| Q73JJ6 | 50S ribosomal protein L7/L12 OS=Treponema denticola (strain ATCC 35405 / CIP 103919 / DSM 14222) OX=243275 GN=rplL PE=3 SV=1 | 2575 | 3177.1 | 1037.5 | 1030.7 | 2867.3 | 3645.7 |
| Q73RR6 | Formate--tetrahydrofolate ligase OS=Treponema denticola (strain ATCC 35405 / CIP 103919 / DSM 14222) OX=243275 GN=fhs PE=3 SV=1 | 2645.6 | 2594.7 | 3522.3 | 3700 | 2657 | 2644.6 |

| | | | | | | | |
|---|---|---|---|---|---|---|---|
| Q04595 | Protein PyrBI OS=Treponema denticola (strain ATCC 35405 / CIP 103919 / DSM 14222) OX=243275 GN=pyrBI PE=3 SV=3 | 2967.4 | 3072.5 | 2480.8 | 2422.2 | 1941 | 2089.1 |
| Q73KM3 | 8-amino-7-oxononanoate synthase OS=Treponema denticola (strain ATCC 35405 / CIP 103919 / DSM 14222) OX=243275 GN=TDE_2194 PE=3 SV=1 | 3458.6 | 3523.2 | 6731.9 | 6494.3 | 4758.1 | 4662.3 |
| Q73KI2 | Glutamate mutase epsilon subunit OS=Treponema denticola (strain ATCC 35405 / CIP 103919 / DSM 14222) OX=243275 GN=glmE PE=3 SV=1 | 4695.7 | 4623.3 | 4779.5 | 4788.4 | 4523.4 | 4479 |
| Q73Q16 | Chaperone protein DnaK OS=Treponema denticola (strain ATCC 35405 / CIP 103919 / DSM 14222) OX=243275 GN=dnaK PE=3 SV=1 | 4977.2 | 5059.6 | 5542.5 | 5552.6 | 6126.1 | 6391.6 |
| Q73NH7 | 60 kDa chaperonin OS=Treponema denticola (strain ATCC 35405 / CIP 103919 / DSM 14222) OX=243275 GN=groL PE=3 SV=1 | 5290.7 | 6263.3 | 7548.5 | 7751.9 | 2843.4 | 3591 |
| Q73KL7 | L-methionine gamma-lyase OS=Treponema denticola (strain ATCC 35405 / CIP 103919 / DSM 14222) OX=243275 GN=megL PE=1 SV=1 | 5348.8 | 5273.4 | 5665.6 | 5687.6 | 3100.7 | 3343.2 |
| Q73PN3 | Elongation factor Tu OS=Treponema denticola (strain ATCC 35405 / CIP 103919 / DSM 14222) OX=243275 GN=tuf PE=3 SV=1 | 5572.5 | 5670.1 | 7839.7 | 7674.5 | 6599.2 | 6393 |
| Q73PM6 | 30S ribosomal protein S3 OS=Treponema denticola (strain ATCC 35405 / CIP 103919 / DSM 14222) OX=243275 GN=rpsC PE=3 SV=1 | 8230.3 | 7524.9 | 1942.6 | 1941.9 | 6810.5 | 6247.9 |
| Q73P70 | Ornithine carbamoyltransferase, catabolic OS=Treponema denticola (strain ATCC 35405 / CIP 103919 / DSM 14222) OX=243275 GN=arcB PE=3 SV=1 | 8270.3 | 8189.6 | 3960.6 | 3761.9 | 4839.9 | 4380.2 |
| P62031 | Probable glycine dehydrogenase (decarboxylating) subunit 2 OS=Treponema denticola (strain ATCC 35405 / CIP 103919 / DSM 14222) OX=243275 GN=gcvPB PE=3 SV=1 | 15293.1 | 13435.5 | 10299.4 | 9987.8 | 13864.4 | 12810.5 |

| | | | | | | | |
|---|---|---|---|---|---|---|---|
| Q73QV6 | Glucosamine-6-phosphate deaminase OS=Treponema denticola (strain ATCC 35405 / CIP 103919 / DSM 14222) OX=243275 GN=nagB PE=3 SV=1 | | | | | | |
| Q73R77 | Cyclic di-GMP binding protein TDE_0214 OS=Treponema denticola (strain ATCC 35405 / CIP 103919 / DSM 14222) OX=243275 GN=TDE_0214 PE=1 SV=1 | | | | | | |
| Q73L91 | UDP-N-acetylglucosamine--N-acetylmuramyl-(pentapeptide) pyrophosphoryl-undecaprenol N-acetylglucosamine transferase OS=Treponema denticola (strain ATCC 35405 / CIP 103919 / DSM 14222) OX=243275 GN=murG PE=3 SV=1 | | | | | | |
| P60794 | Elongation factor 4 OS=Treponema denticola (strain ATCC 35405 / CIP 103919 / DSM 14222) OX=243275 GN=lepA PE=3 SV=1 | | | | | | |
| P60941 | Undecaprenyl-diphosphatase OS=Treponema denticola (strain ATCC 35405 / CIP 103919 / DSM 14222) OX=243275 GN=uppP PE=3 SV=1 | | | | | | |
| Q73PH4 | UDP-N-acetylmuramyl-tripeptide synthetase OS=Treponema denticola (strain ATCC 35405 / CIP 103919 / DSM 14222) OX=243275 GN=murE PE=3 SV=1 | | | | | | |
| Q73KN7 | tRNA modification GTPase MnmE OS=Treponema denticola (strain ATCC 35405 / CIP 103919 / DSM 14222) OX=243275 GN=mnmE PE=3 SV=1 | | | | | | |
| Q73KT5 | Putative ABC transporter ATP-binding protein TDE_2132 OS=Treponema denticola (strain ATCC 35405 / CIP 103919 / DSM 14222) OX=243275 GN=TDE_2132 PE=3 SV=1 | | | | | | |
| P61038 | Apolipoprotein N-acyltransferase 2 OS=Treponema denticola (strain ATCC 35405 / CIP 103919 / DSM 14222) OX=243275 GN=lnt2 PE=3 SV=1 | | | | | | |

| | | | | | | | |
|---|---|---|---|---|---|---|---|
| Q73NP6 | Translation initiation factor IF-2 OS=Treponema denticola (strain ATCC 35405 / CIP 103919 / DSM 14222) OX=243275 GN=infB PE=3 SV=1 | | | | | | |

## 9.2 Conference abstracts

1. Shoker, S. S., Milward, M. R., Landini, G., Shelton, R. M., Cooper, P. R., Ling, M. and Pratten, J., 2019. Periodontal pathogens induce epithelial-mesenchymal transition in a periodontitis model (Poster). *British Society for Oral and Dental Research (BSODR)*, University of Leeds, UK, 3-5 September.

   **Objective**: Bacteria associated with subgingival plaque may initiate periodontitis through a persistent inflammatory response via epithelial-mesenchymal transition (EMT) signalling. This study aimed to determine the effects of periodontal pathogens on oral keratinocyte proliferation and viability and to investigate whether pathogen challenge increased EMT inducing pro-inflammatory cytokine release and associated changes in gene expression.

   **Methods**: *Porphyromonas gingivalis* (*P.gingivalis*), *Fusobacterium nucleatum* (*F. nucleatum*), *Campylobacter rectus* (*C. rectus*) and *Treponema denticola* (*T. denticola*) were cultured anaerobically and characterised by culture, Gram staining and PCR. Bacteria were then heat-inactivated (HI) at 80$^{o}$C for 1 hour or oxygen-inactivated (OI) in atmospheric conditions and applied to oral keratinocyte cultures in a 100:1 bacteria to epithelial cell ratio. Enzyme-linked immunosorbent assay (ELISA) was performed for IL-1β and TGF-β1 on culture supernatants collected at days 1, 5 and 8. Semi-quantitative reverse transcriptase-polymerase chain reaction (Sq-RT-PCR) was performed for epithelial and mesenchymal markers at 8-day cultures.

   **Results**: OI *F. nucleatum* challenge reduced keratinocyte growth significantly ($1.06x10^{6}$ to $6.6x10^{5}$ cells) and viability significantly (99.2% to 92.4%) when

compared with control. Cultures challenged with HI *P. gingivalis* and HI *F. nucleatum* caused significant increase in TGF-β1 (282.6ng/ml to 414.6ng/ml) and IL-1β (116.1pg/ml to 155.8pg/ml) secretion. OI *F. nucleatum* caused significant release of IL-1β (62.5pg/ml to 102.7pg/ml) compared with control. HI *F. nucleatum* down-regulated epithelial marker E-cadherin expression (1-fold) and up-regulated mesenchymal marker N-cadherin expression (1-fold). HI *P. gingivalis* and *F. nucleatum* significantly upregulated expression of the key-EMT transcriptional factor, Snail-1 (1-2-fold).

**Conclusion**: Oral keratinocyte exposure to HI periodontal pathogens caused significant release of pro-inflammatory cytokines IL-1β and TGF-β1 and up-regulated expression of Snail-1, which is a strong repressor of E-cadherin. This loss of E-cadherin and increased N-cadherin after HI *F. nucleatum* exposure may lead to EMT induction characterised by breakdown of epithelium cell adhesion and loss of associated barrier function in periodontitis.

Conference poster for the abstract detailed above:

# Periodontal Pathogens Induce Epithelial-Mesenchymal Transition In A Periodontitis Model

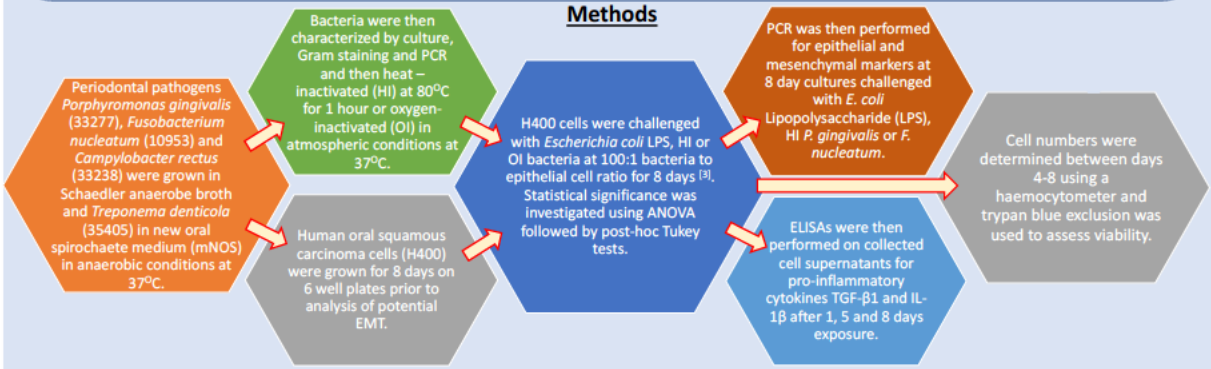
Satvir S. Shoker Paul R. Cooper, Gabriel Landini, Richard M. Shelton, Martin Ling[1], Jonathan Pratten[1], Michael R. Milward
University of Birmingham, School of Dentistry, Birmingham, UK
[1]GlaxoSmithKline, Weybridge, Surrey, UK

## Introduction

Chronic adult periodontal disease is a major disease which affects almost half of the UK adult population and has a complex multi-factorial aetiology [1]. The disease is initiated by an aberrant host response to pathogenic bacteria that colonise in the subgingival plaque biofilm. This inflammatory response may initiate epithelial-mesenchymal transition (EMT), which is a highly conserved process where epithelial cells lose polarity and gain migratory properties and is implicated in diseases such as fibrosis of the liver, lung and kidney and tumour metastasis [2].

Bacteria associated with the subgingival plaque may initiate periodontitis through a persistent inflammatory response via epithelial-mesenchymal transition (EMT) signalling. This study aimed to determine the effects of *Porphyromonas gingivalis, Fusobacterium nucleatum*, *Campylobacter rectus* and *Treponema denticola* on oral keratinocyte proliferation and viability and to investigate whether pathogen challenge increased EMT inducing pro-inflammatory cytokine release and changes in molecular markers associated with both epithelial and mesenchymal phenotype.

## Methods




## Results

OI *F. nucleatum* resulted in a significant reduction (P<0.001) in H400 growth and viability compared with controls and HI *F. nucleatum* after 8 days exposure. H400 exposure to both HI *P. gingivalis* and *F. nucleatum* resulted in significant increase in TGF-β1 (P<0.01) and IL-1β (P<0.001) compared with controls (Fig. 1). Gene expression data showed significant up-regulation (P<0.05 and P<0.001) of the key EMT transcription factor Snail-1 after pathogen challenge at day 8 (Fig. 2).

***TGF-β1 and IL-1β release***

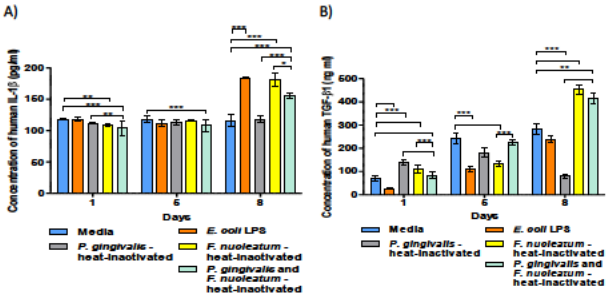



**Figure 1:** H400 cultures challenged with *E.coli* LPS or HI *P. gingivalis* or *F. nucleatum* and both *P. gingivalis* and *F. nucleatum* and supernatants collected for A) TGF-β1 and B) IL-1β ELISA analysis. The error bars represent one standard deviation from the mean (n 9). * P<0.05, ** P<0.01 and *** P<0.001.

***EMT-related gene expression***

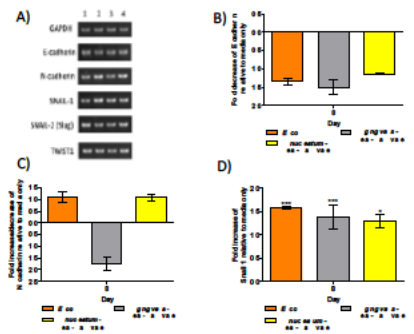



**Figure 2** A) Gene expression on H400 cultures challenged with 1) media only 2) *E.coli* LPS, 3) HI *P. gingivalis* (33277) and 4) *F. nucleatum* (10953) after 8 days for housekeeping gene GAPDH and genes E- cadherin. N-cadherin and SNAIL-1. % change in gene expression relative to media only is shown in genes B) E- cadherin, C) N-cadherin and D) Snail-1. The error bars represent one standard deviation from the mean (n 3). * P<0.05 and *** P<0.001.

## Discussion and Conclusion

Pathogen-epithelial barrier interactions occurring in periodontitis were replicated by using OI pathogens instead of commonly used HI pathogens. OI *F. nucleatum* may have reduced cell growth and viability because of increased reactive oxygen species (ROS) produced after oxygen exposure, which have shown to accelerate cell death [4]. Oral keratinocyte exposure to heat-inactivated periodontal pathogens caused significant release of EMT-inducing pro-inflammatory cytokines IL-1β and TGF-β1 and up-regulated expression of the key EMT transcription factor Snail-1, which up-regulates expression of EMT inducing cytokines and is a strong repressor of E-cadherin. This loss of E-cadherin and increased N-cadherin after heat-inactivated *F. nucleatum* exposure may lead to EMT induction characterised by breakdown of epithelium cell adhesion and loss of associated barrier function in periodontitis.

## References

1. Nagarajan R. M ller C. Dawson D. Al-Sabbagh M. and Ebersole J. (2016). Cross-talk between clinical and host-response parameters of periodontitis in smokers. *Journal of Periodontal Research* 52(3). pp. 342-352.
2. Davis F. Stewart T. Thompson E. and Monteith G. (2014). Targeting EMT in cancer: opportunities for pharmacological intervention. *Trends in Pharmacological Sciences* 35(9). pp.479-488.
3. Abdulkareem A. (2017). Potential involvement of epithelial-mesenchymal transition in the pathogenesis of periodontitis.' PhD thesis University of Birmingham Birmingham pp.1-258.
4. Zhao M. Tang S. Xin J. and Liu D. (2017). Influence of reactive oxygen species on secretory component in the intestinal epithe ium during hyperoxia. *Experimental and Therapeutic Medicine*. pp. 259-267.

## Acknowledgements

The authors gratefully acknowledge financial support from the BBSRC (BIDS3000031260) through an iCASE studentship award with GlaxoSmithKline.

2. Shoker, S. S., Milward, M. R., Landini, G., Shelton, R. M., Cooper, P. R., Ling, M. and Pratten, J., 2021. Epithelial-mesenchymal inhibitors may have a role in inhibiting pathogen-induced EMT (Oral Presentation). *British Society for Oral and Dental Research (BSODR)*, University of Birmingham, UK, 1-3 September.

**Objective**: Subgingival plaque bacteria can initiate periodontitis by eliciting a persistent, excessive host inflammatory response caused by bacterial invasion into host tissue. This may induce an epithelial-mesenchymal transition (EMT) that compromises the epithelial barrier. This study aimed to determine the effects of periodontal pathogens on potential induction of oral keratinocyte EMT, migration and gene expression changes and to investigate potential EMT inhibitors for prevention or management of disease.

**Methods**: *Porphyromonas gingivalis* (*PG*), *Fusobacterium nucleatum* (*FN*) and *Treponema denticola* (*TD*) were cultured anaerobically, then oxygen-killed (OK) in atmospheric conditions at 37ºC and applied to oral keratinocyte cultures in a 100:1 bacterium to epithelial cell ratio. 5µM curcumin was dissolved in 0.15M sodium hydroxide (NaOH) and sterilised PBS before addition to cell cultures. Cell counts were determined manually and cell migration was assessed in a 500µm wound area formed by Ibidi® 2-well inserts. Quantitative real-time polymerase chain reaction (qRT-PCR) was performed for epithelial and mesenchymal markers after 8-days in culture.

**Results**: Cell numbers of keratinocytes grown in the presence of OK *TD* were significantly increased ($P<0.01$) but increased keratinocyte cell numbers were significantly reduced by addition of curcumin after 8-day exposure ($P<0.05$).

Curcumin significantly reduced OK *TD* induced % wound gap closure from 56.15% to 29.54% ($P<0.001$) after 48hrs. Significant down-regulation of epithelial markers E-cadherin, Cytokeratin-5 and Desmoplakin-1 after 8-day exposure to OK *PG*, *FN* and *TD* were significantly inhibited by curcumin addition after qRT-PCR analysis ($P<0.05$ to $P<0.001$). Simultaneously, up-regulation of mesenchymal markers, Snail-1, N-cadherin, Vimentin and MMP-9 was significantly inhibited by curcumin ($P<0.05$ to $P<0.001$).

**Conclusion**: OK periodontal pathogens promote an EMT response in oral keratinocytes through gene expression changes leading to increased cell growth and migration. Curcumin appears to inhibit the responses eliciting EMT by periodontal pathogens, providing a potential therapeutic role in preventing or managing periodontitis progression by maintaining epithelial barrier integrity.